Two Contrasting Approaches to Auto-Ignition Modelling for HCCI Engines

by Gareth Floweday

A Thesis Presented for the Degree of
Doctor of Philosophy

Sasol Advanced Fuels Laboratory
Department of Mechanical Engineering
University Of Cape Town

February 2010

Acknowledgements

I wish to acknowledge and thank the following people for their contributions and support of this project:

- Sasol Technology Fuels Research, who funded the project and well as the laboratory in which it was conducted.

- The Faculty of Engineering and the Built Environment and the Department of Mechanical Engineering at the University of Cape Town, for their support of the Sasol Advanced Fuels Laboratory.

- My supervisor, Professor Andy D.B. Yates, whose encouragement, astute technical guidance and wise mentorship were instrumental in the success of this project.

- Mr Marlan Perumal and Dr Chris Woolard, for the endless technical discussions regarding global auto-ignition model formulations and for enduring my cyclic agonies and ecstasies during this phase of the project.

- Mr Kyle Collair and Mr Ian Lemberger, my Masters students, for their hard work in setting up and testing the engines used for the experimental validation of the thermodynamic engine models.

- My colleagues within the SAFL and Mechanical Engineering Department, for the healthy environment of technical challenge and discussion.

This thesis is dedicated to my wife Dr Clare Louise Floweday, who has been my rock during this season and has made countless sacrifices to my benefit. Perhaps we will share the same title.

Soli Deo Gloria

Abstract

This body of work entailed the broad contrasting of two hydrocarbon fuel auto-ignition models formulated for the emulation of combustion dynamics in Homogeneous Charge Compression Ignition (HCCI) engines.

The first (empirical) auto-ignition model was adapted from its previously published form, for HCCI engine model implementation. This model was then combined with an explicit, single zone, thermodynamic engine model in order to investigate combustion phasing control strategies over a wide range of engine design parameters, experimental conditions and hydrocarbon fuels. This investigation yielded new techniques for HCCI combustion phasing control using convergent control parameter values and operation along curves of constant combustion phasing. These techniques were validated experimentally using two HCCI engines of novel design.

The second (functional global) auto-ignition model was formulated in this study, drawing on an analysis of chemical kinetic schematics, a detailed auto-ignition behavioural study and a critical evaluation of existing global auto-ignition models. The performance of this new functional global model was evaluated using detailed chemical kinetic simulation data for a variety of hydrocarbon fuels, across a wide range of experimental conditions.

The two studies, although different in approach and scope, enabled a broad and detailed comparison of the two auto-ignition models, thereby highlighting their respective values and limitations. The two models were shown to each possess particular advantages in the context of HCCI auto-ignition modelling, which were unmatched by existing models of similar classification. The models were also shown to exhibit individual drawbacks which played to each other's strengths. Both models were shown to be configurable to real world, full boiling range fuels and were designed to accurately emulate the dynamics of two-stage auto-ignition with excellent computational efficiency.

These two hydrocarbon fuel auto-ignition models, together with the engine modelling techniques developed in this study, represent a novel and valuable contribution to the field of HCCI engine combustion control and effectively move this technology one incremental step closer to its anticipated commercial realisation.

Table of contents

List of figures

List of tables

List of equations

Glossary of terms and abbreviations

Active Radical (AR) combustion: An exemplification of CAI which refers specifically to the case where the inlet heating is accomplished through the use of hot internal or external EGR.

Bottom-Dead-Centre (BDC): The point of engine crankshaft rotation when the piston is furthest from the cylinderhead and the combustion chamber volume is at its maximum value.

Brake Mean Effective Pressure (BMEP): A comparative measure of engine torque output given by the engine crankshaft measured cycle work divided by the displaced cylinder volume.

Co-operative Fuels Research (CFR) engine: The engine required and used for the determination of Research and Motor Octane Numbers, RON and MON respectively.

Compression Ignition (CI) engine: An ICE where the fuel is injected into the combustion chamber and ignited by the high temperature and pressure environment. Combustion is controlled by the rate of fuel injection into the combustion chamber.

Compression ignition engine knock: This phenomenon occurs in a CI engine if the fuel ignition quality and/or the compression ratio are too low for fuel ignition to occur rapidly after injection. In this case a significant amount of fuel has been injected at the time of initial ignition and the initial heat release rate is uncontrolled and very high.

Compression Ratio (CR): The ratio of volumes in the combustion chamber given by the volume at BDC divided by the volume at TDC.

Computational Fluid Dynamics (CFD): The study of fluid flow physics by the discretisation of the flow domain into elements wherein mathematical conservation equations are numerically solved.

Controlled Auto-Ignition (CAI): An exemplification of HCCI operation in a gasoline engine where the engine is run with a lean mixture and sufficient inlet heating to produce auto-ignition without the aid of the spark plug.

Detailed Kinetic Model (DKM): The detailed chemical kinetic mechanism used for the generation of auto-ignition delay data in this study.

Dual-mode HCCI: An engine operation strategy where HCCI operation is used in the section of the operational map where it can be achieved, reverting to conventional gasoline or diesel combustion in other parts of the engine map.

Equivalence ratio (φ or phi): The ratio of a given fuel-air ratio to a stoichiometric fuel-air ratio. $\Phi = 1$ is stoichiometric, $\Phi < 1$ is lean and $\Phi > 1$ is a rich mixture.

Exhaust Gas Recirculation (EGR): The method of internal or external reintroduction of exhaust gas products into the inducted fuel-air mixture for combustion and/or emissions control.

Functional Global Model (FGM): The name given to the auto-ignition model developed in this study due to its functional characteristics and concise formulation.

Homogeneous Charge Compression Ignition (HCCI): An engine technology involving the induction (or subsequent creation) of a nominally homogeneous fuel-air mixture which is then ignited by compression alone without any form of additional ignition system

Hydrocarbon (HC) emissions: Engine exhaust emissions consisting usually of partially oxidised species of hydrocarbon radicals and molecules

Ignition quality: The propensity of a given fuel to spontaneously ignite under conditions of elevated pressure and temperature.

Ignition Quality Tester (IQT^{TM}): A patented constant volume combustion bomb apparatus used for determining the “derived cetane number” (a measure of ignition quality) of fuels according to ASTM 6890.

Internal Combustion Engines (ICEs): A thermodynamic heat engine that liberates heat via a chemical combustion process inside the combustion chamber of the engine device

Motor Octane Number (MON): A standard test method (ASTM D 2700) for determining the octane rating of a fuel. The method involves running the fuel at 900rpm in a CFR engine with a heated inlet air temperature.

Negative Temperature Coefficient (NTC): A generic term related to some fuels that exhibit a 2-stage heat release, where a region exists wherein auto-ignition delay can be shortened by decreasing temperature – converse to conventional ignition delay behaviour.

Original Equipment Manufacturers (OEMs): Manufactures of vehicles and engines.

Oxides of nitrogen (NOx) emissions: The regulated emission combination of NO and NO_2 formed during combustion at high temperatures

Premixed Charge Compression Ignition (PCCI): An exemplification of HCCI operation in a diesel engine where the diesel fuel is injected early enough to evaporate and mix significantly prior to auto-ignition by piston compression.

Primary Reference Fuels (PRFs): Iso-octane and n-heptane are the two fuels used to define the octane scale in the Research and Motor Octane test methods (ASTM D2699 and ASTM D2700 respectively). Iso-octane is defined as having an octane rating of 100, while n-heptane is defined as having an octane rating of zero. Linear volumetric interpolation is used to determine the octane rating of PRF blends.

Quasi-Steady-State Assumption (QSSA): A mathematical technique for simplifying a chemical kinetic system where a fast reversible equilibrium reaction pair is followed by a slower forward reaction.

Rapid Compression Machine (RCM): A device used for testing the auto-ignition characteristics of a given fuel. The device operates by rapidly compressing the given fuel and oxidant mixture from a given state of pressure and temperature by a set compression ratio. The mixture is then held at the elevated conditions and the ignition delay measured.

Research Octane Number (RON): A standard test method (ASTM D 2699) for determination of octane number. This method involves running the fuel in a CFR engine at standard knock intensity at 600rpm and bracketing the test fuel using PRF blends.

Spark-ignition (SI) engine: An ICE that ignites the fuel-air mixture with the aid of an electrical spark plug. SI engines usually run on gasoline like fuels and combustion is controlled by the timing of the spark discharge.

Spark-ignition engine knock: An abnormal and potentially damaging combustion phenomenon where unburned mixture within the cylinder is compressed by the piston and advancing flame front to the point of auto-ignition before it is consumed by flame propagation.

Top-Dead-Centre (TDC): The point of engine crankshaft rotation when the piston is closest to the cylinderhead and the combustion chamber volume is at its minimum value.

Two-stage auto-ignition: A spontaneous combustion behaviour exhibited by some fuels where an initial delay and relatively small preliminary heat release is followed by a secondary delay and larger primary heat release

1. Introduction

1.1. General background to the study

Simulation of fuel combustion within Internal Combustion Engines (ICEs) has long been an integral part of the design and study of both fuels and engines. Engines and fuel combustion must be simulated together due to the intricate thermodynamic interaction of the machine and the fuel that it uses. Engine and fuel combustion simulations vary widely in aim and implementation. However, all such simulations aim for a balance between accuracy and computational efficiency. Generally these two requirements form a classical trade-off, since the detailed mathematical formulations required for accurate description of the complex phenomena inherently carry the burden of greater computational expense. Detailed engine combustion chamber simulations generally make use of Computational Fluid Dynamics (CFD) methods to discretise the combustion chamber volume in order to study the physical and thermodynamic phenomena with spatial resolution. Detailed combustion reaction simulations on the other hand generally make use of detailed chemical kinetic mechanisms to accurately capture the numerous elemental reactions active in fuel combustion processes. The accurate simulation of combustion within an engine environment therefore poses a significant challenge, since both engine CFD and detailed chemical kinetic simulations require significant computing power and their combination is currently impractical even using today's most advanced computing hardware systems.

In the field of Homogeneous Charge Compression Ignition (HCCI) engines, simulations of fuel auto-ignition reactions face a particular challenge due to the following factors:

1. CFD methods are frequently required in order to capture spatial dynamics of fluid flow and heat transfer, since this has a significant bearing on the HCCI engine simulation solution.
2. Fuel auto-ignition timing accuracy forms a very important aspect of the simulation since it is directly related to the engine's power and efficiency prediction.
3. Two-stage auto-ignition fuels are often used. These fuels exhibit an initial delay and relatively small preliminary heat release, followed by a secondary delay and larger main heat release. This necessitates the need for accurate prediction of these complex thermo-chemical dynamics.
4. The prediction of heat release rate, as opposed to mere phasing prediction, is very important due to the fact that the maximum HCCI engine power output is generally limited by this factor.

5. There are no hydrocarbon fuel auto-ignition models available in the open literature that are capable of accurately predicting the full heat release dynamics (including “cool-flame” heat release) of full boiling range, two-stage auto-ignition, hydrocarbon fuels.
6. Even if the full boiling range fuel is approximated using a suitable surrogate blend of single component fuels, the only method available for accurate prediction of the full heat release dynamics entails the use of extremely computationally expensive detailed chemical kinetics mechanisms or perhaps one of the better reduced kinetics models which in many cases, renders the simulation effort impractical.

A significant international research effort has been directed towards addressing this gap in the fuel auto-ignition modelling toolset with the publishing of various reduced, skeletal, global and empirical fuel auto-ignition models. Reduced kinetics models are generally constrained to remain true to the base detailed kinetics mechanisms with the result that they remain fairly complex and retain significant computational expense. The skeletal mechanisms, and to a lesser extent the global models, have proven reasonably successful in accurately predicting overall ignition delay timing and have therefore been incorporated in many CFD and detailed engine modelling codes. The skeletal, global and empirical models have not, however, proven successful in capturing the full heat release dynamics (including accurate “cool-flame” timing and heat release rates) of fuels exhibiting two-stage auto-ignition.

1.2. Description and explanation of the study thesis

One recently published empirical fuel auto-ignition model [1] has, however, demonstrated the ability to predict the timing and heat release magnitudes of the “cool-flame” as well as overall ignition delay. The model has been fitted to a number of PRF blends of iso-octane and n-heptane (2-stage ignition fuels) as well as methanol (a single stage ignition fuel) blends. This model does not, however, predict the rates of heat release. The functionality and computational efficiency of this recently developed model opened the potential for wide exploration of the combined effects of fuel formulation and HCCI engine design and operation. The *thesis of this first study section* was that valuable synergistic performance could be obtained by studying fuel auto-ignition characteristics and HCCI engine design and operation in a manner which allowed virtual variation of parameters in both areas. This is in stark contrast to typical HCCI studies where either the fuel auto-ignition parameters are studied using a given engine, or the engine parameters are varied to optimise operation on a given fuel. An obvious weakness in this first section was the model’s limitation to ignition phasing prediction only, i.e., the lack of heat release rate modelling ability. Since heat release rate is the primary limiting factor in the power

output of an HCCI engine, this represented a serious limitation to the broader application of this computational technique.

In an attempt to address this issue, various computationally efficient, rate oriented skeletal and global auto-ignition models were considered, but were found lacking in the accuracy of their cool flame heat release predictions, compared with the recently developed empirical model [1]. However, in view of the various established skeletal and global mechanisms capable of reaction rate and overall auto-ignition delay prediction and the more recently published formulation of an empirical 2-stage auto-ignition delay model incorporating “cool flame” dynamics functionality, it was *the thesis of the second section of this study* that a new fully functional global kinetic model could be formulated to predict reaction rate dynamics of two-stage auto-ignition fuels, over a wide range of pressure, temperature, fuel equivalence ratio and inert exhaust product dilution, incorporating prediction of “cool-flame” timing, “cool-flame” heat release magnitude, main heat release timing and overall heat release magnitude. Such a functional global model could prove ideal for incorporation in CFD HCCI engine models, allowing significantly improved combustion modelling accuracy within reasonable simulation run times. Such a functional global model could also prove useful in other ICE combustion simulations.

1.3. Outline of the study scope and methodology

This study approached the challenge of synergistic HCCI engine and fuel modelling by developing a single zone discrete HCCI engine model using the recently developed empirical two-stage fuel auto-ignition model. A second simplified explicit engine model formulation was also developed. This explicit engine model was first validated using experimental data from a single cylinder variable compression ratio engine running in HCCI mode. The model was then used to identify promising and problematic areas for the combination of fuel properties, engine configurations and operational ranges.

This study approached the challenge of the proposed functional global model formulation in three manners. Firstly, published literature relating to the study and modelling of hydrocarbon chemical kinetics was reviewed and analysed in detail. Secondly the basic observable characteristics of fuel auto-ignition reactions were systematically studied using detailed chemical kinetic simulations as being closely representative of the real-life physical and chemical phenomena. In view of the extensive experimental validation of the detailed chemical kinetics mechanisms, the assumption was made that these simulations were sufficiently representative of the experimental auto-ignition data. These detailed chemical kinetics simulations also provided results across the functional range of a number of experimental

testing devices and provided idealised results free of the experimental challenges and uncertainties (heat loss, mixture homogeneity, leakage etc.) of these experimental testing devices. The third source of insight for the development of the new functional came through the critical evaluation of existing models in comparison with the functional requirements identified in the behavioural study. The insights gleaned from these three approaches were then used to formulate a number of proposed functional global mechanisms which were tested against the detailed chemical kinetics simulation data. The results dictated a number of model form adjustments and the model coefficients were re-solved in order to achieve enhanced accuracy using the detailed chemical kinetics data set. The new functional global model therefore did not aim to test a hypothesis related to combustion kinetics, or to reduce the computational expense of existing detailed fuel auto-ignition models, but rather sought to describe the behavioural dynamics of fuel auto-ignition as simply as possible within the bounds of reasonable accuracy. However, since schematic representations of combustion chemistry were considered in the formulation of the model, some insights were gained from the model's form and agreement with detailed kinetic simulation data.

The approaches and scopes of the two thesis investigations were different. In the *first investigation*, the already published empirical model was adapted for HCCI implementation and used to gain valuable insights into new control techniques. This was done without altering the essential formulation or function of the empirical model. The *second investigation* followed from the first, due to challenges in heat release rate prediction and CFD implementation which could not be achieved using the empirical model. The *second investigation* therefore involved the formulation of a new functional global auto-ignition model which was rigorously evaluated using detailed chemical kinetic simulation data. The scope of this investigation did not include implementation of the new model into an engine model since this was not needed in order to demonstrate the model's functional attributes. In spite of the different approaches and scopes of the two investigations, they effectively enabled the values and limitations of the respective auto-ignition models to be highlighted and contrasted against one another.

1.4. Thesis structure and flow

This thesis document has been structured to guide the reader logically through the project.

The document begins with an introduction of the background and context to the study. This is followed by an explanation of the two study theses as well as an overview of the methodology and scope of the work. A thorough literature review on the topics of HCCI technology and fuel auto-ignition then provides the foundation upon which the study is conducted. A systematic fuel

auto-ignition behavioural study, conducted using detailed chemical kinetics simulations, then builds on the literature review foundation and forms the yardstick to which the fuel auto-ignition models are later compared.

The study then focuses on an existing recently published empirical fuel auto-ignition model which is adapted and implemented into two thermodynamic engine models, formulated as part of the study. The experimental validation and research use of these models is summarised although the details of this are provided in the appendices.

Limitations in the use of the empirical model lead to the formulation of a new functional global fuel auto-ignition model. The formulation of this new functional global model is described in detail, drawing from insights provided by schematic kinetic descriptions in the literature, the previous auto-ignition behavioural study and critical evaluation of existing auto-ignition models. The mathematical implementation of the new functional global model is discussed with reference to software choices, thermo-chemical and kinetic calculation principles, and numerical solving strategies. The optimisation of the model parameters and performance evaluation of the new functional global model is presented using the results of detailed auto-ignition delay and temperature-time plots.

Results and findings of the study are then discussed and the attributes of the two modelling approaches are contrasted and evaluated before final conclusions and recommendations are given.

2. Literature review of HCCI

2.1. Introduction to the concept of HCCI

Homogeneous Charge Compression Ignition (HCCI) is a term used to describe an advanced form of internal combustion engine technology involving the induction (or subsequent creation) of a nominally homogeneous fuel-air mixture which is then ignited by compression alone, without any form of additional ignition system [2;3]. In many ways this engine concept is a hybrid between conventional spark ignition (SI) gasoline engines and compression ignition (CI) diesel engines. HCCI operation offers considerable efficiency benefits [4], but also brings significant implementation challenges, particularly in the area of combustion control [2;3].

HCCI terminology

HCCI has become a generic term for describing this mode of internal combustion engine operation where a pre-prepared mixture of fuel, air and residual combustion product gas is ignited by compression alone without the aid of sparkplugs, glow plugs or other ignition devices. The term HCCI was originally used with other terms such as Premixed Charge Compression Ignition (PCCI) to describe the use of early injection and mixture preparation ignited by compression, specifically in diesel engines. However, the term HCCI has evolved to include Controlled Auto-Ignition (CAI) and Active Radical (AR) combustion techniques (among other terms) used in specific reference to implementation in gasoline engines [2;3].

The term HCCI has actually become somewhat of a misnomer since developments of this combustion mode often include charge preparations that intentionally use stratification of air-fuel ratio, Exhaust Gas Recirculation (EGR) and temperature to help control heat release rates [5-12]. However, HCCI remains the generic term for this form of internal combustion engine operation [2;3].

2.2. Operational principles of HCCI

The propensity of the fuel to spontaneously auto-ignite under conditions of elevated pressure and temperature is known as the fuel's ignition quality [13;14]. Fuel ignition quality may be measured in a cetane engine or by measuring the "derived cetane number" using an Ignition Quality Tester (IQT^{TM}) constant volume combustion bomb [14]. The very critical mixture preparation for HCCI engine operation may be achieved using port and/or early direct fuel injection along with use of EGR [5;7;9]. EGR can be achieved by external cooled or un-cooled

linking of exhaust and inlet systems, as well as variable valve-train exhaust gas recompression or re-breathing strategies [15-17].

The compression ratio (CR) of the engine and the ignition quality of the fuel must be matched to result in combustion phasing approximately 10 crank angle degrees after Top-Dead-Centre (TDC) for optimal efficiency [2;8;18], minimising the need for torque output reducing inlet air heating [2]. The ignition quality of the fuel can also be varied by dual-fuelling with an online controlled blend of high and low ignition quality fuels [2;3]. Combustion phasing before TDC results in excessive compression work and very high heat release rates, while combustion phasing more than 15-20 degrees after TDC can result in partial or total misfire and the associated increase in hydrocarbon (HC) emissions [8;18]. HCCI engine and fuel design therefore requires a thorough understanding of fuel auto-ignition behaviour.

HCCI engines typically operate without throttling and load control is achieved through mixture adjustment and charge boosting. Since air-fuel ratio and boosting directly affect charge ignition quality (ignition delay), controls such as inlet air heating, EGR, variable CR and injection timing must be used to maintain appropriate combustion phasing across the engine load and speed ranges. In-cylinder pressure sensors are generally necessary for closed-loop control of combustion phasing using these parameters [2;3].

2.3. Benefits and challenges of HCCI

Benefits of HCCI

HCCI engine technology promises to combine the high efficiency of the compression ignition diesel engine with the low emissions of the spark ignition gasoline engine [2;3]. High compression ratio, rapid heat release and throttle-less operation allows high ideal cycle efficiencies, based on the Otto Cycle, to be approached. Lean-burn operation further contributes to high thermodynamic efficiency and also reduces peak temperatures, resulting in low oxides of nitrogen (NOx) emissions. Homogeneous, or near homogeneous fuel-air mixture preparation avoids fuel rich zones which are the cause of soot and smoke formation in a diesel engine [2;3].

Challenges of HCCI

HCCI technology has a number of significant challenges which can be divided into technical, cost, competition and marketing issues:

Technical challenges for HCCI are centred on combustion control. Current commercial engine technologies allow for direct control over the ignition timing (phasing) of the fuel, by either fuel

injection (diesel) or spark timing (gasoline) [13]. HCCI concepts rely on the auto-ignition characteristics of the fuel (ignition delay time) to achieve the desired heat release phasing required ensuring efficient and dependable operation. At best, only indirect control over ignition phasing is possible through adjustment of mixture properties such as temperature, pressure, fuel, oxygen and inerts, as well as the in-cylinder distribution thereof. Complex electronic control systems using in-cylinder pressure sensing and closed-loop feedback control are therefore required and have significant associated development and parts costs [15].

In broad terms, HCCI engine operation is limited by two factors. Firstly, due to the homogeneous nature of the mixture, the heat release occurs near-simultaneously throughout the combustion chamber, leading to very rapid heat release rates. This leads to objectionable noise and very high cylinder peak pressures with associated engine component stresses. This can limit HCCI mode operation to the lower load end of the engine map [15;16;19;20]. A second limitation is limited speed range, since optimal ignition delay time must be matched with the time-scales applicable to the engine operation [8;9;18]. This means that HCCI operation is again confined to a limited part of the engine speed range, outside of which combustion instabilities or complete misfire are possible. For operation in these regions the engine must revert to conventional spark or fuel injection controlled combustion modes.

Technical challenges for HCCI therefore include the development of engine hardware and closed-loop control systems that enable stable and optimised HCCI mode operation over as wide a speed-load range as possible, including typical speed-load transients and mode transitions to the base gasoline or diesel mode [2;3]. Understanding of the complex engine and fuel interactions affecting auto-ignition dynamics is a critical part of this challenge. Additional technical challenges exist in the area of exhaust gas after-treatment for HCCI emissions since conventional oxidation catalysts often cannot reach “light-off” temperatures under the lean burn operational conditions typical of HCCI engines at low load, where hydrocarbon and carbon monoxide emissions may be relatively high [2;3].

Cost challenges include the need to achieve HCCI operational benefits without disproportionate expenditure on development and engine hardware costs. While technical advances in modern engines have provided many of the features required for HCCI, such as direct and port fuel injection, cooled EGR, fully variable valve trains, super/turbo charging and complex electronic control units (ECUs), other hardware such as accurate in-cylinder pressure sensors will impose significant additional cost, as will the complex ECU programming required for HCCI mode implementation [3].

Competition challenges also exist, not only from ever improving diesel and gasoline engine power, efficiency and emissions performance, but also from emerging electric and hybrid electric vehicle technologies [3]. Cutting edge diesel technology promises significant emissions reductions through the use of higher pressure injection systems, piezo injectors and selective catalytic reduction (SCR) exhaust catalyst systems. Modern gasoline engines promise significant reductions in fuel consumption through the use of lean-burn high pressure direct fuel injection technologies. Electric and electric hybrid technologies promise zero-emission-at-vehicle performance, but are reliant on significant improvements in current battery technology [3].

Marketing challenges associated with the introduction of any new technology need to be addressed, especially if the technology is likely to carry a premium price tag, as is expected with HCCI, due to its significant hardware and control system complexities [3].

2.4. Dual-mode HCCI

While full time HCCI operation holds promise for full realisation of the benefits of this technology through simultaneous optimisation of engine and fuel design, the current speed and load limitations dictate that this avenue is unlikely to be commercially realised within the medium term [3]. Considering the tremendous benefits that HCCI promises, albeit confined to a limited part of the engine operating map, dual-mode HCCI operation is seen as a means to utilise HCCI benefits where achievable, reverting to conventional gasoline or diesel combustion in other parts of the engine map [11;12]. This approach necessitates the use of conventional fuels (gasoline or diesel) to allow for normal operation outside of the HCCI range and this concept has been demonstrated by various researchers and Original Equipment Manufacturers (OEMs) [11;12;15;21-30].

Unfortunately, the dual-mode approach does impair the optimisation of both the fuel formulation and engine design for HCCI performance, due to the constraints of the conventional engine operation mode. Dual-mode HCCI operation still, however, offers significant benefits to the diesel or gasoline engine to which it is applied. Gasoline-HCCI hybrid engines offer between 12 and 15% efficiency benefit over conventional gasoline engines while diesel-HCCI hybrids can offer up to 5% efficiency benefits with significant reductions in NOx and particulate emissions [2-4].

In spite of the compromises in engine and fuel optimisation for HCCI mode dictated by gasoline or diesel hybridisation with HCCI, this approach has many advantages:

- The technology can be introduced in a way that captures most of the advantages of HCCI since the current HCCI speed-load range covers all/most of standard driving cycles' ranges [15;16;19;20].
- While smooth and rapid mode transitions require significant development time, these have been successfully achieved in lab and vehicle prototypes and the backup of the standard engine mode offers a "safety net" for concerns regarding HCCI sensor reliability and durability [11;12;15].
- Given the current limitations in speed and load of HCCI operation, dual-mode roll-out of HCCI technology will showcase HCCI benefits in the market as well as offering the opportunity of progressive improvement of this technology.

If the technology progresses closer towards realisation of full time HCCI engines, the case for a dedicated HCCI fuel will be strengthened and the cost and logistical implications of this would have to be addressed.

2.5. Speed and load engine map coverage and emissions drive cycle results

Typical passenger vehicle applications of HCCI mode operation currently cover a speed range from approximately 700 – 3500rpm and a load range from zero to approximately 6bar Brake Mean Effective Pressure (BMEP) [2;3] although some laboratory HCCI engines have achieved high loads of up to 20bar BMEP using forced induction [26;31]. Drive cycle emissions data is scarce since only dual-mode HCCI engines with fully integrated mode switching systems are able to complete a drive cycle analysis and such engines are the proprietary property of OEM research laboratories.

2.6. Fuels for HCCI

HCCI is essentially a middle ground between conventional gasoline and diesel engine combustion modes and has consequently been studied from both sides, using both gasoline and diesel engines as the base engine for modification to HCCI mode. From a base engine hardware perspective diesel engines are in some ways better suited to HCCI modification, since they have higher (sometimes too high) CRs and are designed to withstand higher cylinder peak pressures [13]. Older gasoline engines perhaps have more suitable combustion chamber

geometries, since modern gasoline and diesel engines are designed for high turbulence in order to aid flame propagation and diffusion flame mixing [13;32]. While high turbulence in modern combustion chambers do not aid HCCI combustion and simply cause excessive convective heat transfer [13;32], modern gasoline engines make use of valuable variable valve-train hardware that can be effectively used for HCCI combustion control [17;20].

While gasoline has advantages in terms of volatility and associated ease of mixture preparation, its resistance to auto-ignition poses a significant challenge to HCCI operation with standard gasoline engine CRs. Diesel has ignition quality that is too high for typical diesel engine CRs and its low volatility also presents difficulties in terms of mixture preparation. Diesel also has a higher density and volumetric energy content than gasoline, resulting in lower volumetric fuel consumption for diesel fuelled HCCI engines. Although OEMs have developed both gasoline-HCCI and diesel-HCCI hybrid prototypes, it seems that the former is acknowledged to be the preferred roll-out method of HCCI technology [2;3].
The study of desirable fuel properties to enlarge the HCCI operating envelope has followed a mostly empirical approach where fuel properties, mostly ignition quality and cool flame heat release, were varied and the effects on combustion characteristics measured and/or modelled [2;3;33-35].

The development of “designer” fuels for both dual-mode and dedicated HCCI engines requires a fundamental understanding of the desired auto-ignition characteristics of the fuel and how those characteristics are affected by changes in in-cylinder conditions such as temperature, pressure, levels of residual combustion product gasses and oxygen concentration. Most importantly, the interaction between the chemical (auto-ignition) and physical properties of the charge mixture in relation to engine design needs to be rigorously understood [2;3].

Ignition quality:
Due to the nature of ignition in HCCI combustion, the ignition quality of the fuel is of critical importance. While wide varieties of ignition quality have been successfully used in HCCI engines, it is generally accepted that ideal HCCI ignition quality for dedicated HCCI engines, falls in the cetane range of 35 to 45 (approx. 70 to 50 RON respectively) [2;3;33-35].

Volatility:
Since the air-fuel mixture must be at least nominally vaporised and premixed, volatility is also of great importance. Fuels in the gasoline boiling range have therefore been targeted for HCCI in many cases [2;3;35]. However, higher density fuels provide better volumetric fuel economy and

use of early injection of relatively low cetane fuels in the diesel boiling range at very high injection pressures has been shown to produce sufficiently premixed charges [34].

Composition:

While early investigations concluded that fuel composition had negligible consequence for a given volatility and ignition quality, more recent findings have shown that composition is important to HCCI applications. Paraffinic fuels exhibit a low temperature heat release (cool flame) prior to the main (peroxide) heat release [33;36]. This behaviour is associated with a "negative temperature coefficient" (NTC) behaviour in the intermediate temperature region where ignition delay can be shortened by decreasing temperature – converse to conventional ignition delay behaviour. This obviously has significant impact on combustion phasing control system requirements where such 2-stage fuels are used [9;18;37]. Single stage fuels (exhibiting no NTC behaviour), such as certain aromatic, oxygenated and olefinic fuels, exhibit high octane sensitivity – the numerical difference between octane values obtained by the Research and Motor Octane tests. Gasoline fuels with "high RON and high sensitivity" have been indicated as particularly desirable for gasoline-HCCI hybrid applications [38]. Bio-derived oxygenates, ethers and natural gas have received significant attention for HCCI fuel applications [15;33;39;40].

2.7. Notable examples of HCCI implementation

OEM HCCI prototype vehicles:

Volkswagen is currently developing both gasoline-HCCI and diesel-HCCI hybrid vehicles. Their "Gasoline Compression Ignition" (GCI) engine runs on conventional gasoline while their "Combined Combustion System" (CCS) engine runs on "sunfuel" – a synthetic biodiesel. Press statements have indicated that both technologies will be in commercial production by 2015 [21].

General Motors is developing a gasoline-HCCI hybrid engine for two prototype vehicles – the Vauxhall (Opel) Vectra and the Saturn Aura. The vehicles have been developing well from their first test-drive introduction to the motoring press in September 2007. Notable improvements include seamless mode transitions and the achievement of idle in HCCI mode [11;12]. Press articles indicate that the vehicles will reach production in 2012.

Daimler is developing a gasoline-HCCI hybrid called the DiesOtto engine for their Mercedes F700. The prototype engine has been introduced to the motoring press who were allowed to test drive it in an S-class sedan and were later driven around a test track in the prototype F700. Press statements indicate that the engine will reach production in 2012 [22-24].

Other OEMs such as *Nissan, Caterpillar, Volvo and Scania* are also developing HCCI hybrid engines [25-30] . They are contributing to the growth of this technology through collaborative research projects and publications, but have not yet demonstrated their engines in prototype vehicles.

Research achievements:

While most of the advances in HCCI technology achieved in academic institutions and research organisations have already been consolidated and implemented in the above mentioned OEM prototypes, five additional aspects bear mention:

- High load HCCI operation has been achieved up to 16-17bar IMEP on gasoline at Shell Global solutions [31] and 20bar BMEP on diesel at Caterpillar Inc. [26].
- Dual-fuel HCCI with closed loop combustion phasing control has been demonstrated at the Lund Institute of Technology, using iso-octane and n-heptane [41].
- Very wide ranges of fuel properties have been investigated in HCCI engines, including PRF blends, aromatic blends, olefinic blends, oxygenate and ether blends, gaseous fuels, kerosenes and wide varieties of full boiling range gasolines, diesels and blends of the two [2;3;33-35].
- Extremely rigorous experimental and theoretical research on HCCI combustion control methods, including combustion phasing retard, EGR, thermal and mixture stratification has been conducted at Sandia National Laboratories [6-10;18;42]
- Valuable chemical kinetic mechanisms and CFD HCCI modelling strategies have been investigated by researchers at Lawrence Livermore National Laboratory [43-48].

3. Literature review of fuel auto-ignition

Combustion has undoubtedly been studied at least informally since its very first discovery. Modern numerical combustion studies have been divided into a number of methodologies generally related to the level of detail required and associated computational expense afforded. Broad classifications of these levels of complexity are common in the literature, although there are numerous discrepancies regarding their formal definitions. Zheng et al. [49] defined the commonly used classifications as shown in Table 3.1 below:

Table 3.1: Categories of chemical kinetic models (taken directly from [49])

Category	Description	Species	Reactions
Detailed	the latest “comprehensive” reaction set	100’s	1000’s
Lumped	uses a lumped description for larger species	100’s	1000’s
Reduced	a subset of the detailed model	10’s	10’s- 100’s
Skeletal	employs class chemistry and lumping concepts	10’s	10’s
Global	utilizes global reactions to minimize reaction set	<10	<10

It may appear from Table 3.1 above that there is overlap between the categories, particularly in the characteristics of the lumped, reduced and skeletal models. An excellent and comprehensive review of lumped, reduced, skeletal and global models, their development and experimental validation, has been provided by Griffiths [50]. This review notes that skeletal and global models have mostly been developed from “building up” the model according to representative classes of compounds and schematics of formal kinetic structures, rather than the numerous and complex mathematical detailed kinetic mechanism reduction strategies which are themselves described in fair detail. Reduced and skeletal models that are applied over a wide range of hydrocarbon structures have been observed [50] as being associated with greater empiricism than more complex versions of single component reduced models. An additional category of fuel auto-ignition model is the empirical model. This sixth category is not included in table 1 above because these models are not true rate based kinetic models. Empirical models usually take on an Arrhenius form and are calculated using the “knock integral method” first proposed by Livengood and Wu [51] in their seminal paper, but only so termed in later developments of the method [52;53].

While discussion of the intricacies of detailed fuel auto-ignition is beyond the scope of this work, schematics of hydrocarbon reaction kinetics were considered. Such schematics are by nature gross simplifications of the detailed processes involved. However, these schematics provide

some insight into the dominant chemical pathways and resulting kinetic behaviour. Schematics and summaries of hydrocarbon reaction schemes are widely available in the literature [1;2;36;37;47;49;50;54;55]. These schematics generally follow similar trends although there are a number of variations. For the purposes of this study, the reactions schematic for alkane fuels presented by Zhao et al. [2] was used as a reference for auto-ignition model structures, since it shows good general agreement with other schematics in the literature and was written in the context of HCCI combustion studies. The chemistry in this schematic is divided into three broad temperature ranges given at a reference pressure of 1atm. The schematic is presented in [2] as follows:

Low temperature chemistry (<600K at 1atm)

1.	RH + O_2 => R• + HO_2•	(fuel hydrogen abstraction by oxygen to form alkyl and hydroperoxy radicals)
2.	R• + O_2 => olefin + HO_2•	(2^{nd} hydrogen abstraction by oxygen to form conjugate olefin & hydroperoxy radical – slow at low temperatures)
3.	R• + O_2 <=> RO_2•	(oxygen addition to form alkylperoxy radical – temperature and pressure sensitive equilibrium reaction: forward rate is fast for all temperatures, reverse reaction is fast only at high temperatures)
4.	RO_2• => •ROOH	(internal isomerisation to form hydroperoxyalkyl radical)
5.	•ROOH => CARBONYL + R'• + OH•	(decomposition to lighter alkene or cyclic ether and hydroxyl radical)
6.	•ROOH + O_2 <=> •OOROOH	(oxygen addition to form hydroperoxyalkylperoxyl radical - small heat release)
7.	•OOROOH => HOOROOH	(internal hydrogen abstraction of hydroperoxyalkylperoxyl to form alkylhydroperoxide)
8.	HOOROOH => RCHO + R'O + 2 OH•	(decomposition to form aldehyde and 2 hydroxyl radicals - small heat release)

Intermediate temperature chemistry (650 - 700K at 1atm)

9. $RH + HO_2\bullet <=> R\bullet + H_2O_2$ (fuel hydrogen abstraction by hydroperoxy radicals to form hydrogen peroxide – forward rate is pressure dependent)
10. $H_2O_2 + M => 2\ OH\bullet + M$ (decomposition of hydrogen peroxide to form hydroxyl radicals – reaction rate is strongly dependent on peroxide concentration)

High temperature chemistry (>800 K at 1atm)

11. $RH + OH\bullet => R'\bullet + R''\bullet + H_2O$ (fuel pyrolysis at high temperature– small heat release)
12. $R'\bullet + R''\bullet + H_2O => CO + H_2O$ (hydroxyl radicals reacting to form carbon monoxide – small heat release)
13. $CO + H_2O => CO_2 + heat$ (carbon monoxide reacts to form carbon dioxide - large heat release)

Seven additional reactions are included in this high temperature region. These involve various chain branching reactions involving hydrogen, hydroxyl, oxygen, hydroperoxy and water species. These reactions are stated [2] as being extremely reactive and therefore occurring at very high reaction rates. These reaction details were therefore considered outside of the scope of this study.

It should be noted that while HCCI combustion typically occurs within relatively narrow ranges of time and temperature, an auto-ignition model aimed at HCCI applications must be valid over the entire condition history experienced by the reactants and products in the engine. This means that the model must be applicable from nominally ambient pressure and temperature, through to the extreme pressures and temperatures experienced under high load knocking HCCI operation. The model should also be valid for wider ranges of fuel equivalence ratio and combustion product dilution than normal HCCI operation so that such abnormal combustion can be modeled. The extremely wide range of reaction rates and ignition delay timescales associated with this wide range of conditions is therefore important in spite of the relatively narrow range of time scales associated with engine operation.

3.1. Review of experimental auto-ignition studies

There is a wide range of experimental auto-ignition data available in the literature. These studies include the testing of numerous fuels, from single component fuels, through blends to full boiling range fuels. A valuable summary of the experimental data (available prior to 1995) from a wide variety of auto-ignition test devices has been provided in [50]. These devices include rapid compression machines (RCMs), shock tubes, constant volume vessels, flow tubes, jet-stirred reactors, mechanically stirred flow reactors, flat flame burners, motored engines and variations of these devices.

Further experimental auto-ignition studies have been conducted using shock tubes [56;57] and rapid compression machines [37;47;58;59]. One of the primary reasons for the wide variety in auto-ignition testing devices is the fact that all the available devices have limitations in the kinds of tests that can be done and the range of temperature and pressure at which the fuel can be tested. Detailed descriptions of the challenge of obtaining quality experimental fuel auto-ignition data is provided by [50] and alluded to by [57] in the detailed and complex descriptions of their experimental rigour.

The challenge of obtaining reliable experimental data in a given auto-ignition testing device is intensified when different devices of similar operating principle are compared and give inconsistent results. This challenge becomes even more onerous when devices of different natures are considered. This is a significant problem due to the fact that a single fuel generally requires the use of two or more devices in order to obtain auto-ignition characterisation over a wide range of operating parameters. Correlation between data in areas of overlapping range is often poor and leads to particular challenges in cases where fuels requiring quantitative comparison have not been or cannot be tested in the same device. This field therefore remains an oyster of opportunity for valuable quality contributions of skilled experimentalists as indicated in [50].

3.2. Review of detailed chemical kinetics mechanisms

Detailed chemical kinetic mechanisms for hydrocarbon oxidation have historically sought to provide the modeller with the complete set of chemical reaction permutations for a given overall reaction, including all participating and non participating molecule and radical species, as well as calculated or estimated thermo-chemical and reaction rate parameters. As chemical kinetic models have incorporated progressively larger molecules, these mechanisms have “exploded” in size and detailed models incorporating many thousands of reactions and over a thousand

species are now available [45]. An extensive review of hydrocarbon detailed kinetic modelling has been provided by [60].

The study of fuel auto-ignition characteristics conducted for this project (discussed in chapter 3) was started originally using the detailed mechanism for Iso-octane provided by Curran et al. [44]. This mechanism was an extension of a previously published mechanism for n-heptane [43] and is thus able to simulate PRF blends as well as smaller molecules such as methanol and butane. The mechanism consists of 3600 reactions and 860 chemical species and has been validated across a wide range of temperature (550 - 1700K), pressure (1 – 42 atm), equivalence ratio (0.3 – 1.5) and inert dilution (70 – 99%) using a wide variety of experimental devices. However, recently published chemical kinetic mechanisms have achieved the long pursued goal [46] of modelling quaternary surrogate gasoline blends consisting of iso-octane, n-heptane, toluene and isomers of hexene [45;61]. Other useful fuel components such as methanol, ethanol and butane are also included in these mechanisms.

Due to the extensive validation used in the development of detailed kinetic mechanisms [43-45;61] and the challenges of obtaining agreement from experimental auto-ignition data sources, researchers often use the predictions of detailed kinetic models to validate the performance of their skeletal models [62], global models [63-65] and empirical ignition delay models [1;53;54]. It should be noted that a reduced model should only be validated against the detailed model from which it is derived as done in [66]. While comparison of reduced models to experimental data may be worthwhile, any improvement in agreement over its detailed mechanism actually represents a discrepancy in performance. While validating a model with another model may be regards as poor scientific practise in other fields, the practise in this field is generally accepted and even encouraged [50].

In order to gain an appreciation for the level of agreement between these recent detailed models and the experimental data upon which they are validated, the ignition delay curves for n-heptane and its experimental validation data presented in [45], were scanned and digitised for quantitative comparison with its earlier version [44]. Detailed kinetic simulations using these mechanisms (kindly supplied by the authors of [44;45]) were also conducted and included in this comparative analysis. The ignition delay curves for stoichiometric n-heptane-air mixtures at 20bar are shown in Figure 3.1 below. The mean absolute percentage errors as defined in Equation 3.1 are indicated in Table 3.2.

$$\text{mean abs \% error} = \frac{\sum_{i=1}^{n} \frac{\text{abs}\left(x_{\text{ref,i}} - x_i\right)}{x_{\text{ref,i}}}}{n}$$

Equation 3.1: Definition of the mean absolute percentage error used as an indicator of model agreement in this study

Table 3.2: Comparison of average mean percentage errors between detailed models and shock tube experimental data for n-heptane

mean absolute % error between the digitised Mehl mechanism ID prediction and experiments at 20 bar	10.2%
mean absolute % error between the digitised Mehl mechanism ID prediction and experiments across all eight pressures presented in [45].	24.3%
mean absolute % error between the simulated Mehl mechanism ID prediction and experiments at 20 bar	13.5%
mean absolute % error between the simulated Curran mechanism ID prediction and experiments at 20 bar	42.3%
mean absolute % error between simulated Curran mechanism ID prediction and simulated Mehl mechanism ID prediction	37.8%

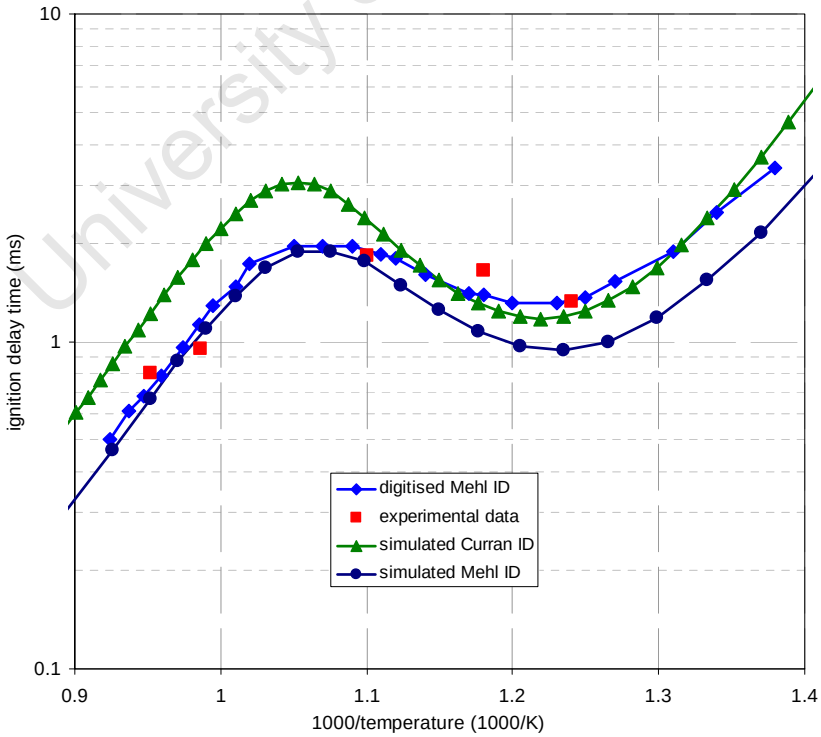

Figure 3.1: Comparison of detailed kinetic model performances with experimental shock tube data for stoichiometric n-heptane-air mixtures at P_i=20 bar. The Mehl mechanism and experimental data are presented in [45], while the Curran model is presented in [44]and [43].

It is worth noting that the agreement between the Mehl mechanism and the experimental data at 20bar was more than twice as good as that for the other seven pressure ranges presented in the paper. It is also concerning that the results presented in the paper could not be replicated with the mechanism provided by the authors. However, perhaps the most concerning finding of this comparison was the relatively poor agreement between these two detailed mechanisms, especially in view of their use as validation for other models.

It is perhaps true to say that fuel auto-ignition behaviour is not an easy phenomenon to measure or model accurately, even with the most complex equipment and detailed kinetics models. Detailed models remain, however, the best currently available tool for fuel auto-ignition prediction.

In view of the improved scope of the Mehl mechanism and its apparent accuracy improvement over its predecessor, the study of fuel auto-ignition characteristics (discussed in chapter 4) was repeated using the mechanism developed by Mehl et al. [45] (for consistency) and extended to other fuels included in this mechanism.

3.3. Review of reduced chemical kinetics mechanisms

It is generally agreed that many of the possible reactions making up a detailed kinetics mechanism have insignificant influence on the function of the mechanism or its numerical predictions [46;50] and are included merely for completeness. Scope therefore exists to reduce detailed mechanisms to the subset of reactions that play an active role in the function of the mechanism, especially where the range of conditions is narrowed to address a particular application. Various techniques have been developed for this purpose, including sensitivity, reaction lumping, reaction flow, extended lifetime analysis, quasi-steady-state analysis (QSSA), “brute force”, Morris-one-at-a-time and Monte-Carlo methods [50;67]. Recent examples of such reduction studies are provided by [67-70].

Reduced models suffer a particular difficulty in that they generally seek to remain true to the detailed model from which they are drawn in terms of rate parameter values. As these models are reduced in size they begin to deviate from the performance of the detailed versions. In most cases [67;69;70] the mechanisms are reduced to some compromise between computational efficiency and prediction accuracy. However, other researchers are prepared to adjust the reduced mechanism parameters in order to allow further reduction while maintaining reasonable agreement with experimental or detailed simulation data [68]. The justification for modification of rate parameters from the detailed models is generally the assertion that the values of these

parameters are not certain in the detailed mechanisms [68;70]. In addition, [67] noted that uncertainty in the thermo-chemical parameters of a kinetic mechanism can have an even greater effect in some cases than uncertainty in the reaction rate parameters. It has also been noted [71] that reduction from detailed mechanisms often does not result in sufficiently reduced models and so a “bottom up” building process of reduced models from skeletal models is sometimes preferred.

3.4. Review of skeletal auto-ignition models

It is the difficulty discussed in the paragraph above which has lead to the formulation of skeletal auto-ignition models. It has been noted by [70] that skeletal mechanisms afford much better opportunity for parameter solving and uncertainty studies than reduced mechanisms due to their significantly reduced complexity and chemistry class lumping approach.

Researchers at the Shell Thornton Research Centre developed a generalised skeletal model consisting of 11 reactions for all hydrocarbon fuels [72]. The authors state that: “The value of these (skeletal) models lies in the demonstration that the phenomenological complexity of hydrocarbon combustion systems is not necessarily a result of their chemical complexity”. The development of the model entailed behavioural examination of the characteristics of two-stage ignition, including cool flame ignition timing and heat release, as well as overall ignition delay for iso-octane. Experimental data from a rapid compression machine was used for validation. The effects of temperature were well simulated, but effects of pressure, equivalence ratio and dilution were less successful.

This model was later developed [73] to comprise of 8 reactions and 7 species and this model became known as the “Shell model”. While this original Shell model may be better classified as a global auto-ignition model, it is included in this section because it formed the basis for most of the later developed skeletal models discussed below. Although automated parameter optimisation was attempted in [73], it was found that significant “insight and judgement” was needed in order to make appropriate changes to model parameters and the optimisation of rate parameters was therefore done manually.

As a further development to the Shell model’s already high computational efficiency, Sazhin et al. [74] developed a mathematical method for reducing its computational expense. This procedure did not alter the structure or functionality of the model, but rather the manner in which the differential equations were computed. The process essentially involved a substitution of the time independent variable with “fuel depletion” as the new independent variable. All other

variables including temperature were then expressed using the Shell model formulation in terms of the new independent variable. This enabled various algebraic and analytical solving methods to be used and allowed decoupling of the differential equations such that the burden of numerical integration was significantly reduced with almost imperceptible differences in output values. This technique may hold promise for application to other more recently developed global fuel auto-ignition models and may be valuable for the implementation of these models into engine thermodynamic and CFD models.

Cox and Cole [75] extended the Shell model [73] for auto-ignition of hydrocarbon fuels in general, but focussing on PRF90. The extended model consisted of 15 generalised reactions involving 10 species and incorporated a more detailed description of the chain propagation of alkylperoxy radical isomerisation and oxidation in that the 2nd oxygen addition and internal hydrogen abstraction were not lumped together with the first sequence. This allowed the model to predict a “sharp” (suddenly initiated) 2nd stage ignition as the hydroperoxide branching agent formed from the RO_2 at higher temperatures post cool flame accumulated to promote 2nd stage ignition.

Hu and Keck [76] further developed the work of Cox and Cole [75] and formulated a reduced mechanism consisting of 18 reactions and 13 active species. The fitting of parameters and comparison to experimental data was done using data from a spherical combustion bomb (with central laminar flame ignition) and a RCM. A further reduced model consisting of the first 10 reactions of their scheme was discussed and appeared to agree fairly well with the experimental data, even in the absence of additional tuning. Consideration of the model in relation to various alkane fuels indicated that only the first H abstraction equilibrium reaction constant was affected by fuel structure. Unfortunately, the level of experimental agreement of these fuels was not presented.

Li et al. [36] further developed the Hu and Keck reduced AI model, adding an additional 11 reactions and 5 species to obtain a better agreement with total heat released. The model performance was compared and fitted to experimental results from a motored engine using partial combustion of PRF 63 fuel. The additional reactions catered for oxidation of aldehydes, olefins, carbonyls as well as the formation of CO and its oxidation to carbon trioxide (CO_3) to reduce overall heat release. The model rate parameters were stated as being largely empirical fits and deviating from the calculated or estimated detailed kinetic reaction values in an “arbitrary”, but “not unrealistic” manner. This model was developed further in [71] by adding a further 11 reactions and 7 species to form a model consisting of 29 reactions and 20 active species. The extended model was capable of predicting PRF ID and heat release rate with

improved accuracy. The extended model was structured to result in oxidation of all species, i.e. all reactions paths ultimately produced product species. In spite of having increased the size of their model, the authors stated that they were confident that a significantly reduced model could represent the important kinetic features adequately. Unfortunately, such a significantly reduced model was neither suggested nor demonstrated.

The 29 reaction model developed in [71] was tested with an HCCI engine model in the prediction of heat release in the engine cylinder [77]. Unfortunately the experimental validation using engine cylinder pressure traces was sparse. This model was further extended by Zheng et al. [78] by incorporating the high temperature reactions from the Griffiths unified model [68]. The model was aimed at HCCI applications and consisted of 69 reactions and 45 active species. The model was used for some HCCI parametric studies, but these were of little value since they indicated effects of parameters such as inlet temperature and equivalence ratio on indicated efficiency without maintaining constant combustion phasing - a dominant factor in determining efficiency in HCCI engines [8;18].

A versatile skeletal mechanism was recently developed by Machrafi et al. [62] for the gasoline and diesel surrogate blend components: iso-octane, n-heptane and toluene. The mechanism was developed by merging 3 reduced mechanisms of the respective pure components and incorporating some additional simplifications (such as removing details of the extremely high temperature kinetics) to result in the surrogate mechanism comprising 62 reactions and 49 species. The mechanism was validated against detailed mechanisms in a zero dimensional kinetic engine code as well as comparison with shock tube, RCM and real engine data. General agreement of ignition delay times were shown across wide ranges of temperature, pressure and equivalence ratio. Since no temperature-time plots or predictions of cool-flame dynamics were presented, it is assumed that the model does not predict cool flame behaviour accurately.

3.5. Review of global auto-ignition models

Müller et al. [63] developed a 4-step (5 reactions in total) skeletal model to describe n-heptane auto-ignition. The model used 2 reactions for the high temperature chemistry and two reactions for the low temperature chemistry with the first LT reaction being reversible:

1) $F \rightarrow X$
2) $X + 11\ O_2 \rightarrow P$
3) $F + 2\ O_2 <=> I$
4) $I + 9\ O_2 \rightarrow P$

This model produced reasonable agreement to experiments for such a simple model and obtained the characteristic “S” shaped ignition delay vs. temperature behaviour. The model could not, however, obtain true NTC behaviour (increasing ignition delay for increasing temperature) due to the lack of chain branching species and thermal dependency of the model, and has attracted criticism regarding this weakness [50;64]. Unfortunately, no attempt was made to compare or validate the temperature-time histories predicted by the model.

Schreiber et al. [64] developed a 5-step (6 reactions in total) mechanism for PRF blends in an attempt to resolve the above mentioned shortcomings of [63]. The model is shown below:

1) $F \rightarrow X$
2) $X + 12.5\ (11)\ O_2 \rightarrow P$
3) $F + 2\ O_2 <=> I$
4) $I \rightarrow 2\ Y$
5) $Y + 0.5\ F + 11.5\ (10)\ O_2 \rightarrow P$

The model parameters were fitted to detailed chemical kinetic simulations and also compared with limited shock tube and RCM data. The model used the reversible reaction and the chain branching species Y to produce NTC behaviour, resulting in improved accuracy of ignition delay prediction. However, the temperature-time traces revealed a lack of accuracy in the cool-flame heat release timing, shape and magnitude predictions. The model also defied Hess’ law (the heat release of the HT path was higher than that of the LT path) in spite of specifically mentioning this requirement. An additional problem was that the heat releasing reaction 5 was not dependent on the reactant fuel species, thereby allowing the reaction to continue after the fuel was depleted.

Zheng et al. [49] developed an improved global mechanism for PRF mixtures. The model used 7-step scheme (nine reactions in total) and included the reversible formation and dissociation of CO and CO_2 in the high temperature chemistry. The model is shown below:

1) $F + 7.5\ O_2 \rightarrow 8\ H_2O + 7\ CO$
2) $CO + 0.5\ O_2 <=> CO_2$
3) $F + 2\ O_2 <=> I_1$
4) $I_1 \rightarrow 2\ Y$
5) $Y + 0.5\ F + 6.5\ O_2 \rightarrow 8\ H_2O + 7\ CO$
6) $I_1 \rightarrow I_2$
7) $I_2 \rightarrow 2\ Y$

Experimental validation across different PRF blends was not given and claimed validity for model sensitivity to the effects of pressure and air-fuel ratio was weakly presented. Prediction of overall ID was reasonably good for the results shown. However, in spite of cool flame heat release prediction being a primary aim of the study, the authors admitted that "… the model does not predict the discrete temperature and heat release jump that was observed experimentally."

Bourdon et al. [65] developed the 5-step scheme proposed by Schreiber [64]. Some valuable modifications were made to the original model, such as compliance to Hess' Law and inclusion of fuel concentration dependence in the fifth reaction. The model optimisation was done using a genetic algorithm, but the fitness function was based purely on over-all ignition delay, without inclusion of cool-flame heat release dynamics. The model was then incorporated into a 3D CFD code (FIREV8) to simulate HCCI combustion of n-heptane. Limitation of conditions was done by assuming that HCCI either uses air or exhaust products for dilution and not a combination of the two. The model showed reasonable agreement with the detailed kinetics on overall ignition delay although understandably (due to the fitness function definition) it showed poor cool-flame dynamics agreement. Incorporation into the 3D CFD engine model used de-coupling of the flow and kinetics solver to eliminate differential equation stiffness problems and enable robust time stepping, with run times of around 5 hours on a standard desktop computer. This therefore indicated that global auto-ignition models could be incorporated into 3D CFD HCCI engine models while still achieving reasonable run times.

3.6. Review of empirical auto-ignition models

In 1955 Livengood & Wu [51] conducted an investigation into fuel auto-ignition delay times in rapid compression machines and engines for the purpose of better understanding SI engine knock. Using assumptions of constant reaction rate under conditions of constant pressure and temperature, they developed a simple empirical approach for the calculation of ignition delay where the Arrhenius delay expression was integrated over the pressure-temperature time history experienced by the fuel-air mixture. This later became known as the Knock-Integral approach to ignition delay prediction [52;53]. The approach relied heavily on the assumption of intermediate reaction species reaching a critical concentration which was independent of temperature and pressure. Although this independence is unlikely, it was shown that the model worked well for single stage ignition prediction. Livengood and Wu acknowledged that 2-stage ignition and deflagration reactions would not be well described by this model and a double ignition integral approach was suggested for the former case [51]. The form of the ignition delay equation was slightly unusual in the location of the pressure term. This may have been a

misprint and has been revised to a pre-exponential term in most later works [1;14;79;80], with the notable exceptions of [52;53]

Douaud and Eyzat [79] developed a four-octane-number method for quantifying model parameters and predicting knock behaviour in conventional engines. The octane tests included the standard RON and MON tests as well as modified versions of these tests in order to solve the A, n and B coefficients of the single Arrhenius expression given in Equation 3.2 below, and provide an estimate of the model error. Basic estimation of real octane requirements in conventional engines was demonstrated, although the single Arrhenius expression must effectively plot a straight line through the "S" ID curve of 2-stage ignition fuels and therefore lacks accuracy for wider application.

$$\tau = A\, p^{n} e^{\frac{B}{T}}$$

Equation 3.2: The conventional single Arrhenius ignition delay expression used in [79].

Swan et al. [53] developed a single Arrhenius knock-integral-method model for the prediction of auto-ignition timing of PRF mixtures in an HCCI engine. The model was set up to use measurable engine parameters such the cylinder temperature and pressure at BDC and equivalence ratio, Polytropic compression laws were then used to model pressure and temperature histories for the integration of the auto-ignition model . Correlation with experiments and a more detailed thermodynamic-kinetic model did not show very good agreement. This is perhaps because the cool-flame heat release invalidates the polytropic compression assumption used in the model.

Shahbakhti et al. [52] extended the single Arrhenius form knock-integral auto-ignition model [53] for predicting real-time HCCI engine combustion phasing. The model was extended to include EGR and equivalence ratio, but due to its single Arrhenius nature, it was stated to only be configurable to predict either cool flame or main heat release. In spite of claimed accuracy for PRF (NTC) fuels, no ability to model NTC behaviour was included in the model formulation and the ability of the model to predict main ignition timing for 2-stage fuels is therefore questionable.

Yates et al. [14] developed a 3-part Arrhenius auto-ignition model capable of good agreement to the ignition delay times of NTC fuels. The model performance was based on experiments using an Ignition Quality Tester (IQT^{TM}) at different pressures and temperatures in order to characterise fuel auto-ignition. This work was extended [54;80] using the vehicle knock limited spark advance data, RON and MON test data and detailed chemical kinetics simulations of a

variety of fuels in order to calculate their model parameters. This model could be used with the "knock integral method" but did not predict cool-flame dynamics.

Yates and Viljoen [1] subsequently developed an Arrhenius empirical model for predicting the cool-flame timing, cool flame temperature rise and overall auto-ignition delays of PRF and methanol blends. The model was calibrated to fit a wide range of pressures, temperatures and fuel equivalence ratios, but did not include inert or active radical dilatants. The model's auto-ignition prediction was applied by using the "knock integral method" to RON and MON experimental data and good correlation was shown.

3.7. Application of auto-ignition models in HCCI engine models

Apart from already mentioned examples of the application of auto-ignition models to the study of HCCI engines, the following examples bear mention:

Flowers et al. [48] modelled HCCI combustion using a single zone reduced kinetics Hydrodynamics Chemistry and Transport model. This formulation modelled the engine as a homogeneous continuously stirred reactor with volume varied according to a crank-slider relationship. Trends in results were compared with experimental results obtained from a CFR engine modified to run in HCCI mode on propane and a 15% dimethyl-ether in methane blend. Multi-zone modelling techniques have also been shown to be an effective approach for combining engine thermodynamic models with chemical kinetic models [81;82].

Zheng et al. [83] used their previously developed [78] skeletal model (69 reactions and 45 active species) in an attempt to explain various aspects of abnormal HCCI combustion, focussing on extremely late cycle auto-ignition and post exhaust auto-ignition. These phenomena were unstable and repeatable only in random (skip-fire) fashion. The authors attempted to explain post compression and expansion auto-ignition by hypothesising that under conditions of high EGR, reactive radicals could be formed during compression but only reacted to produce heat long after TDC in spite of the rapidly dropping temperatures during the expansion stroke. These late ignitions were not attainable experimentally using synthetic EGR, suggesting that the partially reacted fuel radicals may have been critical in achieving these late ignitions. Similar findings have been described in the experimental work of [7]. The authors [83] found this phenomena surprising, since, according to their model, the activation energy required for final decomposition stages of chain branching required higher temperatures than were likely at the initiation of these very late ignitions. This meant that the phenomena could not be replicated with the current skeletal models and indicated perhaps that additional low temperature pathways existed for the liberation of heat. Since internal EGR retained heat and seemed to add

additional reactivity through chemical means, internal EGR was suggested to enhance low load HCCI stability and enable easier SI-HCCI transitions. It was further proposed that high internal EGR may also enhance low load SI flame propagation and combustion stability.

Machrafi et al. [66] developed a semi-reduced (210 reactions) and a reduced (29 reactions) mechanism for auto-ignition of iso-octane. The reduced mechanism and the Chalmers mechanism were put into an adiabatic Chemkin thermo-kinetic engine simulation and compared with Co-operative Fuels Research (CFR) HCCI engine experiments. Agreement appeared reasonable although the method of comparison was poorly presented and ill defined:

- The paper discusses engine inlet temperatures up to 1100K – far removed from typical inlet temperatures.
- Expression of ignition delays in crank angle degrees – inappropriate due to the changing pressure and temperature conditions during compression.

Londleni et al. [84] used the 3-part Arrhenius auto-ignition model form [80] in conjunction with a discrete implicit engine model to model the HCCI combustion characteristics of a Ricardo E6 engine. Model results were compared with experimental tests for n-heptane and methanol. While the methanol case showed reasonable agreement, the n-heptane results were poor due to the fact that the auto-ignition model [80] did not predict 2-stage heat release.

4. Auto-ignition behavioural study

4.1. Introduction to the auto-ignition behavioural study

In order to model fuel auto-ignition in an HCCI engine one must have a thorough understanding of the manner in which different fuels behave under conditions of auto-ignition and how these behaviours are influenced by the experimental conditions. This understanding is crucial in selecting a suitable auto-ignition model for use in HCCI engine modelling and is even more important in the formulation of a new auto-ignition model.

This understanding was pursued through a review of open literature as discussed in chapter 2, with particular attention being paid to experimental studies [37;47;56-59;85]. In addition, a total of over 2200 detailed chemical kinetic simulations were run for iso-octane, n-heptane, 1-hexene, toluene, methanol and a quaternary gasoline surrogate defined in [45], consisting of iso-octane, toluene, hexene and n-heptane in the ratio 44/30/18/8% by moles. These simulations were run using Chemkin Collection™ software, Release 3.7 (Reaction Design, Inc.) as perfectly stirred, constant volume reactor simulations using the detailed mechanism from [45]. The simulations covered a wide range of experimental conditions of temperature, pressure, fuel equivalence ratio and inert exhaust product dilution. An example of the auto-ignition characteristics of different fuels is given in Figure 4.1 below. More detailed and comprehensive data is presented in Appendix A and this simulation data formed the data base used for the fitting and accuracy assessment of the new functional global auto-ignition model.

For the purpose of this study, the following definitions were used:

- The cool flame ignition delay (CFID) was defined as the elapsed time corresponding to the first peak in the derivative of temperature w.r.t. time for a fuel exhibiting a two-stage heat release.
- The overall ignition delay (ID) was defined as the elapsed time corresponding to the final peak in the derivative of temperature w.r.t. time for a given fuel.
- The cool flame ceiling temperature (CFCT) was defined as the temperature at the time halfway between the cool flame ignition delay and the overall ignition delay.
- The post cool flame ignition delay (ID – CFID) was defined as the elapsed time between the cool flame event and the main auto-ignition event.

Figure 4.1 below illustrates the marked differences that exist between different fuels, both in terms of ignition quality and their characteristic response to temperature. In this figure label (and

subsequent labels) P refers to the constant pressure value of the simulation, Phi refers to the fuel-air equivalence ratio and R refers to the mass percentage of reaction product or exhaust residual dilution included in the starting air-fuel mixture. Some fuels, such as toluene and methanol are shown to exhibit straight-line-Arrhenius ignition delay behaviour. Other fuels, such as iso-octane, n-heptane, 1-hexene and the gasoline surrogate blend are shown to exhibit Negative Temperature Coefficient (NTC) behaviour in an intermediate range of temperatures.

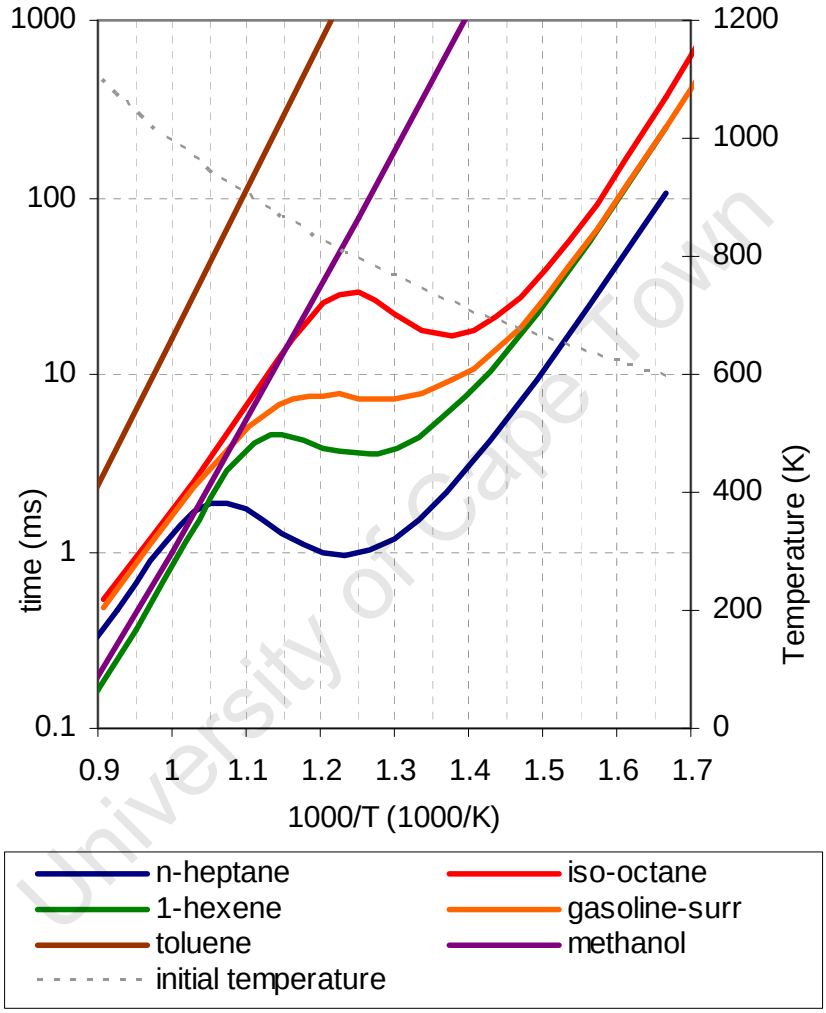

Figure 4.1: A comparison of auto-ignition delay times for different fuels; P_i=20bar; Phi=1; R=0%

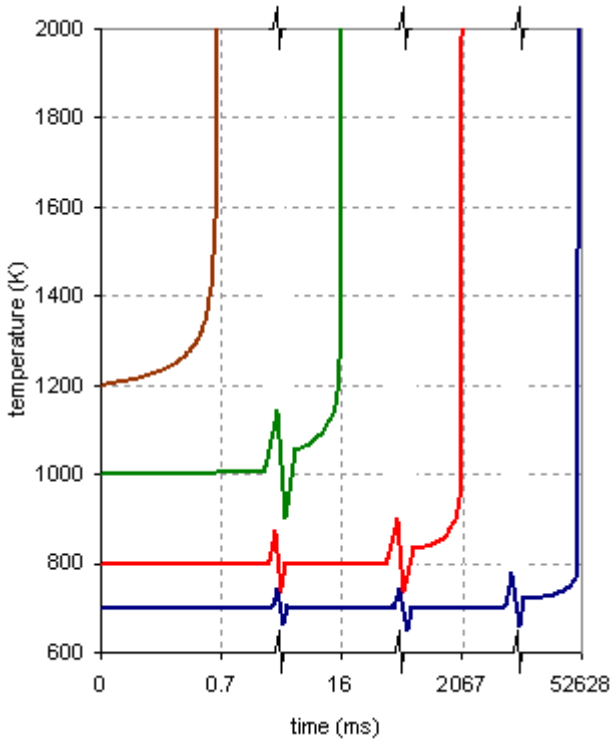

Figure 4.2: Temperature-time profiles for toluene at P_i=20bar, phi=1.0, R=0%

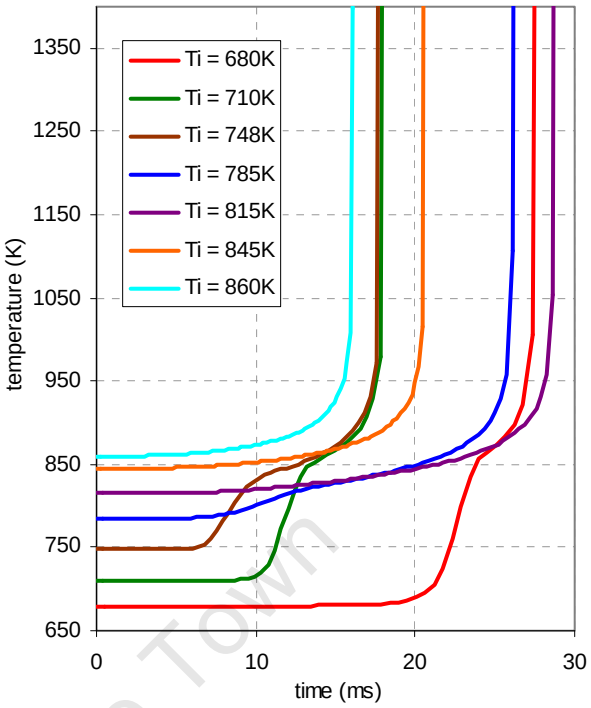

Figure 4.3: Temperature-time profiles for iso-octane at P_i=20bar, phi=1.0, R=0%

4.2. Single and two-stage auto-ignition characteristics

As an example of a straight-line-Arrhenius fuel, a series of temperature-time curves are shown for toluene in Figure 4.2 above. Toluene was chosen due to its relevance for surrogate fuel blending. As an example of an NTC fuel, a series of temperature-time curves are shown for iso-octane in Figure 4.3 above.

From Figure 4.2 above, it may be observed that straight-line-Arrhenius fuels exhibit a delay period followed by a single, full heat release. These fuels are therefore known as “single stage” fuels. From Figure 4.3 above, it is easily observed that for NTC fuels, some of the temperature-time profiles exhibit a single stage heat release, while others exhibit a preliminary minor heat release and a second delay period prior to the main heat release. These fuels are therefore known as “two-stage” fuels. The preliminary minor heat release has been observed experimentally to exhibit a blue fluorescence and has become known as the “cool flame” heat release. This cool flame heat release results in an increase in temperature from the starting temperature to a “cool flame ceiling temperature” after which the rate of heat release decreases significantly. This cool flame ceiling temperature marks a transition from low to high temperature chemical kinetic pathways [43-45;47;58] and due to the numerous chemical reactions involved, this transition does not occur instantaneously at an absolutely defined ceiling temperature, but rather occurs within a narrow temperature range. The cool flame ceiling temperature is

therefore not easy to define and for the purposes of this study the cool flame ceiling temperature is defined as the temperature at the mid point (in time) between the highest rate of cool flame temperature rise and the highest rate of main ignition temperature rise.

It should be noted that all NTC fuels exhibit 2-stage heat release. However, not all 2-stage fuels exhibit true NTC behaviour (displaying a region of increasing overall ignition delay with increasing initial temperature), although they may still exhibit a characteristic “S-shaped” profile on the ignition delay vs. temperature plot. This 2-stage, non NTC behaviour can also be seen with conventional NTC fuels under conditions of high pressure and lean air-fuel ratio as seen in Appendix A. For this reason, fuels in this study are referred to as either single stage or 2-stage auto-ignition fuels and the NTC characteristic is not used as a fuel type classification.

4.3. Effects of temperature on the characteristics of two-stage auto-ignition

A careful observation of Figure 4.3 reveals a number of important characteristics relating to the effects of temperature on 2-stage auto-ignition:

1. Starting from the lower initial temperature curves, the cool flame temperature rise magnitude decreases as the initial temperature (Ti) increases, until it merges with the main ignition delay and becomes difficult to distinguish clearly. The cool flame ceiling temperature also decreases as the initial temperature increases, until it can no longer be defined (no clear cool flame heat release).
2. Starting from the lower initial temperature curves, the cool flame ignition delay initially becomes shorter as the initial temperature is increased, but later remains approximately fixed in timing as the cool flame heat release magnitude dies away.
3. It is interesting to note that the ceiling temperature of the 748K curve is similar to the starting temperature of the 845K curve. However, the post cool flame ignition delay (time from the cool flame heat release to the main heat release) is significantly shorter than the overall single stage ignition delay of the 845K curve. This enhanced reactivity attribute is extremely significant in auto-ignition modelling [1] and is discussed in further detail below.

Figure 4.4 below illustrates a number of significant temperature effects on the auto-ignition characteristics of the 2-stage fuel, n-heptane. The ignition delay data is presented on the orthogonal scales of logarithm of time vs. 1000/temperature in order to emphasise straight-line-Arrhenius behaviour where it occurs. For ease of deciphering the inverted temperature scale, the light grey series allows the initial temperature to be read across onto the secondary y-axis.

In this figure, the post cool flame ignition delay (ID – t1) is plotted twice: firstly as a function of the initial temperature (Ti) as is common in the literature [72;73] and secondly as a function of the cool flame ceiling temperature (Tcf). The reason for this latter presentation is that the chemistry subsequent to the cool flame is subjected to this ceiling temperature and not the initial temperature. It therefore seems more appropriate to consider the post cool flame ignition delay as a function of the post cool flame temperature. It is acknowledged that the temperature during the post cool flame ignition delay is not constant, but it is considered that this nonetheless represents a better qualitative presentation than the former alternative. Additional benefits to this presentation and perspective are discussed later.

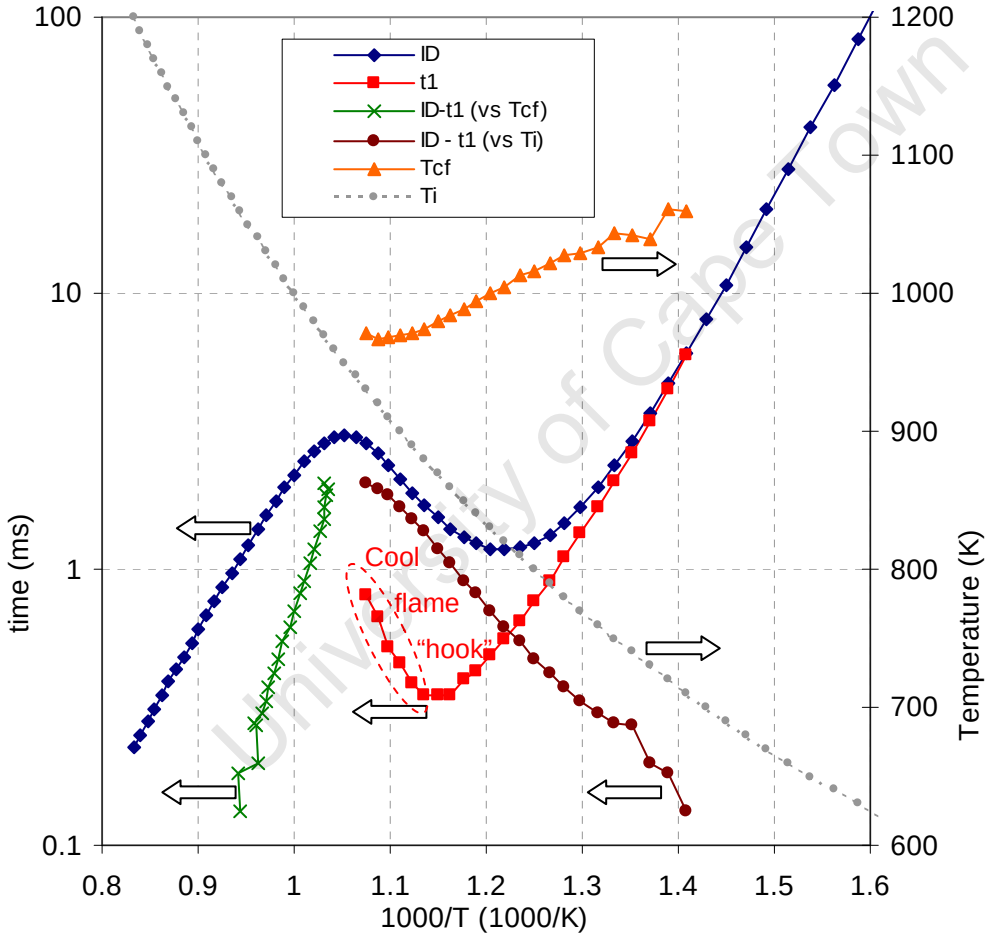

Figure 4.4: Temperature effects on the auto-ignition of n-heptane; P_i=20bar; Phi=1; R=0%

Figure 4.4 above illustrates an important feature of cool flame ignition delay timing. The discussion of Figure 4.3 made reference to the change in behaviour of the cool flame timing as the initial temperature is increased. However, the increased resolution of Figure 4.4 clarifies this issue and indicates that the cool flame timing not only deviates from its initial straight-line-Arrhenius behaviour, but also exhibits a region of NTC behaviour before the cool flame heat release magnitude dies away completely. This deviation from the straight-line-Arrhenius

behaviour has been observed experimentally for 2-stage fuels in [43;45;59;61;73], but the NTC "hook" in the cool flame timing has seemingly only been observed experimentally in [72]. The experimental evidence for a real cool flame NTC hook is therefore tenuous. Perhaps the reason for this sparse experimental evidence of the cool flame NTC hook is highlighted in [85] where the authors state that the cool flame timing appears to follow a straight-line-Arrhenius behaviour but that the CF ID becomes difficult to distinguish and record as the cool flame heat release reduces to low values and merges into the main ignition delay. This cool flame hook was observed in simulations using both the detailed mechanism from [44] and from [45]. It was therefore assumed to be a real and relevant aspect of 2-stage auto-ignition chemical kinetic behaviour, although unequivocal experimental evidence of this phenomenon does not appear to be available.

A careful examination of Figure 4.4 illustrates the fact that the post cool flame ignition delays (ID-t1 vs cool flame ceiling temperature, series shown in green) are significantly shorter than the overall ignition delays (series shown in blue) in the high temperature region (temperatures higher than 980K) for similar cool flame ceiling temperatures and initial temperatures respectively. It may be argued that the high temperature chemistry does achieve progress prior to the cool flame heat release and that comparison of the high temperature reactivity with the post cool flame reactivity is not entirely appropriate. However, due to the exponential temperature sensitivity of these reactions (assuming Arrhenius reaction rates), it is easily shown that the progress of the high temperature chemistry prior to the cool flame heat release is negligible. It is also interesting to note that both the cool flame ceiling temperature and the post cool flame ignition delay exhibit nominally straight line behaviour in Figure 4.4.

While fuel auto-ignition chemistry is usually discussed in terms of low, intermediate and high temperature regions [43-47;50], Figure 4.4 indicates that the auto-ignition behaviour of 2-stage fuels should be considered in detail within in six distinct regions. The thermal separations of these regions are given below in the context of Figure 4.4 but differ according to the particular 2-stage fuel and the experimental conditions concerned.

1. For temperatures below 710K, the cool flame (t1) and main ignition (ID) are not separated by a discernable second delay period. This appears to be due to the fact that the cool flame ceiling temperature (Tcf) is so high under these conditions, that the main heat release does not suffer a measurable delay.
2. For temperatures between 710K and 810K, the cool flame becomes clearly distinguishable from the main heat release. In this region the cool flame ignition delay dominates determination of the overall ignition delay which decreases with increasing temperature in

spite of the decreasing cool flame ceiling temperature and corresponding increasing post cool flame ignition delay (ID – t1).

3. From 820 - 870K, the cool flame heat release magnitude and ceiling temperature continues to decrease with increasing initial temperature, resulting in an increased post cool flame ignition delay. The post cool flame ignition delay now dominates the overall ignition delay and therefore overall NTC behaviour is observed.
4. From 870 – 930K a NTC phenomenon is seen in the cool flame timing. This behaviour, together with the continued reduction in ceiling temperature with increasing initial temperature, results in further NTC behaviour in the overall ignition delay.
5. While the cool flame position cannot be distinguished between 930K and 950K, it is believed that some low temperature chemistry is still active in this region, causing enhanced reactivity (deviation from the high temperature straight-line-Arrhenius ignition delay behaviour) compared with the higher temperature region.
6. For temperatures over 950K, no cool flame or enhanced reactivity is observed and the main ignition follows the straight-line-Arrhenius behaviour once more.

4.4. Effects of pressure on the characteristics of fuel auto-ignition

The effects of pressure on auto-ignition behaviour were investigated using detailed chemical kinetics simulations in the same manner as discussed previously. The detailed results of these simulations are given in Appendix A. For single stage fuels, pressure effects on auto-ignition delay are relatively simple and are observed in the example of toluene in Figure 4.5 below. Increasing pressure results in a decrease in ignition delay and this effect is relatively constant through the temperature range.

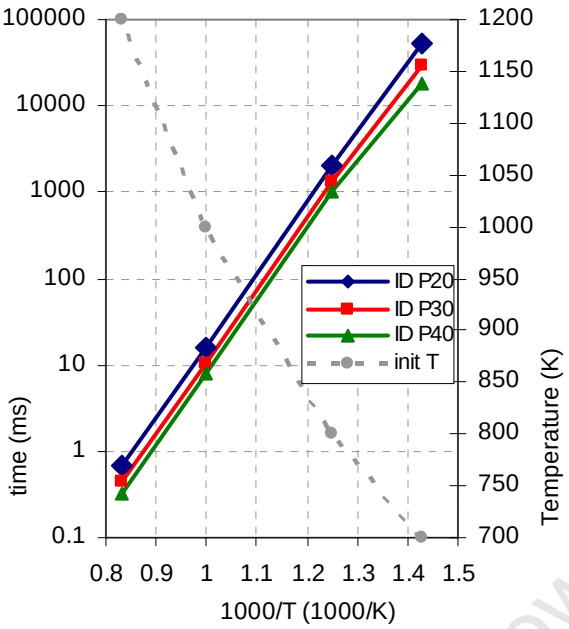

Figure 4.5: Pressure effects on the auto-ignition of toluene; P_i= 20, 30, 40bar; Phi=1.0; R=0%

For 2-stage ignition fuels, the effects of pressure are more complex, since pressure affects different temperature regions in different ways. These effects are illustrated for stoichiometric mixtures of n-heptane in Figure 4.6 below. Starting from the low temperature region, pressure has minimal effect on the cool flame ignition delay until it approaches the cool flame NTC hook. Higher pressures delay the occurrence of the cool flame hook, resulting in significantly shorter cool flame ignition delays seen at intermediate temperatures. Cool flame ceiling temperatures are also significantly increased with increasing pressure. The post cool flame ignition delay remains almost unaffected by pressure changes. These three effects result in a very large decrease in ignition delay with increasing pressure in the intermediate temperature region. The high temperature region exhibits decreased ignition delay with increased pressure as seen for single stage fuels.

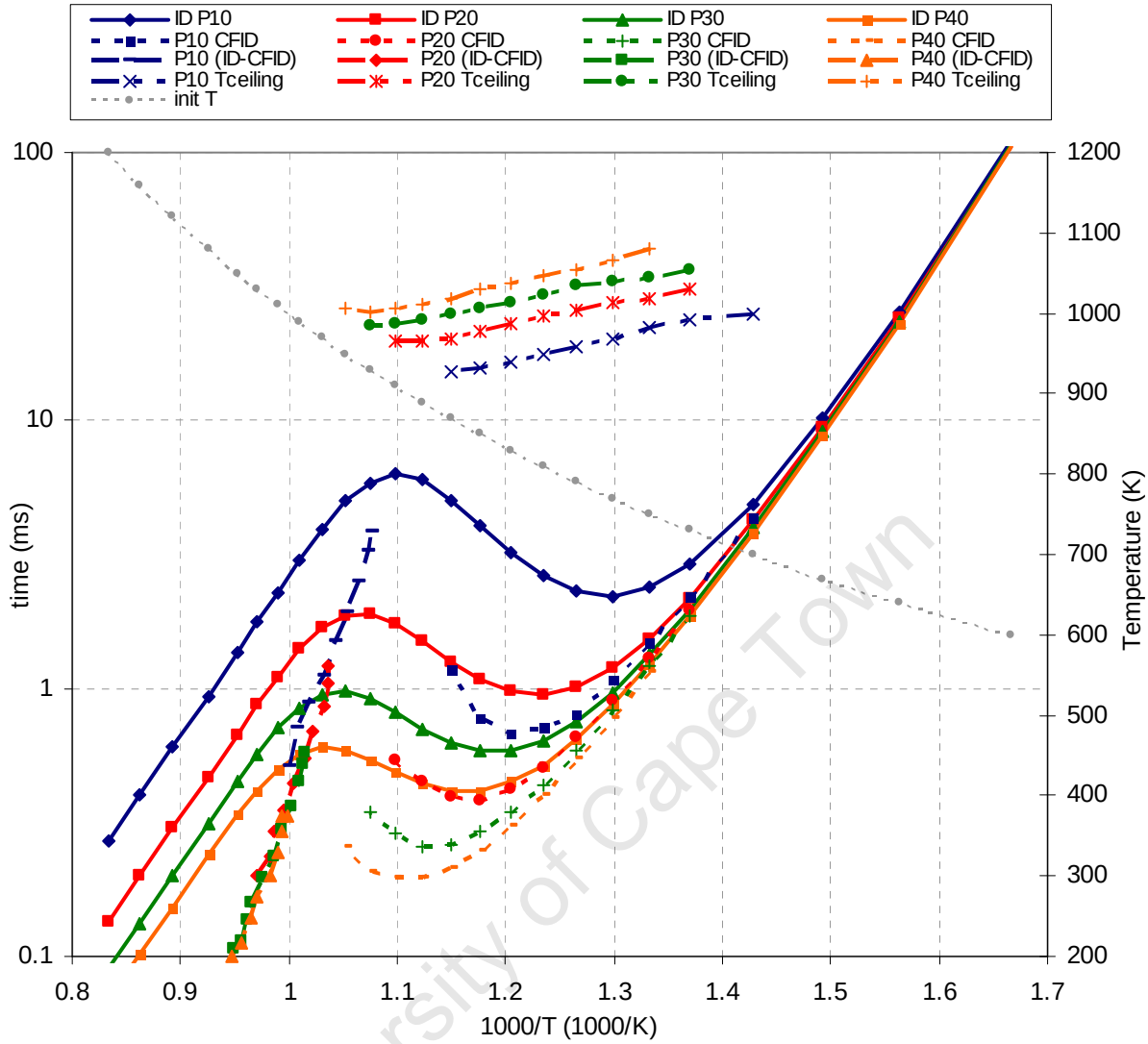

Figure 4.6: Pressure effects on the auto-ignition of n-heptane; P_i=10, 20, 30, 40bar; Phi=1.0; R=0%

4.5. Effects of air-fuel ratio on the characteristics of fuel auto-ignition

The effects of fuel-air equivalence ratio on auto-ignition behaviour were similarly investigated. The detailed results of these simulations are given in Appendix A. For single stage fuels, fuel-air equivalence ratio effects on auto-ignition delay are relatively simple and are observed in the example of toluene in Figure 4.7 below. Leaner fuel ratios results in slightly increased ignition delay times (bear in mind the magnitude of the y-axis scale) and this effect is relatively constant through the temperature range.

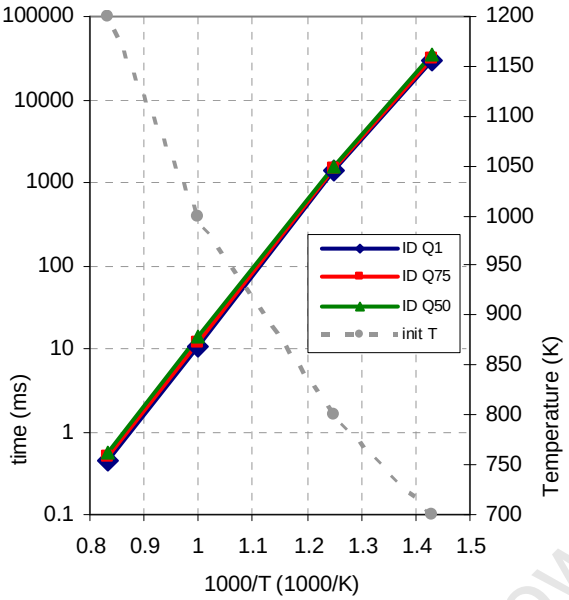

Figure 4.7: Fuel-air equivalence ratio effects on the auto-ignition of toluene; P_i=30bar; Phi=1.0, 0.75, 0.5; R=0%

For 2-stage ignition fuels, the effects of fuel-air equivalence ratio are again more complex, since fuel-air equivalence ratio affects different temperature regions in different ways. These effects are illustrated for mixtures of n-heptane at 20bar in Figure 4.8 below. Starting from the low temperature region, equivalence ratio has minimal effect on the cool flame ignition delay until it approaches the cool flame NTC hook. Higher equivalence ratios delay the occurrence of the cool flame hook, resulting in slightly shorter cool flame ignition delays seen at intermediate temperatures. Cool flame ceiling temperatures are also increased with increased equivalence ratio, although the effect is strong at lower temperatures and diminishes significantly as the cool flame heat release magnitude decreases (with increasing initial temperature). As with pressure influences, the post cool flame ignition delay remains almost unaffected by equivalence ratio changes, with the possible exception of very lean mixtures. These three effects result in a significant decrease in ignition delay with increasing equivalence ratio in the intermediate temperature region. The high temperature region exhibits decreased ignition delay with increased equivalence ratio as seen for single stage fuels, except that the effect appears to diminish slightly with increasing temperature.

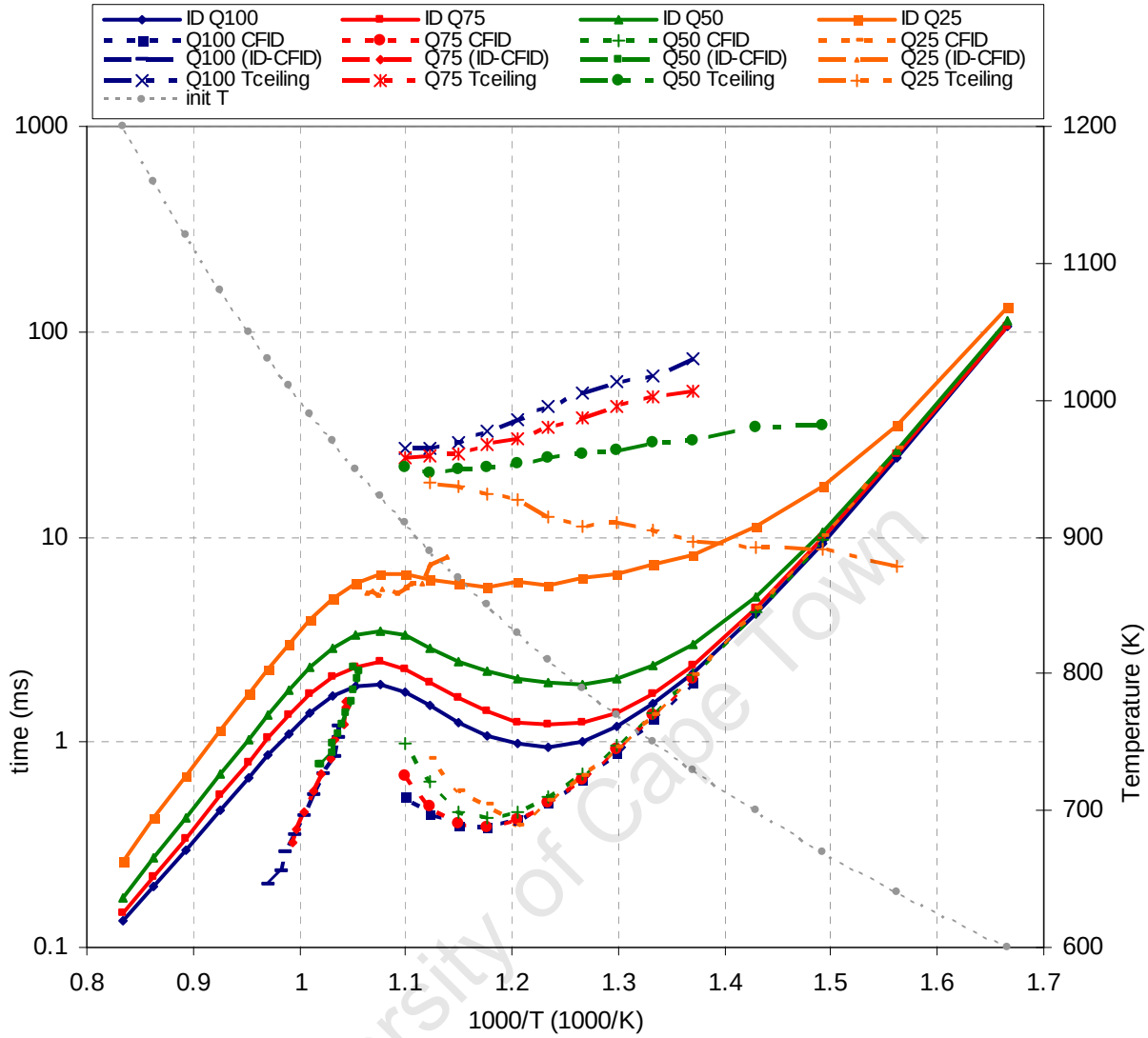

Figure 4.8: Fuel-air equivalence ratio effects on the auto-ignition of n-heptane; P_i=20 bar; Phi=1.0, 0.75, 0.5, 0.25; R=0%

4.6. Effects of inert dilution on the characteristics of fuel auto-ignition

The effects of inert dilution (using completed combustion product species) on auto-ignition behaviour were investigated using detailed chemical kinetics simulations in the same manner as discussed previously. The detailed results of these simulations are given in Appendix A. For single stage fuels, inert dilution effects on auto-ignition delay are relatively simple and are observed in the example of toluene in Figure 4.9 below. Increased inert dilution percentage results in slightly increased ignition delay times (bear in mind the magnitude of the y-axis scale) and this effect is relatively constant through the temperature range.

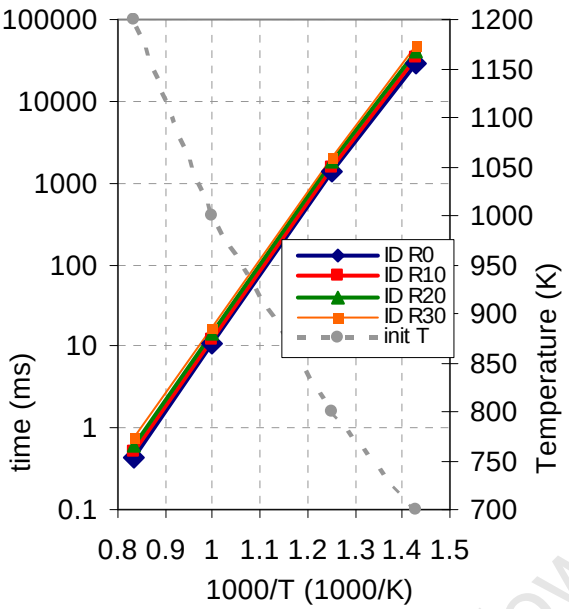

Figure 4.9: Inert combustion product dilution effects on toluene; P_i=30bar; Phi=1.0; R=0, 10, 20, 30%

For 2-stage ignition fuels, the effects of inert dilution are again more complex, since inert dilution affects different temperature regions in different ways. These effects are illustrated for mixtures of n-heptane at 20bar in Figure 4.8 below. Starting from the low temperature region, inert dilution has minimal effect on the cool flame ignition delay until it approaches the cool flame NTC hook. Lower inert dilution percentages delay the occurrence of the cool flame hook, resulting in slightly shorter cool flame ignition delays seen at intermediate temperatures. Cool flame ceiling temperatures are also increased with lower inert dilution and the effect is slightly stronger at lower temperatures, diminishing slightly as the cool flame heat release magnitude decreases (with increasing initial temperature). As with pressure and equivalence ratio influences, the post cool flame ignition delay remains almost unaffected by inert dilution changes. These three effects result in a significant decrease in ignition delay with decreasing inert dilution in the intermediate temperature region. The high temperature region exhibits increased ignition delay with increased inert dilution as seen for single stage fuels, except that the effect appears to become marginally more pronounced with increasing temperature.

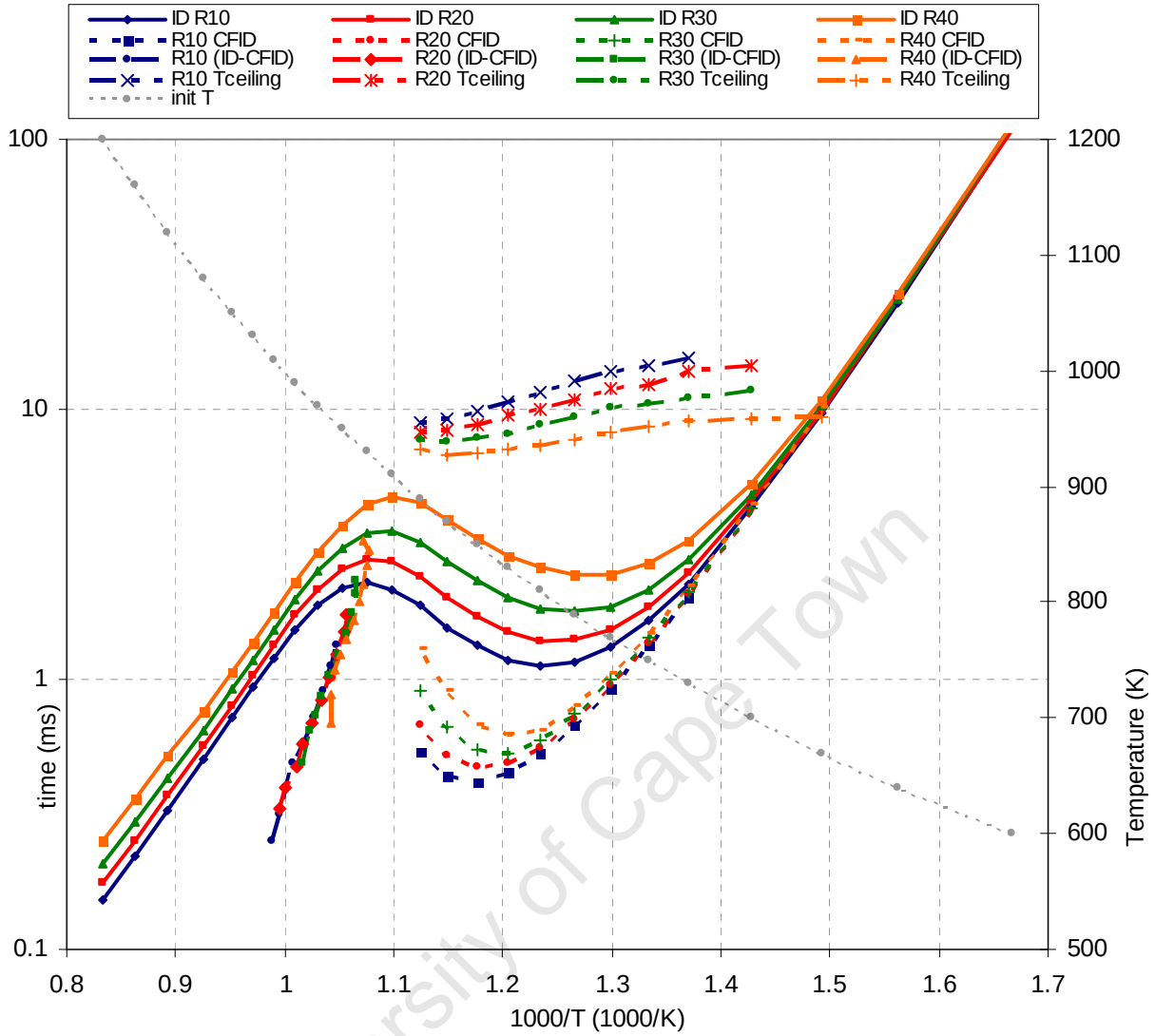

Figure 4.10: Inert combustion product dilution effects on n-heptane; P_i=20 bar; Phi=1.0; R=10, 20, 30, 40%

5. Application of an empirical AI model

The recent development of the empirical model by Yates and Viljoen [1], offered an opportunity for HCCI engine modelling, since this model was able to predict, with remarkable computational efficiency and accuracy, single and 2-stage fuel auto-ignition behaviour (including cool flame timing and cool flame temperature rise) for PRF blends as well as ternary blends of the PRFs and methanol. The model was also valid over a suitable range of pressures and equivalence ratio, making it well suited for HCCI auto-ignition modelling. This empirical model was therefore formulated for HCCI engine modelling and used for a very wide range investigation of fuel and engine parameter optimisation. The complete report of this work is given in Appendix B.
A summary of this work is provided below.

5.1. Formulation of an empirical auto-ignition model for HCCI use

The empirical auto-ignition model presented in [1] was formulated in the context of constant volume combustion simulations. The application of the model was therefore adapted to an environment of changing pressure and temperature using the “conservation-of-delay” or knock-integral method as discussed in Chapter 3.

Prediction of the cool flame ignition delay was given by:

$$t_1 = \phi^{\beta_1} A_1 p^{n_1} e^{\frac{B_1}{T}}$$

Equation 5.1: Cool flame ignition delay as given in [1]

Where:
Φ is the fuel-air equivalence ratio
β: is the exponent of air-fuel ratio
A: is the pre-exponential constant of proportionality
p: is the pressure
n: is the auto-ignition pressure coefficient
B: is the exponential temperature coefficient
T: is the temperature
and the subscript 1 refers to the cool flame heat release event

In an environment of changing pressure and temperature, by using the knock-integral approach [51-53] the cool flame ignition delay was given by:

$$\int_{t_{BDC}=0}^{t_1} \frac{1}{\left(\phi^{\beta_1} A_1 p^{n_1} e^{\frac{B_1}{T}}\right)} dt = 1$$

Equation 5.2: Integral form of cool flame ignition delay

For the purposes of discrete time stepping in the HCCI engine model, a discrete form of Equation 5.2 was given by:

$$\sum_{t_{BDC}=0}^{t_1} \frac{1}{\left(\phi^{\beta_1} A_1 p^{n_1} e^{\frac{B_1}{T}}\right)} \Delta t = 1$$

Equation 5.3: Discrete form of cool flame ignition delay

This summation was then calculated during the discretised pressure-temperature history experienced by the fuel-air mixture. At the point where the cool flame integral = 1 (if this did actually occur), the cool flame temperature rise was calculated using the conditions at this point using a slightly modified form of the expression from [1]:

$$\Delta T_{CF} = \omega \left(T_i - T_{EQ} . p^k . \phi^{\mu} \left(\frac{100}{99 + \phi} \right)^{\sigma} \right)$$

Equation 5.4: Cool flame temperature rise

Where:

T_i and **p** are the temperature and pressure at the point of the start of cool flame heat release

ω, k, μ and σ are empirically fitted coefficients.

The empirical termination function for gradually nullifying the influence of the cool flame temperature rise when the calculated value became negative [1], was also used:

$$T_{CF} = T_i + 0.5\left(\Delta T_{CF} + \sqrt{(\Delta T_{CF})^2 + C_0}\right)$$

Equation 5.5: Empirical termination function for cool flame temperature rise from [1]

Where the constant C_0 = 684

Since the engine model was formulated to calculate basic species concentrations and solve for temperature in order to satisfy the laws of thermodynamics, a simple temperature rise could not be directly applied in the engine model. For this reason the cool flame temperature rise was applied by calculating the amount of fuel-air mixture that would be required to burn at the point of the cool flame heat release in order to attain the cool flame temperature rise calculated with Equation 5.4 and Equation 5.5, while still applying conservation of energy to the cylinder volume.

The main (peroxide) heat release ignition delay was also calculated in discrete integral form similarly to Equation 5.3, but was split into pre and post cool flame integral contributions in order to incorporate the post cool flame enhanced reactivity factor X described in [1]. The discrete formulation for the peroxide ignition delay was therefore formulated as:

$$\sum_{t_{BDC}=0}^{t_1} \frac{1}{\left(\phi^{\beta_h} A_h p^{n_h} e^{\frac{B_h}{T}}\right)} \Delta t + \sum_{t_1}^{t_{Perroxide}} \frac{1}{\left(\phi^{\beta_h} A_h p^{n_h} e^{\frac{B_h}{T + X\ \Delta T_{CF}}}\right)} \Delta t \Rightarrow 1$$

Equation 5.6: Discrete formulation for the peroxide ignition delay

The model formulation presented in [1] did not address the issue of burn duration for the cool flame and main heat release events, which were treated as instantaneous events. Some effort was therefore spent formulating an empirical model to emulate the burn durations for the cool flame and peroxide reactions using the underlying Chemkin simulation data used to formulate the auto-ignition model in [1]. However, when these burn durations were compared with typical durations measured during the experimental validation, it was found that the real burn durations were more than an order of magnitude longer than those calculated by considering only the

chemistry effects. This is perhaps not surprising, given the work by many researchers on the effects of thermal and charge stratification on HCCI burn durations [5-12].

It was therefore deduced that the burn durations were dominated by these stratification effects. Based on the empirical data, burn duration values were very similar throughout the limited range of validation and burn durations of 9 and 16 crank angle degrees were used for the cool flame and peroxide burn durations respectively. The cool flame and peroxide heat release rates were modelled using a Wiebe burn function as described in [13]. While the heat release rate treatment was regarded as a pragmatic simplification of the model formulation, this was justified because the application of the model aimed at timing prediction rather than burn durations.

5.2. Formulation of a discrete thermodynamic engine model

In order to simulate various aspects of HCCI engine combustion behaviour, a discrete, single zone thermodynamic engine model was formulated using Microsoft Excel 2003. The engine model consisted of six modules as described below:

1. Parameter database

This module was used to store all the user defined variables and input parameters needed for the model to function. User defined variables included engine geometry values, fuel composition, atmospheric conditions and operational specifications. Input parameters included thermo-chemical data for air components and various single component fuels as well as their basic combustion products. This data was sourced from the JANAF thermo-chemical tables [86]. Parameters for the auto-ignition model, engine heat transfer model and port flow models were also included in this module.

2. Fuel blending module

This module was used to perform blending calculations to enable an “equivalent hydrocarbon” species to be defined for the stoichiometry and composition module. The module also calculated mass, mole and volume fractions as well as the density of a given fuel blend.

3. Reactant and product stoichiometry and composition module

This module was used to calculate the stoichiometric and specified non stoichiometric proportions of reactants as well as their combustion products. The module calculated the number of moles and mole fractions of each species involved.

4. Mixture properties module

This module calculated the mixture properties within the inlet port, engine cylinder and exhaust port while the engine model was running. The detailed equations and derivations used in this module can be found in Appendix C. A summarised outline of these calculations is presented below. The module made use of the thermo-chemical data and calculated species specific heats using the conventional polynomial equation:

$$C_P = a + bT + cT^2 + dT^3 + eT^4$$

Equation 5.7: polynomial specific heat expression

Mixture specific heats (and other thermodynamic mixture parameters below) were calculated using the species values and the species mole fractions. Enthalpy values were calculated using the standard enthalpy derivation of the specific heat polynomial expression and the enthalpies of formation given in the JANAF data:

$$h_{sensible,(T)} = \int_0^T C_p\, dT = aT + \frac{b}{2}T^2 + \frac{c}{3}T^3 + \frac{d}{4}T^4 + \frac{e}{5}T^5$$

Equation 5.8: Sensible enthalpy expression

$$h_{state,(T)} = \left(\Delta h^0_{f_{298}} - h^0_{sensible\,298}\right) + h_{sensible,(T)}$$

Equation 5.9: State enthalpy expression

The species internal energy values were calculated from the enthalpy values according to the expression:

$$u_{state,(T)} = h_{state,(T)} - R_u T$$

Equation 5.10: State internal energy expression

Species entropy values were used in the reaction dissociation calculations and were calculated using the expressions:

$$\int_1^2 dS = \left[a\ln T + aT + \frac{cT^2}{2} + \frac{dT^3}{3} + \frac{eT^4}{4} \right]_1^2 - R\left(\ln P_2 - \ln P_1\right)$$

Equation 5.11: Change in entropy expression

$$S^0_{state} = S^0_{sens}\Big|_T - S^0_{sens}\Big|_0 + (S_{f,T=298K} - (S^0_{sens}\Big|_{298} - S^0_{sens}\Big|_0))$$

Equation 5.12: State entropy expression

Combustion gas product dissociation was modelled in terms of the water-gas shift reaction and carbon dioxide dissociation reaction. Nitrogen oxide dissociation reactions were not considered due to the relatively low temperatures reached in lean HCCI combustion. The dissociation calculations assumed chemical equilibrium of combustion product species. The composition of the reaction products was calculated by application of the second law of thermodynamics using the standard concepts of Gibbs free energy and the equity of the two Kp expressions:

$$K_{\mathrm{p1}} = e^{-\Delta \mathrm{G}^* / R_u T}$$

Equation 5.13: First Gibbs energy Kp expression

$$K_{\mathrm{p2}} = \left[\Pi N_i^{\nu_i}\right]\left(\frac{P_{\mathrm{total}}}{N_{\mathrm{total}}}\right)^{\Sigma \nu_i}$$

Equation 5.14: Second Gibbs energy Kp expression

Atomic balances were maintained for all calculations.

5. Fuel auto-ignition module

Fuel auto-ignition was modelled using the Yates and Viljoen empirical auto-ignition model [1] modified to discrete form as described in section 5.2 above.

6. Engine and port module

The engine and port module used the standard crank-slider relationship and the basic geometry of the targeted engine to calculate the volume dynamics. Pressure and Temperature were solved simultaneously at each discrete time step (crank angle increment) using the ideal gas law and 1st law of thermodynamics (conservation of energy). These two parameters were iteratively solved using the standard Excel solver function (Secant method). Heat transfer to and from the combustion chamber walls was modelled using the standard Woschni correlation and parameters as described in [13].

Flow through the inlet and exhaust ports with their associated valve obstructions, was modelled using a combined plug flow and pipe friction formulation to replicate both dynamic ram flow and frictional effects on engine breathing characteristics. The first law of thermodynamics for open

systems and the law of conservation of mass were applied to the port and cylinder systems to resolve flow magnitudes. This treatment allowed the port and valve geometric parameters to influence the flow friction and momentum characteristics. Important parameters affecting dynamic flow, such as port surface roughness coefficients, valve and elbow drag coefficients and effective plenum geometric sizes, were tuned to fit typical volumetric efficiency performance data given in literature [13]. The valve lift profile was measured on the Ricardo E6 engine used for validation of the model. The computational efficiency of the model was reasonable and a four stroke cycle required about 100 seconds solving on a standard office computer.

5.3. Formulation of an explicit thermodynamic engine model

For the HCCI engine modelling study detailed in Appendix B, the engine model was formulated differently in a manner which allowed the inlet air temperature to be solved in order to attain a given HCCI combustion phasing. The iterative solving of the engine model for this purpose added significantly to the model run time and the very large number of simulations required in the study provided motivation for a much more computationally efficient HCCI engine model to be formulated. The primary goal of this formulation was to use the previous principles in a manner which allowed the energy and conservation equations in the model to be solved explicitly rather than iteratively.

The formulation of the engine model was aimed at being as generic as possible in order to be able to explore wide ranges of setup and operating conditions. This explicit generic model was also set up in Microsoft Excel and formulated to allow easy manipulation of conditions, multiple copies solving simultaneously and instant visual assessment of the effects of changes to conditions.

The variables used to define the setup condition were:

- cylinder swept volume
- compression ratio
- bore/stroke ratio
- connecting rod length/stroke ratio
- Fuel choice

The variables used to define the extremely wide operational conditions were:

- engine speed – varied from 300 - 15000rpm
- inlet charge temperature (mixture entering the cylinder) - varied from 300 - 800K
- inlet charge P (mixture entering the cylinder) - varied from 0.2 – 2bar absolute
- air fuel equivalence ratio – varied from 0,25 – 1.0
- residual combustion product gas pressure at exhaust valve closure – held constant.

These variables were used in a full factorial parametric sensitivity investigation.

Exhaust gas product species and mole fractions were calculated from stoichiometric and lean burn balanced chemical equations assuming no dissociation due to the typically low burned temperatures in HCCI combustion. Exhaust valve closure was assumed to occur at TDC and residual combustion product gas temperature was assumed to be a linear function of equivalence ratio as indicated by spark ignition engine exhaust temperature data in [13].

Instead of using the breathing model from the previous engine model, mixture properties at the start of compression were calculated empirically. The calculated mass of trapped exhaust gas was adiabatically adjusted to the inlet gas pressure with the associated changes in volume and temperature. The inlet gas was assumed to fill the remainder of the volume to BDC at its inlet pressure and temperature. The moles of both mixtures were summed and the temperature and pressure of the mixture calculated for start of compression at BDC. Using the mole fractions and JANAF coefficients for specific heats of each component, the expression for gamma as a function of temperature for the specific mixture could be calculated. Values of gamma were related to an appropriate polytropic compression coefficient using a relationship derived from data showing speed effects on polytropic compression coefficient [13] and pressure data from a number of different engine sizes including very small displacement engines [40;87-90]. The expressions for this empirical formulation are given in Appendix B.

This effectively simulated the effects of engine speed and displacement on heat loss during compression and associated effects on the compression pressure and temperature history. Temperature and pressure during compression were discretely calculated using this polytropic approximation, resulting in a pressure and temperature history showing sensitivity to inlet and exhaust boundary conditions, fuel type and equivalence ratio, engine speed, compression ratio and size. The formulation also removed the need for iterative solving of the energy and conservation equations, resulting in fast simulation times in the order of 1.3 seconds on a standard issue Pentium 4 desktop PC.

5.4. Experimental validation

Experimental validation of the more detailed discrete engine model was addressed using a 25cc, single cylinder Honda engine that was modified to run in HCCI mode. This experimental work is attached as Appendix D.

The validation of the simplified explicit engine model was conducted using two engines. The first was a Ricardo E6, variable compression ratio, E6 engine that had been modified to run in HCCI mode. The details of this experimental work are given in Appendix B. An example of the good agreement between the model and experimental results is given in Figure 5.1 below. The fit in this figure was obtained by tuning the inlet mixture temperature rise through the inlet port and valve to a value of 60^0C and using a post cool flame reactivity enhancement factor [1] value of 2.0.

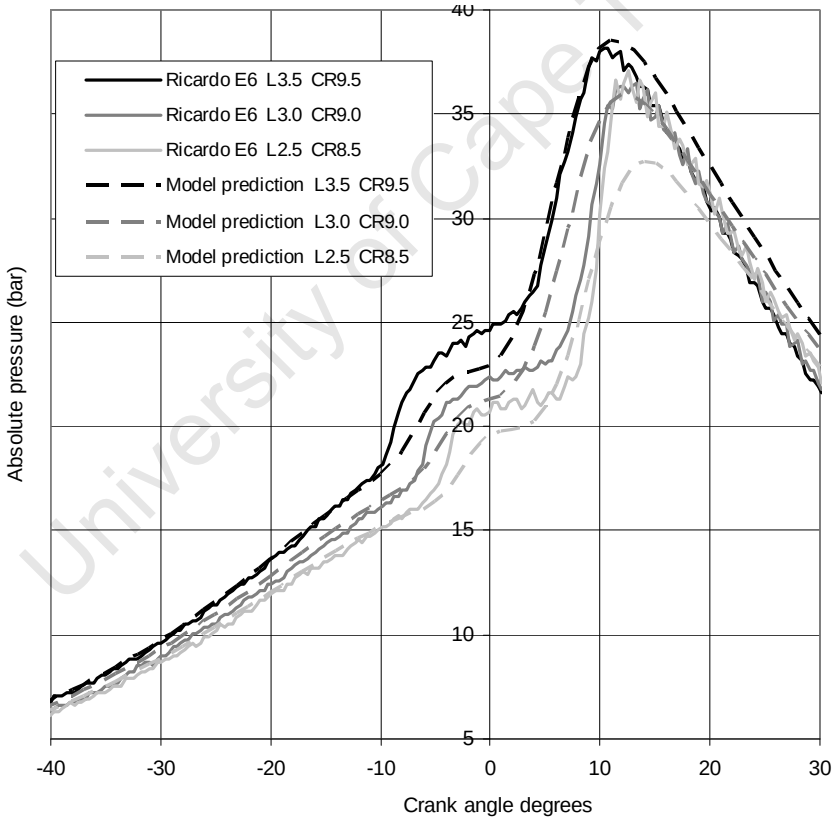

Figure 5.1: Experimental validation of the simplified discrete HCCI engine model using the Ricardo E6 engine for a range of air-fuel ratio (Lambda) values

A second attempt at validation of the simplified explicit engine model was conducted using a 2-stroke model aeroplane “diesel” engine. While this form of model aeroplane engine is known as model “diesel” it functions as an HCCI engine since it draws in a premixed charge via a carburettor and ignites the mixture by compression of the piston alone [40;87-90]. This

experimental work is attached as Appendix E. An attempt was made to run this engine on a mixture of n-heptane and 2-stroke lubricant in order to validate the HCCI engine model. This attempt failed due to the very high ignition quality fuel appetite of the very small engine whose heat loss characteristics made HCCI running with n-heptane impossible. Unfortunately the explicit model that was formulated for this engine could not be used, since the fuel auto-ignition model parameters for the model aeroplane fuel were not available. The study did, however, yield valuable findings regarding the HCCI characteristics of this rather unique engine. These findings are discussed in the next two sections.

5.5. Application of the model for prediction and insight

The simplified explicit engine model was used to investigate “convergent zones of operation” where the complex interplay of engine speed, engine breathing, heat transfer and fuel auto-ignition characteristics resulted in “sweet spot” operational zones where one or more parameters (e.g. speed or load) could be changed without altering the combustion phasing. Examples of such behaviour have been specifically noted in literature [18]. Details of the motivation for this study and the explanations of this phenomenon are given in Appendix B. Key findings from this study were:

- In general, engine speed effects on combustion phasing exhibited convergence to a speed range where engine speed could be varied independently of combustion phasing without phasing correction adjustment of other variables.
- Within these speed convergence areas, zones also existed where fuel equivalence ratio could be varied independently of combustion phasing without phasing correction adjustment of other variables. For n-heptane, zones also existed where inlet pressure could be varied independently of combustion phasing without phasing correction adjustment of other variables, but this was not the case with fuels that do not exhibit any significant cool flame heat release within the convergent zone even if they do in fact exhibit negative temperature coefficient behaviour within their broader auto-ignition characterisation.
- HCCI operational zones also existed where multiple constant combustion phasing lines of differing engine speed intersect to allow very large ranges of phasing independent speed variation.
- This formulation of HCCI modelling could also be used to find fixed constant combustion phasing lines that run through the speed-load map from low speed and low load to high speed and high load, much like a propeller speed-load line. Load control could be achieved by equivalence ratio and/or inlet pressure in the case of fuels exhibiting cool

flame behaviour, but only by equivalence ratio in fuels exhibiting no cool flame heat release.

- Engine cylinder size played an important role in determining the fuel ignition quality appetite of an HCCI engine and strongly influenced the speed range where speed could be varied without affecting combustion phasing.
- Appropriate combustion phasing could not be achieved for slow cranking engine speeds without unrealistic charge heating due to excessive compression heat loss. Spark ignition, multiple single charge compressions, high speed cranking or some other means of starting HCCI engines would therefore be required.
- HCCI engine compression ratio, size and fuel formulation are therefore critical parameters in determining the most effective operational range and mode of combustion control.

5.6. Small engine HCCI experimental work

Thermal gradients within the engine combustion chamber have been shown by a number of researchers [6;8;10;42] to offer significant potential for control of heat release rates in HCCI engine combustion. The very small engine sizes used in the studies given in Appendix D and E were chosen to investigate whether small HCCI engine combustion chamber size offers a method of heat release rate control due to the inherently larger combustion chamber surface to volume ratios and associated more pronounced thermal gradients.

The findings of the studies in Appendices D and E indicated that very small combustion chambers certainly do enhance the percentage of mixture affected by the thermal boundary layer of the chamber wall. Such small combustion chamber sizes may, however, be too extreme for this finding to be implemented in a commercially valuable manner.

The study of thermal stratification on HCCI engines requires the use of multi-zone or CFD engine models. The fuel auto-ignition models available in literature, however, did not offer a suitable computationally efficient reaction rate based model capable of accurately representing cool flame heat release behaviour. Such a functional global fuel auto-ignition model therefore became the target of further study.

6. Formulation of a new global AI model

6.1. Motivation for a new functional global model

The literature review as discussed in chapter 3, revealed that none of the currently available global fuel auto-ignition models [49;63-65;73] were capable of accurately reproducing the dynamics (timing, rate and magnitude) of the cool flame heat release associated with 2-stage auto-ignition fuels, particularly the cool flame “hook” and enhanced post cool flame reactivity.

Such a functional global model, if it could be formulated, could prove ideal for incorporation in CFD HCCI engine models, allowing significantly improved combustion modelling accuracy within reasonable simulation run times. Such a functional global model could also prove useful in other ICE combustion simulations.

6.2. Feature requirements for the new functional global model

The fuel auto-ignition behavioural study presented in chapter 4 distilled a number of key behavioural features that a global fuel auto-ignition model must possess if it is targeted to predict the full heat release dynamics of 2-stage auto-ignition. Therefore, in order to satisfy the needs of this project, the new functional global fuel auto-ignition model must possess the following basic functional features, defined in general terms:

1. The virtual lack of heat released during the cool flame ignition delay period (constant temperature period) indicated that an intermediate species concentration must be used in the model formulation between the fuel species and the reaction/s resulting in heat release to control the ignition time delay.

2. The “cool flame hook” (or cool flame NTC behaviour in some cases) required a reverse reaction to act on this low temperature intermediate species in a manner which slowed its rate of formation at higher temperature.

3. The cool flame heat release triggering reaction must be strongly dependent on the concentration of the low temperature intermediate species. This reaction rate must, however, also be dependent on temperature to ensure that the low temperature intermediate species does in fact oxidise, even if this concentration is only depleted during the high temperature phase.

4. The arrest of the cool flame heat release indicates that a reverse reaction activates at an intermediate ceiling temperature. The cool flame heat release cannot simply be halted by the depletion of the low temperature intermediate, since this intermediate will continue to be produced in the absence of a reverse reaction or alternative termination path. It was not clear from the outset whether this reverse reaction could be combined with the reverse reaction required in item 2 above. Thermally activated reverse reaction/s would effectively shut down the low temperature reaction path for experiments conducted at high temperature.

5. For such high temperature experiments, the virtual lack of heat released during the single ignition delay period indicated that a high temperature intermediate species must be used in the model formulation between the fuel species and the reaction/s resulting in heat release, to control the ignition delay timing. This species cannot be combined with the low temperature intermediate, since the cool flame arrest reaction would prevent high temperature heat release from occurring.

6. The high temperature heat release triggering reaction must be strongly dependent on the concentration of the high temperature intermediate species. This reaction rate must, however, also be dependent on temperature to ensure that the high temperature intermediate species does in fact oxidise, even if this concentration is only depleted near the peak adiabatic flame temperature.

7. The enhanced post cool flame reactivity relative to that exhibited in the high temperature experiments indicates a requirement for enhancing or earlier triggering of the main heat release event where cool flame activity has been present. This requirement for post cool flame enhanced high temperature reactivity is illustrated in Figure 4.4. This post cool flame enhanced high temperature reactivity was specifically addressed in [1] with the use of a reactivity enhancement factor X which was applied as a virtual temperature increase in order to reduce the post cool flame ignition delay. It is believed that this attribute is one of the key factors in this model's [1] successful prediction of 2-stage auto-ignition dynamics.

8. It is known that hydrocarbon fuels do not react to completion in engine combustion chambers and rather form dissociated products that remain in chemical equilibrium [13]. Primary examples of these dissociations include the dissociation of CO_2 and the "water-gas shift' reactions as shown below:

$$CO_2 \longleftrightarrow CO + \frac{1}{2}O_2$$

Equation 6.1: CO2 dissociation equilibrium reaction

$$CO + H_2O \longleftrightarrow CO_2 + H_2$$

Equation 6.2: Water-gas shift equilibrium reaction

A simplistic complete reaction of fuel and air to their basic combustion products results in an over prediction of the adiabatic flame temperature by liberating the full calorific value of the fuel. Such full heat liberation will result in over prediction of combustion heat release and dissociation reactions must be at least partially addressed for accurate prediction of post combustion temperatures.

9. Reaction rate expressions must incorporate the appropriate coefficients needed to attain sensitivity to the experimental conditions of temperature, pressure, fuel equivalence ratio and inert combustion product dilution. These reaction rate coefficients should be applied only where required in order to attain appropriate agreement without suffering additional model complexity. Apart from temperature sensitivity, these requirements for a given 2-stage auto-ignition fuel (as demonstrated previously in Figure 4.6, Figure 4.8 and Figure 4.10) are as follows:
    a. The cool flame ignition delay at low temperature (before the cool flame hook) does not exhibit sensitivity to pressure, equivalence ratio or inert dilution.
    b. The reverse reaction responsible for the cool-flame hook exhibits sensitivity to pressure, equivalence ratio and inert dilution.
    c. The cool flame ceiling temperature exhibits sensitivity to pressure, equivalence ratio and inert dilution.
    d. The post cool flame (enhanced reactivity) ignition delay does not exhibit sensitivity to pressure, equivalence ratio or inert dilution.
    e. The high temperature (no prior cool-flame activity) ignition delay exhibits sensitivity to pressure, equivalence ratio and inert dilution.

6.3. Existing global model formulation critique

Existing model formulations were analysed in view of the above mentioned requirements, before alternative formulations were considered:

The Shell global model by Halstead et al. [73]

As was discussed in section 3.4, this global model comprised 8 reactions and 7 species as follows:

1) RH + O_2 → 2R’
2) R’ → R’ + products and heat
3) R’ → R’ + B
4) R’ + Q → R’ + B
5) R’ → out
6) R’ → R’ + Q
7) 2R’ → out
8) B → 2 R’

Although the presentation of the model’s performance in [73] indicated a reasonably good fit to the experimental data upon which it was validated, subsequent studies [91] indicated that the model did not perform well for different fuels and under conditions outside those presented in [73]. Even when effort was made in [91] to re-fit the model parameters, the model yielded “completely unrealistic results”. This failure was attributed to the fact that the model lacked basic agreement to the schematic of alkane chemistry (as presented in Chapter 3) and was therefore regarded as “no more than a very complex empirical model”, unlikely to yield valid results beyond the extent of its original validation data. This model was therefore not considered as useful in formulating the new functional global model.

The 4-step model by Müller et al. [63]

As was discussed in section 3.5, this model used 2 reactions for the high temperature chemistry and two reactions for the low temperature chemistry with the first LT reaction being reversible as follows:

1) F → X
2) X + 11 O_2 → P
3) F + 2 O_2 <=> I
4) I + 9 O_2 → P

The model satisfied the functional global model requirements 1, 3, 4, 5 and 6 as described above. Unfortunately, this model did not allow for enhanced post cool flame reactivity as detailed by requirement 7 above. The presentation of this model [63] also indicated that no provision was made for correctly capturing the cool flame hook as described by requirement 2,

nor was any form of high temperature dissociation included, thereby failing to meet requirement 8.

The 5-step model by Schreiber et al. [64]

Also discussed in section 3.5, this model used 2 reactions for the high temperature chemistry and 3 reactions for the low temperature chemistry with the low temperature intermediate formation reaction being reversible. The model was given [64] as follows:

1) $F \rightarrow X$
2) $X + 12.5\ (11)\ O_2 \rightarrow P$
3) $F + 2\ O_2 <=> I$
4) $I \rightarrow 2\ Y$
5) $Y + 0.5\ F + 11.5\ (10)\ O_2 \rightarrow P$

While this model aimed to improve NTC predictive accuracy through the use of the branching intermediate Y, the model still failed to meet the enhanced post cool flame reactivity as detailed by requirement 7 above. As with [63], the presentation of this model [64] also indicated that no provision was made for correctly capturing the cool flame hook as described by requirement 2, nor was any form of high temperature dissociation included, thereby failing to meet requirement 8.

The 7-step model by Zheng et al. [49]

This model used a single reaction to describe the high temperature oxidation reactions. The low temperature reactions scheme also made use of branching dynamics as demonstrated by [64], however, in this model, an extra chain branching intermediate was included. This model also included a reversible carbon dioxide formation reaction, thereby allowing dissociation effects for the reduction of the adiabatic flame temperature. The model was presented as follows:

1) $F + 7.5\ O_2 \rightarrow 8\ H_2O + 7\ CO$
2) $CO + 0.5\ O_2 <=> CO_2$
3) $F + 2\ O_2 <=> I_1$
4) $I_1 \rightarrow 2\ Y$
5) $Y + 0.5\ F + 6.5\ O_2 \rightarrow 8\ H_2O + 7\ CO$
6) $I_1 \rightarrow I_2$
7) $I_2 \rightarrow 2\ Y$

This model did not, however, include provision for the cool flame hook or the post cool flame enhanced reactivity. The model also failed to include the high temperature intermediate species and therefore failed to meet requirements 2, 5 and 7 as described above.

6.4. Model formulations development

6.4.1. Approach of a new formulation

Review of the literature provided an overview of the schematic chemical reaction classes active during alkane combustion. Schematics such as the example presented in Chapter 3, were carefully reviewed in an effort to formulate the new functional global model to be representative of the underlying chemical class reactions, in the hope of minimizing the empirical limitation criticisms directed towards the Shell model in [91]. However, significant effort was made to keep the model as simple and concise as possible while still achieving a fit of the kinetic behaviour. The approach used during the formulation of the new functional global auto-ignition model may be likened to a principle attributed to Albert Einstein:

"*It can scarcely be denied that the supreme goal of all theory is to make the irreducible basic elements as simple and as few as possible without having to surrender the adequate representation of a single datum of experience.*" [92]. This principle is often paraphrased in the form: "Everything should be made as simple as possible, but no simpler."

In his excellent and comprehensive review on the subject of reduced chemical kinetic modelling [50], John F. Griffiths mentions a rule of thumb that is paraphrased (to capture context) as follows:

"*For any fluid-mechanical calculation of reactive systems involving two or three spatial dimensions, the kinetics must be reduced to the simplest possible representation which satisfies the modelling requirements*."
A key aspect in the approach was to aim for a formulation that allowed direct behavioural adjustment of the model using the reaction rate parameters with the intension that these parameters could then be solved in a direct and robust fashion.

The fact that all four of the models described in the previous section, made no separate provision for the cool flame hook behaviour led to a preliminary suspicion that the achievement of this characteristic might possibly be simultaneously achievable with the cool flame arresting reverse reaction. However, all the models that were formulated to combine the cool flame hook

and the cool flame arrest resulted in poor agreement with the detailed simulation data. Models of this form that were tuned to fit the cool flame hook predicted overly high cool flame heat release, while fitting of the cool flame heat release resulted in the cool flame hook shifting to lower temperatures (overly retarded cool flame timing in the intermediate temperature region). It was therefore concluded that these two characteristics would need to be controlled by separate reactions.

The post cool flame enhanced reactivity requirement was regarded as an obvious area of potential improvement for the new global model formulation, especially since the need for this characteristic has been so clearly illustrated in [1].

6.4.2. Dominant chemistry identification

As discussed in Chapter 3, various researchers have studied the detailed and reduced models of alkane reaction kinetics with a view to identifying the dominant reaction pathways. In view of the auto-ignition behavioural study presented in Chapter 4, the alkane oxidation schematic presented by Zhao et al. [2] was revisited in order to distil insight regarding an optimal formulation for the new functional global model. This schematic is repeated in below for ease of reference.

Low temperature chemistry (<600K at 1atm)

1. $RH + O_2 \Rightarrow R\bullet + HO_2\bullet$ (fuel hydrogen abstraction by oxygen to form alkyl and hydroperoxy radicals)
2. $R\bullet + O_2 \Rightarrow$ olefin $+ HO_2\bullet$ (2^{nd} hydrogen abstraction by oxygen to form conjugate olefin & hydroperoxy radical – slow at low temperatures)
3. $R\bullet + O_2 \Leftrightarrow RO_2\bullet$ (oxygen addition to form alkylperoxy radical – temperature and pressure sensitive equilibrium reaction: forward rate is fast for all temperatures, reverse reaction is fast only at high temperatures)
4. $RO_2\bullet \Rightarrow \bullet ROOH$ (internal isomerisation to form hydroperoxyalkyl radical)
5. $\bullet ROOH \Rightarrow$ CARBONYL $+ R'\bullet + OH\bullet$ (decomposition to lighter alkene or cyclic ether and hydroxyl radical)
6. $\bullet ROOH + O_2 \Leftrightarrow \bullet OOROOH$ (oxygen addition to form hydroperoxyalkylperoxyl radical - small heat release)
7. $\bullet OOROOH \Rightarrow HOOROOH$ (internal hydrogen abstraction of hydroperoxyalkylperoxyl to form alkylhydroperoxide)
8. $HOOROOH \Rightarrow RCHO + R'O + 2\ OH\bullet$ (decomposition to form aldehyde and 2 hydroxyl radicals - small heat release)

Intermediate temperature chemistry (650 - 700K at 1atm)

9. $RH + HO_2\bullet \Leftrightarrow R\bullet + H_2O_2$ (fuel hydrogen abstraction by hydroperoxy radicals to form hydrogen peroxide – forward rate is pressure dependent)
10. $H_2O_2 + M \Rightarrow 2\ OH\bullet + M$ (decomposition of hydrogen peroxide to form hydroxyl radicals – reaction rate is strongly dependent on peroxide concentration)

High temperature chemistry (>800 K at 1atm)

11. $RH + OH\bullet \Rightarrow R'\bullet + R''\bullet + H_2O$ (fuel pyrolysis at high temperature– small heat release)
12. $R'\bullet + R''\bullet + H_2O \Rightarrow CO + H_2O$ (hydroxyl radicals reacting to form carbon monoxide – small heat release)
13. $CO + H_2O \Rightarrow CO_2 +$ heat (carbon monoxide reacts to form carbon dioxide - large heat release)

Viljoen et al. [55] used density function theory to examine dominant reaction pathways and made a convincing argument for the hydrogen abstraction of the alkylperoxy radical being the rate determining step in the low temperature chemistry of alkanes. This reaction is presented as reaction 4 in the schematic above. Other researchers [36;71;76] have found that differences in the ignition quality of alkane fuels can largely be addressed by changing the reaction rate parameters of this reaction. This reaction therefore seemed an appropriate choice for controlling the cool flame heat release timing in the new functional global model.

According to the schematic, the preceding reaction 3 (oxygen addition to form the alkylperoxy radical) is a temperature and pressure sensitive equilibrium reaction, whose forward rate is fast for all temperatures, while the reverse reaction is fast only at high temperatures. This reverse reaction therefore seemed an appropriate choice of reaction for controlling the cool flame hook characteristic.

The only remaining reverse reaction in the low temperature chemistry section of the schematic, was the reverse reaction of reaction 6 - the oxygen addition to form the hydroperoxyalkylperoxyl radical. This reverse reaction was therefore chosen to control the arrest of the cool flame heat release.

The high temperature chemistry rate limiting reaction is generally agreed [2;43-45;47] as being reaction 9 in the schematic - fuel hydrogen abstraction by hydroperoxy radicals to form hydrogen peroxide. This reaction is slow at low temperatures and is also pressure dependent.

The post cool flame enhanced reactivity was addressed by assuming that the reverse reaction of the schematic's reaction 6 (the cool flame heat release arrest reaction) traps the hydroperoxyalkyl radicals in the low temperature chemical pathway and that the dominant alternative pathway is the decomposition of hydroperoxyalkyl radicals to lighter alkenes or cyclic ethers and hydroxyl radicals. This reaction is represented as reaction 5 in the schematic. It was simultaneously assumed that this reaction is more reactive than reaction 9 (the high temperature chemistry rate limiting reaction) at temperatures typical of the cool flame ceiling temperature. Reaction 5 can only feature in reactions that start at relatively low temperatures (below ~800-950K – depending on the fuel) since the reverse reaction 3 blocks the low temperature chemistry pathway for experiments that are started at relatively high temperatures (above ~800-950K – depending on the fuel). The enhanced cool flame reactivity was therefore assumed to be achieved by the trapped hydroperoxyalkyl radicals reacting through reaction 5 and triggering the high temperature chemistry through the enhanced availability of the very reactive hydroxyl radicals.

The heat release of the cool flame and the early stages of the main heat release were assumed to occur through the formation of carbon monoxide, which was assumed to be formed through the decomposition of the alkylhydroperoxide and/or ketohydroperoxide species in the low temperature pathway and hydrogen peroxide in the high temperature pathway. Zhao et al indicated [2] that the decomposition of these species yields the very reactive hydroxyl radicals which in turn undergo rapid chain branching and decomposition reactions to ultimately form carbon monoxide, water and carbon dioxide with the associated significant release of thermal energy. The concentrations of the alkylhydroperoxide/ketohydroperoxide and hydrogen peroxide species were therefore regarded as important in the reaction rates of reactions forming carbon monoxide and water.

The important final chain branching reactions resulting in the main heat release are referred to in chapter 3, but were not dealt with in detail in this thesis, since the compact formulation of the new functional global model required use of only the most critical species. The formation and dissociation of carbon monoxide and carbon dioxide were therefore treated in a lumped global manner similar to the approach taken in the global model developed by Zheng et al. [49].

The reversible reactions between carbon monoxide and carbon dioxide are temperature dependent such that they only reach fast equilibrium at high temperatures [13]. This means that carbon monoxide formed during the cool flame reaction does not rapidly react further to form carbon dioxide until additional carbon monoxide (and associated heat release) is produced through the high temperature chemistry. This approach was supported by preliminary analysis of species concentrations from detailed chemical kinetic simulations as shown in Figure 6.1 below. The logarithmic concentration scale should be noted with regard to the fact that while carbon dioxide is formed during the cool flame heat release, these concentrations are negligible compared with its later formation during the main heat release.

The process of development of the new functional global model progressed through several iterations before arriving at a satisfactory formulation. Two of the preliminary model formulations are presented in the sections below. Although they do not necessarily conform to all of the principles discussed previously, they do illustrate part of the process through which the final model formulation was achieved.

These preliminary model formulations and the final functional global model formulation were implemented as is described in the following Chapter 7.

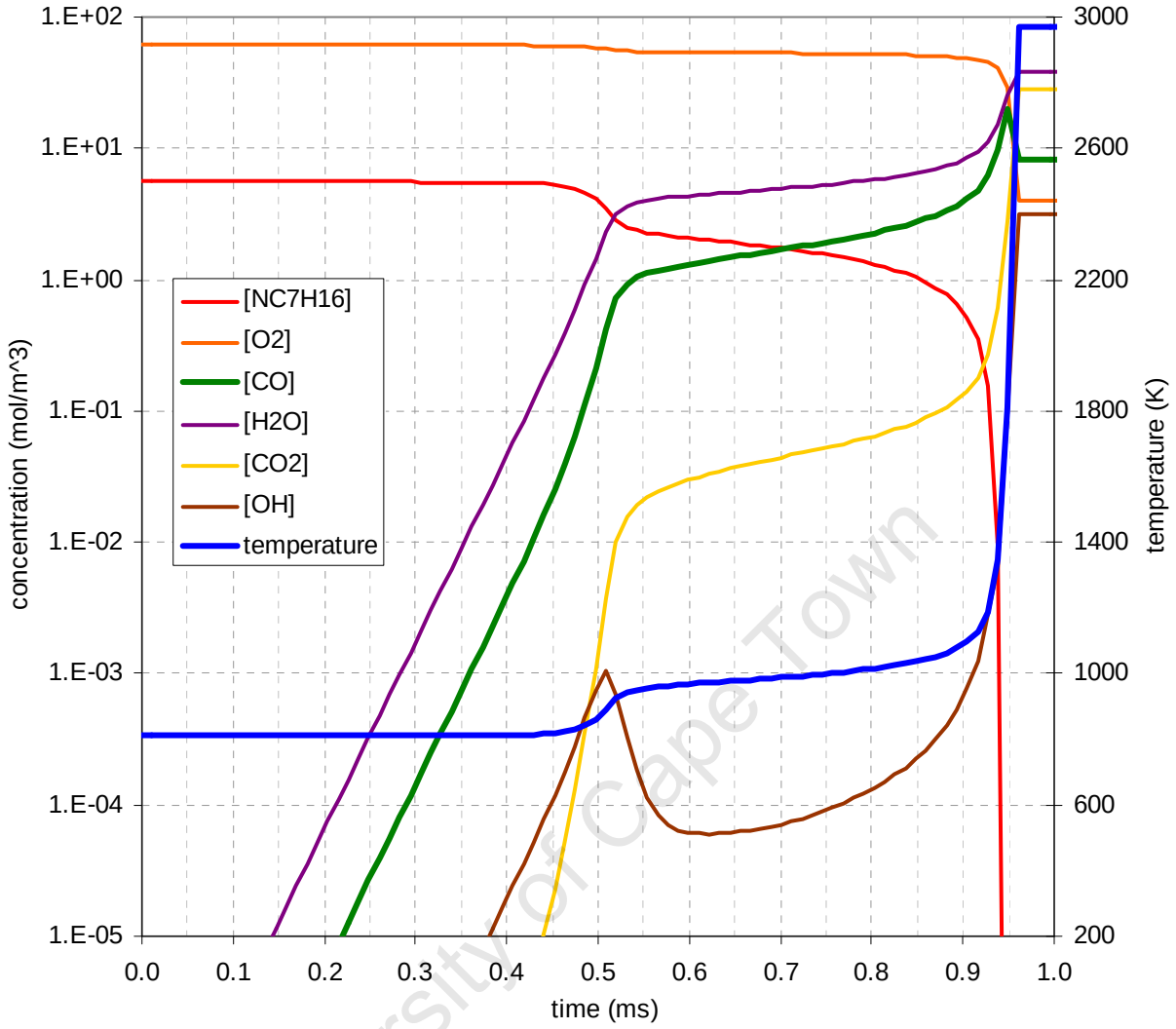

Figure 6.1: Temperature and concentrations during the constant volume oxidation of n-heptane at T=810K, P_i=20bar, phi=1.0, R=0%

6.4.3. First example of a preliminary global model formulation

A schematic example of a considered global model formulation is given in Figure 6.2 below. In this schematic the letter symbols are representative of species classes as follows:

F: fuel, oxygen and the alkyl radical pool
J: alkylperoxy radical pool
I: hydroperoxyalkyl radical pool
CO: carbon monoxide and water (and preceding hydroperoxyalkylperoxyl and alkylhydroperoxide and/or ketohydroperoxide radical pools)
Q: carbonyl, lighter alkenes and ethers
Y: hydrogen peroxide (which decomposes and reacts with other species to eventually form CO)
CO_2: carbon dioxide

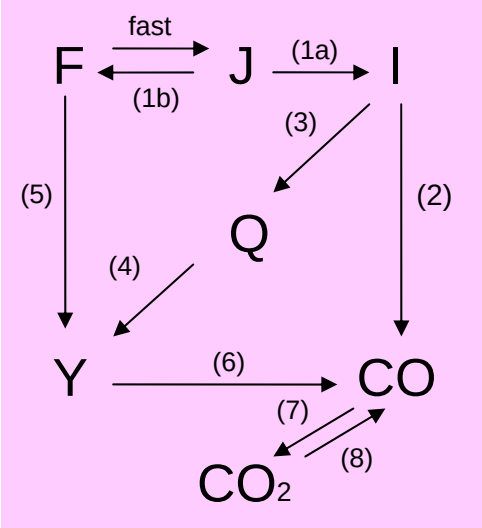

Figure 6.2: Schematic of the first example preliminary global model formulation

This model formulation used the various reactions to fit the alkane kinetic behaviour as follows:

Reaction 1a: the cool flame ignition delay
Reaction 1b: the cool flame hook
Reaction 2: the cool flame heat release
Reaction 3: the cool flame arrest
Reaction 4: the post cool flame ignition delay
Reaction 5: the high temperature ignition delay
Reaction 6: the first phase of the high temperature heat release
Reaction 7: the second phase of the high temperature heat release
Reaction 8: the control of the adiabatic flame temperature by dissociation effects
Each of the reactions used the conventional Arrhenius form and the reaction sequence from F to J was simplified to a single two-Arrhenius reaction rate descriptor using an empirical formulation similar to the quasi-steady-state assumption (QSSA) as has been used by other researchers [50;67-70]. The derivation for this simplification is given in Appendix F.

In spite of the crude assumptions and simplifications used in the formulation of the model in Figure 6.2, this model (with suitably solved reaction rate parameters) achieved an excellent fit to n-heptane oxidation behaviour across the temperature range (600 - 1200K) for a fixed initial pressure and fuel equivalence ratio with no inert dilution. One of the reasons for this strong performance was the direct control of the model's behaviour by adjustment of the various reaction rate parameters.

Unfortunately when attempts were made to extend the model's application to a variety of initial equivalence ratios, the model's performance could not be sustained. One of the key reasons for this breakdown was the dynamic nature of the cool flame ceiling temperature. It can be noted from Figure 4.8 that the cool flame ceiling temperature is reduced as the initial mixture is made leaner. If the cool flame arrest is achieved by reaction 3 of this model, then the reaction rate would need to be inversely proportional to the fuel concentration, i.e. the lower the fuel concentration, the higher the rate of reaction 3, the lower the cool flame ceiling temperature. This, however, was not feasible, since it is not chemically defensible and the reaction rate became undefined when fuel concentration was depleted.

6.4.4. Second example of a preliminary global model formulation

A second schematic example of a considered global model formulation is given in Figure 6.3 below. In this schematic the letter symbols are representative of species classes as follows:

F: fuel, oxygen and the alkyl radical pool
J: alkylperoxy radical pool
I: hydroperoxyalkyl radical pool
L: hydroperoxyalkylperoxyl radical pool
Q: alkylhydroperoxide and/or ketohydroperoxide radical pools
Y: hydrogen peroxide, carbonyl radicals, lighter alkenes and ethers
CO: carbon monoxide and water
CO_2: carbon dioxide

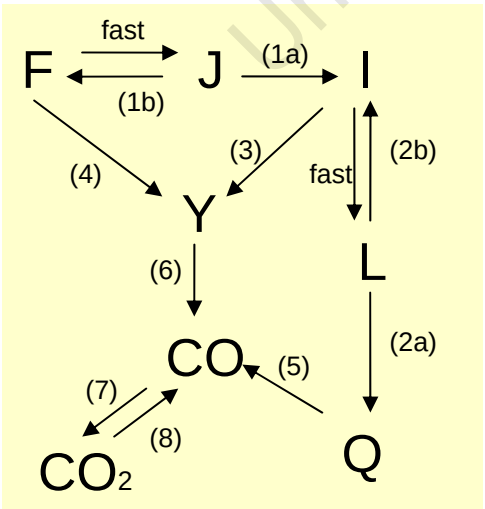

Figure 6.3: Schematic of the second example preliminary global model formulation

This model formulation used the various reactions to fit the alkane kinetic behaviour as follows:

Reaction 1a: the cool flame ignition delay
Reaction 1b: the cool flame hook
Reaction 2a: fast reaction - no specific attribute control
Reaction 2b: the cool flame arrest
Reaction 3: the post cool flame ignition delay
Reaction 4: the high temperature ignition delay
Reaction 5: the cool flame heat release
Reaction 6: the first phase of the high temperature heat release
Reaction 7: the second phase of the high temperature heat release
Reaction 8: the control of the adiabatic flame temperature by dissociation effects

Each of the reactions again used the conventional Arrhenius form and both the reaction sequence from F to J and the sequence from I to Q were simplified to a single semi-empirical two-Arrhenius reaction rate descriptor.

This model formulation was viewed as being neatly representative of the schematic alkane chemistry and the model was also able to achieve a reasonable fit to the kinetic behaviour of n-heptane.

This model, however, had two fundamental problems:
Firstly, the cool flame arrest reaction was not able to shut off the low temperature path as abruptly as needed (within the bounds of reasonable rate parameter values) in order to achieve the required fit to temperature time curves from the detailed kinetics simulations.
Secondly, and more importantly, a similar problem to that of the previously described model existed in that the cool flame ceiling temperature could not be correctly controlled with regard to equivalence ratio effects. Reaction 2b of the model would need to be inversely proportional to the fuel concentration. This was again unsatisfactory, since it was not chemically defensible and the reaction rate became undefined when fuel concentration was depleted. This issue posed a challenge since the only way to make the ceiling temperature proportional to the fuel equivalence ratio was to allow it to affect a *forward* reaction rate in the low temperature chemistry. This in turn posed a significant problem since the cool flame timing prior to the cool flame hook and the post cool flame ignition delay exhibited almost no sensitivity to fuel equivalence ratio as shown in Figure 4.8.

It was also noted that changing the low temperature cool flame timing reaction to 2a, the cool flame hook reaction to 2b and the cool flame arrest reaction to 1b would not alleviate this problem, since this would result in starvation of species “I” during the cool flame arrest stage, thereby resulting in insufficient species concentration for the post cool flame enhanced reactivity via reaction 3. A solution to this dilemma was, however, found for the final model formulation.

6.5. Final model formulation

The final functional global model formulation is given in Figure 6.4 below. In this schematic the letter symbols are representative of species classes as follows:

F: fuel, oxygen and the alkyl radical pool
J: alkylperoxy radical pool
I: hydroperoxyalkyl radical pool
Q: hydroperoxyalkylperoxyl and subsequent alkylhydroperoxide and/or ketohydroperoxide radical pools
Y: hydrogen peroxide, carbonyl radicals, lighter alkenes and ethers
CO: carbon monoxide and water
CO_2: carbon dioxide

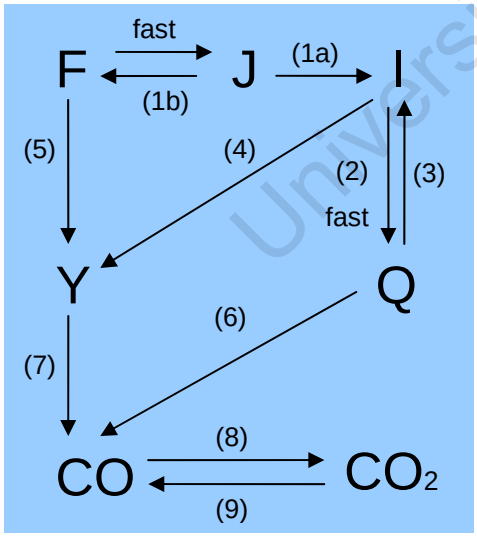

Figure 6.4: Schematic of the final formulation for the new functional global model

This model formulation used the various reactions to fit the alkane kinetic behaviour as follows:

Reaction 1a: the cool flame ignition delay
Reaction 1b: the cool flame hook
Reaction 2: the equivalence ratio effect on cool flame ceiling temperature during the cool flame arrest.
Reaction 3: the cool flame arrest
Reaction 4: the post cool flame ignition delay
Reaction 5: the high temperature ignition delay
Reaction 6: the cool flame heat release
Reaction 7: the first phase of the high temperature heat release
Reaction 8: the second phase of the high temperature heat release
Reaction 9: the control of the adiabatic flame temperature by dissociation effects

Each of the reactions again used the conventional Arrhenius form and the reaction sequence from F to J was simplified to a single two-Arrhenius reaction rate descriptor using the semi-empirical form as previously. The reaction rate equations and reaction "constant" equations are given in Figure 6.5 below.

$$RR_1 = 1/(1/K_{1a} + [F]^{a1}[O_2]^{b1}K_{1b})$$
$$RR_2 = [F]^{a2}[I]^{c2}K_2$$
$$RR_3 = [Q]^{d3}K_3$$
$$RR_4 = [I]^{c4}K_4$$
$$RR_5 = [F]^{a5}[O_2]^{b5}K_5$$
$$RR_6 = [Q]^{d6}[O_2]^{b6}K_6$$
$$RR_7 = [Y]^{e7}[O_2]^{b7}K_7$$
$$RR_8 = [CO]^{f8}[O_2]^{b8}K_8$$
$$RR_9 = [CO_2]^{g9}K_9$$

$$K_{1a} = A_{1a}e^{B_{1a}/T}$$
$$K_{1b} = A_{1b}P^{n_{1b}}e^{B_{1b}/T}$$
$$K_2 = A_2P^{n_2}e^{B_2/T}$$
$$K_3 = A_3e^{B_3/T}$$
$$K_4 = A_4e^{B_4/T}$$
$$K_5 = A_5P^{n_5}e^{B_5/T}$$
$$K_6 = A_6P^{n_6}e^{B_6/T}$$
$$K_7 = A_7P^{n_7}e^{B_7/T}$$
$$K_8 = A_8e^{B_8/T}$$
$$K_9 = A_9e^{B_9/T}$$

Figure 6.5: Reaction rate equations and reaction rate "constant" equations for the final functional global model

This model formulation exhibited very good agreement to a number of 2-stage ignition fuels, through a wide range of temperatures, pressures, fuel equivalence ratios and inert exhaust product dilution. Examples of this agreement can be found in Appendices G and H.

The challenge of obtaining the correct cool flame ceiling temperature sensitivity to fuel equivalence ratio, while maintaining the correct insensitivity of both the low temperature cool flame ignition delay and the enhanced post cool flame ignition delay, was achieved as follows:

- The insensitive cool flame ignition delay was achieved by making reaction 1a fairly insensitive to fuel concentration.
- The insensitive enhanced post cool flame ignition delay was achieved by making reaction 4 insensitive to fuel concentration.
- The sensitivity of the cool flame ceiling temperature to fuel concentration was achieved by making reaction 2 sensitive to fuel concentration. The Arrhenius parameters for this reaction rate were chosen to ensure that this reaction remained faster than reaction 1a, thereby ensuring that reaction 1a (with its negligible fuel concentration sensitivity) remained the rate limiting step determining the low temperature cool flame ignition delay.
- However, at higher temperatures during the cool flame reaction, the reverse reaction 3 was set up to slow down the low temperature chemical pathway and arrest the cool flame heat release.
- The effect of reaction 3 during the cool flame arrest therefore changed the rate limiting reaction in the low temperature chemical pathway from the F to I sequence, to the I to Q sequence, thereby bringing into effect the previously ineffective sensitivity of the low temperature pathway to fuel concentration.

It may be argued that this solution is not chemically defensible since reaction 2 essentially represents the internal hydrogen abstraction of hydroperoxyalkylperoxyl to form alkylhydroperoxide and this reaction is unlikely to be directly affected by fuel concentration. There is no good defense for this objection, other than the fact that on the whole, this formulation still remains representative of the basic schematic of alkane oxidation chemistry and the formulation allows excellent agreement between the global model and the numerous behavioral requirements of the detailed chemical kinetic simulation data across a wide range of 2-stage fuels, temperature, pressure, fuel equivalence ratio and inert dilution as shown in Appendix G.

7. Implementation of the functional global model

7.1. Overview of the computational implementation

The process of formulation of the new functional global model required significant development in terms of the form of the reaction scheme, the reaction rate formulations, plotting of model and data outputs, parameter solvers and parameter variation effect visualisation in real-time. For these reasons, Microsoft Excel 2003 was chosen and used with its powerful VBA functionality to investigate the various model formulations, solve the model simulations and optimise the model parameters.

The models were set up in Excel using separate sheet modules for thermo-chemical data, stoichiometry calculations and calculation of the reverse reaction constant parameters and equilibrium constant for the carbon monoxide dissociation reaction using Gibbs free energy principles. Additional separate sheet modules were used for solving each separate condition of constant volume ignition delay experiment and comparison with its detailed simulation data (solved separately in Chemkin). The experiment sheets were formulated to solve in a pseudo-explicit manner without using the solver or goal-seek functions in Excel and rather coding user-defined worksheet functions in VBA to use secant method solvers or perform complex logic controlled calculations where values could not be easily solved analytically. VBA code for these user defined functions is given in Appendix H.

This format allowed numerous experiments under different conditions to be solved simultaneously in real-time, thereby allowing visualisation of parameter effects across ranges of conditions for a given fuel. The computational efficiency of the implementation was such that a model solving 48 separate experiment conditions could be achieved in less than 6 seconds on a standard office computer. This format also allowed optimisation of the model parameters across the range of temperature, pressure, fuel equivalence ratio and inert dilution conditions for a given fuel. This parameter solving time depended strongly on the proximity of the initial parameter values to their final optimised values, but if structured and progressive manual manipulation of the parameters was done prior to numerical optimisation, the optimisation solving could usually be achieved on a set of 48 experiment conditions within 24 hours.

The Excel implementation also made extensive use of VBA macros for importing and sorting the data from the detailed kinetic simulations, various model parameter solving strategies, and plotting the model and detailed kinetic data results. The coding of these macros is given in Appendix H.

7.2. Thermo-chemical calculation principles

Calculation of the thermo-chemical parameters used in the global models was approached in the same manner used in the discrete engine model described in Chapter 5. Temperature dependent specific heats, enthalpy, entropy, Gibbs energy and internal energy parameters were therefore calculated using the polynomial expressions described previously. Since the global model made use of classes of intermediate species rather than specific species and since the formation of these species from fuel and oxygen liberates relatively little thermal energy compared to the formation of carbon monoxide, water and carbon dioxide, these intermediates were treated as fuel molecules in terms of their thermo-chemical properties.

Solving of the temperature dependent thermo-chemical values for the individual species and the mixture as a whole at each time step was achieved through the use of user defined worksheet functions. These functions allowed logical operations such as selection of the correct polynomial coefficients according to the given temperature range. These functions also allowed detailed calculations such as temperature dependent mixture internal energy to be efficiently calculated in a single cell for each time step. The coding of these functions is given in Appendix H.

7.3. Chemical kinetics principles

Chemical kinetic reaction rates were calculated according to the standard Arrhenius form shown in Equation 7.1 below.

$$\frac{d[\text{Product}]}{dt} = [\text{reactant 1}]^{a}[\text{reactant 2}]^{b} A\ P^{n}\ e^{B\ /T}$$

Equation 7.1: Standard Arrhenius reaction rate expression

Where:

A: pre exponential factor

P: pressure

B: exponential factor (nominally representative of activation energy divided by the universal gas constant)

As mentioned in the previous section, the quasi-steady-state assumption was used to simplify the sequence of fast equilibrium chemistry followed by slow forward reactions. Details of this assumption and its derivation can be found in [50;67-70]and Appendix F.

7.4. Numerical solving strategies

7.4.1. Adaptive time-stepping algorithm

One of the challenges of solving chemical kinetics models is the “stiffness” of the coupled differential reaction rate equations. This generally requires the use of specialised solving strategies such as Green’s method [50] or Gear’s method [49]. A simple numerical adaptive time-stepping algorithm was developed for this study. The algorithm selected the smallest iterative time-step from the following four criteria:

1. A default time-step calculated by dividing the overall ignition delay of the detailed kinetic simulation by a user defined number (e.g. 50). This criterion provided resolution to temperature-time plots in regions of negligible heat release.

2. The maximum time step possible was calculated for each reaction such that the reactant concentration/s were depleted. The smallest time-step value from these calculations was the value used for this criterion. This criterion provided protection against negative species concentrations being produced by overly large time-steps. More conservative depletion strategies were investigated. However this total depletion approach allowed robust temporal progress and yielded acceptable accuracy.

3. The rate of temperature increase was calculated for the current time and the time step producing a user defined temperature resolution (e.g. 20K) was calculated. This criterion provided resolution to temperature-time plots in regions of rapid heat release.

4. Using the rate of temperature increase from the current and previous time steps, the angular difference between these rates was defined in the temperature-time domain and used with a user defined arc length to calculate a time-step value. This criterion essentially provided resolution to temperature-time plots in regions of rapid change from low heat release rates to high heat release rates.

This simple algorithm provided efficient, robust and relatively accurate solving of the model kinetics within a typical maximum of 100 time steps. Although the solver was not validated against other existing solvers, the consistent performance and agreement to detailed kinetic solution indicated reliable performance. The coding of this function is given in Appendix H.

7.4.2. Numerical fitness function definition and solver strategy

The new functional global model was targeted at fitting the cool flame timing, the cool flame heat release magnitude, the overall ignition timing and the general overall shape of the temperature-time plot from the detailed kinetic simulations. Adiabatic flame temperatures were controlled to some degree by the carbon dioxide dissociation equilibrium reaction, but since this equilibrium is controlled by the Gibbs energy parameters and since other dissociation reactions such as the “water-gas shift” reaction were not included, the modelled adiabatic flame temperatures were slightly over predicted. Prediction of the flame temperature was, however, significantly better than would have been the case if carbon dioxide dissociation had not been included.

The numerical fitness function used for optimisation of the model parameters was defined by a normalised integration of the difference between the temperature-time plots of the model and detailed kinetic simulations as shown in the schematic Figure 7.1 below:

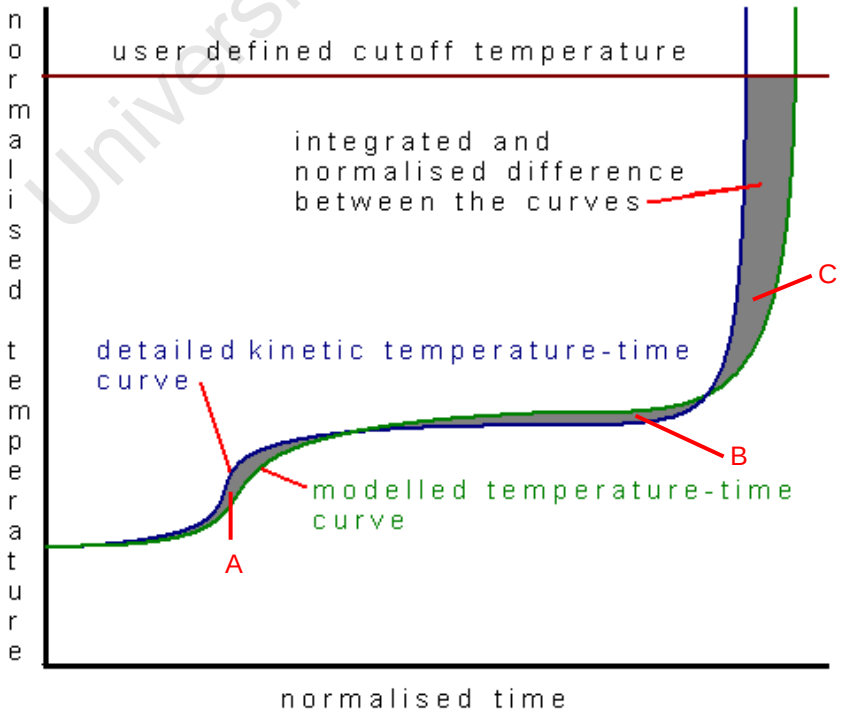

Figure 7.1: Schematic of the numerical fitness function

The definition of the fitness function was normalised using the overall ignition delay time and adiabatic flame temperature of the detailed kinetic simulations. The user defined cut off temperature allowed the fitness function to be weighted between the cool flame and main ignition delays according to the user's preference. A cut off temperature of 1500K was generally used. The coding of the fitness function is given in Appendix H. Care was required using the fitness function since behavioural characteristics were not always easily resolved by its use. As an example referring to Figure 7.1 above, the cool flame ceiling temperature may be difficult to solve since the fitness function allows a trade-off between the integrated areas A and B. These trade-off challenges were addressed by sometimes solving for specifically identified features on the temperature–time profiles, such as cool flame ignition delay, cool flame ceiling temperature and overall ignition delay. These features also, however, sometimes held challenges in terms of their definition.

7.4.3. Model parameter solving strategy

Solving of the model parameters in order to optimise the agreement with the detailed kinetic simulation results proved challenging due to the extreme non-linearity of the model's mathematics. The model reaction rate parameters were therefore solved in three sequential phases:

Phase one

In the first phase, the parameters were adjusted manually using "spin buttons" set up in the Excel model for this purpose. This phase was executed in a progressive fashion using the following order:

1. The low temperature cool flame timing (prior to the cool flame hook) and fuel consumption of the low temperature chemical pathway were adjusted using the parameters of reactions 1b and 6. Other model parameters were made suitably large or small so that they did not affect the function of these reactions during this sub-phase.

2. The cool flame hook behaviour was then fitted using the parameters of reaction 1b.

3. The arrest of the cool flame was then produced by adjusting the parameters of reaction 3 and the cool flame ceiling temperature fitted by adjustment of these parameters.

4. The high temperature ignition delay and fuel consumption rate during this delay were then introduced and fitted using the parameters from reactions 5 and 7.

Steps 1 -4 above resulted in the typical “S curve” of 2-stage fuels with a good fit of the low and high temperature regions. The intermediate region showed retarded overall ignition delay due to the lack of enhanced post cool flame reactivity.

5. The post cool flame ignition delay was then enhanced using the parameters of reaction 4 to produce a good fit to the entire 2-stage ignition delay curve.

6. Parameters of the carbon monoxide oxidation reaction 8 were estimated based on literature values and the reverse reaction parameters were calculated via calculation of the equilibrium constant.

Phase two

In the second phase, the Arrhenius “A” and “B” pair parameters of each reaction rate expression were solved in turn to optimise the behavioural characteristic relevant to the reaction:
e.g. the Arrhenius “A” and “B” pair of reaction 1a was solved to optimise the low temperature cool flame ignition delay, the Arrhenius “A” and “B” pair of reaction 1b was solved to optimise the position of the cool flame hook, etc.

Phase three

A macro was written in VBA to optimise the fitness function by solving each of the reaction rate parameters separately and sequentially. The macro made use of the standard secant method solver in Excel. This method of sequential single variable solving is much slower than the conventional multivariable use of this solver function. However, due to the extreme non-linearity of the coupled Arrhenius rate equations, this method was found to be robust and capable of parameter optimisation. The coding of this macro is given in Appendix H.

8. Model calibration

8.1. Choice of data domain and population

Due to the computational expense of solving the model's reaction rate parameters, the total population of experiments used in this procedure was limited to 48 experiments. These experiments were therefore carefully selected for each fuel, to allow as wide a range of parameter variation as reasonably possible. Due to the complex behavioural sensitivity of 2-stage fuel auto-ignition to temperature, 8 temperature data points were selected for each condition of pressure, fuel equivalence ratio and inert dilution ratio. The selection of these 8 data points is shown in Figure 8.1 below

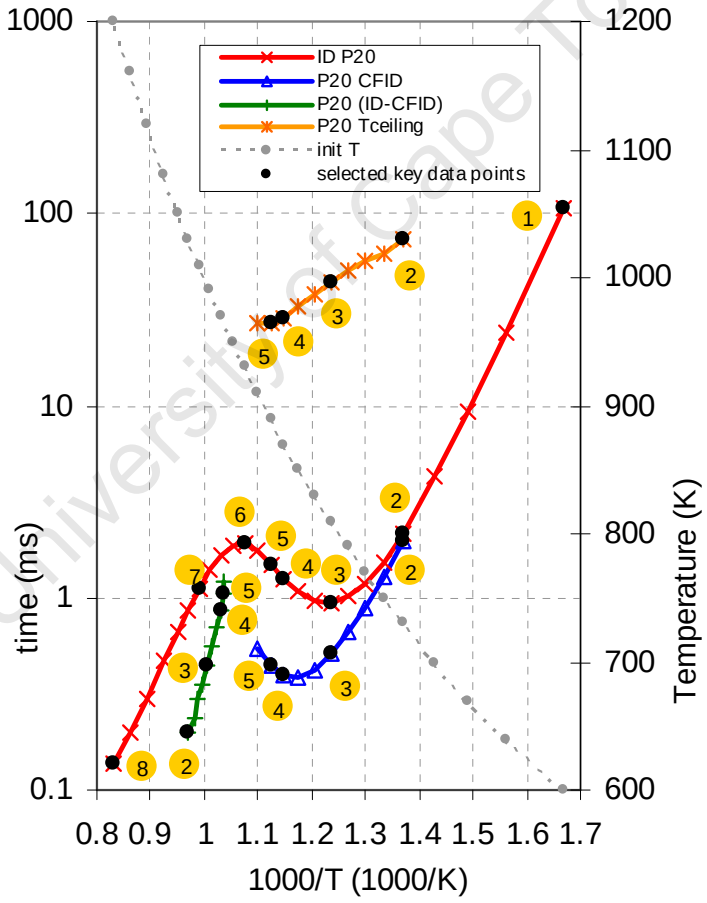

Figure 8.1: Selected key data points for n-heptane at P_i=20bar; Phi=1.0; R=0%

Figure 8 above indicates the positions chosen for key data points used in the solving of reaction rate parameters for 2-stage ignition fuels. Starting from the low temperature side, the selected key data points defined critical behavioural points as follows:

Point 1: Anchored the low temperature cool flame and overall ignition delay position.
Point 2: Defined the slope of the overall ignition delay and the start of a distinct cool flame heat release.
Point 3: Defined the start of the NTC behaviour in the overall ignition delay.
Points 4 & 5: Defined the slope of the cool flame hook (with due care to ensure that a distinct cool flame heat release was discernable)
Point 6: Defined the end of the NTC behaviour in the overall ignition delay.
Points 7 & 8: Defined the slope of the high temperature ignition delay.

The selection of pressure and temperature variables for preliminary model parameter optimisation was defined to be typical of HCCI engine conditions as follows:

1. P = 30bar, Phi = 0.75, R=0%
2. P = 20bar, Phi = 1.0, R=0%
3. P = 20bar, Phi = 1.0, R=0%
4. P = 40bar, Phi = 0.5, R=0%
5. P = 40bar, Phi = 0.5, R=0%
6. P = 20bar, Phi = 1.0, R=40%

This represented a matrix of 48 constant volume experimental conditions that were used to tune the model parameters.

8.2. Use of detailed chemical kinetic simulation data

Detailed chemical kinetics simulations were run for constant volume experiments of n-heptane, iso-octane, 1-hexene, toluene, methanol and a quaternary gasoline surrogate consisting of iso-octane, toluene, hexene and n-heptane in the ratio 44/30/18/8% by moles. Results from these simulations are given in Appendix A. The temperature definition of the auto-ignition delay curves was resolved using 25 selected points for each condition of pressure, equivalence ratio and inert dilution ratio. From these 25 points, the 8 key behaviour defining points were selected. Temperature-time data for these points was reduced to 100 time-steps for each experiment and was used as fitting data for the new functional global model. The new functional global model parameters were then solved as discussed previously.

8.3. Solutions for the new functional global model parameters

Preliminary solutions for optimisation of the model parameters are presented in Table 8.1 below. Units are P (bar), T (K), concentration (mol/m^3) and reaction rate (mol/m^3.s).

	n-heptane	iso-octane	1-hexene	gasoline surrogate	toluene	methanol
ln(A1a) =	23.09	25.98	22.24	25.94	-	-
B1a =	-12300	-14900	-12500	-15100	-	-
a1 =	-0.14	-0.15	-0.13	-0.25	-	-
b1 =	0.922	0.702	0.923	0.702	-	-
ln(A1b) =	20.87	20.1	24.43	14.98	-	-
n1b =	-2.72	-2.71	-2.72	-2.9	-	-
B1b =	-21300	-15200	-21400	-10700	-	-
a2 =	0.986	1.191	0.743	1.154	-	-
c2 =	0.638	0.603	0.589	0.657	-	-
ln(A2) =	24.92	22.94	34.55	23.69	-	-
n2 =	-1.17	-1.17	-1.15	-1.17	-	-
B2 =	-8120	-8110	-8110	-7310	-	-
d3 =	2.853	2.858	2.698	2.343	-	-
ln(A3) =	43.66	42.09	42.59	43.58	-	-
B3 =	-29900	-27800	-27300	-24800	-	-
c4 =	0.05	0.016	0.045	0.05	-	-
ln(A4) =	52.27	37.61	54.82	56.17	-	-
B4 =	-41300	-24400	-36700	-36100	-	-
a5 =	0.983	0.927	0.91	0.878	0.877	0.927
b5 =	0.855	0.854	0.849	0.85	0.834	0.854
ln(A5) =	21.83	21.42	23.03	20.09	22.74	23.36
n5 =	-0.61	-0.58	-0.61	-0.61	-0.61	-0.59
B5 =	-17700	-16600	-19300	-16700	-22100	-20400
d6 =	5.92	5.742	5.58	6.064	-	-
b6 =	0.145	0.166	0.143	0.146	-	-
ln(A6) =	26.59	25.53	27.8	40.84	-	-
n6 =	-0.04	-0.03	-0.04	-0.04	-	-
B6 =	-15800	-16000	-15000	-21700	-	-
e7 =	5.792	3.22	7.375	7.057	7.057	7.057
b7 =	0.141	0.152	0.155	0.165	0.166	0.162
ln(A7) =	12.42	11.52	13.49	13.36	13.34	12.81
n7 =	1.804	1.804	1.804	1.804	1.804	1.804
B7 =	-13600	-14900	-6610	-7150	-6610	-6610
f8 =	3.823	2.727	2.8	2.8	2.8	2.8
b8 =	0.164	0.229	0.23	0.23	0.23	0.23
ln(A8) =	17.27	16.92	18.05	18.05	18.05	18.05
B8 =	-12900	-14000	-13500	-13900	-13900	-13900
g9 =	1	1	1	1	1	1
ln(A9) =	21.74	21.39	22.52	22.52	22.52	22.52
B9 =	-44900	-46000	-45400	-45900	-45900	-45900
overall ID error	17.5%	23.1%	18.9%	19.3%	14.5%	11.3%

Table 8.1: Functional global model parameter values for various fuels

These parameters should be regarded merely as preliminary examples of appropriate values for the rate parameters of the given fuels and not necessarily the optimal solution even for the domain of condition variables considered. Effort during this study was aimed primarily at investigating the model's validity for a variety of fuels rather than the extremely time consuming task of fitting the model to a very wide and detailed set of condition variables. The parameter values should also be regarded as fuel specific solution sets rather than individual chemically representative values.

9. Demonstration of the model's performance

The average absolute percentage error for overall ignition delay between the detailed chemical kinetic simulations and the new functional global model's predictions were defined as previously according to Equation 3.1 and are given in the last line of Table 8.1 of the previous section. These errors should not be regarded as the best fit possible for the model, but merely as preliminary example indications of the model's performance. The agreement may, however, be considered relatively good considering the discrepancies of the detailed chemical kinetic models given in Table 3.2, where a randomly selected n-heptane auto-ignition curve showed an average absolute percentage error for overall ignition delay between the Curran [44] and Mehl [45] detailed mechanisms of 37.8%.

Examples of the comparative overall auto-ignition performance of the new functional global model for n-heptane are given in Figure 9.1 to Figure 9.6 below. Figure key abbreviations are DKM for the detailed kinetic model and FGM for the functional global model. Details of this agreement for other fuels are provided in Appendix G. These figures indicate that the model's agreement with the detailed simulation data breaks down for the cool flame timing prediction under conditions of inert dilution as shown in Figure 9.6.

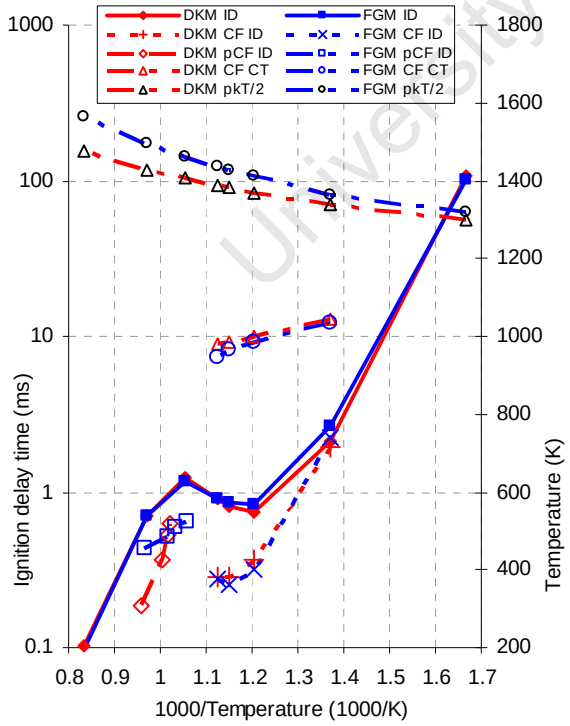

Figure 9.1: Comparison of auto-ignition performance for n-heptane at P_i=30 bar, Phi=0.75, R=0%

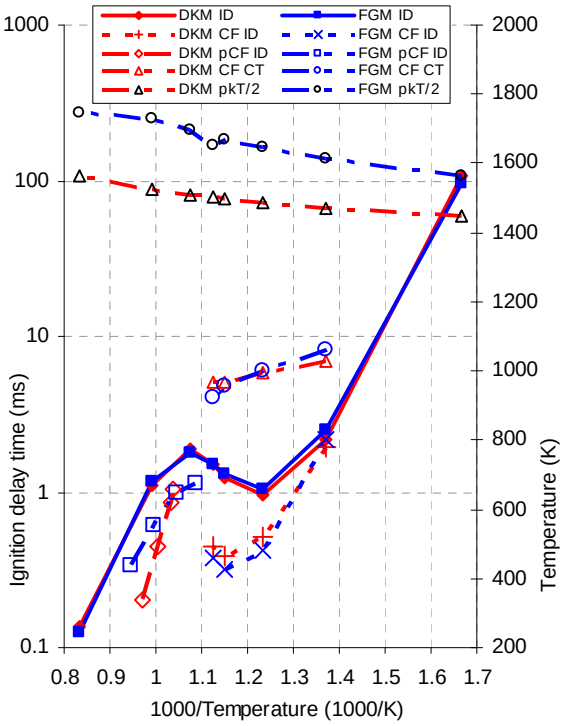

Figure 9.2: Comparison of auto-ignition performance for n-heptane at P_i=20 bar, Phi=1.0, R=0%

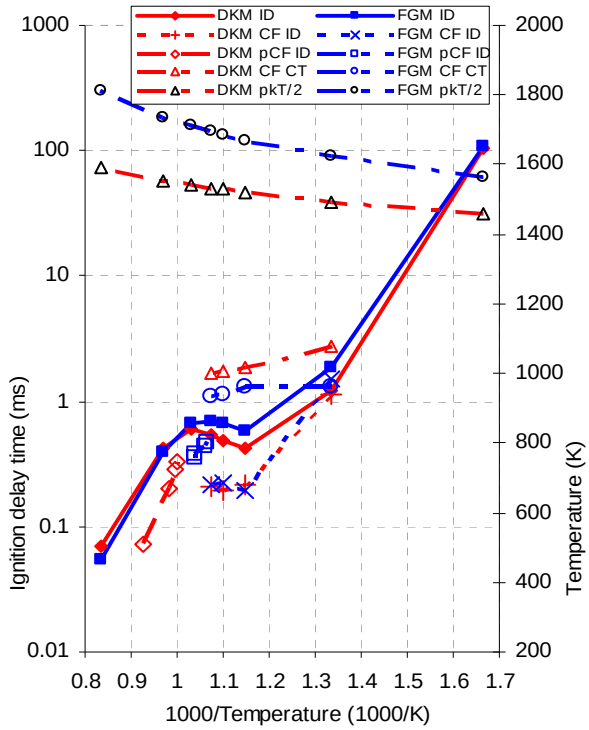

Figure 9.3: Comparison of auto-ignition performance for n-heptane at P_i=40 bar, Phi=1.0, R=0%

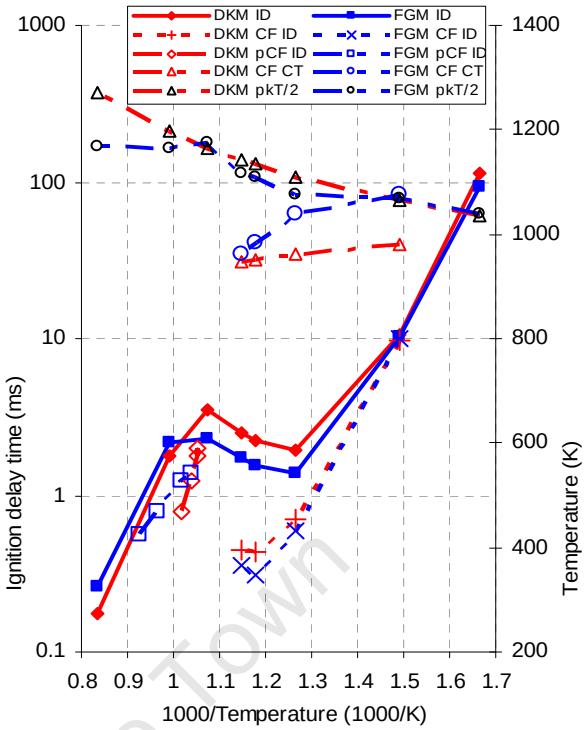

Figure 9.4: Comparison of auto-ignition performance for n-heptane at P_i=20 bar, Phi=0.5, R=0%

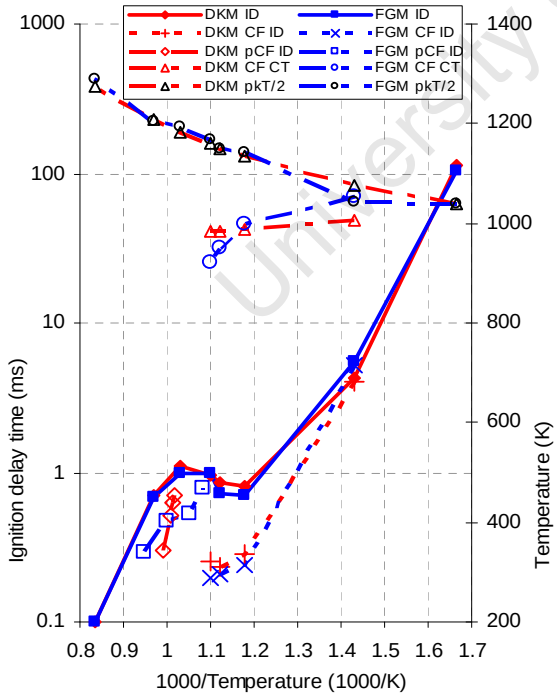

Figure 9.5: Comparison of auto-ignition performance for n-heptane at P_i=40 bar, Phi=0.5, R=0%

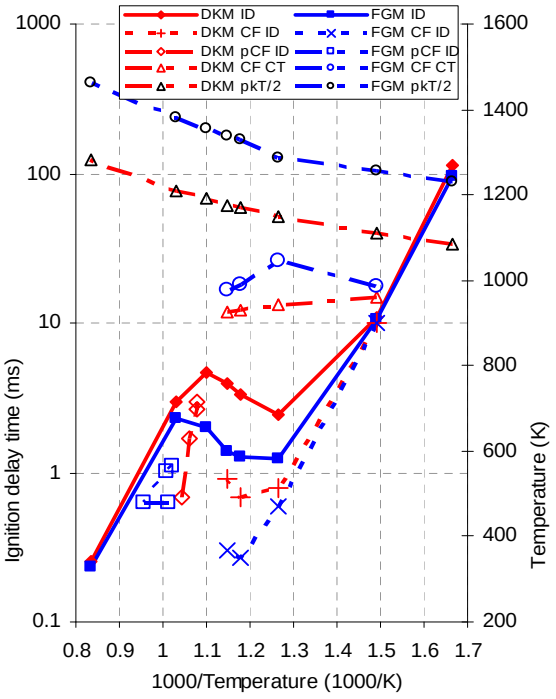

Figure 9.6: Comparison of auto-ignition performance for n-heptane at P_i=20 bar, Phi=1.0, R=40%

Examples of the comparative temperature-time profile performance of the new functional global model for n-heptane are given in Figure 9.7 to Figure 9.14 below. Figure key abbreviations are again DKM for the detailed kinetic model and FGM for the functional global model. Details of this agreement at other conditions and for other fuels are provided in Appendix G. These figures indicate that the model's agreement with the detailed simulation data is generally of good form.

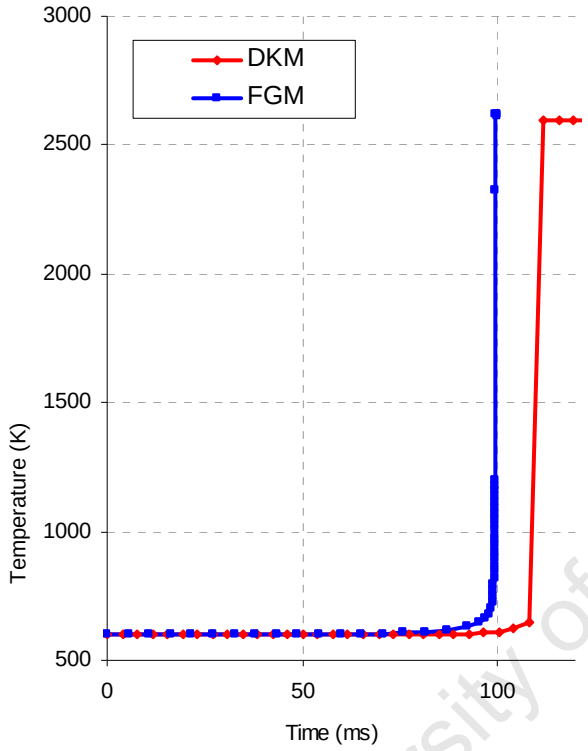

Figure 9.7: Comparison of temperature-time performance for n-heptane at P_i=30 bar, Phi=1.0, R=0%, Ti=600K

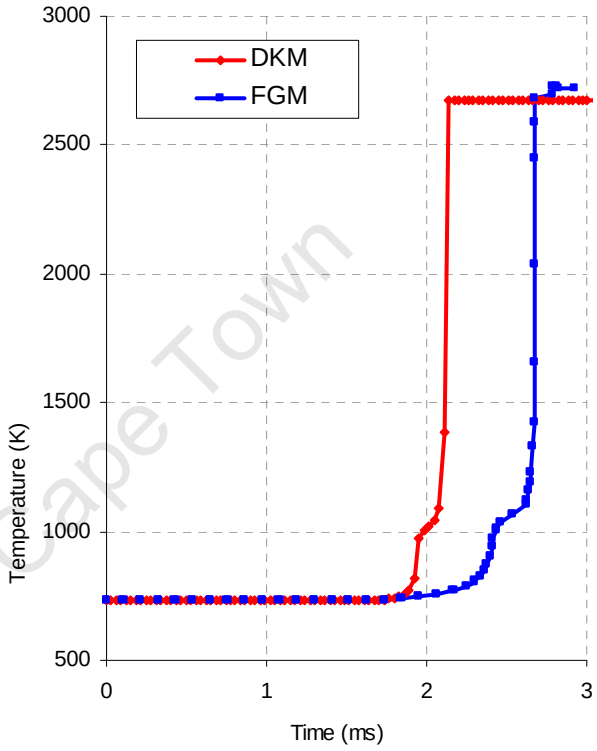

Figure 9.8: Comparison of temperature-time performance for n-heptane at P_i=30 bar, Phi=1.0, R=0%, Ti=730K

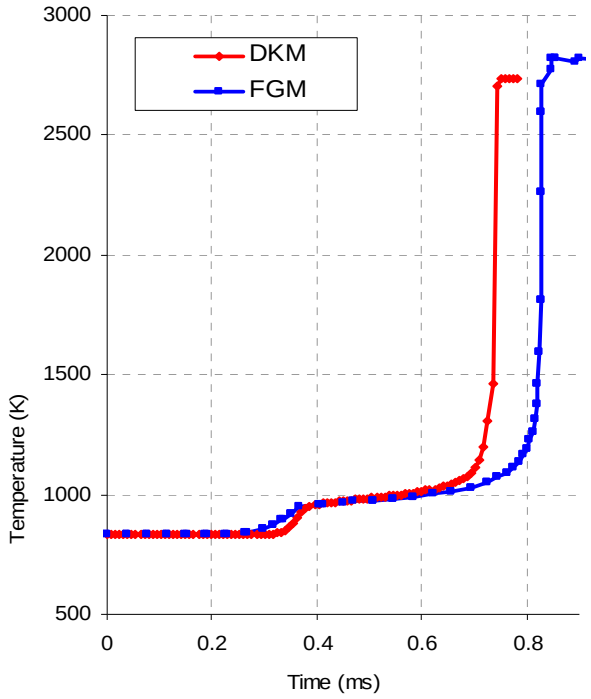

Figure 9.9: Comparison of temperature-time performance for n-heptane at P_i=30 bar, Phi=1.0, R=0%, Ti=830K

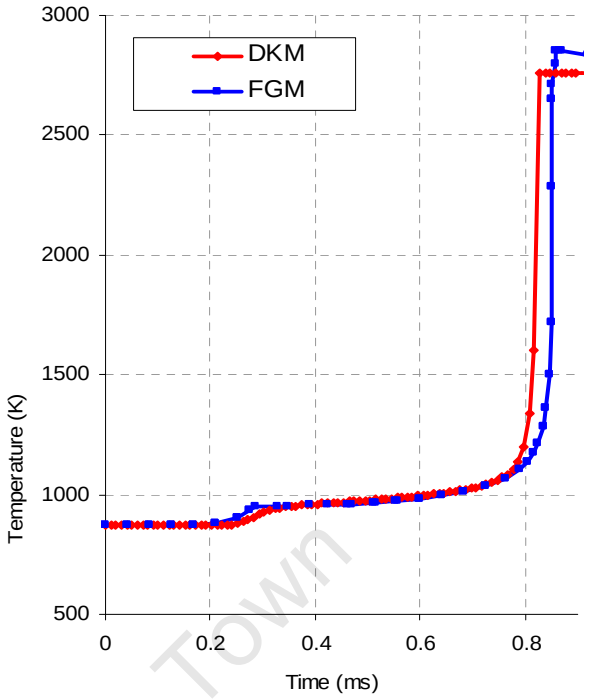

Figure 9.10: Comparison of temperature-time performance for n-heptane at P_i=30 bar, Phi=1.0, R=0%, Ti=870K

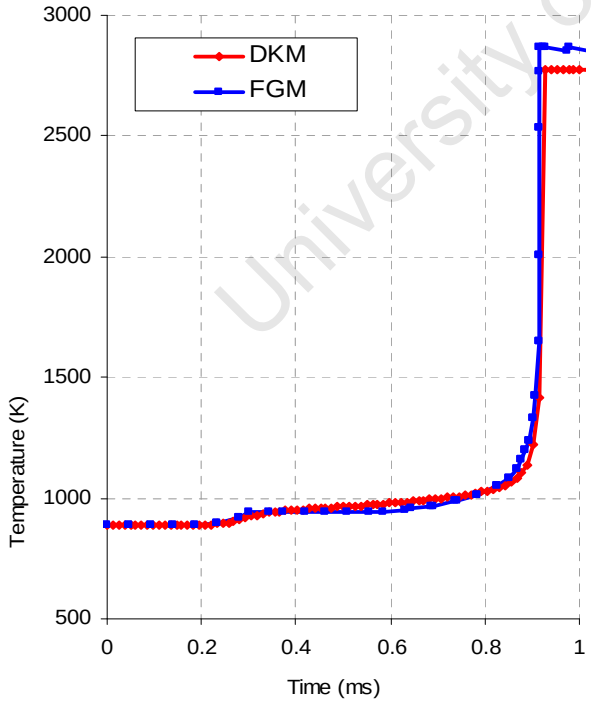

Figure 9.11: Comparison of temperature-time performance for n-heptane at P_i=30 bar, Phi=1.0, R=0%, Ti=890K

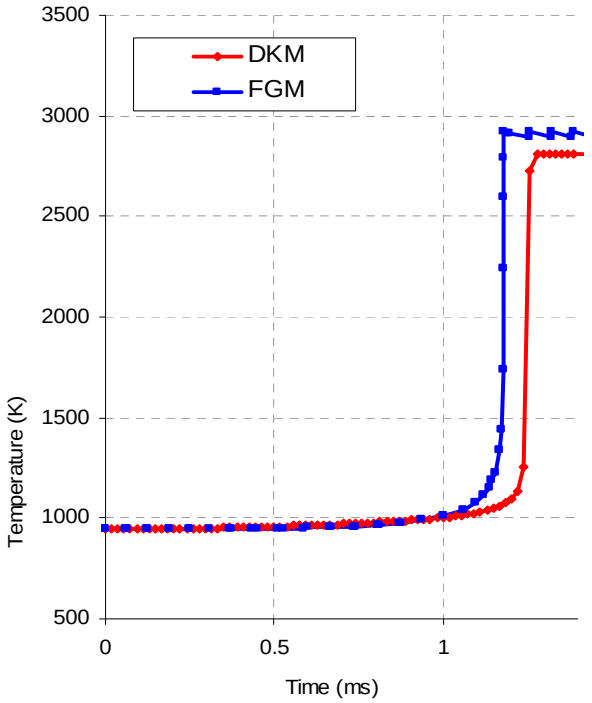

Figure 9.12: Comparison of temperature-time performance for n-heptane at P_i=30 bar, Phi=1.0, R=0%, Ti=950K

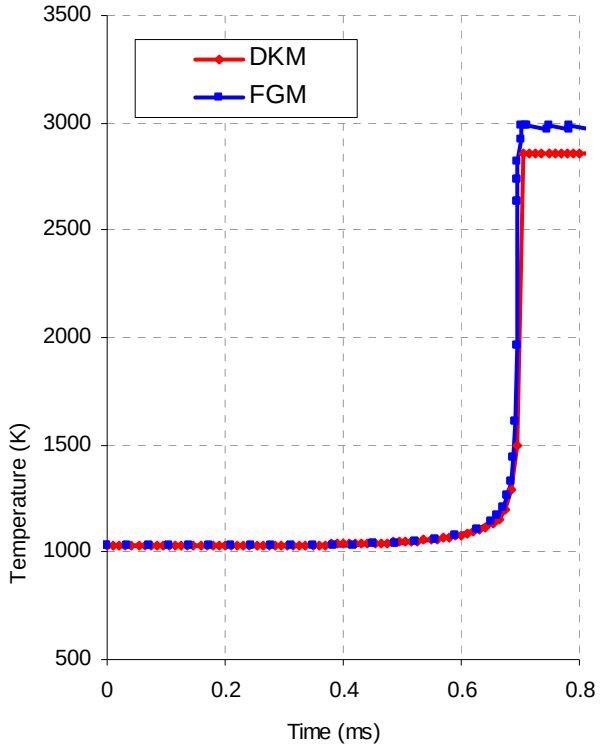

Figure 9.13: Comparison of temperature-time performance for n-heptane at P_i=30 bar, Phi=1.0, R=0%, Ti=1030K

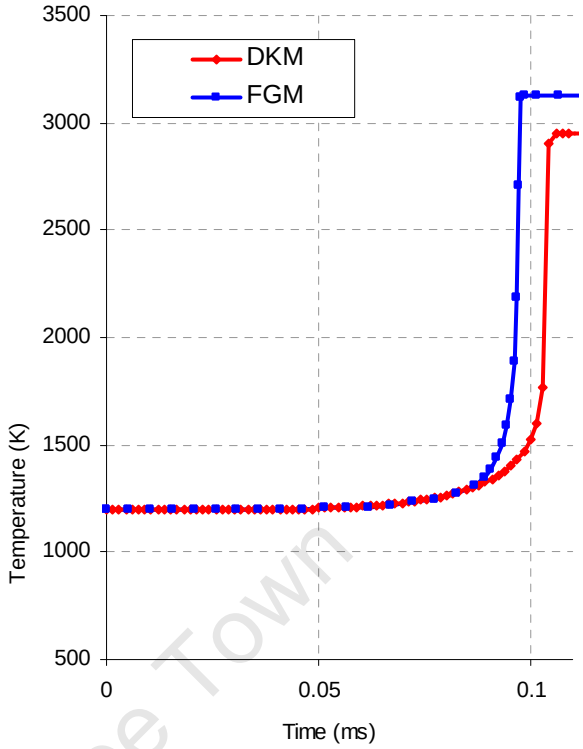

Figure 9.14: Comparison of temperature-time performance for n-heptane at P_i=30 bar, Phi=1.0, R=0%, Ti=1200K

It was noted during the parameter optimisation phase of the model development that the concentration powers of reaction 6 and 7 tended to be slowly reduced by the solving algorithm. This had the effect of smearing the definition of the cool flame heat release and resulting in overly large cool flame burn durations. Interestingly, the definition of the cool flame heat release could usually be recovered without significantly increasing the fitness function error value by manually increasing these concentration powers and then allowing the solver algorithm to operate on only the Arrhenius terms in the model.

10. General discussion

The recently developed empirical fuel auto-ignition model by Yates and Viljoen [1] provided a valuable tool for auto-ignition timing prediction within the HCCI engine modelling context. Application of this model into a single zone, discrete, thermodynamic HCCI engine model provided a reasonably accurate and extremely computationally efficient tool for virtual fuel behaviour investigations in HCCI engines. The even more computationally efficient, but somewhat crudely simplified explicit version of this model allowed HCCI engine operation to be mapped over a wide range of operating conditions for 3 basic fuels with the possibility of further investigations with blends. This investigation provided valuable insight into the complex relationships between fuel auto-ignition characteristics and dynamic in-cylinder environment conditions with particular focus on the pressure and temperature history experienced by a given fuel-air mixture.

Combustion phasing studies conducted with this model yielded valuable information regarding the magnitudes of basic combustion phasing control variables such as inlet temperature, inlet pressure and effects of fuel-equivalence ratio. The model also provided a powerful virtual tool for investigating convergent control parameter phenomenon which had been identified but not fully investigated in previously published experimental work [18]. This convergent behaviour may hold promise for rapid speed and/or load changes in HCCI operation where response times of conventional control systems would be challenges. The discovery of constant combustion phasing speed-load curves within the HCCI operational map holds significant value for rapid transitions in power output without the need for rapid acting control systems. This feature was elegantly demonstrated through the experimental work conducted using the model aeroplane HCCI engine which operates from idle through to high speed wide-open-throttle without any form of combustion phasing control system.

The empirical model used in the early part of this study imposed two limitations on the study. Firstly, the model was not able to capture the chemical effects of residual combustion product gas dilution on HCCI auto-ignition behaviour, although the thermo-dynamic effects could be captured in the engine model formulation. Secondly, the empirical auto-ignition model did not allow the rate of combustion to be studied since the model only predicted the timing of the cool flame and main heat release events as well as the magnitude of the cool flame heat release. These two weaknesses in the early part of the study necessitated finding or developing a rate based model sensitive to exhaust residual effects.

The review of available global auto-ignition models revealed no existing model capable of accurately capturing the effects of cool flame and main heat release subject to the effects of pressure, temperature, fuel equivalence ratio and exhaust residual dilution.

The fuel auto-ignition behavioural study provided a wealth of valuable fuel auto-ignition characterisation data, which some researchers argue to be almost more valuable than its experimental verification [50]. This simulation data along with various published schematics of alkane oxidation proved invaluable to the development process of the new functional global model. The behavioural study also highlighted key areas of weakness in existing global auto-ignition models which guided the development process.

The improved functionality of this new global model in comparison to currently available global models adds significant value to this field of research. In spite of the additional numerical cost of non integer concentration powers, the concise form and associated computational efficiency of the new global model is likely to far out-perform skeletal and reduced chemical kinetic models which may possess similar predictive functionality with regard to 2-stage heat release dynamics. This is an important value addition since it effectively opens the door for computationally efficient 2-stage auto-ignition modelling in the CFD environment. It is acknowledged that the new global model is unlikely to compete with these more complex models with regard to emissions predictive functionality, although scope for such functionality may actually exist for the new global model formulation.

The form of the new functional global model also proved to be flexible enough to adapt to the different fuels to which it was applied. Although specifically formulated to fit alkane fuel behaviour, it was able to fit 1-hexene and a quaternary gasoline surrogate without any changes to the model form. Simple removal of the low temperature chemistry section of the model allowed it to be easily fitted to the methanol and toluene fuels as examples of single stage ignition fuel performance. This flexibility seems to indicate that the model could be fitted to any hydrocarbon fuel with suitable adjustment of the model parameters. This is a valuable attribute, since detailed kinetic models are not able to model full boiling range fuel blends. The fact that the functional global model uses fuel thermodynamic properties for its intermediate species is also an advantage for studies using full boiling range fuels, since the specific dominant intermediate species in the auto-ignition kinetics of full boiling range fuels would be difficult to identify. Use of the new functional global model for auto-ignition simulation of full boiling range fuels would, however, require experimental characterisation of such fuels before the model could be used to simulate them.

The new global model's formulation does appear to exhibit some weakness in the accuracy of its inert exhaust product dilution sensitivity characteristics, particularly in the region of the cool flame hook. This weakness propagated through the formulation resulting in overly advanced overall ignition delays in the NTC region for high levels of exhaust product dilution. It is, however, difficult to compare this weakness to other global and skeletal model performances as published, since these publications generally offer little in the way of detailed validation or performance demonstration.

The use of more complex differential solving strategies and model parameter optimisation algorithms may well result in improved predictive accuracy for the new functional global model. However, the implementation strategy for the new functional global model was valuable for the developmental process, allowing easy manipulation of the model's form and parameters, while also allowing automated solver functionality. The use of Excel does, however, necessitate very careful implementation planning to ensure that the required developmental changes can be made without significant alterations of the set-up in this program. Examples of sound structure include separation of calculations into suitable modules and separation of "experiment calculations" to separate sheets, so that if the model form requires alteration, the altered sheet can be replicated and repopulated with the detailed simulation data in an efficient manner.

The pseudo-explicit approach used for solving the energy equation in the development of the functional global models holds significant potential for use in the engine model. While the simplifying assumptions used in the explicit engine model made this model somewhat crude and possibly subject to inaccuracy, use of these pseudo-explicit methods would allow the original and more accurate discrete model to be solved with similar computational efficiency. This model combined with the new functional global auto-ignition model would provide a powerful virtual tool for the investigation of convergent control and other operational studies on HCCI engines.

A direct comparison of the nature and use of the two fuel auto-ignition models is summarised in Table 10.1below. This table illustrates and contrasts the formulation characteristics, performance attributes and application niches of the two models. Both model formulations have strengths and weaknesses and each should be used in its most suitable application. Both models have also been shown to provide unmatched prediction functionality in their respective classes.

Table 10.1: Summarised comparison of the empirical and functional global auto-ignitions models

		Empirical Auto-ignition Model	**Functional Global Auto-ignition model**
basis	source	- proposed by Yates and Viljoen	- developed in this study
	investigated by	- implementation into an explicit single zone HCCI engine model - wide range virtual operational investigation - experimental validation	- validation against detailed chemical kinetic simulation data - comparison with existing global models
form	mathematical description	- Arrhenius 2-stage empirical model	- Reaction rate based global model
	form advantages	- extreme computational efficiency - simple mathematical function - tuneable to pure components, simple blends and full boiling range fuels	- can be representative of class chemistry - can be easily implemented into CFD - relatively computationally efficient - tuneable to pure components, simple blends and full boiling range fuels - "direct effect" formulation of reaction set, free
	form disadvantages	not easily implemented into CFD models	reaction rate formulation inherently requires numerical solving strategies for the "stiff" coupled differential equation set.
model predictive performance	auto-ignition prediction capabilities	- cool flame ignition delay - cool flame heat release magnitude - main heat release delay	- cool flame ignition delay - cool flame heat release rate - cool flame heat release magnitude - main heat release delay - main heat release rate - main heat release magnitude
	parametric sensitivities	- temperature - pressure - fuel equivalence ratio	- temperature - pressure - fuel equivalence ratio - inert exhaust product dilution
	fuel types	- proven fit to PRF and methanol blends	- proven fit to iso-octane, n-heptane, 1-hexene, toluene, methanol and a quaternary surrogate gasoline blend
	accuracy in comparison to detailed kinetic simulations	~ 11% (excluding extreme air-fuel ratios)	~ 11 - 23% depending on choice of fuel modelled
target implementation		- highly computationally efficient single and multi-zone thermodynamic engine models	- highly computationally efficient single and multi-zone thermodynamic engine models - computational fluid dynamics engine models - crude emissions predictions may be possible

11. Conclusions

Two hydrocarbon fuel auto-ignition models were contrasted in their formulation, predictive accuracy and niche applications.

The first model was a recently published empirical auto-ignition model capable of predicting cool flame ignition delay, cool flame heat release magnitude and overall ignition delay. This empirical model was incorporated into a single zone discrete thermodynamic engine model and a simplified explicit engine model. The latter model was used to study combustion phasing control in HCCI engines. Novel and valuable insights were gained regarding the ability of an HCCI engine to run along fixed speed-load curves while maintaining constant combustion phasing as well as a new method of convergent parameter control. These findings *validated the thesis of the first section of this study* which proposed that valuable synergistic performance could be obtained by studying fuel auto-ignition characteristics and HCCI engine design and operation in a manner which allowed virtual variation of parameters in both areas.

The second model was a new functional global auto-ignition model. Published fuel oxidation schematics, a detailed fuel auto-ignition behavioural study and a critical evaluation of existing global models provided clarity for the formulation requirements of the new functional global model. The behavioural study and analysis of existing global fuel auto-ignition models resulted in identification of key attributes lacking in existing global models such as the “hook” on the cool flame ignition delay curve and the enhanced post cool flame reactivity of two-stage auto-ignition fuels. The formulation of the new functional global auto-ignition model resulted in a computationally efficient model, able to accurately predict heat release dynamics of single and two-stage auto-ignition fuels across a wide range of temperature, pressure, fuel equivalence ratio and inert exhaust product dilution, compared to detailed kinetic simulations. The new functional model exhibited good agreement ranging between 11 and 23% error for the six fuels considered, over the wide range of experimental conditions. This compared favourably with the nominal 38% error seen between successive detailed chemical kinetic mechanisms. This achievement *validated the thesis of the second section of the study* which proposed that a new fully functional global kinetic model could be formulated to predict reaction rate dynamics of two-stage auto-ignition fuels, incorporating prediction of “cool-flame” timing, “cool-flame” heat release magnitude and main heat release timing. The new functional global model did, however, over-predict the adiabatic flame temperature due to the lack of complete dissociation reaction modelling and this aspect of the second study thesis was therefore not fully realised.

The two model studies, although different in approach and scope, enabled a broad and detailed comparison of the two auto-ignition models, thereby highlighting their respective values and limitations. The two models were shown to each possess advantages in the context of HCCI auto-ignition modelling, which were unmatched by existing models of similar classification. The two models were also shown to exhibit drawbacks which played to each other's strengths: The functional global model enabled prediction of heat release rate, but sacrificed a degree of computational efficiency. Both models were shown to be configurable to real world, full boiling range fuels and were able to accurately emulate the dynamics of two-stage auto-ignition with remarkable computational efficiency.

This work revealed potential for unconventional niche convergent control methods in HCCI engines. Such control methods could in theory allow rapid operational transitions without the need for complex combustion control systems. Operation along speed-load curves of constant combustion phasing, could allow HCCI engines to be coupled with electronically controlled CVT drives in order to reduce the complex control systems needed for combustion phasing control.

The development of a new functional global model capable of accurate two-stage fuel auto-ignition predictions proved that simple and concise rate based models can be formulated to accurately model these behaviours for a variety of fuels across a wide variety of conditions. The fact that such models can be form-fitted to experimental data allows full boiling range fuels to be accurately simulated. This opens the door for use of such models in complex CFD HCCI engine models as well as powerful use in simple efficient thermodynamic engine models for the simulation of full boiling range fuels auto-ignition in HCCI engines.

This work therefore moves HCCI technology one incremental step closer to overcoming its combustion control challenges and to commercial realisation of its significant benefits in terms of fuel efficiency and reduced emissions. It is hoped that this work will encourage further research into convergent control methods and the development of improved functional global fuel auto-ignition models.

12. Recommendations for further work

This study has achieved a number of satisfactory preliminary results, but has also highlighted a number of areas in which further work could be done.

The empirical auto-ignition model developed by Yates and Viljoen [1] would benefit significantly if extended to accurately modelling the effects of inert exhaust product dilution on cool flame and main ignition delays as well as cool flame heat release magnitude.

The new functional global model would benefit from additional work on application of the model using appropriate coupled differential equation solving strategies such as Green's method and Gear's method. Additional work could also be done applying suitable parameter optimisation algorithms such as particle swarm and genetic algorithms to this model in order to further optimise the model parameters. While MS Excel formed a versatile programming environment for the initial development of the new functional global model, other programming environments may be more suitable to its optimisation.

Although the effects of pressure, temperature and fuel equivalence ratio appear to be well captured by the new functional global model, a further in-depth auto-ignition behavioural study is needed to gain insight into the effects of the these sensitive variables as well as a study of the sensitivity of auto-ignition to inert exhaust product dilution. This study should be conducted with due consideration to the various dominant chemical kinetic pathways for the given fuel.

While thermal heat release formed the focus of this study for the formulation of the new functional global model, consideration of the detailed kinetics simulated concentration profiles for dominant species could add significant insight into the formulation of the model. Use of these concentration profiles for fitting the behaviour of species represented by the intermediate pseudo-species in the functional global model would add significantly to the chemical kinetic defensibility of the model. Comparisons between the rate parameters values used in detailed kinetic models and those used for representing chemical class reactions could also provide insight for appropriate adjustment of the model parameters and improved chemical kinetic defensibility.

Although use of detailed chemical kinetic simulation data for model fitting and validation is a recognised practise in this field, experimental validation of the new functional global model would certainly add confidence to its validity.

The implementation of the new functional global model into various forms of HCCI engine models is recommended. These engine models could range from computationally efficient models aimed at real time combustion control and high repetition studies of HCCI operational conditions, to complex 3-dimensional computational fluid dynamic simulations. The simpler versions could make use of the pseudo-explicit formulation used in the formulation of the functional global model to avoid unnecessary empiricism and associated deteriorations in accuracy or range validity.

Scope may also exist for investigating the new functional global model's value in terms of carbon monoxide and unburned hydrocarbon emissions prediction. The enhanced reactivity effect of partially burned hydrocarbons on HCCI combustion is another area of potentially valuable application for the new functional global model.

13. References

[1] A. D. B. Yates and C. L. Viljoen, "An Improved Empirical Model for Describing Auto-ignition," in 2008 SAE powertrain, fuels and lubricants conference, SAE 2008-01-1629, 2008.

[2] F. Zhao, T. W. Asmus, D. N. Assanis, J. E. Dec, J. A. Eng, and P. M. Najt, *Homogeneous charge compression ignition (HCCI) engines: key research and development issues*, 1st ed. Warrendale, PA: Society of Automotive Engineers, 2003.

[3] R. Cracknell, J. Ariztegui, K. Barnes, P. Bessonette, W. Cannella, F. Douce, B. Kelecom, H. Kraft, I. Lampreia, D. J. Rickeard, M. C. Savarese, J. Williams, and K.D.Rose, "Advanced combustion for low emissions and high efficiency: a literature review of HCCI combustion concepts," CONCAWE, Brussels, report 4/08, Apr.2008.

[4] A. Kulzer, A. Christ, M. Rauscher, C. Sauer, G. Wurfel, and T. Blank, "Thermodynamic Analysis and Benchmark of Various Gasoline Combustion Concepts," in SAE 2006 World Congress & Exhibition, SAE 2006-01-0231, 2006.

[5] A. W. Berntsson and I. G. Denbratt, "HCCI Combustion using Charge Stratification for Combustion Control," in SAE World Congress & Exhibition, SAE 2007-01-0210, 2007.

[6] M. Sjöberg, J. E. Dec, A. Babajimopoulos, and D. Assanis, "Comparing Enhanced Natural Thermal Stratification against Retarded Combustion Phasing for Smoothing of HCCI Heat-Release Rates," in SAE 2004 Powertrain & Fluid Systems Conference & Exhibition, SAE 2004-01-2994, 2004.

[7] M. Sjoberg, J. Dec, and W. Hwang, "Thermodynamic and Chemical Effects of EGR and Its Constituents on HCCI Autoignition," in SAE World Congress & Exhibition, SAE 2007-01-0207, 2007.

[8] M. Sjoberg and J. Dec, "Effects of Engine Epeed, Fueling Rate and Combustion Phasing on the Thermal Stratification Required to Limit HCCI Knocking Intensity," in 2005 SAE Brasil Fuels & Lubricants Meeting, SAE 2005-01-2125, 2005.

[9] M. Sjoberg and J. Dec, "EGR and Intake Boost for Managing HCCI Low-Temperature Heat Release over Wide Ranges of Engine Speed ," in 2007 SAE Fuels and Emissions Conference, SAE 2007-01-0051, 2007.

[10] M. Sjöberg, J. E. Dec, and N. P. Cernansky, "Potential of Thermal Stratification and Combustion Retard for Reducing Pressure-Rise Rates in HCCI Engines, Based on Multi-Zone Modeling and Experiments," in 2005 SAE World Congress, SAE 2005-01-0113, 2005.

[11] N. Wermuth, H. Yun, and P. Najt, "Enhancing Light Load HCCI Combustion in a Direct Injection Gasoline Engine by Fuel Reforming During Recompression," in 2009 SAE World Congress & Exhibition, SAE 2009-01-0923, 2009.

[12] H. Yun, P. Najt, and N. Wermuth, "Development of Robust Gasoline HCCI Idle Operation Using Multiple Injection and Multiple Ignition (MIMI) Strategy," in 2009 SAE World Congress & Exhibition, SAE 2009-01-0499, 2009.

[13] J. B. Heywood, *Internal Combustion Engine Funamentals*, 1st ed. Singapore: McGraw-Hill, 1988.

[14] A. D. B. Yates, C. L. Viljoen, and A. Swarts, "Understanding the Relation between Cetane Number and Combustion Bomb Ignition Delay Measurements," in 2004 SAE Fuels & Lubricants Meeting & Exhibition, SAE 2004-01-2017, 2004.

[15] H. Kuzuyama, M. Machida, K. Akihama, K. Inagaki, and M. Ueda, "A Study on Natural Gas Fueled Homogeneous Charge Compression Ignition Engine - Expanding the Operating Range and Combustion Mode Switching," in SAE World Congress & Exhibition, SAE 2007-01-0176, 2007.

[16] Y. Kodama, I. Nishizawa, T. Sugihara, N. Sato, T. Iijima, and T. Yoshida, "Full-Load HCCI Operation with Variable Valve Actuation System in a Heavy-Duty Diesel Engine," in SAE World Congress & Exhibition, SAE 2007-01-0215, 2007.

[17] Y. Li, H. Zhao, N. Brouzos, and T. Ma, "Parametric study on CAI Combustion in a GDI Engine with an Air-Assisted Injector," in SAE World Congress & Exhibition, SAE 2007-01-0196, 2007.

[18] M. Sjoberg and J. Dec, "Combined Effects of Fuel-Type and Engine Speed on Intake Temperature Requirements and Completeness of Bulk-Gas Reactions for HCCI Combustion," in SAE Powertrain & Fluid Systems Conference & Exhibition, SAE 2003-01-3173, 2003.

[19] M. Christensen, B. Johansson, P. J. H. Amneus, and F. Mauss, "Supercharged Homogeneous Charge Compression Ignition," in International Congress & Exposition, SAE 980787, 1998.

[20] Y. Ishibashi and H. Morikawa, "An Experimental Approach to the Controlled Auto-Ignition," in SAE World Congress & Exhibition, SAE 2007-01-0173, 2007.

[21] "Das CCS-Brennverfahren von Volkswagen," 2008, pp. 183-192.

[22] "Innovative Mercedes-Benz DIESOTTO Engine Awarded," 2008.

[23] "Diesotto - Towards ACEA and EURO 6 compliance; two birds with one stone?," 2007.

[24] E. Sippel, "First drive: Merc's high-tech DiesOtto engine," 2008.

[25] T. Matsuda, T. Urushihara, T. Nakamura, H. Wada, and T. Kono, "A Study of Gasoline-fueled HCCI Engine—Mode Changes from SI Combustion to HCCI Combustion," in SAE 2008 World Congress & Exhibition, SAE 2008-01-0050, 2008.

[26] P. W. Bessonette, C. H. Schleyer, K. P. Duffy, W. L. Hardy, and M. P. Liechty, "Effects of Fuel Property Changes on Heavy-Duty HCCI Combustion," in SAE World Congress & Exhibition, SAE 2007-01-0191, 2007.

[27] "SCANIA - ENGINE TECHNOLOGY - MASTERING EURO 4, EURO 5 AND BEYOND,", 03.12 enXX1595167 © Scania CV AB ed 2008.

[28] L. Koopmans, I. Denbratt, H. Ström, S. Lundgren, and O. Backlund, "Demonstrating a Si-Hcci-Si Mode Change on a Volvo 5- Cylinder Electronic Valve Control Engine," in SAE 2003 World Congress & Exhibition, SAE 2003-01-0753, 2003.

[29] L. Koopmans, I. Denbratt, and O. Backlund, "Cycle-To-Cycle Variations: Their Influence on Cycle Resolved Gas Temperature and Unburned Hydrocarbons From a Camless Gasoline Compression Ignition Engine," in SAE 2002 World Congress & Exhibition, SAE 2002-01-0110, 2002.

[30] P. Stralin, F. Wahlin, and H.-E. Angstrom, "Effects of Injection Timing on the Conditions At Top Dead Center for Direct Injected Hcci," in SAE Powertrain & Fluid Systems Conference & Exhibition, SAE 2003-01-3219, 2003.

[31] G. T. Kalghatgi, P. Risberg, and H.-E. Angstrom, "Partially Pre-Mixed Auto-Ignition of Gasoline to Attain Low Smoke and Low NOx at High Load in a Compression Ignition Engine and Comparison with a Diesel Fuel," in SAE 2007 Fuels and Emissions Conference, SAE 2007-01-0006, 2007.

[32] R. van Basshuysen and F. Schafer, *Internal Combustion Engine Handbook*. Warrendale, P.A., USA: SAE, 2004.

[33] Y. c. Hou, X. c. Lu, L. l. Zu, L. b. Ji, and Z. Huang, "Effect of High-Octane Oxygenated Fuels on n-Heptane-Fueled HCCI Combustion," *Energy Fuels*, vol. 20, no. 4, pp. 1425-1433, June2006.

[34] P. Risberg, G. Kalghatgi, H.-E. Angstrom, and F. Wåhlin, "Auto-ignition quality of Diesel-like fuels in HCCI engines," in 2005 SAE Brasil Fuels & Lubricants Meeting, SAE 2005-01-2127, 2005.

[35] P. Risberg, G. Kalghatgi, and H.-E. Ångstrom, "Auto-ignition Quality of Gasoline-Like Fuels in HCCI Engines," in SAE Powertrain & Fluid Systems Conference & Exhibition, 2003.

[36] H. Li, D. L. Miller, and Nicholas P.Cernansky, "A Study on the Application of a Reduced Chemical Reaction Model to Motored Engines for Heat Release Prediction," in International Fuels & Lubricants Meeting & Exposition, SAE 922328, 1992.

[37] S. Tanaka, F. Ayala, J. C. Keck, and J. B. Heywood, "Two-stage ignition in HCCI combustion and HCCI control by fuels and additives," *Combustion and Flame*, vol. 132, pp. 219-239, 2003.

[38] G. T. Kalghatgi, "Auto-ignition Quality of Practical Fuels and Implication for Fuel Requirements of Future SI and HCCI Engines," *SAE*, Apr.2005.

[39] I. Lemberger and G. Floweday, "A 25cc HCCI Engine Fuelled with Diethyl Ether," in 2009 SAE Powertrains, Fuels and Lubricants Meeting, SAE 2009-01-1771, 2009.

[40] V. Manente, P. Tunestal, and B. Johansson, "Mini High speed HCCI engine Fuelled with Ether: Load Range, Emission Characteristics and Optical Analysis," in SAE Asia Pacific Automotive Engineering Conference, SAE 2007-01-3606, 2007.

[41] J. Bengtsson, P. Strandh, R. Johansson, P. Tunestal, and B. Johansson, "Cycle-To-Cycle Control of a Dual-Fuel Hcci Engine," in SAE 2004 World Congress & Exhibition, 2004.

[42] M. Sjöberg and J. E. Dec, "Comparing late-cycle autoignition stability for single- and two-stage ignition fuels in HCCI engines," *The Combustion Institute*, vol. 31, no. 2, pp. 2895-2902, Jan.2007.

[43] H. J. Curran, P. Gaffuri, W. J. Pitz, and C. K. Westbrook, "A Comprehensive Modeling Study of n-Heptane Oxidation," *Combustion & Flame*, vol. 114, pp. 149-177, 1998.

[44] H. J. Curran, P. Gaffuri, W. J. Pitz, and C. K. Westbrook, "A Comprehensive Modeling Study of iso-Octane Oxidation," *Combustion & Flame*, vol. 129, pp. 253-280, 2002.

[45] M. Mehl, H. J. Curran, W. J. Pitz, and C. K. Westbrook, "Detailed Kinetic Model of Gasoline Surrogate Mixtures," in Proceedings of the European Combustion Meeting, 2009.

[46] W. J. Pitz, N. P. Cernansky, F. L. Dryer, F. N. Egolfopoulos, J. T. Farrell, D. G. Friend, and H. Pitsch, "Development of an Experimental Database and Chemical Kinetic Models for Surrogate Gasoline Fuels," in SAE World Congress & Exhibition, SAE 2007-01-0175, 2007.

[47] C. K. Westbrook, H. J. Curran, W. J. Pitz, J. F. Griffiths, C. Mohamed, and S. K. Wo, "The Effects of Pressure, Temperature, and Concentration on the Reactivity of Alkanes: Experiments and Modeling in a Rapid Compression Machine," in The Combustion Institute in Proceedings of the Twenty-seventh symposium (International) on Combustion, 1998, pp. 371-378.

[48] D. L. Flowers, S. M. Aceves, J. R. Smith, J. Torres, J. Girard, and R. W. Dibble, "HCCI in CFR Engine: Experiments and Detailed Kinetic Modeling," in SAE 2000 World Congress, SAE 2000-01-0328, 2000.

[49] J. Zheng, D. L. Miller, and N. P. Cernansky, "A Global Reaction Model for the HCCI Combustion Process," in Powertrain & Fluid Systems Conference & Exhibition, SAE 2004-01-2950, 2004.

[50] J. F. Griffiths, "Reduced kinetic models and their application to practical combustion systems," *Prog. Energy Combust. Sci.*, vol. 21, pp. 25-107, 1995.

[51] J. C. Livengood and P. C. Wu, "Correlation Of Autoignition Phenomena In Internal Combustion Engines And Rapid Compression Machines," in The Combustion Institute in Proceedings of the 5th Symposium (International) on Combustion, 1955, pp. 347-356.

[52] M. Shahbakhti, R. Lupul, and C. R. Koch, "Predicting HCCI Auto-Ignition Timing by Extending a Modified Knock-Integral Method," in SAE World Congress & Exhibition, SAE 2007-01-0222, 2007.

[53] K. Swan, M. Shahbakhti, and C. R. Koch, "Predicting Start of Combustion Using a Modified Knock Integral Method for an HCCI Engine," in 2006 SAE World Congress, SAE 2006-01-1086, 2006.

[54] C. L. Viljoen, A. D. B. Yates, A. Swarts, G. Balfour, and K. Moller, "An Investigation of the Ignition Delay Character of Different Fuel Components and an Assessment of Various Autoignition Modelling Approaches," in 2005 SAE Brasil Fuels & Lubricants Meeting, SAE 2005-01-2084, 2005.

[55] C. L. Viljoen, A. D. B. Yates, and R. L. J. Coetzer, "A molecular modelling investigation of selected gasoline molecules to relate oxidation pathways to their autoignition behaviour," in 2007 Fuels and Emissions Conference, SAE 2007-01-0005, 2007.

[56] K. Fieweger, R. Blumenthal, and G. Adomeit, "Self-ignition of S.I. engine model fuels: A shock tube investigation at high pressure," *Combustion and Flame*, vol. 109, no. 4, pp. 599-619, 1997.

[57] B. M. Gauthier, D. F. Davidson, and R. K. Hanson, "Shock tube determination of ignition delay times in full-blend and surrogate fuel mixtures," *Combustion and Flame*, vol. 139, no. 4, pp. 300-311, Dec.2004.

[58] A. Fish, A. Read, W. S. Affleck, and W. W. Haskell, "The controlling role of cool flames in two-stage ignition," *Combustion & Flame*, vol. 13, pp. 39-49, 1969.

[59] G. Vanhove, Petit G., and R. Minetti, "Experimental study of the kinetic interactions in the low-temperature autoignition of hydrocarbon binary mixtures and a surrogate fuel," *Combustion and Flame*, vol. 145, no. 3, pp. 521-532, May2006.

[60] J. M. Simmie, "Detailed chemical kinetic models for the combustion of hydrocarbon fuels," *Progress in Energy and Combustion Science*, vol. 29, no. 3, pp. 599-634, 2003.

[61] R. Bounaceur, P. A. Glaude, R. Fournet, V. Warth, and F. Battin-Leclerc, "Detailed kinetic models for the low-temperature auto-ignition of gasoline surrogates," in Proceedings of the European Combustion Meeting, 2009.

[62] H. Machrafi, S. Cavadiasa, and J. Amouroux, "The development and experimental validation of a reduced ternary kinetic mechanism for the auto-ignition at HCCI conditions, proposing a global reaction path for ternary gasoline surrogates," *Fuel Processing Technology*, vol. 90, no. 2, pp. 247-263, Feb.2009.

[63] U. C. Müller, N. Peters, and A.Liñan, "Global Kinetics for n-Heptane Ignition at High Pressures," in The Combustion Institute in Proc.of 24th Symp.(Int.) on Combustion, 1992, pp. 777-784.

[64] M. Schreiber, A. Sadat Sakak, A. Lingens, and J. F. Griffiths, "A reduced thermokinetic model for the autoignition of fuels with variable octane ratings," in The Combustion Institute in Proceedings of the Twenty-Fifth Symposium (Int.) on Combustion, 1994, pp. 933-940.

[65] A. Bourdon, G. Rymer, and R. Wanker, "Optimization of a 5-Step Kinetic Scheme for HCCI Applications," in 2004 SAE World Congress, SAE 2004-01-0559, 2004.

[66] H. Machrafi, K. Lombaert, S. Cavadias, P. Guibert, and J. Amouroux, "Reduced Chemical Reaction Mechanisms: Experimental and HCCI Modelling Investigations of Autoignition Processes of iso-octane in Internal Combustion Engines," *Fuel*, vol. 84, pp. 2330-2340, 2005.

[67] K. J. Hughes, J. F. Griffiths, M. Fairweather, and A. S. Tomlin, "Evaluation of models for the low temperature combustion of alkanes through interpretation of pressure - temperature ignition diagrams," *Physical Chemistry Chemical Physics*, pp. 3197-3210, 2006.

[68] J. F. Griffiths, K. J. Hughes, M. Schreiber, and C. Poppe, "A Unified Approach to the Reduced Kinetic Modeling of Alkane Combustion," *Combustion & Flame*, vol. 99, pp. 533-540, 1994.

[69] H. S. Soyhan, F. Mauss, and C. Sorusbay, "Chemical Kinetic Modeling Of Combustion In Internal Combustion Engines Using Reduced Chemistry," *Combustion Science and Technology*, vol. 174, no. 11 & 12, pp. 73-91, 2002.

[70] K. J. Hughes, M. Fairweather, J. F. Griffiths, R. Porter, and A. S. Tomlin, "The application of the QSSA via reaction lumping for the reduction of complex hydrocarbon oxidation mechanisms," in Proceedings of the Combustion Institute, 2009, 32, pp. 543-551.

[71] H. Li, D. L. Miller, and N. P. Cernansky, "Development of Reduced Kinetic Model for Prediction of Preignition Reactivity and Autoignition of Primary Reference Fuels," in International Congress & Exposition, SAE 960498, 1996.

[72] M. P. Halstead, L. J. Kirsch, A. Prothero, and C. P. Quinn, "A mathematical model for hydrocarbon autoignition at high pressures," in Proc.Roy.Soc.London, 1975, A346, pp. 515-538.

[73] M. P. Halstead, L. J. Kirsch, and C. P. Quinn, "The Autoignition of Hydrocarbon Fuels at High Temperatures and Pressures -Fitting of a Mathematical Model," *Combustion & Flame*, vol. 30, no. 45, p. 60, 1977.

[74] S. S. Sazhin, E. M. Sazhina, M. R. Heikal, and C. Marooney, "The Shell Autoignition Model: A New Mathematical Formulation," *Combustion & Flame*, vol. 117, pp. 529-540, 1999.

[75] R. A. Cox and J. A. Cole, "Chemical aspects of the autoignition of hydrocarbon-air mixtures," *Combustion & Flame*, vol. 60, pp. 109-123, 1985.

[76] H. Hu and J. C. Keck, "Autoignition of adiabatically compressed combustible gas mixtures," *SAE*, 1987.

[77] J. Zheng, W. Yang, D. L. Miller, and N. P. Cernansky, "Prediction of Preignition Reactivity and Ignition Delay for Using a Reduced Chemical Kinetic Model," in SAE 2001 World Congress, SAE 2001-01-1025, 2001.

[78] J. Zheng, W. Yang, D. L. Miller, and N. P. Cernansky, "A Skeletal Chemical Kinetic Model for the HCCI Combustion Process," in SAE 2002 World Congress & Exhibition, SAE Paper 2002-01-0423, 2002.

[79] A. M. Douaud and P. Eyzat, "Four-octane-number method for predicting the antiknock behaviour of fuels and engines," *SAE*, 1978.

[80] A. D. B. Yates, A. Swarts, and C. L. Viljoen, "Correlating Auto-ignition Delays and Knock-Limited Spark-Advance Data for Different Types of Fuel," in 2005 SAE Brasil Fuels & Lubricants Meeting, SAE 2005-01-2083, 2005.

[81] S. M. Aceves, D. L. Flowers, C. K. Westbrook, J. R. Smith, R. W. Dibble, M. Christensen, and B. Johansson, "A Multi-Zone Model for Prediction of Hcci Combustion and Emissions," in SAE 2000 World Congress, SAE 2000-01-0327, 2000.

[82] S. M. Aceves, D. L. Flowers, F. Espinosa-Loza, A. Babajimopoulos, and D. N. Assanis, "Analysis of Premixed Charge Compression Ignition Combustion With a Sequential Fluid Mechanics-Multizone Chemical Kinetics Model," in SAE 2005 World Congress & Exhibition, SAE 2005-01-0115, 2005.

[83] J. Zheng, D. L. Miller, and N. P. Cernansky, "Two Types of Autoignition and Their Engine Applications," in 2005 SAE World Congress, SAE 2005-01-0178, 2005.

[84] S. C. Londleni, T. Rabe, and A. Swarts, "The Application of an Enhanced Ignition Delay Model to HCCI Engines and Comparison to Engine Measurements," in 2007 SAE Fuels and Emissions Conference, SAE 2007-01-0048, 2007.

[85] H. K. Ciezki and G. Adomeit, "Shock-tube investigation of self-ignition of n-heptane-air mixtures under engine relevant conditions," *Combustion & Flame*, vol. 93, pp. 421-433, 1993.

[86] U.S.Department of Commerce/National Bureau of Standards, "National standard reference data series of National Bureau of Standards," in *NSRDS-NBS 37 (1971): Joint-Army-Navy-Air Force (JANAF) Thermo-chemical Tables* 1971.

[87] V. Devaraj, S. Suryanarayanan, V. M. Janakiraman, K. Subramanian, and V. Devaraj, "Comparative Study of Performance Characteristics of a Glow Plug Fired 2 Stroke Engine for Different Blends of Methanol, Castor Oil and Gasoline by Experimental and ANN Analysis," in 2007 Fuels and Emissions Conference, SAE 2007-01-0058, 2007.

[88] V. Manente, P. Tunestal, and B. Johansson, "Influence of Inlet Temperature and Hot Residual Gasses on the Performance of a Mini High Speed Glow Plug Engine," in SAE Small Engine Technology Conference & Exposition, SAE 2006-32-0057, 2006.

[89] V. Manente, P. Tunestal, and B. Johansson, "A Study of a Glow Plug Ignition Engine by Chemiluminescence Images,", SAE 2007-01-1884, 2007.

[90] R. R. Raine and H. Thorwarth, "Performance and Combustion Characteristics of a Glow-Ignition Two-Stroke Engine," in SAE 2004 World Congress & Exhibition, SAE 2004-01-1407, 2004.

[91] A. D. B. Yates, A. Swarts, and C. L. Viljoen, "An Investigation of Anomalies Identified Within the Astm Research and Motor Octane Scales," *SAE*, May2003.

[92] Albert Einstein, "On the method of Theoretical Physics," *Philosophy of Science*, vol. 1, no. 2, pp. 163-169, Apr.1934.

Appendix A: Auto-ignition behaviour of fuels

This appendix provides the results from detailed chemical kinetics simulations using Chemkin Collection™ software, Release 3.7 (Reaction Design, Inc.). The simulations were run as perfectly stirred, constant volume reactor simulations and used the Mehl et al. (2009) [1] detailed chemical kinetics mechanism for hydrocarbon oxidation reactions. This recently updated mechanism consists of 8000 reactions and 1550 species and includes alkanes up to C8 as well as isomers of hexene and a number of oxygenate compounds. In particular, the inclusion of n-heptane, iso-octane, 1-hexene and toluene make this mechanism a very useful mechanism for formulation and simulation of pure component fuels as well as binary, ternary and quaternary gasoline surrogate blends.

The fuels simulated below are n-heptane, iso-octane, 1-hexene, toluene, methanol and a quaternary gasoline surrogate consisting of iso-octane, toluene, hexene and n-heptane in the ratio 44/30/18/8% by moles as presented in [1]. This data was used as the basis for selection of key points for the fitting of the functional global model developed in this study.

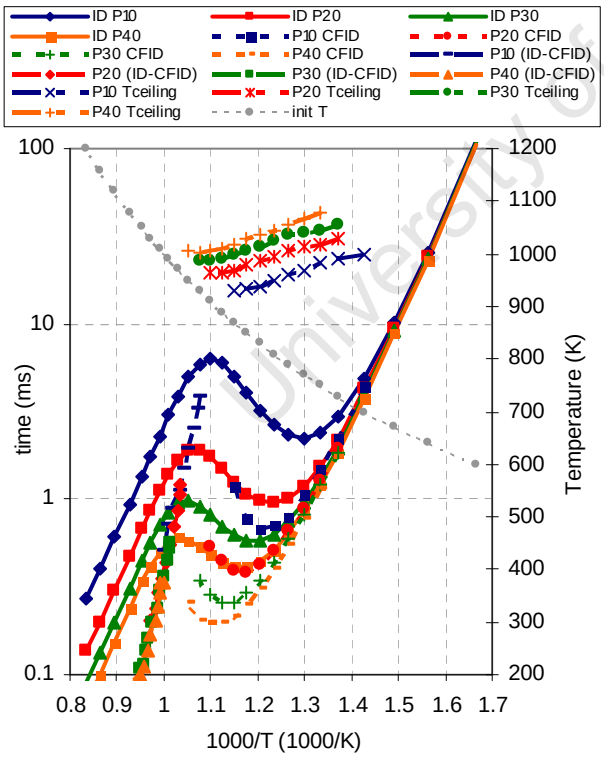

Figure A1: n-heptane; P=10, 20, 30, 40bar; Phi=1.0; R=0%

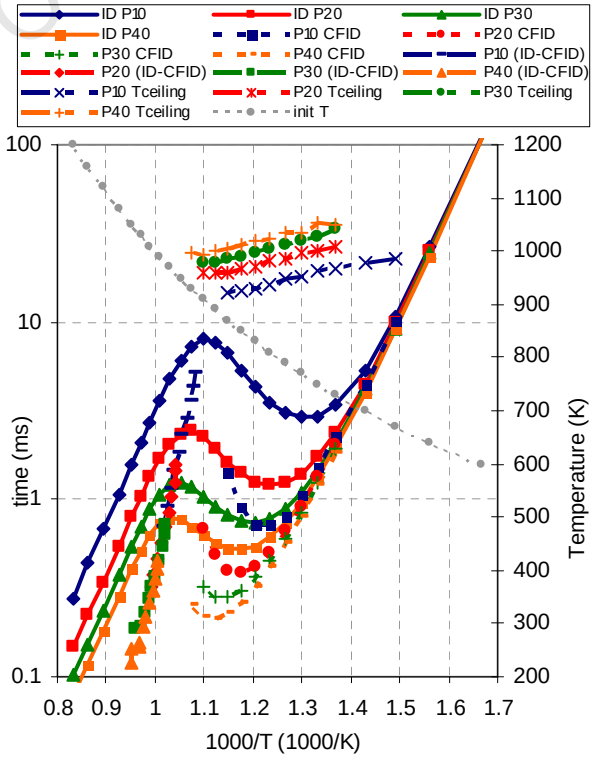

Figure A2: n-heptane; P=10, 20, 30, 40bar; Phi=0.75; R=0%

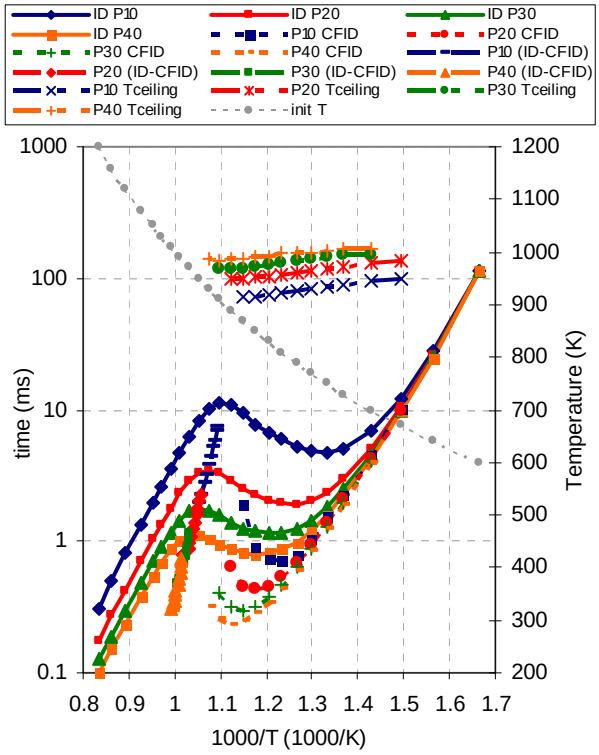

Figure A3: n-heptane; P=10, 20, 30, 40bar; Phi=0.50; R=0%

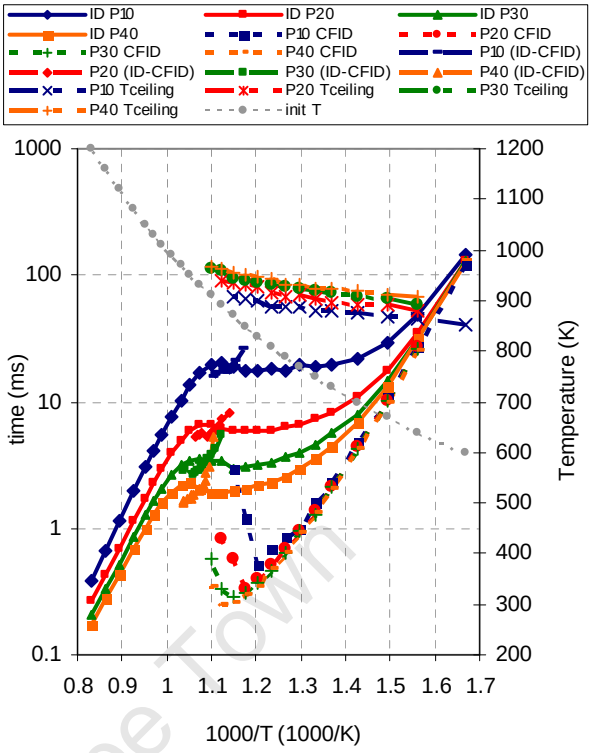

Figure A4: n-heptane; P=10, 20, 30, 40bar; Phi=0.25; R=0%

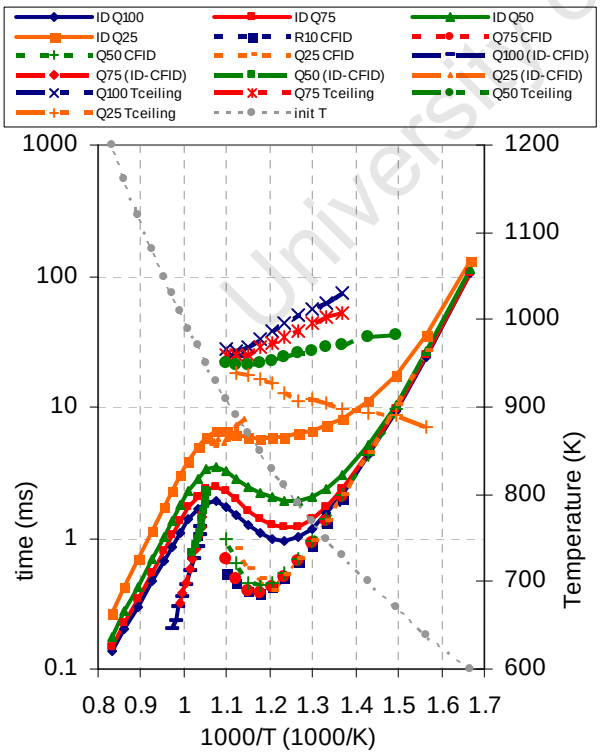

Figure A5: n-heptane; P=20 bar; Phi=1.0, 0.75, 0.5, 0.25; R=0%

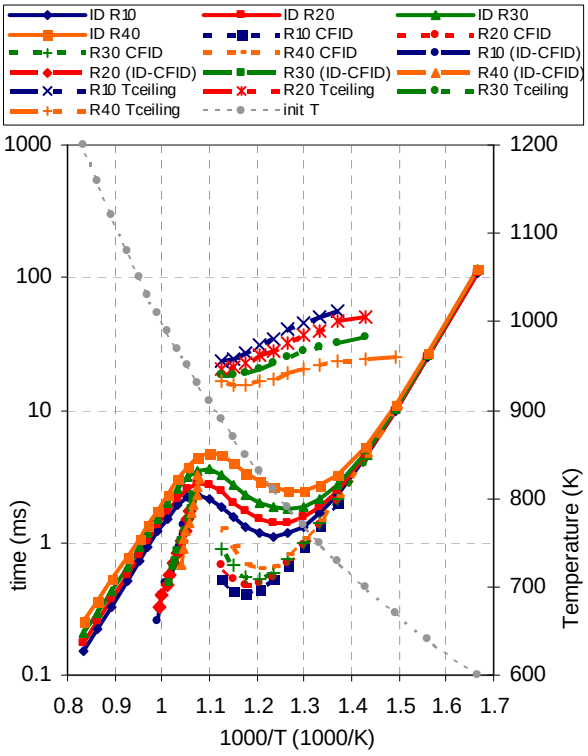

Figure A6: n-heptane; P=20 bar; Phi=1.0; R=10, 20, 30, 40%

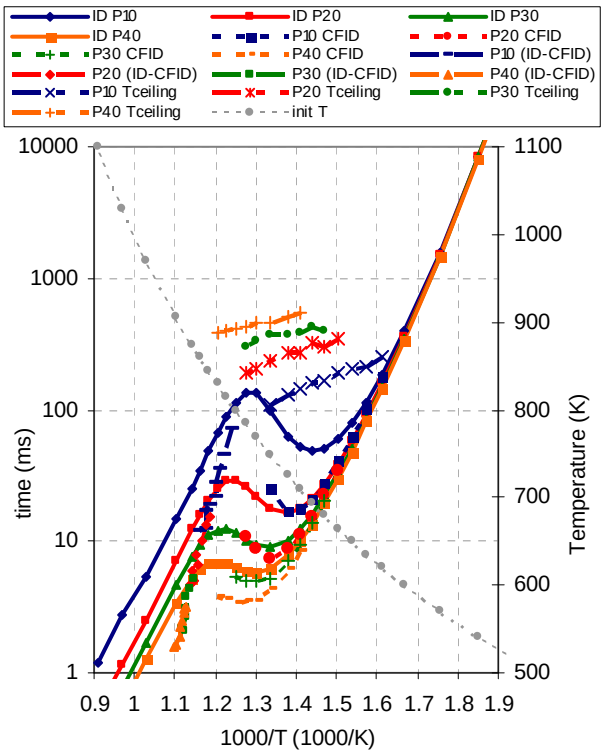

Figure A7: Iso-octane; P=10, 20, 30, 40bar; Phi=1; R=0%

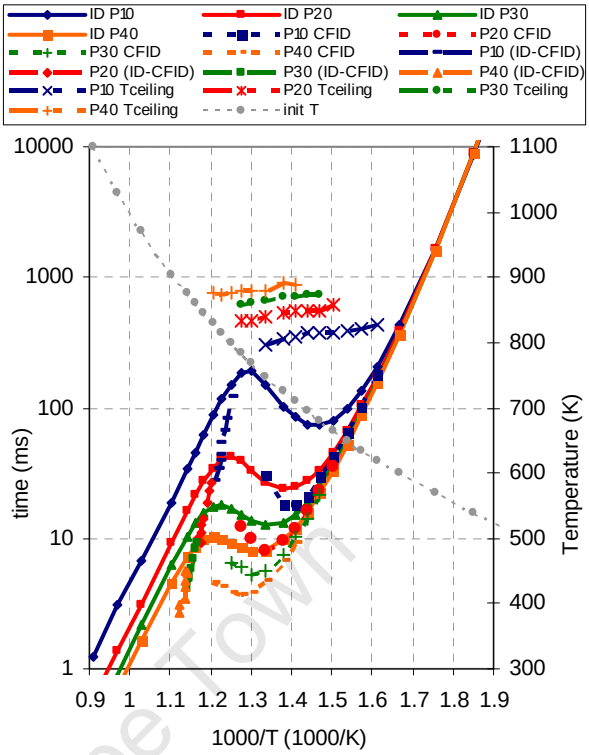

Figure A8: Iso-octane; P=10, 20, 30, 40bar; Phi=0.75; R=0%

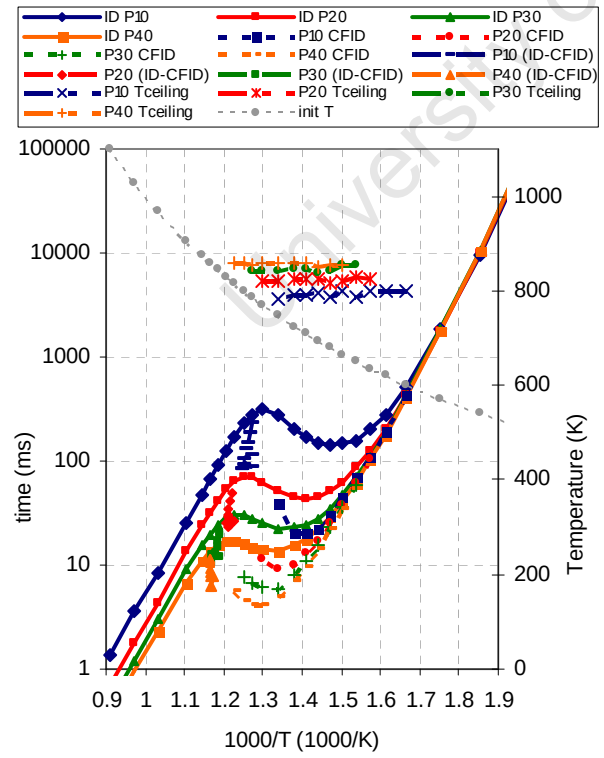

Figure A9: Iso-octane; P=10, 20, 30, 40bar; Phi=0.50; R=0%

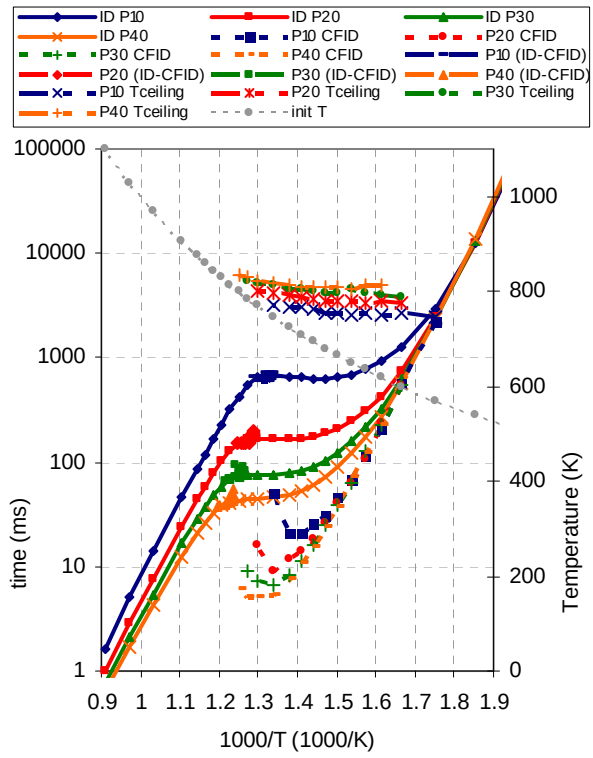

Figure A10: Iso-octane; P=10, 20, 30, 40bar; Phi=0.25; R=0%

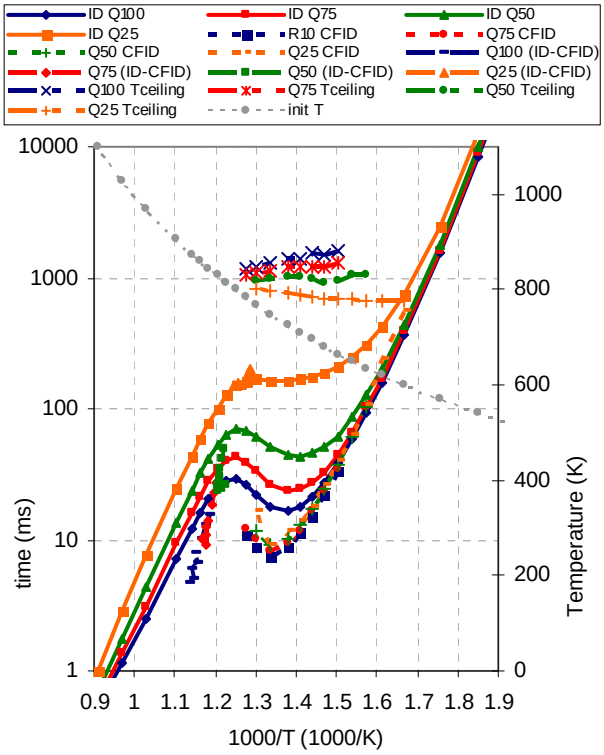

Figure A11: Iso-octane; P=20bar; Phi=1.0, 0.75, 0.5, 0.25; R=0%

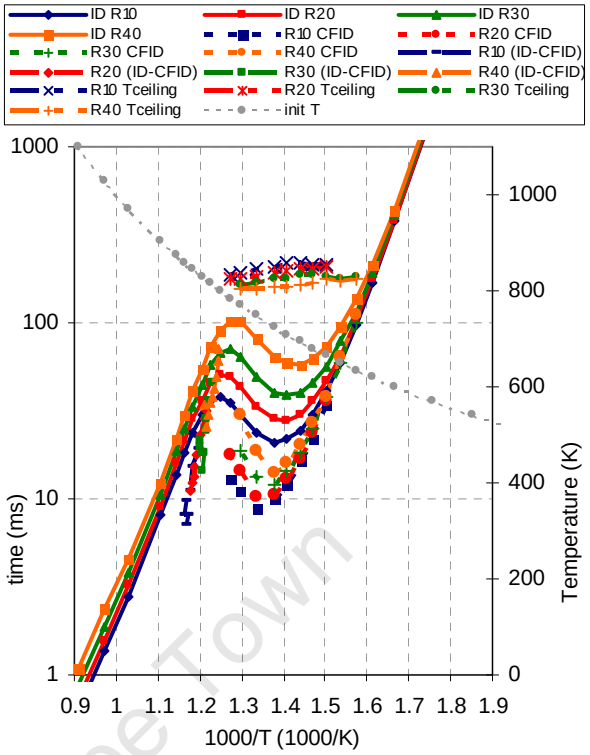

Figure A12: Iso-octane; P=20 bar; Phi=1.0; R=10, 20, 30, 40%

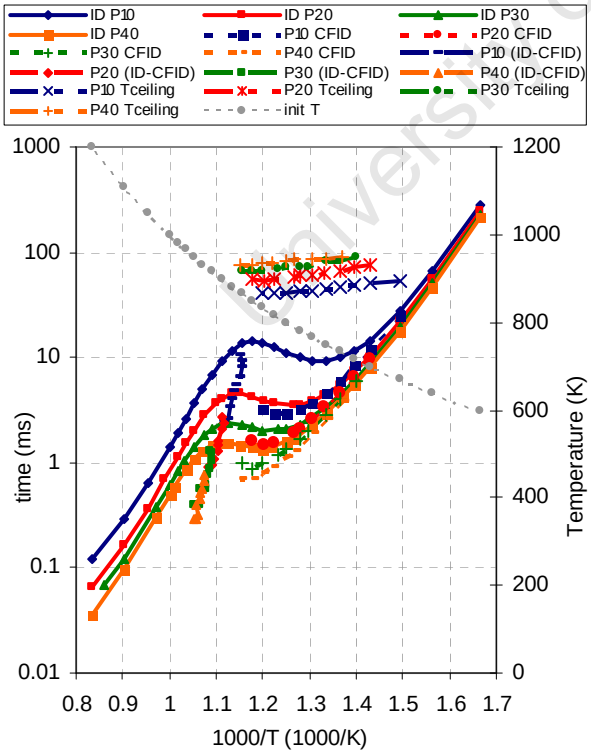

Figure A13: 1-hexene; P=10, 20, 30, 40bar; Phi=1.0; R=0%

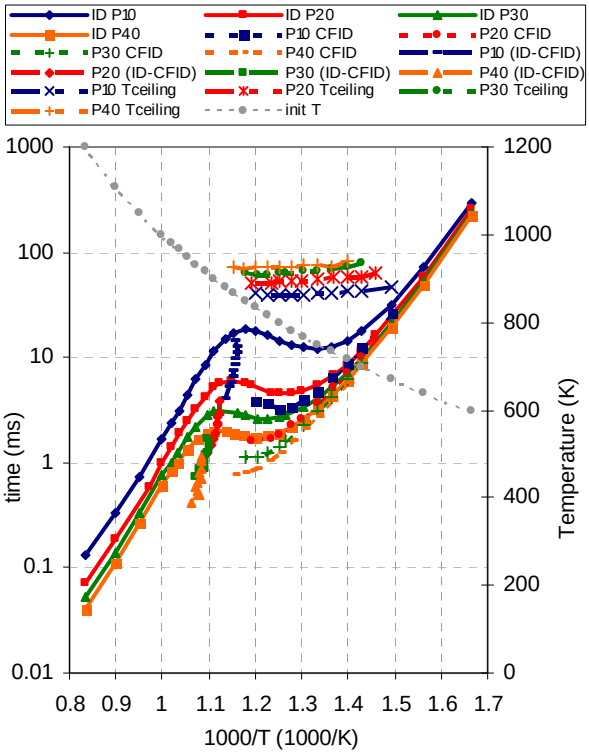

Figure A14: 1-hexene; P=10, 20, 30, 40bar; Phi=0.75; R=0%

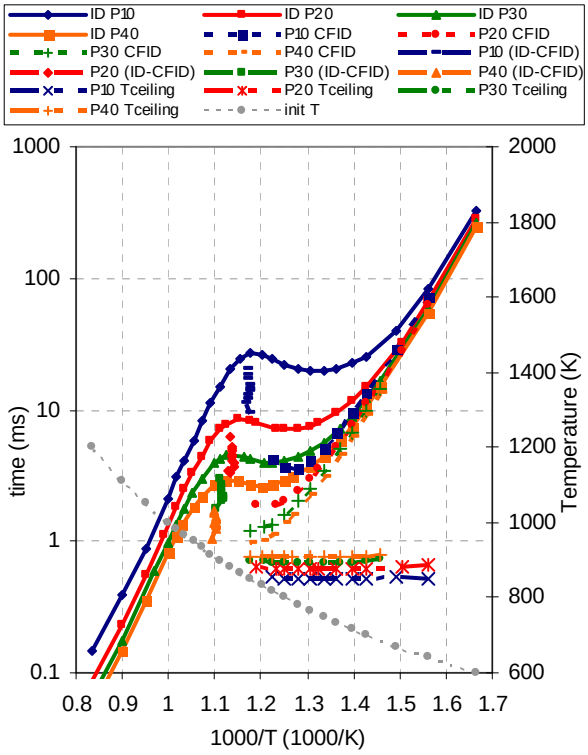

Figure A15: 1-hexene; P=10, 20, 30, 40bar; Phi=0.50; R=0%

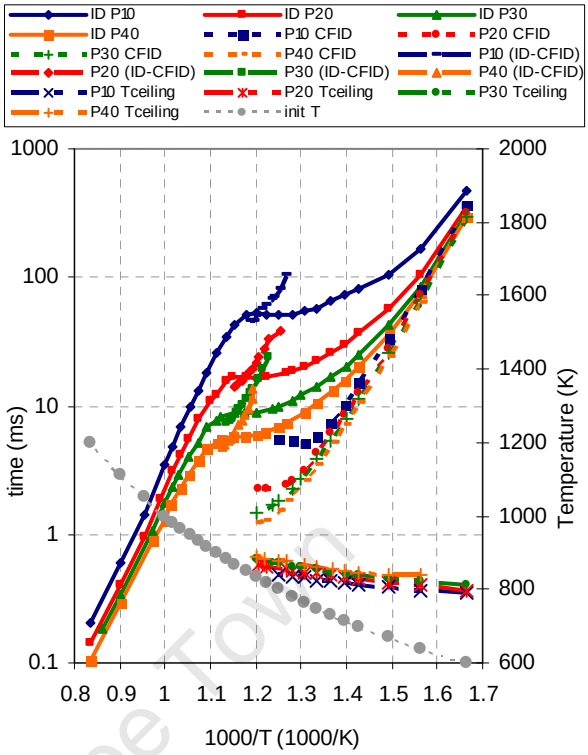

Figure A16: 1-hexene; P=10, 20, 30, 40bar; Phi=0.25; R=0%

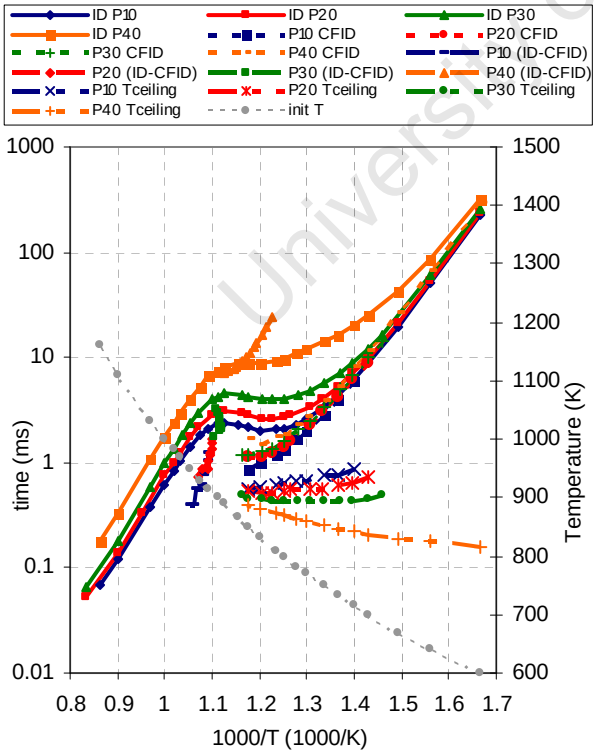

Figure A17: 1-hexene; P=30bar; Phi=1.0, 0.75, 0,5, 0,25; R=0%

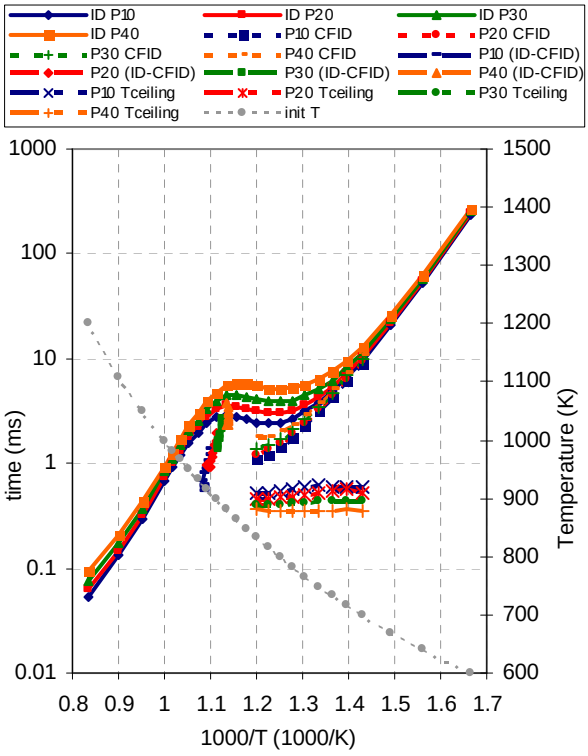

Figure A18: 1-hexene; P=30 bar; Phi=1.0; R=10, 20, 30, 40%

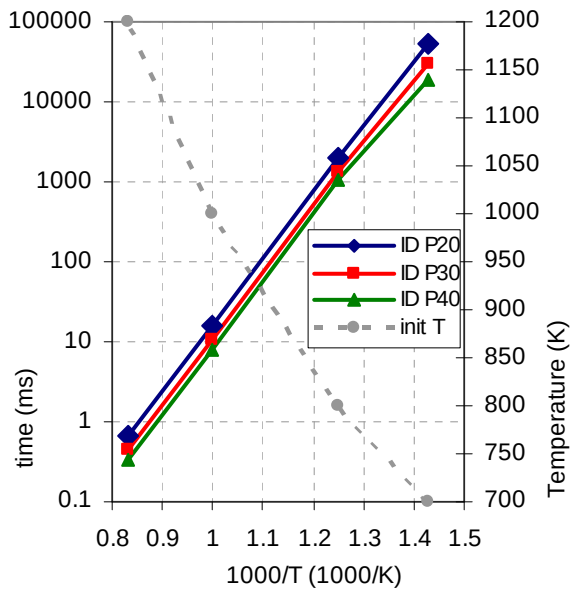

Figure A19: toluene; P= 20, 30, 40bar; Phi=1.0; R=0%

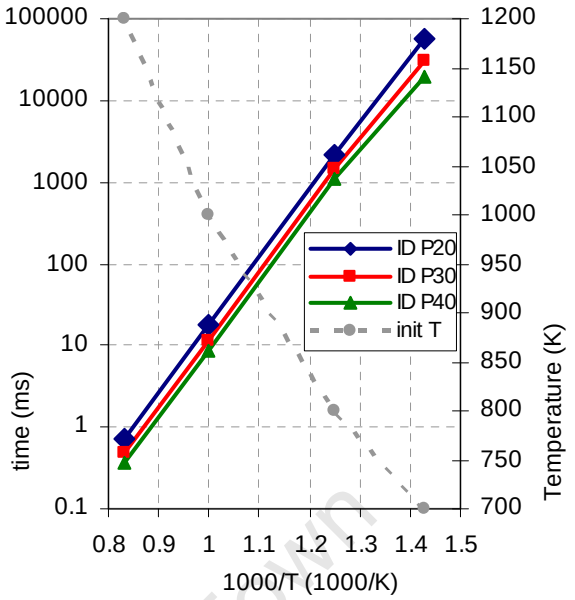

Figure A20: toluene; P=20, 30, 40bar; Phi=0.75; R=0%

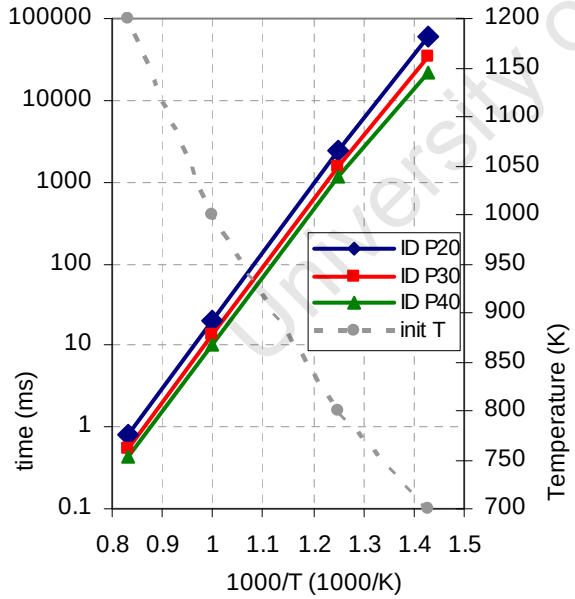

Figure A21: toluene; P=20, 30, 40bar; Phi=0.50; R=0%

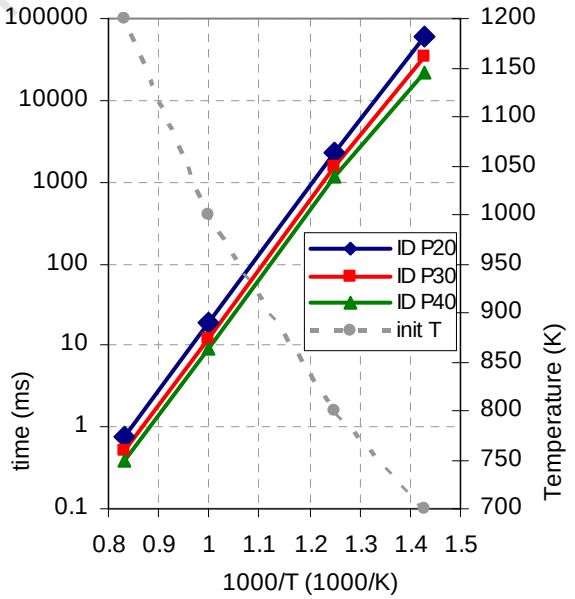

Figure A22: toluene; P=20, 30, 40bar; Phi=1.0; R=10%

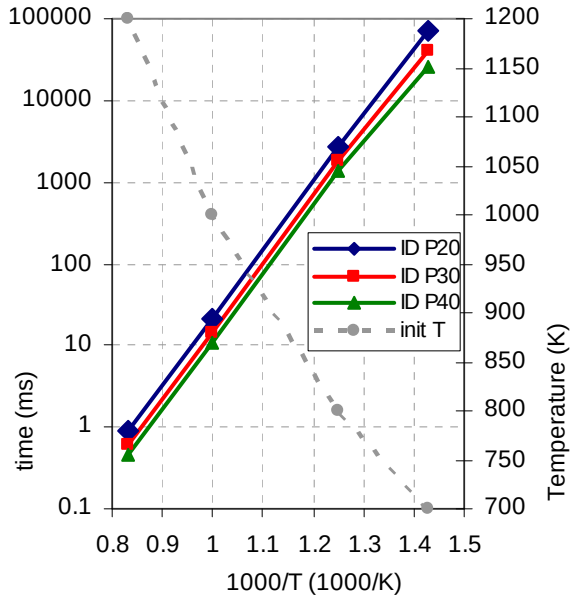

Figure A23: toluene; P=20, 30, 40bar; Phi=1.0; R=20%

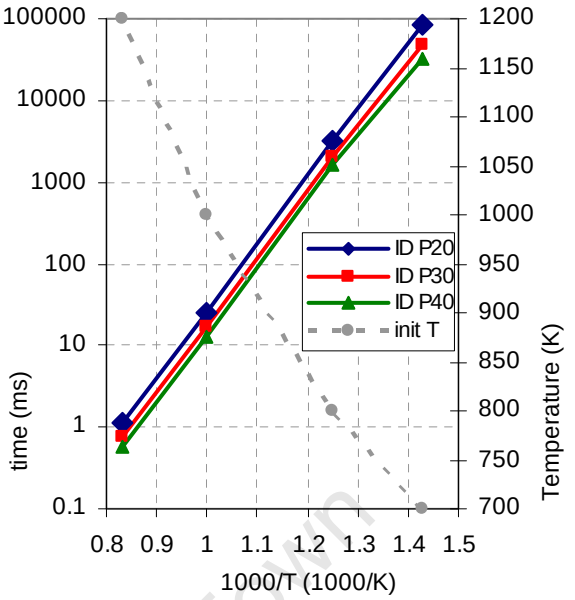

Figure A24: toluene; P=20, 30, 40bar; Phi=1.0; R=30%

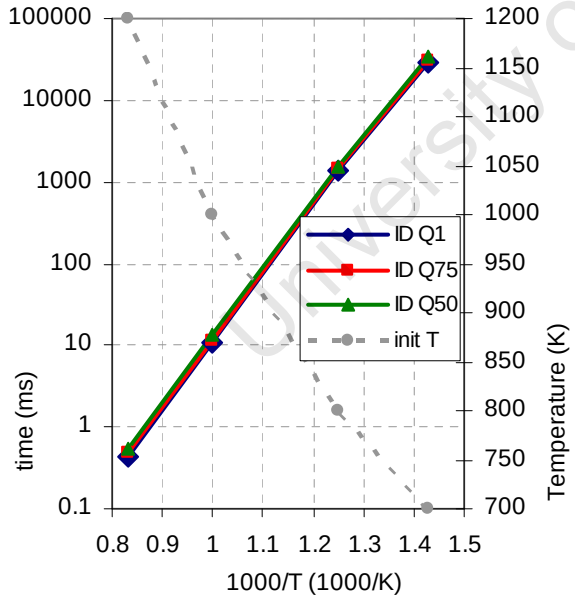

Figure A25: toluene; P=30bar; Phi=1.0, 0.75, 0.5; R=0%

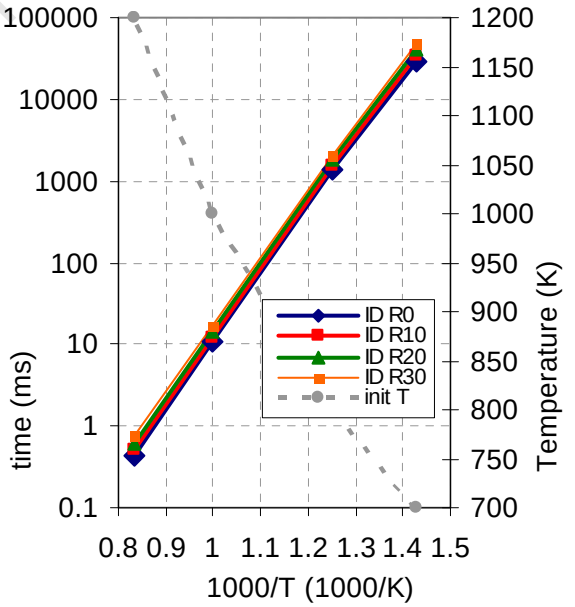

Figure A26: toluene; P=30bar; Phi=1.0; R=0, 10, 20, 30%

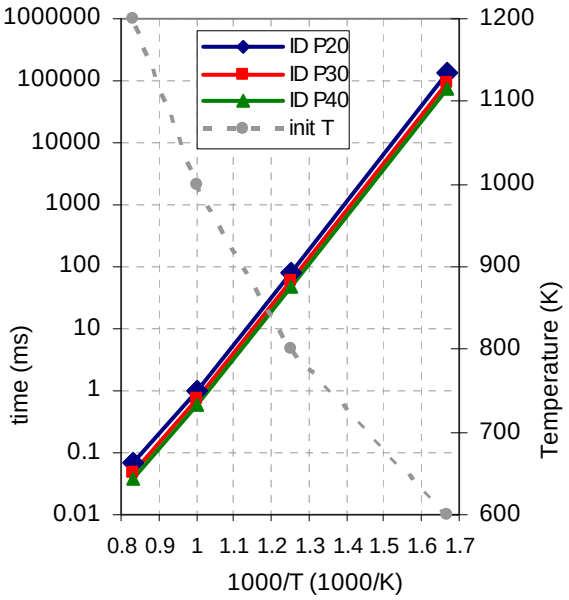

Figure A27: methanol; P=20, 30, 40bar; Phi=1.0; R=0%

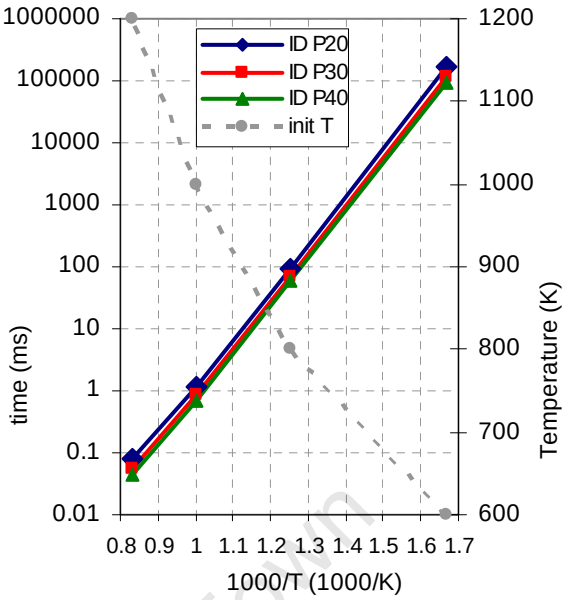

Figure A28: methanol; P=20, 30, 40bar; Phi=0.75; R=0%

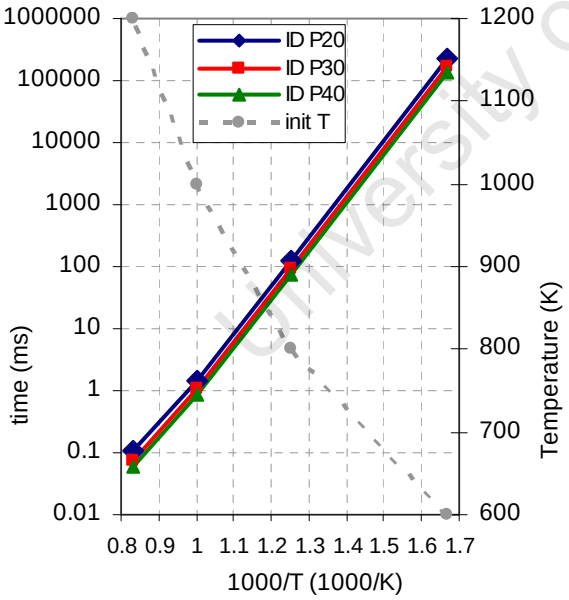

Figure A29: methanol; P=20, 30, 40bar; Phi=0.50; R=0%

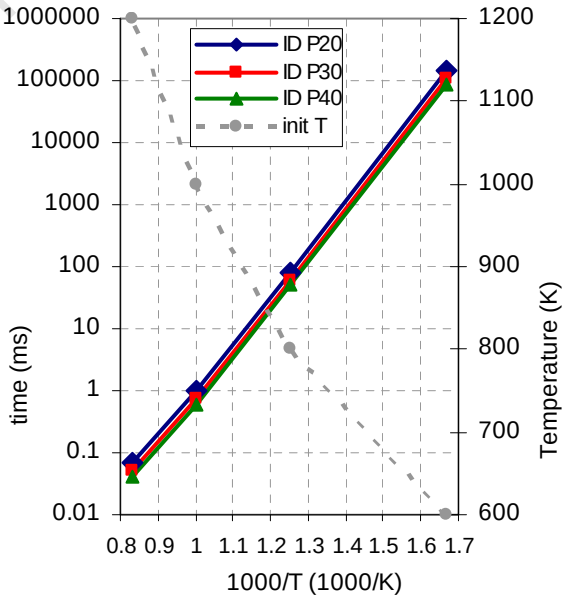

Figure A30: methanol; P=20, 30, 40bar; Phi=1.0; R=10%

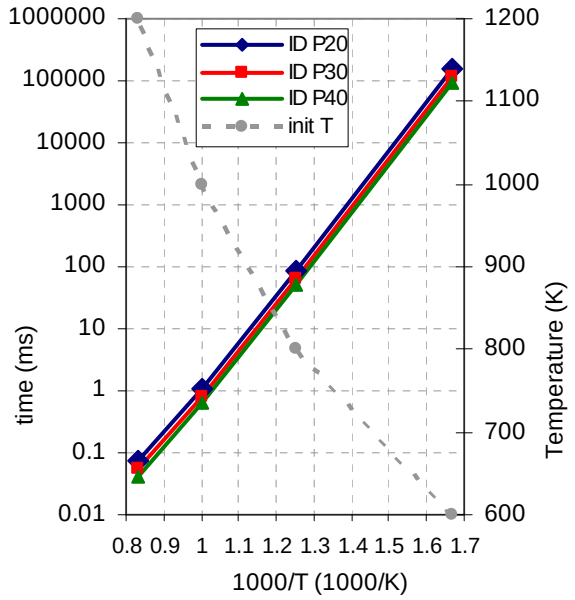

Figure A31: methanol; P=20, 30, 40bar; Phi=1.0; R=20%

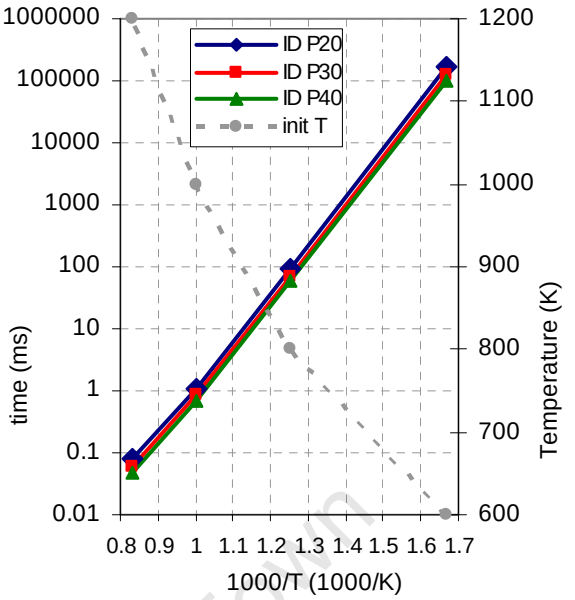

Figure A32: methanol; P=20, 30, 40bar; Phi=1.0; R=30%

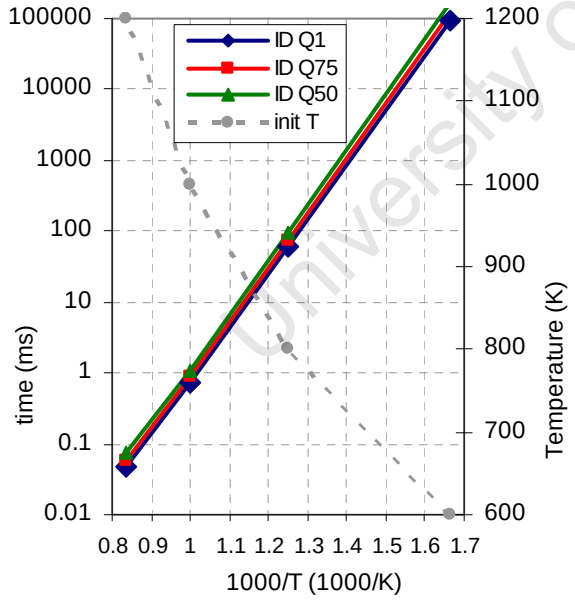

Figure A33: methanol; P=30bar; Phi=1.0, 0.75, 0.5; R=0%

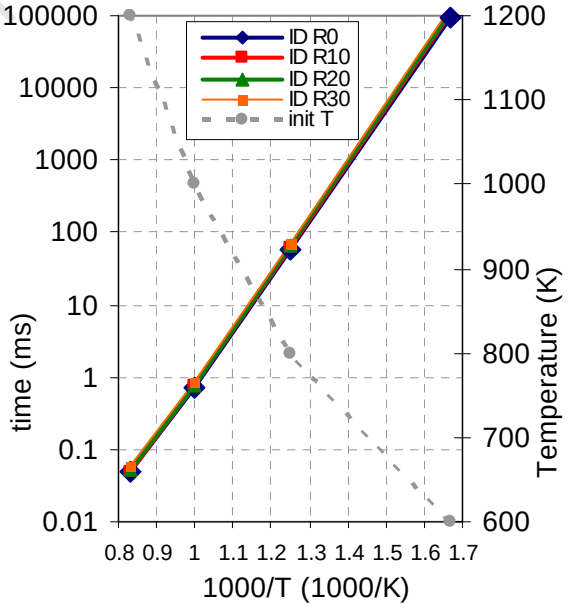

Figure A34: methanol; P=30bar; Phi=1.0; R=0, 10, 20, 30%

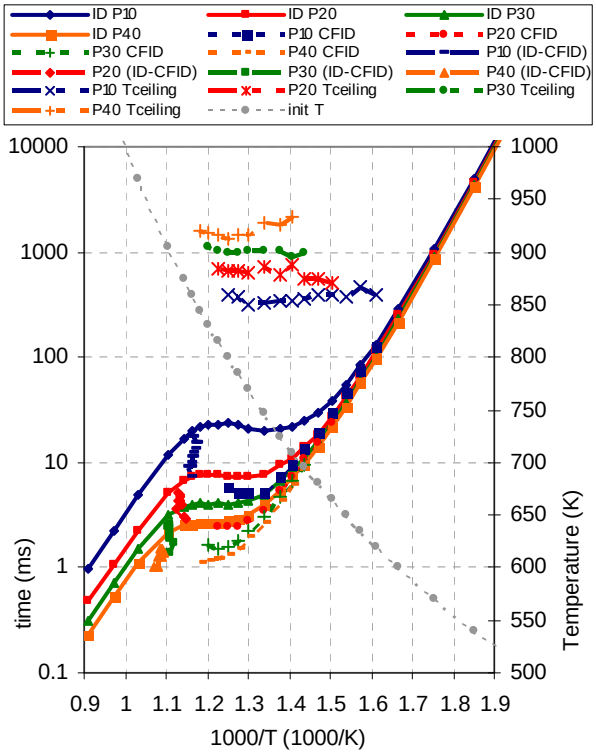

Figure A35: Gasoline Surrogate; P=10, 20, 30, 40bar; Phi=1.0; R=0%

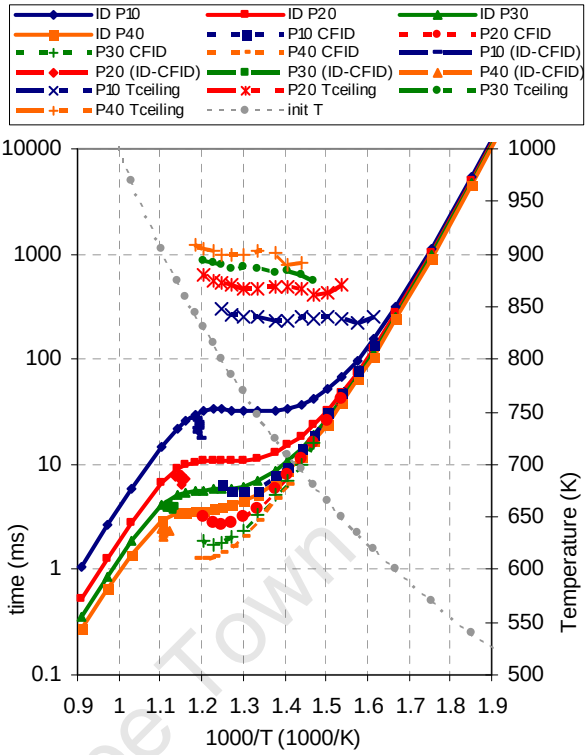

Figure A36: Gasoline Surrogate; P=10, 20, 30, 40bar; Phi=0.75; R=0%

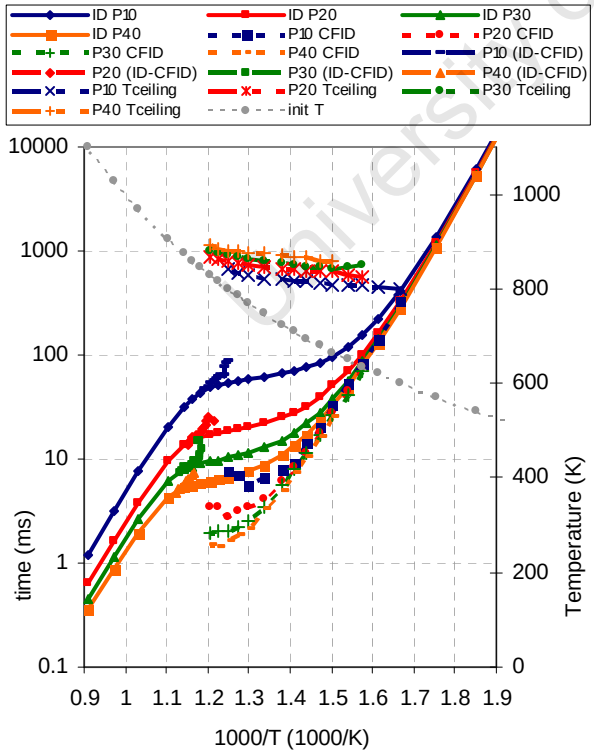

Figure A37: Gasoline Surrogate; P=10, 20, 30, 40bar; Phi=0.50; R=0%

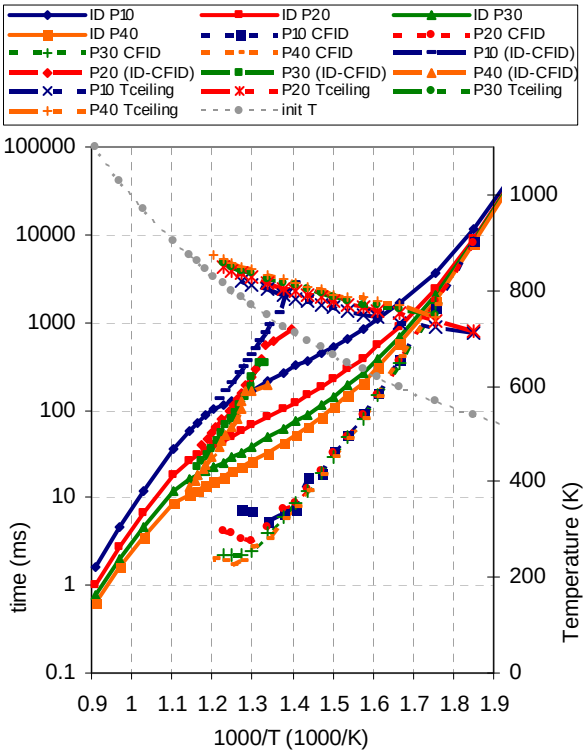

Figure A38: Gasoline Surrogate; P=10, 20, 30, 40bar; Phi=0.25; R=0%

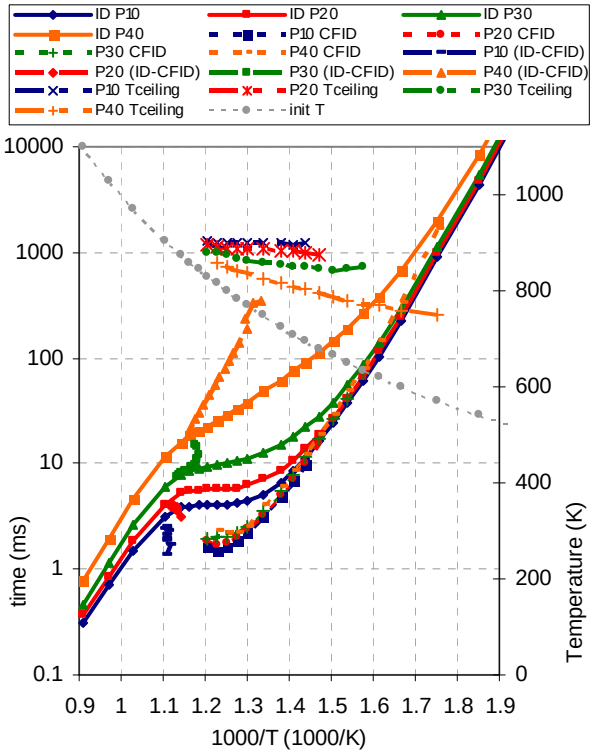

Figure A39: Gasoline Surrogate; P=30bar; Phi=1.0, 0.75, 0,5, 0,25; R=0%

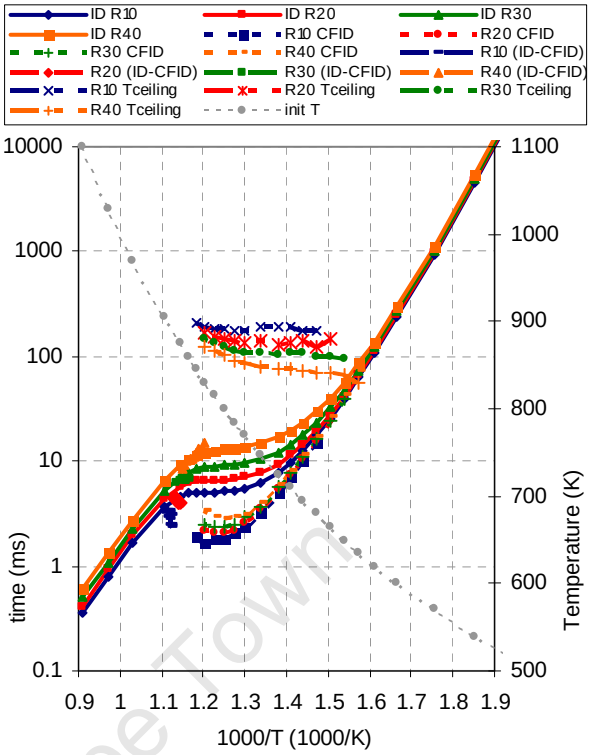

Figure A40: Gasoline Surrogate; P=30 bar; Phi=1.0; R=10, 20, 30, 40%

References

[1] M. Mehl, H. J. Curran, W. J. Pitz, and C. K. Westbrook, "Detailed Kinetic Model of Gasoline Surrogate Mixtures," in Proceedings of the European Combustion Meeting, 2009.

Appendix B: SAE Paper 2008-01-1661

The study contained in this appendix was presented at the 2008 SAE International Powertrain, Fuels and Lubricants Conference, published in the conference proceedings and later published in the SAE International Journal of Fuels and Lubricants, April 2009.

The modelling and experimental work contained in this study was conducted exclusively by Mr Gareth Floweday under the supervision of Professor Andrew D.B. Yates. The paper was also written exclusively by Gareth Floweday with minor editorial guidance from Professor Andrew D.B. Yates.

SAE 2008-01-1661

Integration of Fuel Auto-ignition Characteristics and HCCI Engine Operation

Gareth Floweday, Andy D. B. Yates
Sasol Advanced Fuels Laboratory, University of Cape Town

ABSTRACT

A recently improved Arrhenius fuel auto-ignition model was combined with a single zone explicit discrete Homogeneous Charge Compression Ignition (HCCI) engine model in order to investigate a wide range of combinations of fuel type with engine setup and operational configurations.

The engine model was validated using experimental data from a single cylinder variable compression ratio engine running in HCCI mode.

The model was used to identify promising and problematic areas for the combination of fuel properties, engine configurations and operational ranges. Insights regarding the interaction between trapped gas pressure and temperature histories and auto-ignition reaction rate surfaces in the pressure and temperature domain are presented.

INTRODUCTION

BACKGROUND & LITERATURE REVIEW

Homogeneous Charge Compression Ignition engines offer significant advantages in efficiency over spark ignition engines and engine out emissions advantages over diesel engines [1, 2]. However, due to wide range control and starting challenges HCCI operation is chiefly being developed as part of dual mode systems in spark ignition and diesel engines [1]. While HCCI combustion has been shown to be achievable using almost any hydrocarbon fuel, appropriate choice of fuel characteristics can help in optimising engine operation [1, 4]. This fuel characteristic optimisation is often hampered by the fuel characteristics required for dual mode operation due to the combustion requirements of the non-HCCI mode [1].

Hydrocarbon fuel auto-ignition characteristics can be divided into 2 classes: Single stage ignition fuels such as methanol exhibit decreasing constant volume auto-ignition delay times with increasing temperature and increasing pressure [5-10]. Autoignition delay times of two stage ignition fuels such as n-heptane and iso-octane also decrease with increasing temperature and increasing pressure, with the exception of the "negative temperature coefficient" zone wherein autoignition delay times remain constant or increase with increasing temperature [5-10]. This NTC effect is associated with a cool flame heat release that precedes the main heat release. The cool flame timing and heat release magnitude are also strongly affected by temperature and pressure [5-10].

Fuel mixture composition also dramatically affects fuel autoignition behaviour. Air-fuel ratio, residual exhaust gas fraction and concentrations of oxygen, H_2O, CO and partially oxidised hydrocarbons all affect autoignition delay times [11, 12].

Fuel autoignition behaviour in an HCCI engine is therefore intimately connected with the particular trapped charge composition and thermodynamic history experienced by the charge. The charge's thermodynamic history is in turn a complex function of engine configuration parameters (e.g. compression ratio, combustion chamber wall temperatures, chamber size) and operational parameters (e.g. inlet heating, valve timing, inlet throttling/boosting).

All these factors influence fuel autoignition behaviour in HCCI engines and the complexity is greatly increased by the inter-connectedness of many of these parameters. For example, inlet heating reduces inlet gas density and results in increased exhaust gas fraction and reduced mass of the trapped charge, while compression ratio changes affect in-cylinder turbulence, residual gas fractions and therefore trapped charge composition and temperature [1, 13]. These interactions make research into direct cause and effect relationships in HCCI engines extremely difficult [1].

It has been noted in many studies that HCCI operation is typically limited in speed range due to combustion phasing requirements [1, 4, 14-16]. Combustion phasing is generally retarded to the point of instability at high speed operation limits and advanced to the point of excessive pressure rise rates and excessive pumping work at low speed operation limits unless phasing is corrected by changes to other parameters [17, 18]. However, it is also known that at low engine speeds, heat losses to the combustion chamber walls result in decreased peak pressures and temperatures [19, 20]. In the extreme isothermal compression case, autoignition would never take place due to insufficient temperature required to initiate combustion even within the time scales of the isothermal process. Since high engine speed results in retarded phasing, low speed in advanced phasing and ultra low speed in ultra retarded phasing, it stands to reason that there must exist a speed range where phasing is relatively independent of engine speed changes.

This speed convergence behaviour has been noticed in experimental work conducted by Sjöberg and Dec [19]. Detailed reasons for this behaviour were suggested and the following statement was made in reference to this unique operational zone:

"… we can conclude that the compression and combustion temperatures increase with engine speed in such a manner to almost perfectly compensate for the reduced "real" time available for both autoignition and for completion of the CO-to-CO_2 reactions, as observed for iso-octane." - Sjöberg and Dec [19].

The above example is just one of a number of imaginable "sweet spots" or "convergence zones" where the complex interplay of system variables could result in independence of critical parameters such as engine speed, charge density and air-fuel ratio. Identifying these areas and enlarging them could offer an additional approach to other more complex HCCI combustion controls being researched such as charge stratification [21], thermal stratification [22] and exhaust recompression/rebreathing strategies [11, 12]. Development of this approach could prove helpful in the advance of HCCI technology.

AIM OF THIS STUDY

The aim of this work was to explore the complex engine-fuel interactions in an HCCI engine with a view to identifying and optimising the naturally occurring auto-compensation zones described above. This required the development of a single zone explicit discrete engine model capable of accurately simulating combustion chamber trapped gas thermodynamic histories and the effects of engine configuration and operational changes on these histories without the need for numerical solving techniques. These thermodynamic histories were used in an explicit discrete version of the Arrhenius form Auto-ignition Integral Model improved upon in [9]. The explicit nature of the engine and autoignition model was imposed due to the requirements of demonstrating the effects of a very broad range of engine configuration and operational states simultaneously. The explicit formulation was also able to solve for initial conditions required in order to achieve desired combustion phasing. This enabled easy assessment of trends in effects and rapid identification of optimal configurations of the many variables. Such a model formulation cannot compete with the accuracy of CFD and detailed chemical kinetics models used in other studies [23, 24], but was merely aimed at identifying operational trends in HCCI combustion.

METHODS IN THE STUDY

ENGINE MODEL

The formulation of the engine model was aimed at being as generic as possible in order to be able to explore wide ranges of setup and operating conditions. The generic model was set up in Microsoft Excel and formulated to allow easy manipulation of conditions, multiple copies solving simultaneously and instant visual assessment of the effects of changes to conditions.

The variables used to define the setup condition were:

- cylinder swept volume
- compression ratio
- bore/stroke ratio
- connecting rod length/stroke ratio
- Fuel choice

The variables used to define the operational condition were:

- engine speed
- inlet charge temperature (mixture entering the cylinder)
- inlet charge P (mixture entering the cylinder)
- air fuel equivalence ratio
- residual exhaust gas pressure at exhaust valve closure.

Note that external residual exhaust gas recirculation was kept constant at zero and no chemical effects of exhaust gas residuals on autoignition were included. This was a recognised simplification in the modelling which is a planned future extension to this work.

Exhaust gas product species and mole fractions were calculated from stoichiometric and lean burn balanced chemical equations assuming no dissociation due to the typically low burned temperatures in HCCI combustion. Values for constant volume specific heat were calculated as a polynomial function of temperature using the JANAF thermodynamic tables (National Bureau of Standards, 1971). Exhaust valve closure was assumed to occur at TDC and residual exhaust gas

temperature was assumed to be a linear function of equivalence ratio as indicated by spark ignition engine exhaust temperature data in [13].

The calculated mass of trapped exhaust gas was adiabatically adjusted to the inlet gas pressure with the associated changes in volume and temperature. The inlet gas was assumed to fill the remainder of the volume to BDC at its inlet pressure and temperature. The moles of both mixtures were summed and the temperature and pressure of the mixture calculated for start of compression at BDC. Using the mole fractions and JANAF coefficients for specific heats of each component, the expression for gamma as a function of temperature for the specific mixture could be calculated. Values of gamma were related to an appropriate polytropic compression coefficient using a relationship derived from data showing speed effects on polytropic compression coefficient [13] and pressure data from a number of different engine sizes including very small displacement engines [25-29].

Polytropic compression coefficient, $n = X_1 \gamma$ (Eq.1)

Where $X_1 = 0.7 + 0.3\left(1 - e^{-A_{poly}\ RPM}\right)$ (Eq.2)

And $A_{poly} = 0.000562\ \mathrm{Ln}(V_{swept}) - 0.000694$ (Eq.3)

Where V_{swept} is the displaced cylinder volume in cm^3

And RPM is engine speed in revolutions per minute

This effectively simulated the effects of engine speed and displacement on heat loss during compression and associated effects on the compression pressure and temperature history. Temperature and pressure during compression were discretely calculated using this polytropic approximation, resulting in a pressure and temperature history showing sensitivity to inlet and exhaust boundary conditions, fuel type and equivalence ratio, engine speed, compression ratio and size.

FUEL AUTO-IGNITION MODEL

The Arrhenius form auto-ignition integral model used in this study was originally proposed in [30]. The model was further improved in [5-7], incorporated into a discreet implicit HCCI engine model and compared with experimental HCCI test results in [8]. The model was further improved in [9] to incorporate predictions of cool flame ignition delay and heat release magnitude (for 2 stage ignition cases) in addition to the main heat release timing prediction, and effects of air-fuel ratio were incorporated. The model form and coefficients used were taken directly from [9]. Since the AI model was applied in a discrete engine model, the AI integral calculations were used in their discrete form. A summary of the discrete formulation of the model is given in the appendix.

The cool flame and peroxide heat release rates were modelled using a Wiebe burn function. Some effort was spent formulating an empirical model to describe the burn durations for the cool flame and peroxide reactions using the underlying Chemkin simulation data used to formulate the autoignition model in [9]. However, when these burn durations were compared with typical durations during the experimental validation, it was found that the real burn durations were more than an order of magnitude longer. It was therefore deduced that the burn durations were completely dominated by physical effects such as thermal profile and since the burn duration values were very similar throughout the limited range of validation, constant crank angle degree burn durations of 9 and 16 CAD were used for the cool flame and peroxide burn durations respectively.

RESULTS

EXPERIMENTAL VALIDATION

Limited experimental validation was done using a $507cm^3$ displacement, single cylinder, variable compression ratio engine. The naturally aspirated engine had been modified to incorporate a port fuel injection system and inlet air was heated to 313K to aid fuel evaporation. Geometric information for the engine is given in Table 1 below.

Engine description:	Research test engine
Number of cylinders:	1
swept volume:	$507\ cm^3$
Cylinder bore size:	76.2 mm
Piston stroke length:	111.1 mm
Connecting rod length:	241.3 mm
compression ratio	variable 6:1 – 20:1

Table 1: test engine geometry

The engine was run using n-heptane at 600, 1200 and 1800 rpm and lambda values of 2.0, 2.5, 3.0, and 3.5. The higher engine speeds caused knocking and instability at the lower lambda values, so not all points the test matrix could be achieved. In each test, the HCCI combustion phasing was varied by compression ratio adjustment to produce peak pressure at 10-13 degrees after TDC. Combustion phasing retarded to this range has been shown to optimise efficiency, combustion stability, peak heat release rates and emissions [1, 31].

Representative pressure traces from each test condition were compared to those predicted by the engine model. The polytropic compression and cool flame phasing correlated reasonably well, assuming a fixed inlet mixture temperature rise of 60^0C due to heat transfer from the inlet manifold, port, valve and combustion chamber walls. The cool flame temperature rise was slightly under-predicted. The phasing of the main heat release in the model was slightly retarded compared with experimental results. An attempt was made to rectify this problem by scaling the X factor in the autoignition model, and it was found that multiplying the X factor by 2.0 gave good correlation across the admittedly small range of experimental results. Comparison of resulting pressure traces are shown below in figure 1.

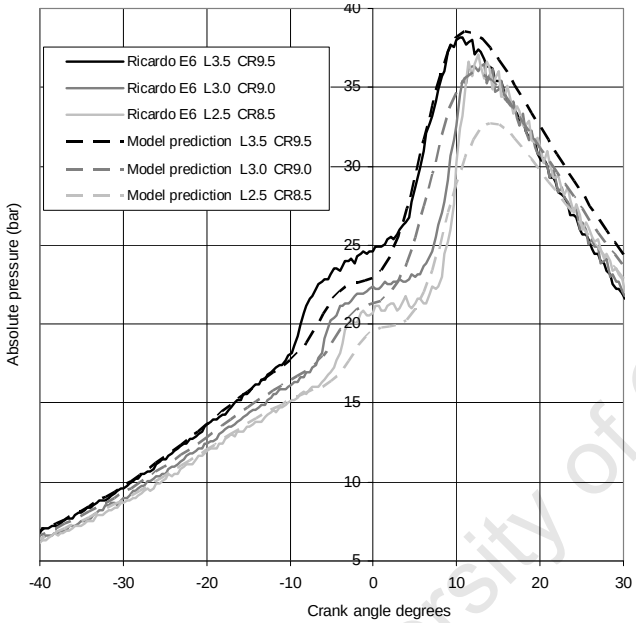

Figure 1: Comparison of experimental and modelled pressure traces at 1200rpm with "X factor" multiplied by 2 (note: combustion phasing controlled by CR adjustment).

OPERATIONAL PARAMETRIC STUDY

A parametric study was conducted using the engine model to predict the inlet charge temperature required to obtain complete combustion and peak pressure at ten degrees after TDC for a very wide range of engine speeds, compression ratios, inlet gas pressures and equivalence ratios. The combustion phasing was chosen as 10 CAD ATDC for reasons stated earlier. This was done for 3 fuels and 3 engine displacement sizes. The fuels used were n-heptane, iso-octane and methanol. The 3 engine displacements were chosen according to 3 HCCI engines currently being studied:

- a research test engine (507 cm^3),
- a small commercial utility engine (25 cm^3)
- a model aeroplane engine (6.5 cm^3).

For each engine and fuel combination, attention was directed towards compression ratios that yielded practically attainable initial temperatures and pressures. Attention was directed towards areas where engine speeds converged, implying speed insensitivity to combustion phasing. Within these areas, attention was directed towards zones that exhibited load (equivalence ratio and/or initial pressure) insensitivity to combustion phasing.

These areas were then investigated for running stability by assessing the effect of small changes in initial temperature and/or engine speed on combustion phasing. Areas that exhibited high phasing sensitivity to these changes were deemed unstable operating points and therefore of little practical value, while areas that exhibited low sensitivity were deemed to be practically achievable and therefore of value. Pressure rise rate limits were not regarded as a limiting factor in this study since many researchers have attained extremely high load operation with corresponding high pressure rise rates and ringing intensities without evidence of engine damage [4, 16]. This is particularly interesting in the light of the modes of auto-ignition damage shown by [32, 33]. In addition, very small engines with large in-cylinder thermal gradients appear to operate at high loads completely free of knocking limitations [25-29]. However, care was taken to steer clear of lean misfire and emissions limits shown by [19, 21, 34]

PARAMETRIC STUDY RESULTS

Parametric study results using n-heptane and the 507cm^3 research engine configuration, a typical set of initial pressure and charge temperature curves are shown in figure 2 below.

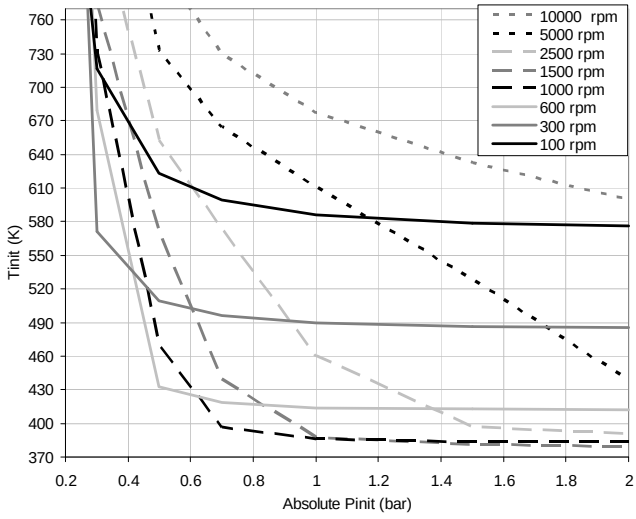

Figure 2: Curves of initial pressure and charge temperature for 507 cm^3 engine at CR = 8 and ϕ = 0.35, using n-heptane.

A number of interesting features can be seen in figure 2:

1. Typical cranking engine speeds (300 rpm or less) require high initial temperatures in order to overcome the significant heat losses. High engine speeds also require high initial temperatures in order to achieve short enough ignition delay times for appropriate combustion phasing.

2. For this particular set of conditions, there is a converging of the speed contours at around 1500 rpm for unthrottled (Pi > 1bar) operation. This means that for changes in speed between 1000 and 1500rpm, very little change in the initial temperature of 380K is needed to maintain correct combustion phasing.

3. The lower speed curves flatten out at higher initial pressures. For example, there is almost no change in the initial temperature of 380K required to maintain correct combustion phasing at 1000rpm as the initial pressure is increased from 1bar to 2bar.

The base of the speed converged Ti-Pi curves tends to slope upward for higher equivalence ratios and downward for lower equivalence ratios than the $\phi = 0.35$ condition shown in figure 2.

Similar curves can be calculated illustrating the effects of equivalence ratio on initial charge temperatures required for correct combustion phasing. A typical set is shown in figure 3 below.

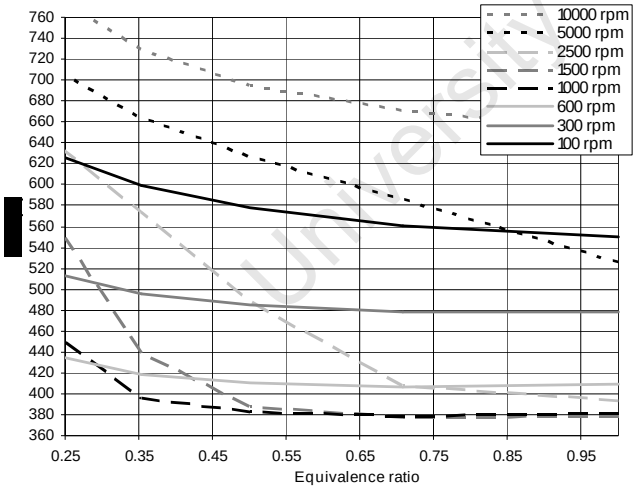

Figure 3: Curves of equivalence ratio and charge temperature for 507 cm^3 engine at CR = 8 and P_i = 0.7 bar, using n-heptane.

A number of interesting observations can be made from the Ti-ϕ curves shown in figure 3:

1. The convergence of speeds can also be observed in the equivalence ratio dimension at an inlet charge temperature of 380K and occur in a similar speed range (1000-1500rpm) to that seen in figure 2.

2. The curves flatten out at higher equivalence ratios. For example, there is almost no change in initial temperature of 380K required to maintain correct combustion phasing at 1000rpm as the equivalence ratio is increased from 0.5 to 1.0.

Note that the base of the converged Ti-ϕ curves tends to slope upward for higher initial pressures and downward for lower initial pressures than the Pi = 0.7 bar condition shown in fig 3.

Increasing compression ratio results in inlet charge temperature convergence over a wider range of engine speeds. This means that inlet heating is not desirable, since it reduces the compression ratio needed to achieve correct combustion phasing.

For n-heptane in the 507 cm^3 engine without inlet air heating, inlet charge temperatures (including port heating of 60 K) were kept constant at 360 K. This allowed the following operation while maintaining peak pressure phasing of CAD 10 ±1 ATDC:

- For Pi = 1.5bar and $\phi = 0.5$ a speed range of 950 – 2600 rpm.

- At 1500 rpm and $\phi = 0.5$ an inlet pressure from 0.6 bar upwards (upper boost pressure limit would be limited by peak cylinder pressures and intercooling requirements)

- At 1500 rpm and Pi = 1.5bar , equivalence ratio $\phi = 0.2 – 0.75$

A stability analysis was conducted on these conditions by testing the phasing sensitivity to small changes in initial conditions. Peak pressure phasing can be seen as a function of inlet charge pressure and temperature in figure 4 below.

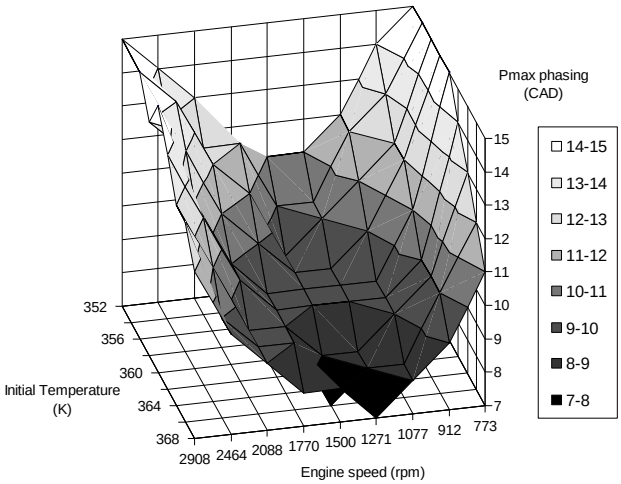

Figure 4: Peak pressure phasing surface showing engine speed and charge temperature effects on phasing for 507 cm^3 engine at CR = 10, P_i = 1 bar, ϕ = 0.5 using n-heptane.

The peak pressure phasing surface plot in figure 4 reveals that the running stability (indicated by the slope of the surface) decreases dramatically as peak pressure phasing is retarded. At the midpoint of the speed convergent zone (~1500 rpm) the phasing is relatively stable with respect to small changes in engine speed. However, at the extremities of the speed convergent zone (900 rpm and 2100 rpm), peak pressure phasing is far more sensitive to small changes in engine speed. Peak pressure phasing sensitivity with respect to inlet charge temperature does not appear to change significantly within the speed convergent zone.

Changing the fuel to iso-octane necessitates much higher compression ratios in order to attain appropriate auto-ignition phasing without significant inlet charge heating due to its low ignition quality. Initial pressure and charge temperature curves for iso-octane are shown in figure 5 below.

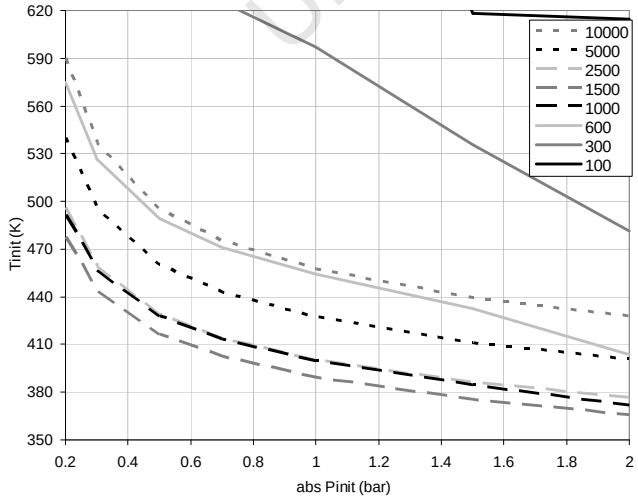

Figure 5: Curves of initial pressure and charge temperature for 507 cm^3 engine at CR = 20 and ϕ = 0.35, using iso-octane.

Observations from the Ti-Pi curves shown in figure 5 include the following:

1. Similar speed convergence behaviour can be observed with iso-octane as was seen using n-heptane: The inlet charge temperatures are fairly constant with respect to speed change for speeds close to 1500rpm.

2. However, with iso-octane the speed convergence applies throughout the inlet pressure range and not only at higher inlet pressure conditions as with n-heptane in figure 2.

3. Iso-octane does not exhibit flattening out of the curves at higher inlet pressures (compare figures 2 and 5), indicating pressure sensitivity of combustion phasing throughout the inlet pressure range.

The Ti-ϕ curves for this engine using iso-octane are shown in figure 6 below:

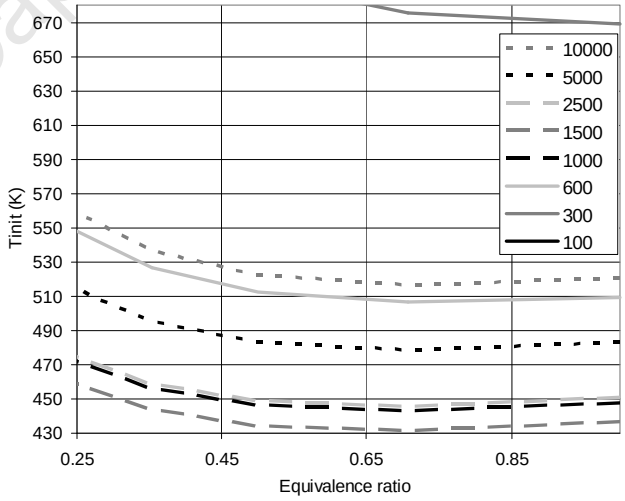

Figure 6: Curves of equivalence ratio and charge temperature for 507 cm^3 engine at CR = 20 and P_i = 0.3 bar, using iso-octane.

Observations form the Ti-ϕ curves in figure 6 include the following:

1. Similar speed induced Ti convergence is seen at at engine speeds around 1500 rpm.

2. Iso-octane exhibits this speed convergence throughout the equivalence ratio range, unlike n-heptane which only exhibits speed convergence at higher equivalence ratios (compare figures 3 and 6)

3. Iso-octane Ti-ϕ curves maintain slight curvature across the equivalence ratio range unlike n-heptane Ti-ϕ curves which flatten and reach constant Ti values for higher equivalence ratios. (compare figures 3 and 6). This means that fueling can only be varied independently of combustion phasing in a small range of equivalence ratios (ϕ = 0.50 to 0.85) with the condition in figure 6.

For iso-octane in the 507 cm^3 engine with some inlet air heating, inlet charge temperatures (including port heating of 60 K) were kept constant at 386 K. This allowed the following operation while maintaining peak pressure phasing of CAD 10 ±1 ATDC:

- For Pi = 1 bar and ϕ = 0.5 a speed range of 1000 – 2800 rpm.
- At 1500 rpm and Pi = 1bar, equivalence ratio ϕ = 0.2 – 0.75
- No areas of inlet pressure insensitivity were found.

A stability analysis was conducted on these conditions by testing the phasing sensitivity to small changes in initial conditions using iso-octane. Peak pressure phasing can be seen as a function of inlet charge pressure and temperature in figure 7 below. Instability trends were remarkably similar to those observed with n-heptane in figure 4.

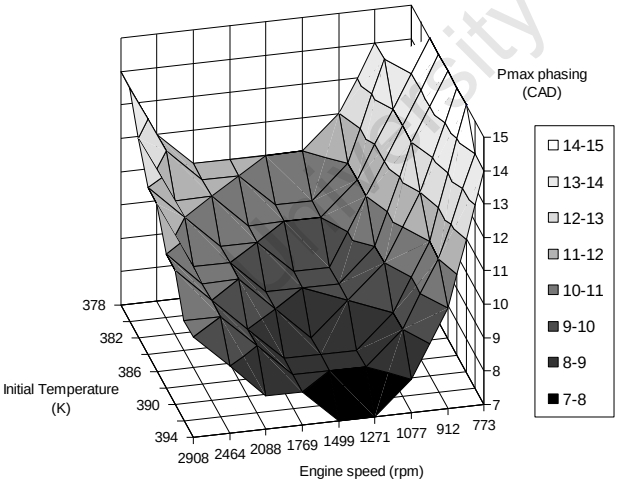

Figure 7: Peak pressure phasing surface showing engine speed and charge temperature effects on phasing for 507 cm^3 engine at CR = 20, P_i = 1 bar, ϕ = 0.5 using n-heptane.

Changing the fuel to methanol also requires high compression ratios in order to attain auto-ignition without significant inlet charge heating. Initial pressure and charge temperature curves for methanol are shown in figure 8. Observations include the following:

1. Methanol exhibits quite linear Pi-Ti relationships, indicating much less sensitivity to inlet throttling effects on inlet charge pressure.
2. Methanol exhibits similar speed convergence behaviour to iso-octane.
3. Methanol does not exhibit pressure insensitive zones (similarly to iso-octane).

The Ti-ϕ curves for methanol shown in figure 9 also maintain the speed convergence throughout the equivalence ratio range (similarly to iso-octane) and are also more sensitive to equivalence ratio than when using n-heptane

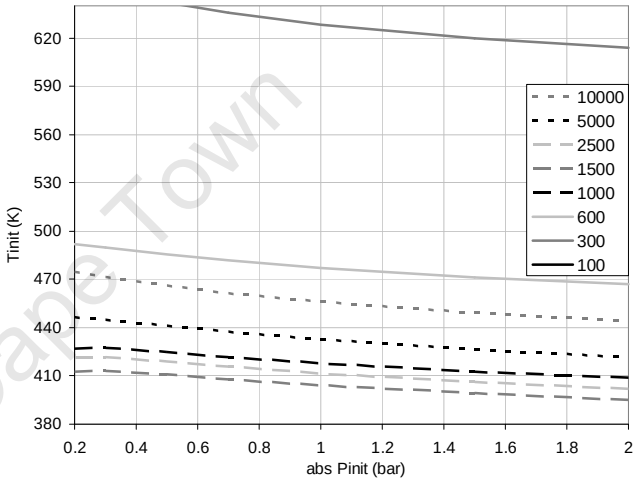

Figure 8: Curves of initial pressure and charge temperature for 507 cm^3 engine at CR = 20 and ϕ = 1.0, using methanol.

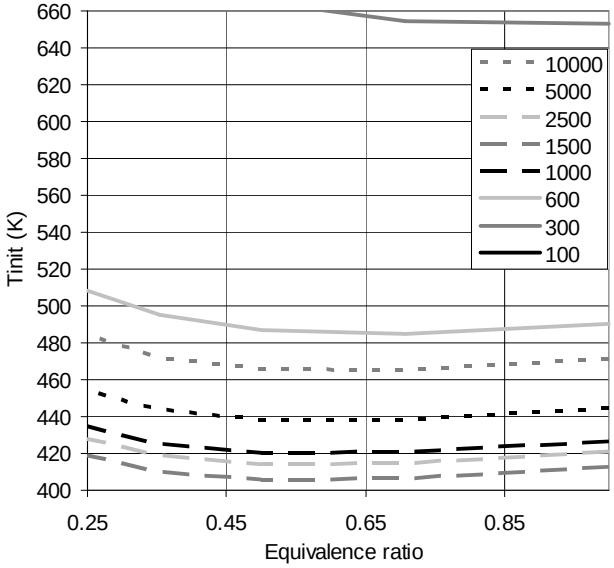

Figure 9: Curves of equivalence ratio and charge temperature for 507 cm^3 engine at CR = 20 and P_i = 0.3 bar, using methanol.

For methanol in the 507 cm^3 engine with some inlet air heating, inlet charge temperatures (including port heating of 60 K) were kept constant at 380 K. This allowed the following operation while maintaining peak pressure phasing of CAD 10 ±1 ATDC:

- For Pi = 1 bar and ϕ = 0.5 a speed range of 1100 – 3100 rpm.
- No areas of inlet pressure insensitivity were found.

If the inlet charge was further heated (including port heating of 60 K) to 402 K,

- At 1500 rpm and Pi = 0.3bar, equivalence ratio ϕ = 0.25 – 1.0

Instability trends for methanol were very similar to those observed with iso-octane and n-heptane in figures 4 and 7.

HCCI behaviour in the 25 cm^3 engine shows significant differences due to size effects. More heat is lost to the combustion chamber walls due to the increased surface to volume ratio. This means that a higher compression ratio must be used to avoid the need for significant inlet heating.

Figures 10 and 11 show the Ti-Pi and Ti –ϕ curves for the 25 cm^3 engine running on n-heptane and the following features can be observed:

1. The broad convergence of speeds covers a far wider speed range than for the 507 cm^3, especially at higher inlet pressures, although the well converged engine speed ratios are similar.
2. The same zones of pressure insensitivity can be observed with this engine.
3. Areas of equivalence ratio insensitivity can also be observed.

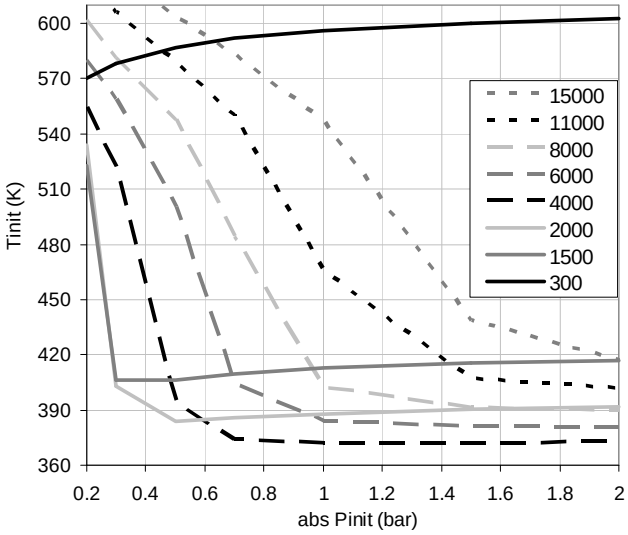

Figure 10: Curves of initial pressure and charge temperature for 25 cm^3 engine at CR = 14 and ϕ = 1.0, using n-heptane.

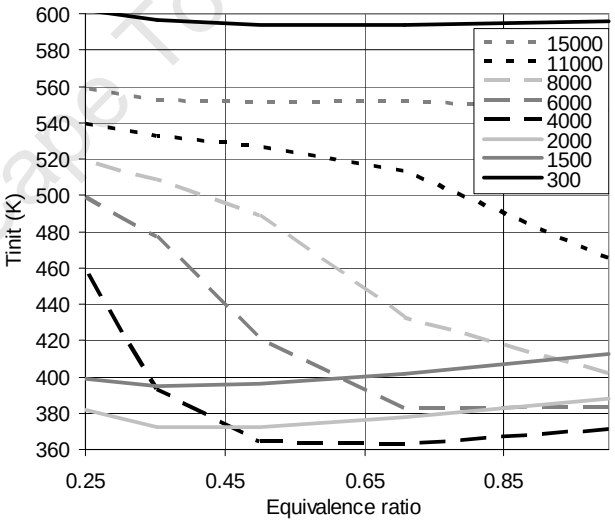

Figure 11: Curves of equivalence ratio and charge temperature for 25 cm^3 engine at CR = 14 and P_i = 1.0 bar, using n-heptane.

For n-heptane in the 25 cm^3 engine without inlet air heating, inlet charge temperatures (including port heating of 60 K) were kept constant at 358 K. This allowed the following operation while maintaining peak pressure phasing of CAD 10 ±1 ATDC:

- For Pi = 1.5bar and ϕ = 0.7 a speed range of 2400 – 6500 rpm.
- At 4000 rpm and ϕ = 0.7 an inlet pressure from 0.7 bar upwards (upper boost pressure limit would be limited by peak cylinder pressures and intercooling requirements)
- At 4000 rpm and Pi = 1.5bar , equivalence ratio ϕ = 0.25 – 0.9

The 25 cm^3 engine model was also combined with the iso-octane and methanol AI models. The results show similar trends to the larger engine, but require higher compression ratios as illustrated above. Thermal and speed sensitivity analyses on phasing stability for all three fuels yielded very similar results to the larger engine.

The 6.5 cm^3 engine geometry was also modelled with the 3 fuel AI models. The general trend was similar to results already presented except that even higher compression ratios were required in order to achieve appropriate combustion phasing without excessive inlet charge heating. Use of n-heptane however, exhibited slightly atypical behaviour as shown in figures 12 and 13. This very small engine did not exhibit any areas of charge pressure insensitivity even with n-heptane and only very narrow areas of equivalence ratio insensitivity. However, with n-heptane (only) this engine does exhibit areas where multiple Pi-Ti or ϕ-Ti lines cross. Examples are shown at Ti = 485 K and Pi = 0.7 bar in figure 12 and at Ti = 490 K and ϕ = 0.68 in figure 13.

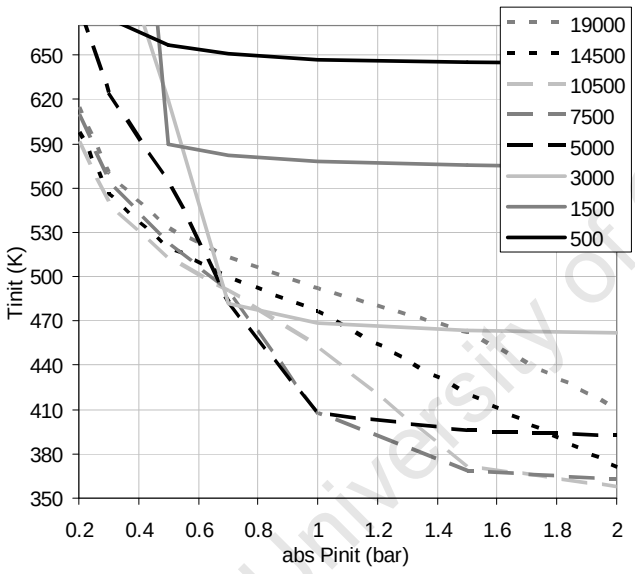

Figure 12: Curves of initial pressure and charge temperature for 6.5 cm^3 engine at CR = 20 and ϕ = 0.5, using n-heptane.

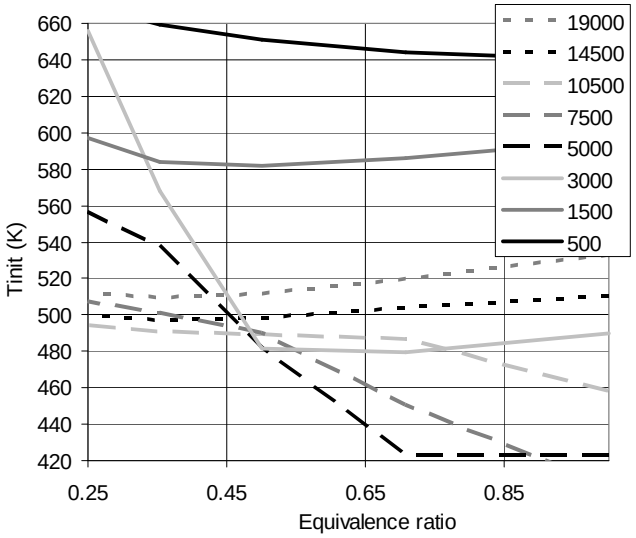

Figure 13: Curves of equivalence ratio and charge temperature for 6.5 cm^3 engine at CR = 20 and P_i = 0.7 bar, using n-heptane.

These areas of intersections in figures 12 and 13 can yield unique areas of operation in terms of speed insensitivity. For example, while maintaining peak pressure phasing of CAD 10 ±1 ATDC in the 6.5 cm^3 engine at CR = 20 using n-heptane: with a slightly throttled charge pressure of 0.68 bar and fixed heated charge temperature of 469±4 K the speed available is 2950 – 15000 rpm.

This represents a five fold increase in speed and is even more significant given the thermal stability of the zone. This speed transition is made possible by a unique combination of the effects of speed and heat transfer on the cylinder pressure and temperature histories (as shown in figure14) and subsequent cool flame timing and heat release magnitude (as shown in figure 15). At the lower speed limit, the cool flame occurs late and yields a significant temperature rise. As the speed is increased, the cool flame timing is advanced and the cool flame heat release is reduced until it becomes insignificant at the high speed limit. At this point it is unable to control the main combustion phasing and further increase in speed results in rapid retardation of combustion timing.

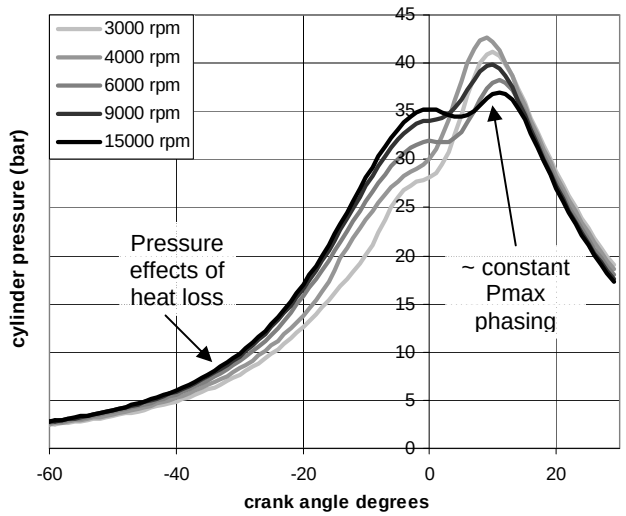

Figure 14: Cylinder pressure traces for the 6.5 cm^3 engine at CR = 20, Pi = 0.68 bar Ti = 469 K, using n-heptane.

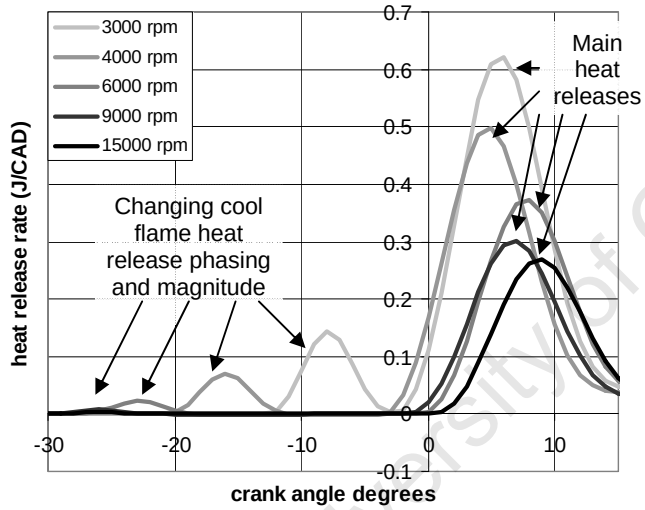

Figure 15: Heat release rate traces for the 6.5 cm^3 engine at CR = 20, Pi = 0.68 bar Ti = 469 K, using n-heptane.

This transition behaviour of cool flame heat release with increasing temperature has been studied in [9] and is shown in figure 16 below, taken from [9].

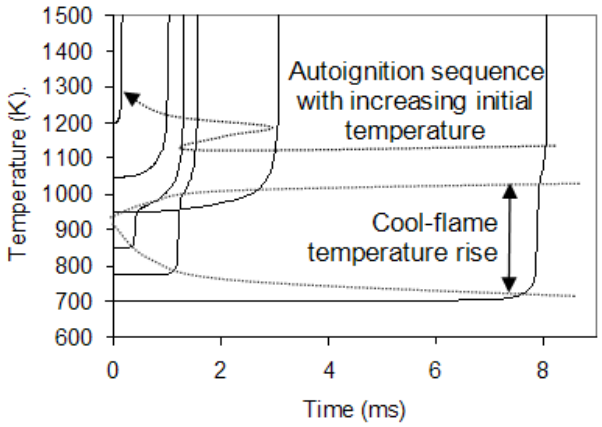

Figure 16: Stoichiometric auto-ignition delay profiles for n-heptane at various initial temperatures in a constant volume simulation at 20 bar, taken from [9].

DISCUSSION

Since the operational range of an engine is typically expressed in terms of speed and load, it is very interesting to note that areas exist within an HCCI engine operating range where engine speed and/or load (equivalence ratio and/or inlet pressure) can be varied without adjustment of any other parameters being required to maintain a particular combustion phasing. Furthermore, these zones seem to exist in areas of operation where the phasing sensitivity to temperature is not high. This indicates that these areas would be naturally stable operating zones and indicates that they would be achievable in reality. These areas could contribute to HCCI control stability as well as offering a means of easily executing speed-load transitions without complex control mechanisms.

N-heptane offers areas of inlet charge pressure insensitivity while iso-octane and methanol do not. This is interesting since n-heptane and iso-octane both exhibit “negative temperature coefficient” (and associated cool flame) behaviour. In an effort to understand this behaviour, several engine compression pressure and temperature histories were plotted on the reaction rate surfaces (average reaction rate = 1/total ignition delay) of n-heptane and iso-octane for comparison in figures 17 and 18.

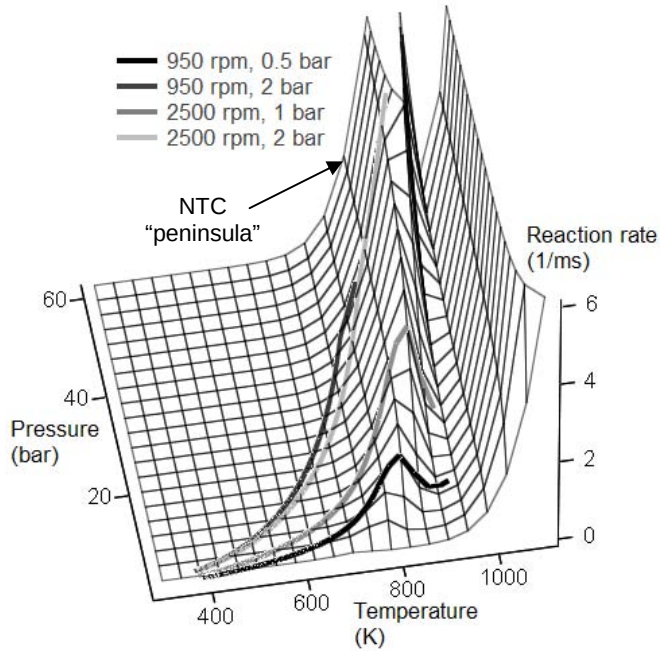

Figure 17: Surface plot showing fuel mixture reaction rate as a function of pressure and temperature. Surface is shown for n-heptane at $\phi = 0.5$. and shows the NTC "peninsula" increasing with pressure at T ≈ 820 K. Four temperature and pressure histories taken from the 507 cm^3 engine are superimposed. All four histories have identical peak pressure phasing, use CR = 10 and Ti = 360 K and show compression histories up to the start of main heat release points.

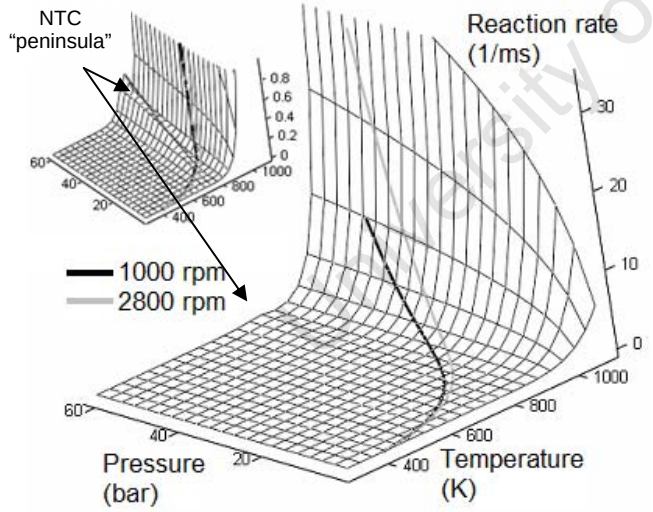

Figure 18: Surface plot showing fuel mixture reaction rate as a function of pressure and temperature. Surface is shown for iso-octane at $\phi = 0.5$. Two temperature and pressure histories taken from the 507 cm^3 engine are superimposed. Both histories have identical peak pressure phasing, use CR = 20, Ti = 402 K, Pi = 1 bar and show compression histories up to the start of main heat release points. The insert version shows the same plot with a significantly reduced reaction rate scale in order to expose the NTC "peninsula" increasing with pressure at T ≈ 800 K.

Figures 17 and 18 yield insight into two reasons for the apparent absence of NTC effect which would normally be expected for iso-octane as a 2 stage ignition fuel:

1. The positioning of the engine compression histories results in the charges missing the iso-octane "NTC wedge" almost completely as shown in the close-up insert of fig 18.

2. The reaction rates experienced by the charge in the iso-octane NTC region are quite insignificant compared with the reaction rates experienced later in the compression. The path through the NTC region therefore has negligible effect on combustion phasing.

Note that although iso-octane and methanol do not display NTC behaviour in an engine combustion environment, they are still affected by heat transfer effects on ignition delay and therefore still exhibit speed convergence behaviour as shown in the parametric study results.

Where Ti-ϕ lines slope downward and move to the right with increasing engine speed, (For example as for the 25 cm^3 engine with n-heptane at T = 460K as shown in figure 11), the possibility exists to operate using speed and equivalence ratio balanced phasing. This results in a single curve of increasing power which can be scribed through the speed-load domain with constant inlet charge temperature and constant combustion phasing. An example would be the 25 cm^3 engine at CR = 14 and P_i = 1.0 bar, using n-heptane and an inlet charge temperature of 453K running from $\phi = 0.25$ at 4000rpm to $\phi = 1$ at 11000rpm. This condition can be deduced from figure 11 and is shown in figure 19 below.

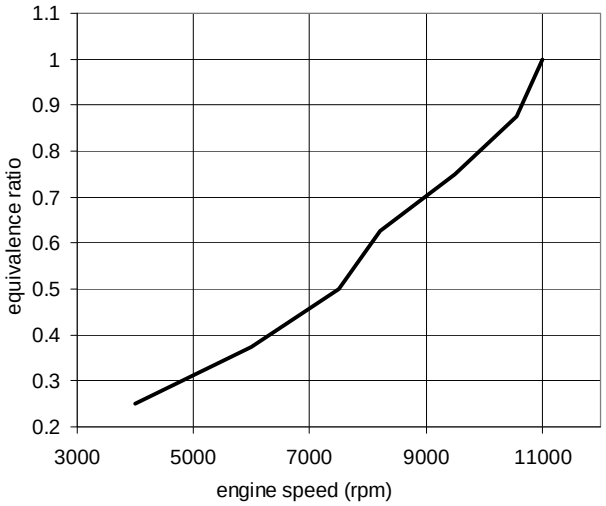

Figure 19: Constant phasing power line for 25 cm^3 engine at CR = 14 and P_i = 1.0 bar, using n-heptane at an inlet charge temperature of 453 K

Given the right setup, similar behaviour can be exploited using charge pressure as indicated in figure 10 at T = 420 K and a speed and charge pressure balance can be created as shown in figure 20 below:

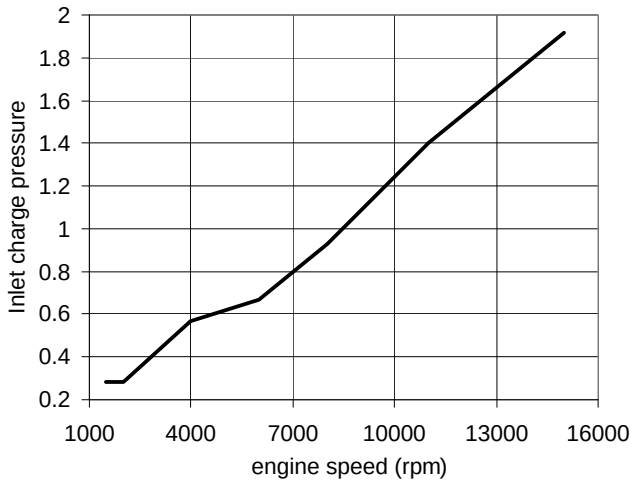

Figure 20: Constant phasing power line for 25 cm^3 engine using n-heptane at CR = 14, ϕ = 1.0 at an inlet charge temperature of 420 K

These lines or curves presented in figures 19 and 20 could represent convenient solutions to applications where fixed speed-load lines are features of the application. Examples would include fixed pitch propellers, blower and pump impellors etc.

The heat loss at very low engine speeds remains a significant challenge even in a firing engine and would be far more severe in a cold engine on crank starting.. Small engines can be cranked at higher speeds but also have higher heat loss. Recent advances in solenoid and pneumatic valve actuation hardware could provide the answer with multiple compressions of a single charge for starting purposes. Another possible answer could be the combination of an electric motor and HCCI engine in a “mild hybrid” configuration. This configuration would provide high speed motoring power for starting the HCCI engine.

The width of a zone of speed independent fixed combustion phasing increases with increasing compression ratio and high CR is therefore a desirable feature which also offers improved thermal efficiency. This means that for passenger car sized engines a fuel of mid range ignition quality is required if inlet heating is to be avoided.

A two stage ignition fuel is also desirable since this holds potential for load control using zones of pressure insensitivity as well as the zones of air-fuel ratio insensitivity offered by both single and 2-stage ignition fuels. This advantage adds to the four distinct advantages of 2-stage ignition HCCI fuels offered by [31] and revisited by [11]. Blending of aromatics in the form of toluene with n-heptane has been shown to reduce the cool flame heat release more severely than addition of iso-octane for a given ignition quality [31]. This indicates that the NTC behaviour of the fuel and hence the tuning of HCCI operational “sweet spot” ranges can be optimised through fuel chemistry as well as careful setup of the engine. As engine displacement decreases, autoignition quality must be improved in order to counter heat loss effects of large combustion chamber surface to volume ratios.

CONCLUSION

A discrete explicit engine model was combined with an empirical fuel autoignition model and used to study the interaction of engine operational characteristics with fuel auto-ignition behaviour in HCCI engine combustion. A variety of insights were highlighted and discussed and conclusions include the following.

- A discrete explicit engine model can be formulated to be sensitive to the effects of inlet pressure and temperature, engine speed and displacement size effects on heat loss as well as inlet heating and compression ratio effects on inlet charge composition, temperature and pressure. This formulation together with an auto-ignition integral method fuel autoignition model therefore provides a realistic and computationally efficient basis for investigating trends across wide ranges of multiple variables in HCCI engine operation.

- In general, engine speed effects on combustion phasing exhibit convergence to a speed range where engine speed can be varied independently of combustion phasing without phasing correction adjustment of other variables.

- Within these speed convergence areas, zones also exist where fuel equivalence ratio can be varied independently of combustion phasing without phasing correction adjustment of other variables. For n-heptane, zones also exist where inlet pressure can be varied independently of combustion phasing without phasing correction adjustment of other variables, but this is not the case with fuels that do not exhibit any significant cool flame heat release within the convergent zone even if they do in fact exhibit negative temperature coefficient behaviour within their broader auto-ignition characterisation.

- HCCI operational zones also exist where multiple constant combustion phasing lines of differing engine speed intersect to allow very large ranges of phasing independent speed variation.

- This formulation of HCCI modelling can also be used to find fixed constant combustion phasing lines that run through the speed-load map from low speed and low load to high speed and high load, much like a propeller speed-load line. Load control can be achieved by equivalence ratio and/or inlet pressure in the case of fuels exhibiting cool flame behaviour, but only by equivalence ratio in fuels exhibiting no cool flame heat release.

- Engine cylinder size plays an important role in determining the fuel ignition quality appetite of an HCCI engine and strongly influences the speed range where speed can be varied without affecting combustion phasing.

- Appropriate combustion phasing cannot be achieved for slow cranking engine speeds without unrealistic charge heating due to excessive compression heat loss. Spark ignition, multiple single charge compressions, high speed cranking or some other means of starting HCCI engines is therefore required.

- HCCI engine compression ratio, size and fuel formulation are therefore critical parameters in determining the most effective operational range and mode combustion control.

ACKNOWLEDGMENTS

This study was funded and supported by the Sasol Technology Fuels Research team which is headed by Dr J.J. Botha.

REFERENCES

1. F. Zhao, T.W. Asmus, D.N. Assanis, J.E. Dec, J.A. Eng and P.M. Najt, (2003), "Homogeneous charge compression ignition (HCCI) engines: key research and development issues", 1st edition, Warrendale, PA, Society of Automotive Engineers.
2. Andre Kulzer, Ansgar Christ, Martin Rauscher, Christina Sauer, Gernot Wurfel, Thomas Blank, (2006), "Thermodynamic Analysis and Benchmark of Various Gasoline Combustion Concepts", SAE 2006-01-0231.
3. Yu chun Hou, Xing cai Lu, Lin lin Zu, Li bin Ji, and Zhen Huang, (2006), "Effect of High-Octane Oxygenated Fuels on n-Heptane-Fueled HCCI Combustion", Energy & Fuels 2006, 20.
4. Christensen, M., Johansson, B., Amnèus, P. and Mauss, F., (1998), "Supercharged Homogeneous Charge Compression Ignition", SAE 980787
5. Andy D.B. Yates, Carl L. Viljoen, Andre Swarts, (2004), "Understanding the Relation Between Cetane Number and Combustion Bomb Ignition Delay Measurements", SAE 2004-01-2017
6. Viljoen, C.L., Yates, A.D.B., Swarts, A., Balfour, G., Möller, K., (2005), "An Investigation of the Ignition Delay Character of Different Fuel Components and an Assessment of Various Autoignition Modelling Approaches", SAE 2005-01-2084
7. Yates, A.D.B., Swarts, A., Viljoen, C.L., (2005), "Correlating Auto-ignition Delays and Knock-Limited Spark-Advance Data for Different Types of Fuel", SAE 2005-01-2083
8. Sibusiso C. Londleni, Tiaan Rabe, Andre Swarts, (2007), "The Application of an Enhanced Ignition Delay Model to HCCI Engines and Comparison to Engine Measurements", SAE 2007-01-0048
9. Yates ADB, (2008) "An improved empirical model for describing autoignition", SAE 2008-01-1629
10. Carl L. Viljoen, Andy D.B. Yates and Roelof L.J. Coetzer, (2007), "A molecular modelling investigation of selected gasoline molecules to relate oxidation pathways to their autoignition behaviour", SAE 2007-01-0005
11. Magnus Sjoberg, John Dec, Wontae Hwang, (2007), "Thermodynamic and Chemical Effects of EGR and Its Constituents on HCCI Autoignition", SAE 2007-01-0207
12. Yufeng Li, Hua Zhao, Tom Ma, Nikolaos Brouzos, (2007), "Parametric study on CAI Combustion in a GDI Engine with an Air-Assisted Injector", SAE 2007-01-0196
13. Heywood, John B, (1988), "Internal Combustion Engine Funamentals", 1st edition, Singapore, McGraw-Hill
14. Morikawa and Ishibashi, (2007), "An Experimental Approach to the Controlled Auto-Ignition", SAE 2007-01-0173
15. Hiroshi Kuzuyama, Kazuhisa Inagaki, Matsuei Ueda, Kazuhiro Akihama, Masahiro Machida, (2007), "A Study on Natural Gas Fueled Homogeneous Charge Compression Ignition Engine - Expanding the Operating Range and Combustion Mode Switching", SAE 2007-01-0176
16. Yuuichi Kodama, Izumi Nishizawa, Takumi Sugihara, Norihiko Sato, Tadashi Iijima, Tatsuya Yoshida, (2007), "Full-Load HCCI Operation with Variable Valve Actuation System in a Heavy-Duty Diesel Engine", SAE 2007-01-0215
17. Kyoungjoon Chang, George A. Lavoie, Dennis N. Assanis, Zoran S. Filipi, Aristotelis Babajimopoulos, (2006), "Analysis of Load and Speed Transitions in an HCCI Engine using 1-D Cycle Simulation and Thermal Networks", SAE 2006-01-1087
18. Mahdi Shahbakhti, Charles R. Koch, Robert Lupul, (2007), "Predicting HCCI Auto-Ignition Timing by Extending a Modified Knock-Integral Method", SAE 2007-01-0222
19. Sjöberg and Dec, (2003), "Combined Effects of Fuel-Type and Engine Speed on Intake Temperature Requirements and Completeness of Bulk-Gas Reactions for HCCI Combustion", SAE 2003-01-3173
20. Sjöberg and Dec, (2007b), "EGR and Intake Boost for Managing HCCI Low-Temperature Heat Release over Wide Ranges of Engine Speed", SAE 2007-01-0051

21. Berntsson and Denbratt, (2007), “HCCI Combustion using Charge Stratification for Combustion Control”, SAE 2007-01-0210
22. Sjöberg and Dec, (2005), “Effects of Engine Epeed, Fueling Rate and Combustion Phasing on the Thermal Stratification Required to Limit HCCI Knocking Intensity”, SAE 2005-01-2125
23. Daniel L. Flowers, J. Ray Smith, Salvador M. Aceves, Robert W. Dibble, John Torres, James Girard, (2000), “HCCI in CFR Engine: Experiments and Detailed Kinetic Modeling”, SAE 2000-01-0328
24. William J. Pitz, Nicholas P. Cernansky, Frederick L. Dryer, Heinz Pitsch, Dan G. Friend, John T. Farrell, Fokion N. Egolfopoulos, (2007), “Development of an experimental Database and Chemical Kinetic Models for Surrogate Gasoline Fuels”, SAE 2007-01-0175
25. Vittorio Manente, Bengt Johansson, Per Tunestal, (2006), “Influence of Inlet Temperature and Hot Residual Gasses on the Performance of a Mini High Speed Glow Plug Engine”, SAE 2006-32-0057
26. Vittorio Manente, Per Tunestal, Bengt Johansson, (2007a), “A Study of a Glow Plug Ignition Engine by Chemiluminescence Images”, SAE 2007-01-1884
27. Vittorio Manente, Per Tunestal, Bengt Johansson, (2007b), “Mini High speed HCCI engine Fuelled with Ether: Load Range, Emission Characteristics and Optical Analysis”, SAE 2007-01-3606
28. Raine and Thorwarth, (2004), “Performance and Combustion Characteristics of a Glow-Ignition Two-Stroke Engine”, SAE 2004-01-1407
29. Vikram Devaraj, Vijay Manikandan Janakiraman, Saikishan Suryanarayanan, Varun Devaraj, Kaushik Subramanian, (2007), “Comparative Study of Performance Characteristics of a Glow Plug Fired 2 Stroke Engine for Different Blends of Methanol, Castor Oil and Gasoline by Experimental and ANN Analysis”, SAE 2007-01-0058
30. Livengood & Wu, (1955), “Correlation of Autoignition Phenomena in Internal Combustion Engines and Rapid Compression Machines”, 5th (Intl) Symp on Combustion,1955, p347-356.
31. Sjöberg and Dec, (2007), “Comparing late-cycle autoignition stability for single- and two-stage ignition fuels in HCCI engines”, Combustion Institute, 31
32. Fitton & Nates, (1996), “Knock Erosion in Spark Ignition Engines”, SAE 962102
33. Nates & Yates, (1994), “Knock damage mechanisms in Spark-Ignition Engines”, SAE 942064
34. Ishibashi and Asai, (1996), “Improving the Exhaust Emissions of Two-Stroke Engines by applying Activated Radical Combustion”, SAE 960742

CONTACT

Mr Gareth Floweday
SASOL Advanced Fuels Laboratory
Mechanical Engineering Department
University of Cape Town
Tel: +27 21 650 5306
email: gareth.floweday@uct.ac.za

DEFINITIONS, ACRONYMS, ABBREVIATIONS

ABDC: After Bottom Dead Centre
ATDC: After Top Dead Center
BBDC: Before Bottom Dead Centre
BTDC: Before Top Dead Centre
CAD: Crank Angle Degrees
CF: Cool flame heat release
CI: Compression Ignition
COV: Coefficient of Variation
CR: Compression Ratio
EGR: Exhaust Gas Recirculation
EVO: Exhaust Valve Opening
HCCI: Homogeneous Charge Compression Ignition
HRR: Heat Release Rate
IC: Internal Combustion
IMEP: Indicated Mean Effective Pressure
IVC: Inlet Valve Closure
NO_x: Nitrous Oxides
NTC: Negative Temperature Coefficient
ON: Octane Number
PM: Particulate Matter
PRF: Primary Reference Fuel
RCM: Rapid Compression Machine
REG: Residual Exhaust Gas
RON: Research Octane Number
RPM: Revolutions per Minute
SI: Spark Ignition
SOC: Start of Combustion

NOMENCLATURE

LIST OF SYMBOLS
A: Pre-exponential constant of proportionality
B: Exponential temperature coefficient
β: Exponent of air-fuel ratio
n: Auto-ignition pressure coefficient
p: Pressure
Q_{LHV}: Low heat value of fuel
R: Universal gas constant
S_p: Average mean piston speed
T: Temperature
t: Time
V_d: Displacement volume
W_c: Work done per cycle
x_b: Mass fraction burnt
λ: Air-fuel ratio
Φ: Fuel-air equivalence ratio
γ: gamma (the ratio of specific heats)

APPENDIX

DISCRETE FORMULATION OF THE FUEL AUTO-IGNITION MODEL DESCRIBED IN [9]

The cool flame ignition delay is given by:

$$t_1 = \phi^{\beta_1} A_1 p^{n_1} e^{\frac{B_1}{T}} \quad \text{(Eq. 1)}$$

In the environment of changing pressure and temperature, the cool flame ignition delay is given in integral form by:

$$\int_{t_{BDC}=0}^{t_1} \frac{1}{\left(\phi^{\beta_1} A_1 p^{n_1} e^{\frac{B_1}{T}}\right)} dt = 1 \quad \text{(Eq. 2)}$$

Or in discrete form by:

$$\sum_{t_{BDC}=0}^{t_1} \frac{1}{\left(\phi^{\beta_1} A_1 p^{n_1} e^{\frac{B_1}{T}}\right)} \Delta t = 1 \quad \text{(Eq. 3)}$$

At the point where the cool flame integral = 1 (if this does occur during compression), the cool flame temperature rise is calculated using the conditions at this point and the expression:

$$\Delta T_{CF} = \omega\left(T_i - T_{EQ}.p^k.\phi^{\mu}\left(\frac{100}{99+\phi}\right)^{\sigma}\right) \quad \text{(Eq. 4)}$$

The empirical termination function for gradually nullifying the influence of the cool flame temperature rise when the calculated value became negative, was also used:

$$T_{CF} = T_i + 0.5\left(\Delta T_{CF} + \sqrt{\left(\Delta T_{CF}\right)^2 + C_0}\right) \quad \text{(Eq. 5)}$$

Where the constant $C_0 = 684$

The main (peroxide) heat release ignition delay is also calculated in discrete integral form but split into pre and post cool flame integral contributions in order to incorporate the cool flame multiplication factor X described in [9]. The discrete formulation for the peroxide ignition delay is therefore:

$$\sum_{t_{BDC}=0}^{t_1} \frac{1}{\left(\phi^{\beta_h} A_h p^{n_h} e^{\frac{B_h}{T}}\right)} \Delta t + \sum_{t_1}^{t_{Perroxide}} \frac{1}{\left(\phi^{\beta_h} A_h p^{n_h} e^{\frac{B_h}{T + X\ \Delta T_{CF}}}\right)} \Delta t \Rightarrow 1 \quad \text{(Eq. 6)}$$

Table 1. The empirical coefficient values derived for some specific fuels

Coeffs	$Ln(A_1)$	n_1	B_1	T_{EQUIL}	ω	κ_{PRESS}	X	$Ln(A_h)$	n_h	B_h	μ_ϕ	σ_ϕ	β_1	β_h
iso-octane	-17.03	-0.237	14764	719.2	-1.221	0.050	1.179	-11.20	-1.012	15022	0.050	0.732	-0.276	-0.777
n-heptane	-18.73	-0.065	14764	819.6	-1.221	0.050	1.550	-10.98	-0.972	15022	0.050	0.732	-0.117	-0.456
methanol	-	0	-	-	0	-	0	-15.90	-0.752	18549	-	-	-	-0.629

Appendix C: Thermodynamic derivations and equations used in the engine models

This appendix provides the derivations of mathematical expressions used in the thermodynamic engine models built during this study. These derivations and mathematical expressions are not novel and can be found in [1;2] and other standard engine modelling and thermodynamics texts.

The engine models were built on the fundamental principles of the ideal gas law:

$$pV = nR_uT$$

Where:

p = pressure

V = volume

n = number of moles

R_u = the universal gas constant (8.3143 J/molK)

T = temperature

The first law of thermodynamics in general form:

$$E = U + KE + PE$$

$$KE \approx 0 \approx PE$$

$$E = U$$

Where

E = total system energy

U = internal energy

KE = kinetic energy

PE = potential energy

The first law of thermodynamics as applied to closed systems:

$$\mathrm{Q} - \mathrm{W} = \Delta \mathrm{E}$$

$$E = U$$

$$U_P - U_R = Q_{R-P} - W_{R-P}$$

Where:

Q = heat added to the system

W = work taken from the system

subscript R refers to reaction reactants

subscript P refers to reaction products

The first law of thermodynamics as applied to flow through a control volume:

total energy in a closed volume, $E = U + KE + PE$

flow work, $w = FL = PAL = PV$

total energy in a open (flow through) volume:

$$\Theta = E + PV = U + PV + KE + PE$$
$$= H + KE + PE$$
$$\therefore 1\text{st Law} \Rightarrow \quad Q - W = \Delta H + \Delta KE + \Delta PE$$
$$\Delta KE \approx 0 \approx \Delta PE$$
$$\therefore \qquad Q - W = \Delta H$$

Where:

F = force

L = length

A = cross sectional area

H = enthalpy (see definition below)

The following standard mathematical definitions were used:

$$W = \int P dV$$

Heat capacity/specific heat from JANAF thermodynamic table, ca. 1971

$$Cp(T) = aT^4 + bT^3 + cT^2 + dT + e$$

Relationships between Cp and C_v:

from defn: $H = U + PV$

mass specific: $h = u + Pv$

& idea gas law: $Pv = R_s T$

differentiating: $dh = du + R_s dT$

substituting: $dh = C_p dT$ and $du = C_v dT$

we get: $C_p dT = C_v dT + R_s dT$

$\therefore R_s = Cp - Cv$ (per unit mass basis)

or $R_u = Cp - Cv$ (per unit mol basis)

$$R = \frac{\partial h}{\partial T} - \frac{\partial u}{\partial T}$$

Relationship of $C_p(T)$ and $h_{sensible}$:

$$\text{note: } h_{\text{state, (T)}} = h_{\text{formation, (T=0K)}} + h_{\text{sensible, (T)}}$$

$$Cp = \left(\frac{\partial h}{\partial T}\right)_p \qquad \therefore\ h_{\text{sensible, (T)}} = \int_0^T C_{p,(T)}\, dt$$

$$\text{empirically, } C_P = a + bT + cT^2 + dT^3 + eT^4$$

$$\therefore\ h_{\text{sensible, (T)}} = \left| aT + \frac{b}{2}T^2 + \frac{c}{3}T^3 + \frac{d}{4}T^4 + \frac{e}{5}T^5 + \text{constant} \right|_0^T$$

$$\therefore\ h_{\text{sensible, (T)}} = aT + \frac{b}{2}T^2 + \frac{c}{3}T^3 + \frac{d}{4}T^4 + \frac{e}{5}T^5$$

Note 1: $h_{\text{formation}}$ given at 298K and not 0K

Note 2: C_P coeff only valid in particular ranges of T

from $h_{\text{state, (T)}} = h_{\text{formation, (T=0K)}} + h_{\text{sensible, (T)}}$

$$\text{reformulate: } h_{\text{state, (T)}} = \left(\Delta h^0_{f_{298}} - h^0_{\text{sensible}_{298}}\right) + h_{\text{sensible, (T)}}$$

$$H_R = \sum_{\text{reactants}} n_i h_i$$

$$H_P = \sum_{\text{products}} n_i h_i$$

$$(\Delta H)_{P,adiabatic} = \left(H_P - H_R\right)_{P,adiabatic} = 0$$

$$u_{\text{state, (T)}} = h_{\text{state, (T)}} - R_u T$$

$$U_R = \sum_{\text{reactants}} n_i u_i$$

$$U_P = \sum_{\text{products}} n_i u_i$$

$$(\Delta U)_{V,adiabatic} = \left(U_P - U_R\right)_{V,adiabatic} = 0$$

Adiabatic flame temperature for a constant volume, adiabatic process:

$$Q_{R-P} = (\Delta U)_V = 0$$
$$\therefore U_P - U_R = 0$$
$$\therefore U_P(T_P) - U_R(T_R) = 0$$

$$\text{Since} \quad U_P(T_0) - U_R(T_0) = (\Delta U)_{V,T_0}$$
$$\therefore \left[U_P(T_P) - U_P(T_0)\right] - \left[U_R(T_R) - U_R(T_0)\right] = -(\Delta U)_{V,T_0}$$
$$\text{\& since} \quad Q_{HV_V} = -(\Delta U)_{V,T_0}$$
$$\therefore \left[U_P(T_P) - U_P(T_0)\right] - \left[U_R(T_R) - U_R(T_0)\right] = Q_{HV_V,T_0}$$

i.e. given thermo-chemical tables for heating values and relative internal energies and given T_R, we can solve for T_P

Adiabatic flame temperature for a constant pressure, adiabatic process:

$$Q_{R-P} = (\Delta H)_P = 0$$
$$\therefore H_P - H_R = 0$$
$$\therefore H_P(T_P) - H_R(T_R) = 0$$

$$\text{Since} \quad H_P(T_0) - H_R(T_0) = (\Delta H)_{P,T_0}$$
$$\therefore \left[H_P(T_P) - H_P(T_0)\right] - \left[H_R(T_R) - H_R(T_0)\right] = -(\Delta H)_{P,T_0}$$
$$\text{\& since} \quad Q_{HV_P} = -(\Delta H)_{V,T_0}$$
$$\therefore \left[H_P(T_P) - H_P(T_0)\right] - \left[H_R(T_R) - H_R(T_0)\right] = Q_{HV_P,T_0}$$

i.e. given thermo-chemical tables for heating values and relative enthalpies and given T_R, we can solve for T_P

Derivations and calculation of entropy:

$$dS_{sys} \geq \frac{dQ}{T}$$

where $dS = \frac{dQ_{\text{int } rev}}{T}$

$dQ_{\text{int } rev} - dW_{\text{int } rev} = dU$ (1st law of thermodynamics)

$dQ_{\text{int } rev} = T\ dS$ (defn of dS)

$dW_{\text{int } rev} = F\ dx = PAdx = PdV$ (defn of W)

Subst : $T\ dS = dU + PdV$ (1st TdS eqn, Gibbs function)

Since : h = u + pv (defn of h)

$dh = du + p\,dv + v\,dp$

Subst into Gibbs : $T\ dS = dh - v\,dp$ (2nd TdS eqn)

since : $dh = C_p dT$ (defn of C_p)

and : $v = \frac{RT}{P}$ (*I*deal gas law)

$$dS = \frac{dh}{T} - \frac{v\,dp}{T} = \frac{C_p dT}{T} - \frac{R\,dp}{P}$$

$$\int_1^2 dS = \int_1^2 \frac{C_p}{T} dT - R\int_1^2 \frac{1}{P} dP$$

$$S_2 - S_1 = \int_1^2 \frac{C_{pA} + C_{p\mathbf{B}}T + C_{pC}T^2 + C_{pD}T^3 + C_{pE}T^4}{T} dT - R\left[\ln P\right]_1^2$$

$$= \left[C_{pA}\ln T + C_{p\mathbf{B}}T + \frac{C_{pC}T^2}{2} + \frac{C_{pD}T^3}{3} + \frac{C_{pE}T^4}{4} + const \right]_1^2 - R\left(\ln P_2 - \ln P_1\right)$$

note :

$S_{state} = S_{sens} + S_{f,T=0K}$

$S^0_{state} = S^0_{sens} + S^0_{f,T=0K} = S^0_{sens} + (S_{f,T=298K} - S^0_{sens,T=298K})$

$= S^0_{sens}\Big|_T - S^0_{sens}\Big|_0 + (S_{f,T=298K} - (S^0_{sens}\Big|_{298} - S^0_{sens}\Big|_0))$

$= S^0_{sens}\Big|_T + (\text{chemkin ref})$

Chemical equilibrium and the Gibbs function:

$$by\ definition: \quad dS_{sys} \geq \frac{dQ}{T}$$

$$dQ - dW = dU \qquad (1st\ law\ of\ thermodynamics)$$

$$dQ \leq T\ dS \qquad (defn\ of\ dS)$$

$$dW_{\text{int } rev} = F\ dx = PAdx = PdV \quad (defn\ of\ W)$$

$$Subst: dU + PdV - T\ dS \leq 0 \qquad (1st\ TdS\ eqn)$$

$$define: G = H - TS$$

$$dG = dH - Tds - SdT$$

$$Since\ h = u + PV$$

$$dh = du + PdV + VdP$$

$$Subst: dG = (du + PdV + VdP) - Tds - SdT$$

$$at\ const\ T\ \&\ P:$$

$$dG_{\text{const T\&P}} = du + PdV - Tds$$

$$from\ previous\ section...$$

$$\therefore \quad dG_{\text{const T\&P}} \leq 0$$

Consider reaction components: A, B, C, D

Stoichiometric coefficients: v_A, v_B, v_C, v_D

$$v_A A + v_B B \rightarrow v_C C + v_D D$$

And equilibrium mole numbers: N_A, N_B, N_C, N_D

$$N_A A + N_B B \xleftrightarrow[equilibrium]{} N_C C + N_D D$$

$$at\ equilibrium: (dG)_{\text{const T\&P}} = \Sigma(g_i dN_i)_{\text{const T\&P}} = 0$$

Where : g_i is molar Gibbs values

dN_i is the differential change in # of moles

From stoichiometric reaction:

$$v_A A + v_B B \rightarrow v_C C + v_D D$$

We don't yet know N_i values, but the differential changes are proportional, so:

$$dN_A = -\varepsilon v_A \qquad dN_C = +\varepsilon v_C$$

$$dN_B = -\varepsilon v_B \qquad dN_D = +\varepsilon v_D$$

Where ε is proportionality constant and represents the extent of reaction movement
NB: sign convention -ve for reactants, +ve for products

at equilibrium : $(\mathrm{dG})_{\text{const T\&P}} = \Sigma\left(g_i dN_i\right)_{\text{const T\&P}} = 0$

$g_A dN_A + g_B dN_B + g_C dN_C + g_D dN_D = 0 \quad (\text{const T \& P})$

subst ε expressions :

$-g_A \varepsilon \nu_A - g_B \varepsilon \nu_B + g_C \varepsilon \nu_C + g_D \varepsilon \nu_D = 0 \quad (\text{const T \& P})$

devide through by ε :

$-g_A \nu_A - g_B \nu_B + g_C \nu_C + g_D \nu_D = 0 \quad (\text{const T \& P})$

$\overset{0}{g}_i = \overset{0}{h}_i - T\overset{0}{s}_i$ i.e. at 1 atm

Note : Gibbs is function of T and P

approach : devide the effects

$$\int_1^2 dS = \int_1^2 \frac{C_p}{T} dT - R\int_1^2 \frac{1}{P} dP$$

$$S_2 - S_1 = \int_1^2 \frac{C_{pA} + C_{p\mathbf{B}} T + C_{pC} T^2 + C_{pD} T^3 + C_{pE} T^4}{T} dT - R\left[\ln P\right]_1^2$$

$$= \left[C_{pA} \ln T + C_{p\mathbf{B}} T + \frac{C_{pC} T^2}{2} + \frac{C_{pD} T^3}{3} + \frac{C_{pE} T^4}{4} + const \right]_1^2 - R\left(\ln P_2 - \ln P_1\right)$$

Note :

$S_{state} = S_{sens} + S_{f,T=0K}$

$S^0_{state} = S^0_{sens} + S^0_{f,T=0K} = S^0_{sens} + (S_{f,T=298K} - S^0_{sens,T=298K})$

$= S^0_{sens}\Big|_T - S^0_{sens}\Big|_0 + (S_{f,T=298K} - (S^0_{sens}\Big|_{298} - S^0_{sens}\Big|_0))$

$= S^0_{sens}\Big|_T + (\text{chemkin ref})$

$$g_i^0 = h_i^0 - T s_i^0 \quad \text{i.e. at 1 atm}$$

$$g_{i(p,T)} = g_{i(T)}^0 + P_{correction,\,T=const}$$

$$P_{correction,\,T=const} \rightarrow \quad \Delta g = \Delta h - T\Delta s$$

$$\Delta h_{T=const} = 0 \qquad \Delta s_{T=const} = -R \ln \frac{P_2}{P_1}$$

$$P_{correction,\,T=const} \rightarrow \quad \Delta g = +RT \ln \frac{P_2}{P_1}$$

$$g_{i(p,T)} = g_{i(T)}^0 + RT \ln P_i \qquad \text{for partial P in atm}$$

$$-g_A \nu_A - g_B \nu_B + g_C \nu_C + g_D \nu_D = 0 \quad \text{(const T \& P)}$$

$$-\left[g_A^0 + RT \ln P_A \right] \nu_A - [...]\nu_B + [...]\nu_C + [...]\nu_D = 0$$

$$\text{define } \Delta G^* = -g_A^0 \nu_A - g_B^0 \nu_B + g_C^0 \nu_C + g_D^0 \nu_D$$

$$\text{subst : } \Delta G^* = -RT(-\nu_A \ln P_A - \nu_B \ln P_B + \nu_C \ln P_C + \nu_D \ln P_D)$$

$$\therefore \Delta G^* = -R_u T \ln \left[\frac{P_C{}^{\nu_C} P_D{}^{\nu_D}}{P_A{}^{\nu_A} P_B{}^{\nu_B}} \right]$$

$$\text{define} \quad K_{p1} = [\ ]$$

$$\text{then} \quad K_{p1} = e^{-\Delta G^* / R_u T}$$

$$K_{p1} = \left[\frac{P_C{}^{\nu_C} P_D{}^{\nu_D}}{P_A{}^{\nu_A} P_B{}^{\nu_B}} \right]$$

$$\text{from partial pressure relation : } \quad P_i = \frac{N_i P_{total}}{N_{total}}$$

$$\text{subst in : } \quad K_{p2} = \left[\frac{N_C{}^{\nu_C} N_D{}^{\nu_D}}{N_A{}^{\nu_A} N_B{}^{\nu_B}} \right] \left(\frac{P_{total}}{N_{total}} \right)^{\Delta \nu}$$

$$\text{where : } \quad \Delta \nu = \nu_C + \nu_D - \nu_A - \nu_B$$

$$\text{so at equilibrium : } \quad K_{p1} = K_{p2}$$

For flow through the ports and past the valves:

Pressure loss due to friction effects :

(from Bernouli) $\Delta P = C_f \frac{1}{2}\rho v^2$

where pipe friction factor, $C_f = \frac{4 f l}{d}$

where surface roughness const, $0.005 \le f \le 0.01$

Pressure loss due to fitting geometry effects :

(empirically) $\Delta P = K_f \frac{1}{2}\rho v^2$

where fitting friction factor, $K_f = 0$ for well radiused corners

$= 0.5$ for sharp corner pipe entry

$= 1$ for exposed pipe entry

Flow area, $A_{actual} = C_D A_{curtain}$

where : $C_D \approx 0.6$

(area affected by proximity to cylinder wall)

and : $A_{curtain} = \pi D_{port} L_v$

where valve lift,

$$L_v = L_{max}\left(\frac{1}{2}\left(1-\cos\left(\frac{\theta-\theta_{IVO}}{\theta_{IVC}-\theta_{IVO}}2\pi\right)\right)\right)^m$$

where : shape effect, $m \approx 0.6$

momentum: $\sum F = \frac{\Delta M}{\Delta t} = \frac{m\Delta v}{\Delta t}$

(pressure force - pipe friction force - elbow friction force - valve friction force) = change in momentum

$$\left[(P_1 - P_2)A_2\right] - \left[\Delta P_{pipe\ frict}\pi DL\right] - \left[\Delta P_{elbow\ frict}A_1\right] - \left[\Delta P_{valve\ frict}A_2\right] = \left[\rho_1 A_1 L\frac{(v_1 - v_0)}{\Delta t}\right]$$

$$\left[(P_1 - P_2)A_2\right] - \left[\frac{1}{2}K_{f,pipe}\rho_1 v_0^2 \pi DL\right] - \left[\frac{1}{2}K_{elbow}\rho_1 v_0^2 A_1\right] - \left[\frac{1}{2}K_{valve}\rho_1 v_0^2 A_2\right] = \left[\rho_1 A_1 L\frac{(v_1 - v_0)}{\Delta t}\right]$$

$$\therefore v_1 = v_0 + \frac{\left\{\left[(P_1 - P_2)A_2\right] - \left[\frac{1}{2}K_{f,pipe}\rho_1 v_0^2 \pi DL\right] - \left[\frac{1}{2}K_{elbow}\rho_1 v_0^2 A_1\right] - \left[\frac{1}{2}K_{valve}\rho_1 v_0^2 A_2\right]\right\}\Delta t}{\rho_1 A_1 L}$$

Derivation of Adiabatic process relations:

from $q - w = \Delta u \quad w = Pdv \quad \Delta u = C_v dT$

for adiabatic process : $-w = \Delta u$

substituting : $Pdv + C_v dT = 0$

from ideal gas law : $T = Pv/R \quad \therefore dT = \frac{1}{R}(Pdv + vdP)$

substituting : $Pdv + \frac{C_v}{R}(Pdv + vdP) = 0$

mult by R : $RPdv + C_v(Pdv + vdP) = 0$

$R = C_p\text{-}C_v$: $(C_p\text{-}C_v)Pdv + C_v(Pdv + vdP) = 0$

devide by C_v : $\frac{(C_p\text{-}C_v)}{C_v}Pdv + (Pdv + vdP) = 0$

since $\gamma = \frac{C_p}{C_v}$: $(\gamma - 1)Pdv + Pdv + vdP = 0$

$\gamma Pdv + vdP = 0$

devide by Pv : $\gamma\frac{1}{v}dv + \frac{1}{P}dP = 0$

integrate : $\gamma\int\frac{1}{v}dv + \int\frac{1}{P}dP = 0$

$\gamma(\ln v_2 - \ln v_1) + (\ln P_2 - \ln P_1) = 0$

$\frac{v_2^\gamma}{v_1^\gamma} = \frac{P_1}{P_2}$

$\therefore P_1 v_1^\gamma = P_2 v_2^\gamma$

using : $P = RT/v$

$\frac{RT_1}{v_1}v_1^\gamma = \frac{RT_2}{v_2}v_2^\gamma$

$\frac{T_1}{v_1}v_1^\gamma = \frac{T_2}{v_2}v_2^\gamma$

$T_1 v_1^{\gamma-1} = T_2 v_2^{\gamma-1}$

$P_1 v_1^\gamma = P_2 v_2^\gamma$

using : $v = RT/P$

$P_1\left(\frac{RT_1}{P_1}\right)^\gamma = P_2\left(\frac{RT_2}{P_2}\right)^\gamma$

$P_1^{1-\gamma}R^\gamma T_1^\gamma = P_2^{1-\gamma}R^\gamma T_2^\gamma$

$P_1^{1-\gamma}T_1^\gamma = P_2^{1-\gamma}T_2^\gamma$

$\left(\frac{T_1}{T_2}\right)^\gamma = \left(\frac{P_2}{P_1}\right)^{1-\gamma}$

$\left(\frac{T_1}{T_2}\right) = \left(\frac{P_2}{P_1}\right)^{\left(\frac{1-\gamma}{\gamma}\right)}$

$\therefore T_1 P_1^{\left(\frac{1-\gamma}{\gamma}\right)} = T_2 P_2^{\left(\frac{1-\gamma}{\gamma}\right)}$

The Woschni convective heat transfer correlation:

$$\dot{q}_s = h_{conv}\Delta T$$
$$q = h_{conv} A\, \Delta T\, \Delta t$$

$$h_c(W/m^2K) = 3.26B^{-0.2}\, P^{0.8}\, T^{-0.55}\, w^{0.8}$$

$$w = \left[C_1 \bar{S}_p + C_2 \frac{V_d T_r}{P_r V_r}\left(p - p_m\right) \right]$$

In general :

for gas exchange period : $C_1 = 6.18 \quad C_2 = 0$

for compression period : $C_1 = 2.28 \quad C_2 = 0$

for combustion and expansion period : $C_1 = 2.28 \quad C_2 = 3.24x10^{-3}$

for high swirl engines :

for gas exchange period : $C_1 = 6.18 \text{ x } 0.417 \frac{v_s}{\bar{S}_p}$

for rest of cycle : $C_1 = 2.28 \text{ x } 0.308 \frac{v_s}{\bar{S}_p}$

where $v_s = B\, w_p/2$, w_p = paddle wheel rotational speed

References for this Appendix:

[1] J. B. Heywood, *Internal Combustion Engine Funamentals*, 1st ed. Singapore: McGraw-Hill, 1988.

[2] Y. Cengel and M. Boles, *Thermodynamics: An Engineering Approach*, 2nd ed McGraw-Hill, Inc., 1994.

Appendix D: SAE Paper 2009-01-1771

The experimental work contained in this appendix was presented at the 2009 SAE Powertrain, Fuels and Lubricants Conference, published in the conference proceedings and later published in the SAE International Journal of Engines, October 2009.

It should be noted, however, that this experimental work was conducted by Mr Ian Lemberger as part of his masters degree project. The project was conceived and supervised by Mr Gareth Floweday and the engine model used in the project was formulated by Mr Gareth Floweday. Mr Ian Lemberger modified the model to suit the geometry of the engine and also modified the parameters of the heat transfer model in order to replicate the engine's unusually high heat transfer rates.

SAE 2009-01-1771

25cc HCCI Engine Fuelled with DEE

Ian Lemberger, Gareth Floweday
Sasol Advanced Fuels Laboratory, University of Cape Town

ABSTRACT

This paper describes the set-up and testing of a single cylinder 25cc, air cooled, 4-stroke Spark Ignition (SI) engine converted to run in Homogeneous Charge Compression Ignition (HCCI) mode with the aid of various combustion control systems. The combustion control systems were investigated regarding their effects on combustion stability and heat release phasing. Engine operation was compared with unique findings from previous work done on a very small 2-stroke HCCI engine.

HCCI engine operation was possible between 1000 - 4000 rpm when using Diethyl Ether (DEE) as the test fuel. Maximum operational fuel-air equivalence ratio (Φ) was 0.75 when operating without Exhaust Gas Recirculation (EGR). This relatively high equivalence ratio was attainable due to thermal gradients induced by the high surface area to volume ratio of the small engine combustion chamber, resulting in high chamber heat transfer. Combustion phasing peculiarities, due to fuel Negative Temperature Coefficient (NTC) auto-ignition behaviour, engine heat transfer and breathing characteristics, were investigated.

Additionally, this paper provides a useful resource for building a compact, inexpensive HCCI engine test bed and matching HCCI engine model.

INTRODUCTION

Fuel efficiency requirements and ever more stringent emissions legislation require internal combustion engines to improve fuel economy and concurrently reduce exhaust emissions. One possible solution is advancing combustion technology in the form of HCCI engines which could operate either as single or dual combustion mode engines [1, 2].

HCCI combustion is the process in which a homogeneous air/fuel mixture is spontaneously auto-ignited through compression of the piston. Combustion characteristics allow HCCI to combine the best features of SI and Compression Ignition (CI) engines. HCCI engines offer significantly reduced engine out NOx emissions and fuel economy improvements up to 20% [2] as compared to SI engines, while reducing particulate emissions when compared to CI Engines. However, due to ignition being via the compression of the piston, combustion stability and combustion timing (phasing) over a wide engine load range is a major technical challenge in the development of HCCI combustion. Various combustion control methods are currently being researched and implemented in order to produce stable and reliable combustion while also expanding the HCCI load range. HCCI Electronic Control Unit (ECU) research is ongoing with respect to closed-loop control of HCCI engine dynamics [3].

HCCI has been demonstrated to work under laboratory conditions achieving low emissions and good efficiency under steady state operation, however technical challenges arise when attempting to extend this performance to transient operating conditions.

Primary technical challenges with HCCI development are: [2]

- Combustion phasing control
- Rapid heat release rates and noise level with possible engine damage especially at higher loads
- Transient operation difficulties
- Excess CO and HC emissions, particularly at light loads
- Increased NOx at high loads
- Cold Start difficulty
- A narrow operation range (as result of the above)

This research forms part of an ongoing HCCI study at the Sasol Advanced Fuels Laboratory to investigate and understand engine configuration and fuel chemistry effects on combustion in HCCI engines. This project continues from a previous project [4] where a small high speed model “diesel” aeroplane engine was found to operate in HCCI mode with surprising ease and flexibility. The engine was shown to run from idle through a fixed speed-load curve (propeller) to the maximum speed and load point of the engine at 11000rpm and stoichiometric air-fuel ratio, while maintaining nominally constant combustion phasing without any form of combustion control system. This study continued the investigation by removing lubricant from the fuel and switching to 4-stroke operation while retaining a very small engine size. A 25cc four-stroke, single cylinder engine possessing 2-valves with an overhead cam and sump lubrication system was used in the study.

Insights were gained regarding which engine characteristics play the primary role in the remarkable operational flexibility of the engine used in [4]. A number of additional features of small engine HCCI are also shown.

Additionally this project aimed to produce a low cost flexible HCCI engine/dynamometer rig for research purposes.

PREVIOUS SMALL HCCI ENGINE RESEARCH

At the Sasol Advanced Fuels Laboratory, a standard issue two-stroke model-aero "diesel" engine (Figure 1) was found to operate using HCCI combustion [4]. This type of engine is of particular interest largely because it operated as a self-regulating HCCI engine over a wide range without any undesirable effects such as engine knock or misfire. This engine, unlike the more common glow-plug versions, operates without any form of combustion initiator. Fuel and air are premixed using a simple carburettor and ignited by piston compression only, thus the engine operates in HCCI mode even though it is referred to as a "model diesel" engine. Engine starting is possible from cold, warm and hot conditions with ability to operate from idle to over 11000rpm. Operation is possible at high load points across the speed range with very conservative pressure rise rates. Furthermore, engine knock (high pressure oscillations) is not experienced during normal engine operation. This posed questions with respect to the possibility of similar full scale HCCI engine operation and the role of engine size and fuel requirements in obtaining HCCI operation over a wide load range.

Figure 1: P.A.W Model Aero-"Diesel" Engine

TEST ENGINE

A 25cc, single cylinder 4-stroke engine was chosen due to it being the smallest commercially available 4-stroke engine operating with no fuel/lubrication mixing. Manufacturer's engine specifications are shown in Table 1 below.

Table 1: Manufacturer's Engine Specifications

Engine Designation	GX25
Engine Type	4-stroke single cylinder
Bore X Stroke	35 x 26 mm
Displacement	25cc
Compression Ratio	8:1
Fuel preparation system	Diaphragm carburettor
Net Power Output	0.72 kW at 7000 rpm
Net Torque	1.0 Nm at 5000 rpm
Oil Capacity	80cc
Maximum No-load Speed	11000 rpm
Operational Speed	4000 - 9000 rpm
Inlet Valve Diameter	12.5 mm
Exhaust Valve Diameter	12.0 mm
Valve Lift	2.5 mm
CAD/Tooth on Timing Belt	24 degrees

The GX25 possesses two valves, inlet and exhaust with a single overhead cam and timing belt. The single overhead cam results in fixed valve lift, fixed relative valve timings - durations between inlet and exhaust valves. However the camshaft timing belt can be offset on the cam by shifting the belt a desired number of teeth, allowing for flexibility in altering of the relative valve timing. The standard valve lift profiles are given in Figure 2 below.

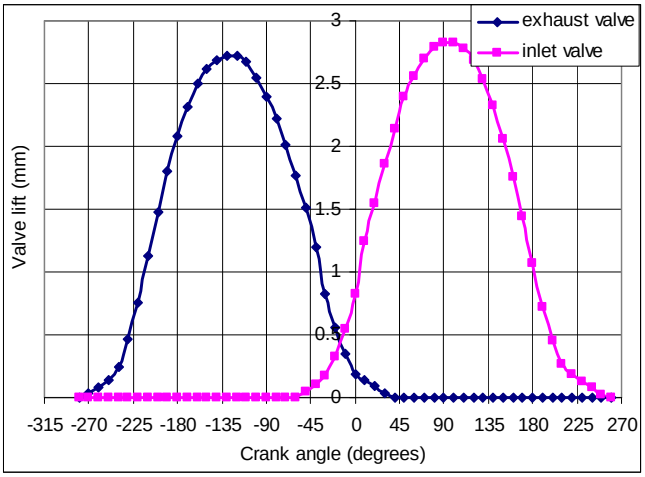

Figure 2: Standard exhaust and inlet valve lift profiles

An oil sump separates the lubricant from the air/fuel mixture (see Figure 3 below), thus allowing for comparison with the model "diesel" engine, which utilised castor oil as a lubricant in its fuel.

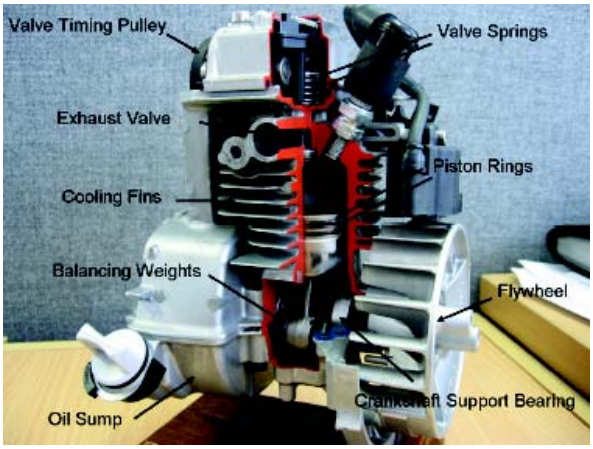

Figure 3: Cut-away Model of the GX25 Engine

Setup for the study therefore involved conversion of the engine to operate in HCCI mode. This required the engine to be operated on a test bench with a reduction drive, regenerative DC dynamometer and electronic control system. Various combustion control systems were added to the engine to obtain HCCI combustion and investigate combustion control mechanism effects on small engine HCCI combustion stability, heat release phasing and exhaust emissions. These controls included, inlet mixture heating, internal and cooled external EGR, inlet pressure boosting, valve timing and external cylinder cooling.

TEST FUELS

The engine's low compression ratio of 8:1, small displacement and associated high combustion chamber heat loss, necessitated the need for a volatile, high ignition quality fuel. Primary testing was conducted using Diethyl Ether as it's high ignition quality and high cetane number (CN > 125 [5]) allows for operation without excessive inlet heating requirements. Properties of this test fuel are given in Table 2.

Table 2: Diethyl Ether Properties ([5], [6])

Property	Value
Molar Mass	74.12 g/mol
Density	0.7134 g/cm^3
Boiling Point	308 Kelvin
Autoignition Temperature	433 Kelvin
Cetane Number	> 125
Stoichiometric Air/Fuel Ratio	11.1 (mass basis)
Lower Heating Value	33892 kJ/kg

DEE is a two-stage fuel [7, 8], exhibiting cool-flame and peroxide autoignition reactions with a corresponding Negative Temperature Coefficient (NTC) region. NTC auto-ignition behaviour is shown by Figure 4 below. The expected trends are such that as the initial temperature increases, the pre-coolflame (period "a" in Figure 5) delay reduces and the associated cool-flame temperature rise also becomes smaller. The NTC region is a region of the ignition delay curve where ignition delay increase as temperature increases. This results from the diminishing magnitude of the cool flame temperature rise as the initial temperature increases [9].

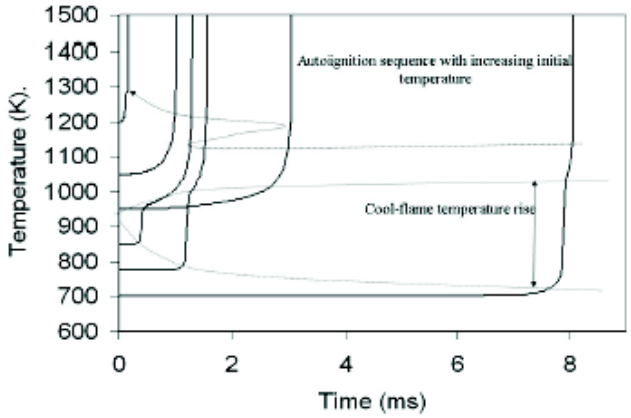

Figure 4: Profiles Showing the Effect of Initial Temperature on Ignition Delay of a 2-Stage Ignition Fuel in a Constant Volume Combustion Chamber [9]

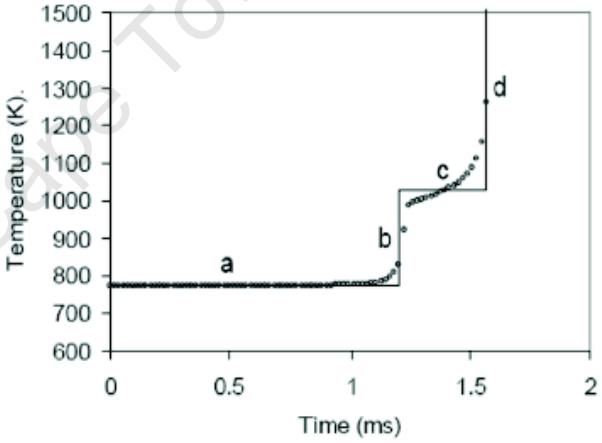

Figure 5: Ignition Delay Curve with Cool Flame Ignition Delay [9]

Engine testing using n-Heptane was completed in order to model observed engine operational characteristics, such as combustion phasing, heat release rates and combustion chamber heat transfer characteristics. n-Heptane was used due to the availability of thermodynamic and auto-ignition data, which was not available for DEE.

Table 3: n-Heptane Properties Table

Properties	Value
Mole Weight	100.20 g/mol
Density	0.682 g/cm3
Boiling Point	371.3 Kelvin
Lower Heating Value	44566 kJ/kg

EXPERIMENTAL SETUP

A secondary goal for this research was to design an inexpensive and compact HCCI rig. Specifications of the

equipment used and a table of equipment costs can be found in Appendix C.

Figure 6 illustrates the engine mounting, which consists of a stand with adjustable feet and slotted plates allowing for component mounting flexibility and shaft alignment.

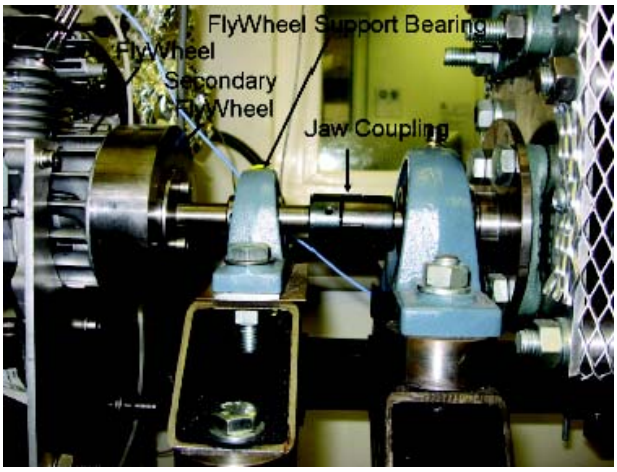

Figure 6: Power Transmission Mechanism

The crankshaft assembly consists of two separate shafts that are press-fitted with counterweights on either side and supported by bearings, creating an inherent misalignment along the crankshaft. A secondary flywheel, supported by a self aligning bearing, was necessary due to the low rotational inertia of the original flywheel. The additional flywheel support minimises the effects of crankshaft misalignment as well as reducing static loading on the crankshaft.

Power from the engine is transmitted to a regenerative DC motor, able to absorb 1.1 kW at a speed of 3000rpm. Operational speed differences between the engine and dynamometer resulted in a speed reduction requirement. A toothed belt reduction drive, see Figure 7, with an overall reduction ratio of 3:1 was installed.

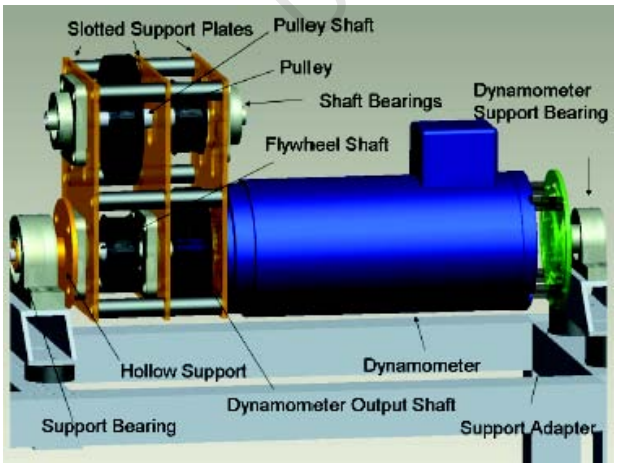

Figure 7: Reduction Drive and Dynamometer Assembly

The reduction drive and dynamometer are assembled as a 'freely' rotational system, supported by two non-rotating trunion bearings, to facilitate the installation of a simple strain gauge to monitor engine load.

MEASUREMENT EQUIPMENT

Various measuring devices were installed for data capturing and engine monitoring during operation. Below is a list of all installed instrumentation and their location:

Table 4: Location of Measurement Equipment

Signal	Description
P_1	Cylinder Pressure
T_{AR}	Air Reservoir Temperature
$T_{mixture}$	Post Injector Mixture Temperature
T_{exh}	Exhaust Gas Temperature
T_{EGR}	EGR Line Pre-injector Temperature
T_{HE}	EGR Heat Exchanger Temperature
T_{cyl1}	Cylinder Wall Temperature 1
T_{cyl2}	Cylinder Wall Temp 2
λ_1	Exhaust lambda value
λ_2	Inlet EGR lambda value
P_2	Air Reservoir Pressure
P_3	Exhaust Back-Pressure
Torque	Reduction/Dyno Assembly
Crank Angle	Engine Rear - Speed
FTIR Analyzer	Exhaust

Cylinder pressure was measured with a water-cooled piezo-electric pressure transducer mounted into the existing spark-plug hole, without the need for any modification. The pressure transducer used was calibrated for a pressure range up to 250 bar.

T_{cyl1} and T_{cyl2} measure temperature in the cylinder wall. These temperature measurements are used to create a linear temperature extrapolation through the cylinder wall, based on their relative placements in the cylinder wall. The extrapolated temperature measurement is then utilised in heat loss modelling of the engine. (See Appendix A for positioning of the thermocouples)

NOx, CO_2 and CO exhaust emissions sampling measurements were measured using a Fourier Transform Infra- Red (FTIR) analyzer connected to the exhaust manifold.

DATA ACQUISITION

Engine control is achieved via an in-house developed Electronic Control System (ECS) using National Instruments LabView$_{TM}$, and a National Instruments FPGA DAQ card, allowing for constant monitoring of engine operation as well as basic control.

The ECS is able to directly control the following operating parameters:

- Engine Speed
- Injection Timing
- Injection Duration

A realtime data acquisition system is used to monitor cylinder pressure, manifold pressures, fuel-air equivalence ratio, temperatures, engine torque, injection control and engine speed. The ECS calculates 50% heat release position as well graphing relative cylinder pressure, heat release rates and cumulative heat release rates. Analysis of the pressure trace is used to obtain pressure rise rates, peak pressures and locations of peak pressure. (See Appendix B for schematic layout of the engine and data capturing setup)

COMBUSTION CONTROL METHODS UTILISED

FUEL INJECTION

Obtaining a homogeneous mixture requires extended mixing time between the fresh charge and fuel. Use of injection timing strategies have shown that when Start of Injection (SOI) is retarded, the combustion timing is also retarded, whereas advancing fuel injection timing would lead to an increase in NOx emissions [10].

A port fuel injection (PFI) system was installed by utilising a fuel injector (Figure 8) from a commercially available 50cc scooter. The injector is housed downstream of a throttle approximately 200mm from the inlet valve, allowing for evaporation and mixing time of the air/fuel mixture. Injection duration is set to a desired value on the ECS and an injector calibration graph is used to obtain mass flow rates at the set injection pressure of 5 bar. Injection timing is determined using a crank angle encoder on the engine, with injection timing being set at a desired crank angle BIVO (Before Inlet Valve Opening).

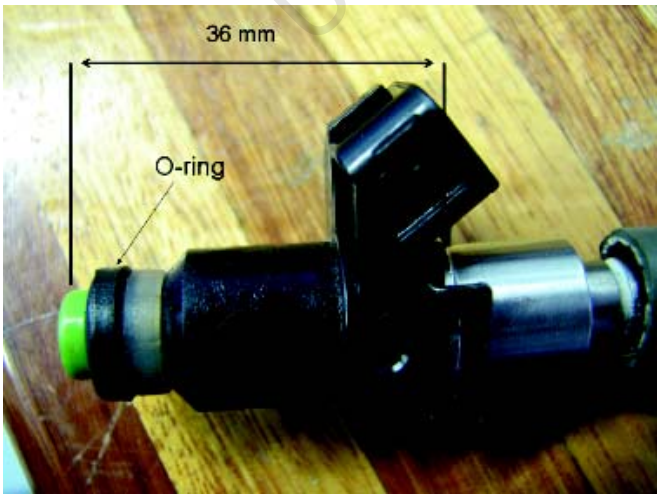

Figure 8: Fuel Injector

INLET MANIFOLD TEMPERATURE CONTROL

Inlet manifold temperature control allows for control of mixture temperatures pre-compression and is thus the primary control for combustion phasing [11, 12]. Inlet charge heating allowed an engine with compression ratio 7.5:1 to produce stable operation over a speed range of 1000 - 4000 rpm [2]. Persson and Johansson [11] utilised a combination of intake temperature (288K - 323K) and negative valve overlap to attain HCCI combustion. Aroonispoon and Foster [12] also researched the impact intake temperature (300K - 400K) had on HCCI combustion, using a CFR single cylinder research engine. A specially designed 0.8 kW cartridge air heating element was installed upstream of the throttle into a reservoir for inlet air heating control. Air temperature was controlled using a K-type thermocouple and heating element control unit, Figure 9.

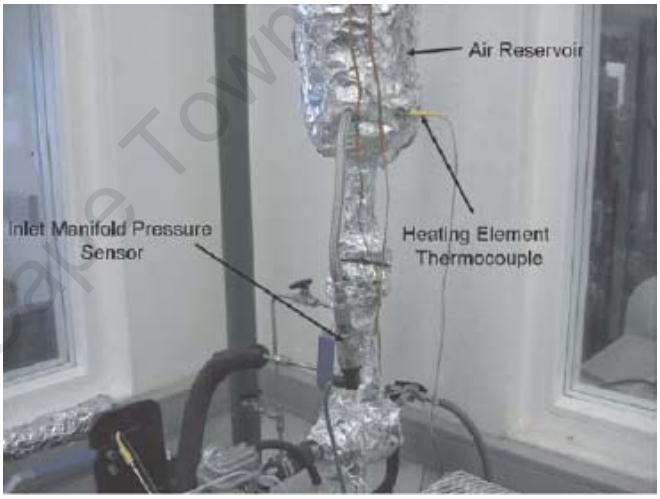

Figure 9: Inlet Manifold Temperature Control Setup

Control of the mixture temperature in the inlet port, allows the ability to compare inlet mixture temperature requirements when operating at various air/fuel ratio's. Combustion Peak Pressure Phasing was maintained at 10^0 ATDC, as this combustion phasing has been shown to produce optimal combustion quality [13]. Experimental inlet temperature and fuelling swings were conducted at this constant combustion phasing as shown in Figure 10.

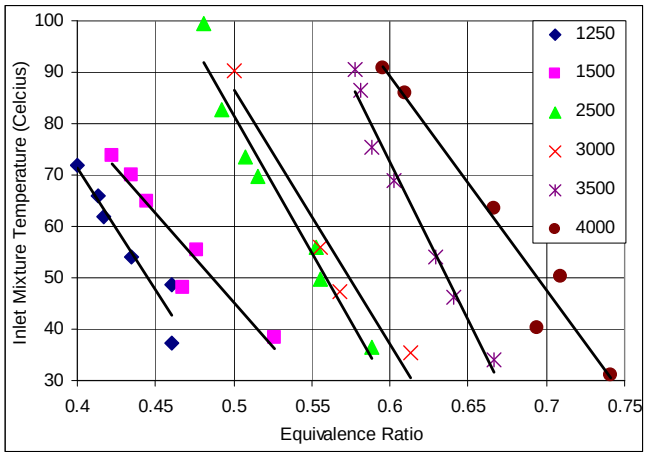

Figure 10: Inlet Mixture Temperature vs. Equivalence Ratio for Constant Phasing with External Cooling Fan

When examining the graph above, several clear trends are visible:

- Increased mixture temperatures are required for Φ reduction for a given engine speed.
- Increasing speeds require significantly increased inlet heating for a given Φ value.
- Minimum mixture temperature was 30^0C. This was due to inlet manifold heating effects as result of engine operation.
- Minimum operational Φ was 0.4, below which combustion quality would deteriorate.
- Maximum allowable operational mixture temperatures were 100^0C. This maximum was set as result of excessive pressure rise rates (greater than 10 bar/- CAD) when operating at high speeds.
- The steepness of the curves in Figure 9 indicates that the engine could be controlled to run with constant inlet air temperature through the indicated speed range, using fuelling to maintain constant combustion phasing. This could result in similar ability to run along a speed load curve as demonstrated by the model aeroplane engine in [4].

Engine operation is possible at increased speeds and increased mixture temperatures if pressure rise rates are allowed to increase. Combustion instability at lower speeds suggests a lower speed 'cap' for mixture temperatures for engine operation as a result of the heat loss characteristics of the engine. However, engine operation was possible at 1000rpm although this was only possible at reduced mixture temperatures whereby any reduction in Φ would result in engine misfire.

The engine's small displacement results in significant combustion chamber thermal gradients and the ability to run close to stoichiometric air/fuel mixtures. This is possible while still achieving conservative pressure rise rates of 10 bar/CAD without the use of EGR. The expected heat loss characteristics associated with small engines were investigated further by operating the engine without the use of the external cooling fan. Combustion Peak Pressure Phasing was again maintained at 10^0 ATDC, and experimental inlet temperature and fuelling swings were conducted as shown in Figure 11 below.

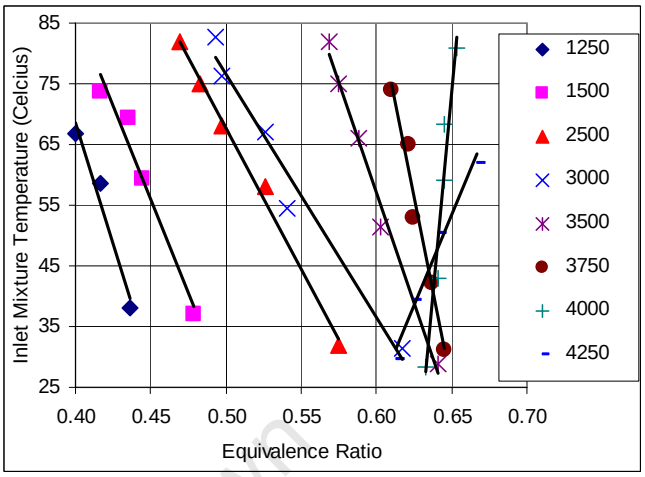

Figure 11: Inlet Mixture Temperature vs. Equivalence Ratio for Constant Phasing - No Cooling Fan in Operation

Operation at a fixed Φ required a reduction in inlet mixture temperature when operating without the external cooling fan. An increase in recorded cylinder temperatures Tcyl1 and Tcyl2 when operating without additional cooling indicated that cylinder temperatures increased. A reduction in required inlet mixtures was prevalent across the entire speed range although the operational variance in Φ reduced with each speed. This occurred as a result of very 6 lean mixtures often resulting in misfire at low speeds and combustion quality deterioration whereas pressure rise rates were exceeded at higher speeds. However there is a distinct reduction in operational Φ at increased engine speeds, suggesting that engine heat transfer characteristics play a major role in engine operation.

Slopes of the high speed bracket (4000 - 4250 rpm) change drastically when operated without external cooling. The slopes illustrate that an increase in operation Φ required increased inlet mixture temperatures. This trend suggests that operation in this zone accesses the fuel's NTC region where phasing is independent of inlet mixture temperature. This is unusual as comparison to other studies have not shown such trends during operation [11, 12, 14].

This was investigated further by examining Pressure (Figure 12) and Heat Release Rate (Figure 13) curves at a speed such that a clear advancing in the cool-flame was visible. Pressure traces were captured at 3800 rpm and Φ = 0.62 where various inlet mixture temperatures were possible at constant Φ and constant phasing.

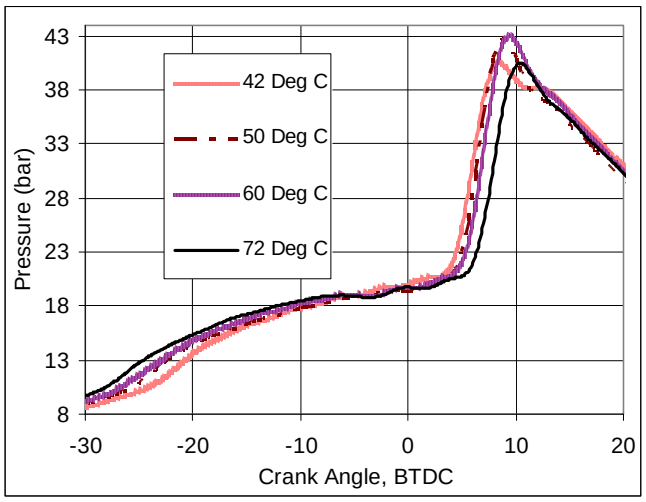

Figure 12: Inlet Mixture Temperature Effects on Cylinder Pressure at 3800 rpm and Φ = 0.62

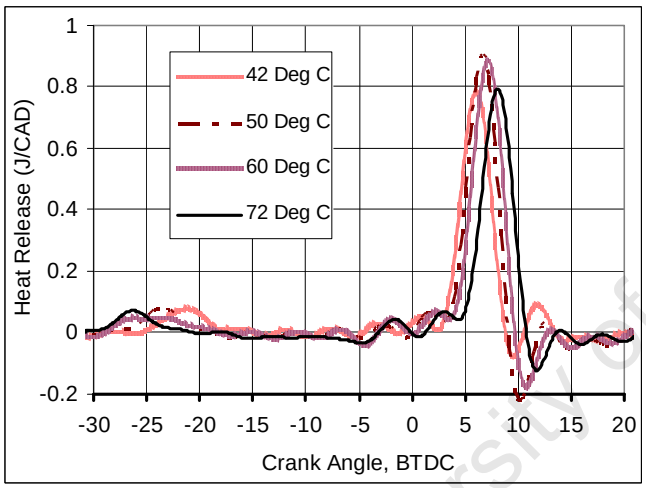

Figure 13: Inlet Mixture Temperature Effects on Heat Release Rates at 3800 rpm and Φ = 0.62

Heat Release Rate plots confirm that an increase in inlet mixture temperature results in a reduction in the cool flame ignition delay and reduced cool flame heat release. The fuel exhibits NTC behaviour such that the main Heat Release ignition delay is independent of inlet mixture temperature. Operation of the engine within the fuel's NTC region can be used to explain the changes that occur when operating without external engine cooling.

INLET MANIFOLD BOOSTING

Inlet boosting by either Turbo/Supercharging increases in-cylinder charge density. The increased density allows for increased allowable fuelling - when the charge is kept at the same Φ. Inlet boosting can provide HCCI with a significant power boost. Boosting increases IMEP, which is a result of increased fuelling and compression pressure. Boosting has been shown to increase the HCCI load range but is then limited by engine knock [15].

Inlet charge boosting is provided by boosting the inlet manifold air with a roots blower and reservoir, located in the test cell allowing for boosting up to 1.0 bar (gauge). Boosted air pressure is altered using a control valve on the blower and monitored in the temperature controlled reservoir upstream using an absolute pressure sensor.

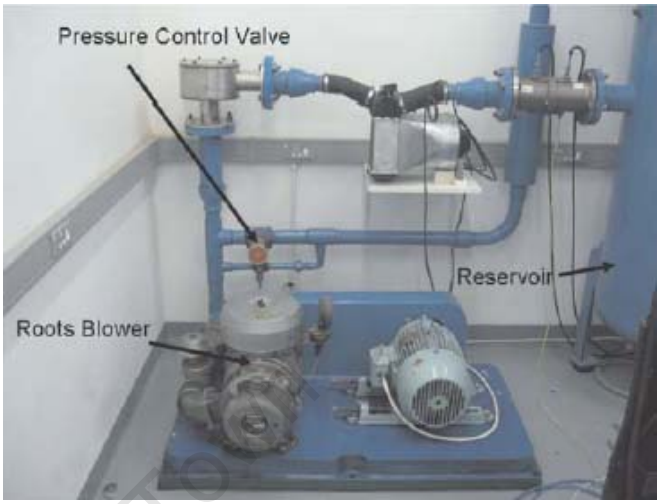

Figure 14: Roots Blower Used For Inlet Manifold Boosting

Manifold pressure effects were investigated for inlet pressures (gauge) of 0.1, 0.15, 0.2 and 0.25 bar, by recording the change in Φ as result of inlet pressure variations, while maintaining constant combustion phasing and inlet mixture temperature of 350C. Figure 15 below illustrates the recorded effects of altering inlet manifold pressures.

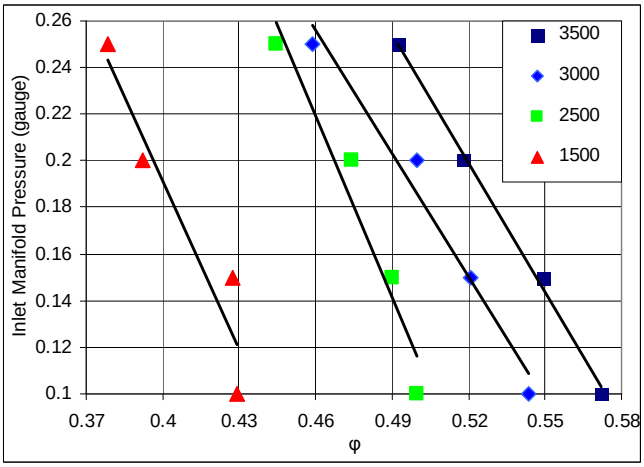

Figure 15: Effects of Inlet Manifold Pressure on Equivalence Ratio for Constant Phasing at Tinlet = 350C

Trends show that a reduction in operational Φ requires increased manifold pressures across the speed range for constant combustion phasing. The requirement is result of increased post-compression cylinder pressures and associated advancing effect of fuel auto-ignition.

TEMPERATURE CONTROLLED EXHAUST GAS RECIRCULATION

External Exhaust Gas Recirculation (EGR) is a widely used method used to suppress NOx emissions in Diesel Engines, and offers the possibility to lower combustion temperatures [16]. Additionally EGR is now being used as a basic control method of ignition timing and burn rates in HCCI engines. EGR has numerous effects on HCCI combustion and emissions [17]:

1. When using hot EGR the inlet charge temperature is increased. This creates a pre-heating effect which raises compression cycle temperatures

2. Dilution effect - which reduces oxygen concentrations and therefore lowers required fuelling

3. Heat capacity effect due to the higher heat capacity of carbon dioxide and water vapour. This leads to a reduction in compression temperatures

4. Chemical effect due to the combustion products in the EGR taking part in the chemical reactions during combustion Unburned Hydrocarbons, CO, CO2, NO, H2O etc, take part in the chemical reaction, which affect the reaction rates

Exhaust Gas Recirculation (EGR) was installed by linking the exhaust manifold to the inlet manifold using stainless steel tubing (Figure 15). EGR passes through a temperature controlled Heat Exchanger. Flow control is achieved using two valves, one which controls exhaust back pressure (backpressure valve) and hence also varies in-cylinder residual exhaust gas (REG), and either EGR control valve 1 or 2, for coarse or fine adjustments respectively.

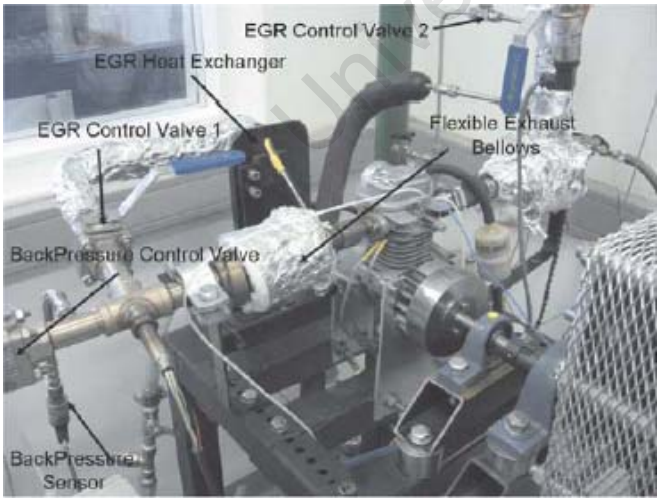

Figure 16: EGR System

EGR flow to the inlet manifold enters downstream of the reservoir and is temperature monitored by two thermocouples, one located at the exit of the EGR Heat Exchanger and the other located at the inlet port as to monitor mixing effects on gas temperature. A non-sampling method was required to predict %EGR due to the small volumes of exhaust gas being circulated. The volume ratio of O2 content between the inlet and exhaust manifolds are compared, using two broadband Lambda sensors, to obtain %EGR using Equation 1 below.

$$EGR(\%) = \frac{\%O_{2intake} - \%O_{2Environment}}{\%O_{2Exhaust} - \%O_{2Environment}} * 100 \quad (1)$$

To compare effects of exhaust gas temperature on engine operation, cooled EGR was introduced into the cylinder via the EGR line. EGR circulates through the heat exchanger, supplied with circulating water temperature controlled to 200C as to obtain lowest possible EGR temperatures. Inlet heating was used to increase mixture temperatures when EGR rate was increased, as to maintain constant combustion phasing. Results obtained during EGR testing can be seen in Figure 17 below.

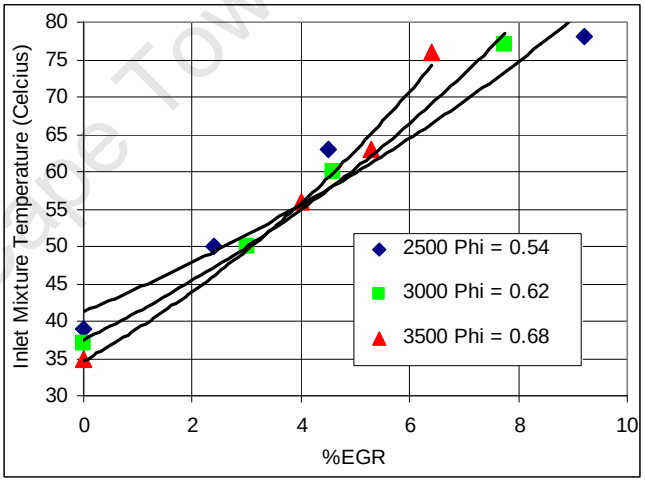

Figure 17: Effects of Cooled EGR on Engine Operation

An increase in EGR rate requires an increase in inlet mixture temperature to maintain constant phasing and Φ. This trend is as result of the dilution and heat capacity effects of EGR on combustion phasing. Cooled EGR reduces combustion pressure and temperatures resulting in a retarding of the auto-ignition timing which is then offset by an increase in inlet mixture temperature. The intersection point observed indicates that an operating range exists where altering of speed has little or no effect on combustion phasing, which occurs at an EGR rate of ± 4%.

RESIDUAL EXHAUST GAS EFFECTS AS RESULT OF BACK-PRESSURE CONTROL

The backpressure valve was used to control the backpressure in the exhaust stream. Changes in exhaust backpressure effect engine volumetric efficiency (η_v) by trapping residual exhaust gas (REG) in the cylinder. This results in reduced fresh charge induction. Varying backpressure was utilised at various mixture temperatures

in order to maintain constant phasing and Φ when operating at fixed speeds.

An initial base Φ was obtained at reduced mixture temperature to obtain a base Φ value for the specified set speed. Inlet mixture temperature could then be increased and the backpressure altered to obtain the preset required variables at speeds of 1500, 2500, 3000 and 3500 rpm. Figure 18 illustrates the obtained results.

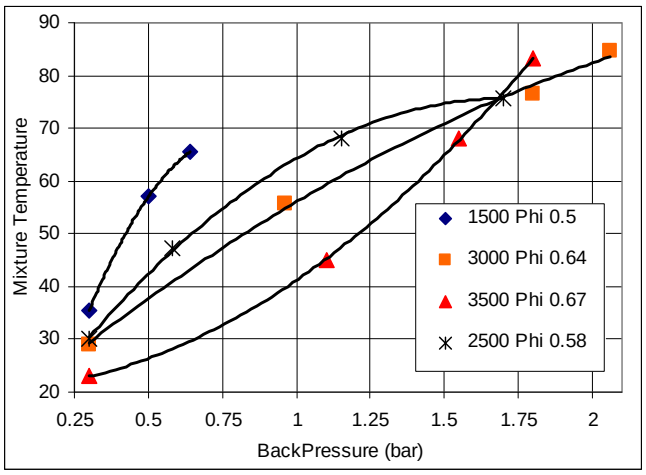

Figure 18: Varying Backpressure for Constant Phasing

A clear trend is visible whereby a point of intersection exists of mixture temperature and backpressure for various speeds. This intersection point describes a range at which the engine can vary speed without affecting the combustion phasing. The expected relationship is such that an increase in REG mass would require an inlet mixture temperature reduction to compensate for the increased cylinder temperature as result of the hot residuals. However this doesn't occur, suggesting that engine characteristics such as cylinder heat transfer and breathing characteristics play a major role in small engine HCCI operation. This is as result of the combination of the dilution, chemical and heat capacity effects of REG having predominant effect in combustion phasing over the temperature preheating effects of the REG.

VALVE TIMING EFFECTS

Valve timing plays a key role in engine breathing and is thus directly related to volumetric efficiency. Engine operating characteristics became apparent when engine operation was altered by varying relative valve timing. Valve timing was altered by adjusting the timing gear 1 or 2 teeth either forward or backwards, with respect to the original timing, resulting in advancing or retarding of the relative valve timing respectively. Volumetric efficiency η_v comparisons were calculated, using Equation 2 [18], across the engine's operating range as to evaluate the effectiveness of the engines induction process as affected by valve timing. Volumetric efficiency is defined as the volume flow ratio of air into the intake system divided by the rate at which volume is displaced by the piston (Figure 19):

$$Volumetric\ \ Efficiency, \eta_v = \frac{2\dot{m}_a}{\rho_{a,i} V_d N} \quad (2)$$

Where $\rho_{a,i}$ is the inlet air density, m_a is the mass of air inducted into the cylinder per cycle, V_d is the displaced volume and N is engine speed.

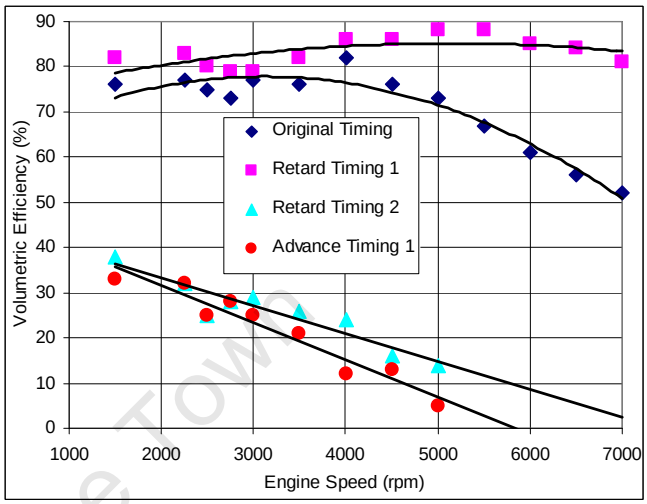

Figure 19: Volumetric Efficiency for Varying Valve Timings with the engine in SI mode

Volumetric efficiency (Figure 19) and torque plots (Figure 20) affirm that retarding the valve timing by 1 tooth produces improved η_v and torque. This suggests that the valve timing is detuned by the engine manufacturer/supplier to improve engine durability. Note that the torque curve measured with this valve timing (Figure 20) matched the engines specifications for the engine. This indicates that engine breathing performance can be significantly improved by retarding the valve timing.

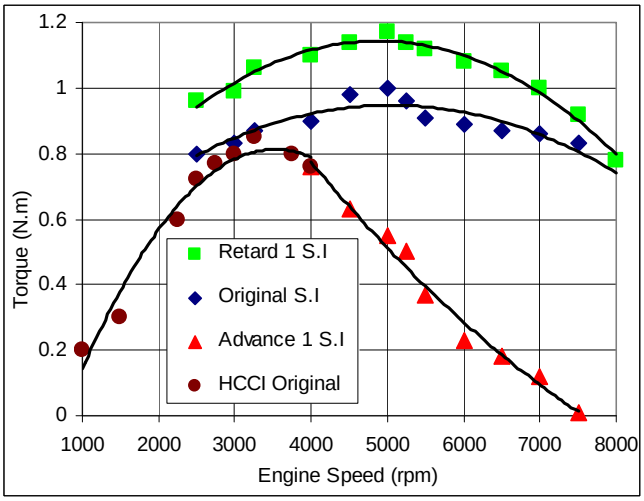

Figure 20: Effects of Valve Timing on Engine Torque (SI fuel used was RON95 and HCCI fuel used was DEE)

COMBUSTION CHAMBER HEAT TRANSFER

High heat loss to the cylinder walls was expected due to the small volume to surface area ratio of the engine. As a result, heat transfer modelling would be an important factor in modelling engine operation. In order to predict heat transfer to the cylinder walls, motored cylinder pressure traces were used to evaluate the heat loss to the cylinder walls from IVC to EVO, since there is no heat release from combustion and thus heat release analysis would show instantaneous heat loss from the cylinder [19]. A motored trace at 2500 rpm was chosen for Heat Release analysis purposes as it was at speed which indicated highest volumetric efficiency (η_v).

A heat release analysis based on pure air with a temperature dependent specific heats was used to evaluate the heat release [18]:

$$\dot{Q}_w = \frac{\gamma(T)}{(\gamma(T)-1)} p \frac{dV}{d\theta} + \frac{1}{(\gamma(T)-1)} V \frac{dp}{d\theta}$$

The well known Woschni Heat Transfer correlation was used as a platform for Heat Transfer modelling due its wide acceptance, robustness and simplicity in implementation. Additionally a modified HCCI Woschni Correlation as proposed by [20] was compared. Errors were expected when using the original Woschni Heat Transfer correlation due the original use of the correlation being used to correlate heat loss in a four-cylinder water-cooled Direct Injection C.I engine.

The global heat transfer coefficient can be written as [20]:

$$h_{global}(t) = \alpha_{scaling} . L(t)^{m-1} . \frac{k}{\mu^m} . p(t)^m . T(t)^{-m} . v(t)^m$$

The global heat transfer coefficient is dependant on engine characteristics such as length, transport properties, pressure, temperature and characteristic velocity. The value of $\alpha_{scaling}$ is used to match specific engine geometry and the exponent m has been proposed by several different authors, m = 0.5 for Elser and Oguri, 0.7 for Annand and Sitkei, 0.75 for Taylor and Toong and 0.8 for Woschni and Hohenberg [20]. A fitted heat loss model was formulated modifying the Woschni Correlation's exponent to fit cumulative heat loss of experimental heat release analysis. Results from utilising heat release analysis as well as the Woschni Heat Transfer Correlation [20] are shown in Figure 21, from which is clear that the Woschni Heat Transfer correlation doesn't accurately account for heat loss from the cylinder. The fitted heat transfer model using coefficient m = 0.55 shows better accuracy.

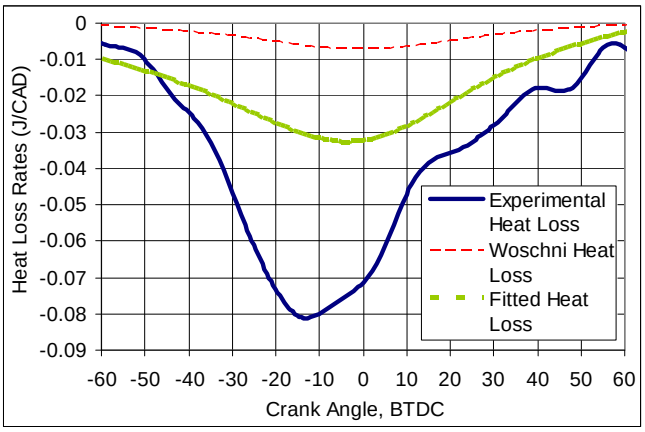

Figure 21: Heat Loss Rates for Motoring at 2500 rpm

ENGINE MODELLING

A numerical engine model was formulated to utilise measured engine parameters to model engine operating characteristics such as peak pressure as well as gauge effects of various heat loss model terms on engine operation predictions.

The model consists of two separate portions, a breathing model (EVO to IVC) which predicts the cylinder blow-down, exhausting and induction process and the resultant REG at IVC. A single zone combustion model (IVC to EVO) is used to compute the combustion portion of the cycle, by utilising fuel properties based on in-cylinder conditions using thermodynamic principles to predict engine operational behaviour.

Motored pressure traces were simulated in the model to determine a fitted heat loss parameter. Figure 22 below is the result of the fitting of the heat loss parameters to the experimentally obtained motored trace.

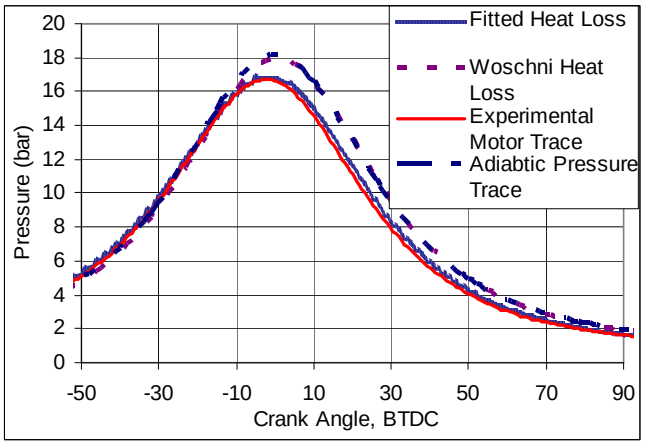

Figure 22: Modelled and Experimental Motored Traces Utilising Heat Loss Parameters

The fitted motored pressure trace was obtained by adjusting the m coefficient used in Woschni's Heat Transfer Correlation to m = 0.55.

In order to evaluate the effectiveness of the adjusted coefficient in predicting engine operation during combustion, the adjusted coefficient Heat Transfer Model was run in the combustion model. The method of comparison was conducted by:

1. Running the combustion model from IVC to EVO using:
   - REG fraction as estimated by the breathing model
   - Inlet Port conditions as measured during operation
   - Cycle averaged cylinder wall temperatures as provided by thermocouples
2. Utilise combustion timing obtained from the experimental trace using two Wiebe burn functions to describe burn progression of cool flame and main combustion
3. Utilise the Woschni Correlations as well as the proposed HCCI Woschni Correlation [20] and the fitted correlation as obtained from Motored Pressure Traces

Figure 23 below shows the results as obtained from modelling of a n-Heptane experimental trace at 1500 rpm. Both the original Woschni and Modified Woschni Correlations underestimate the heat loss during operation. It is clear from the plots that the fitted heat loss trace best describes the heat loss during the combustion cycle, although it seems to over estimate heat loss during the expansion stroke. Fuel auto-ignition was triggered manually to match experimental results for the purpose of heat transfer modelling development. However, once good thermal agreement was obtained, auto-ignition predictions could be obtained using the empirical auto-ignition model developed by Yates [9].

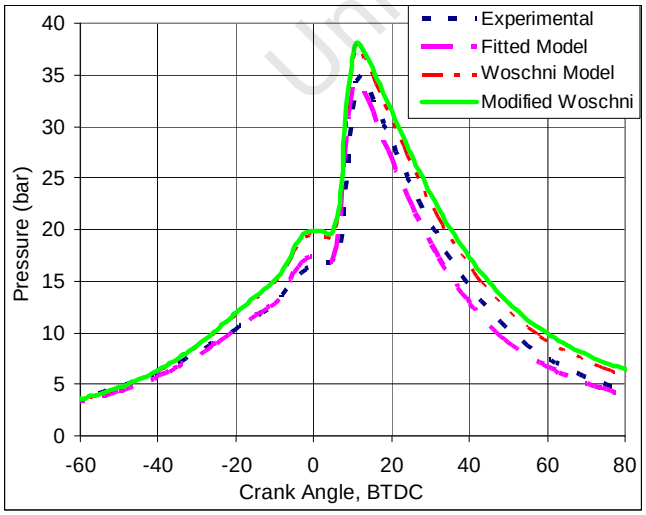

Figure 23: Effects of Various Heat Transfer Correlations on Predicted Cylinder Pressure

In spite of clear differences between HCCI, SI and CI combustion dynamics, a change in the m coefficient of the Woschni model allows it to predict cylinder heat loss with surprising accuracy. Effects of cylinder wall temperatures used in the modelling play a major role in predicting overall heat loss from the combustion chamber. Thermocouple placement is therefore critical in order to obtain cylinder wall temperatures which are representative of the bulk combustion chamber temperature.

CONCLUSIONS

ENGINE OPERATION

• An inexpensive HCCI test rig capable of performing various HCCI fuel and engine tests with a high degree of accuracy and repeatability was constructed.

• Stable HCCI operation is possible between 1000 - 4000 rpm with combustion quality and pressure rise rates being the key factors in operational envelope limits when operating with Diethyl Ether

• Engine design and operational characteristics in the form of breathing and heat loss are major factors in small engine operation and dictate required control strategies and fuel selection

• Testing of the various control strategies seem to indicate points of optimal operation and so called "sweet spot" operation; where engine operation is possible under varying speed and load conditions with no required altering of control strategy conditions such that there is no effect on combustion phasing. These "sweet spots" are expected to be completely engine dependent and thus engine characteristics including heat-loss and breathing characteristics dominate.

• Diethyl Ether is an effective fuel choice for small engine operation, allowing for operation over a wide operating envelope. However DEE can exhibit NTC behaviour at increased speeds under certain operating conditions. Access to the NTC region is primarily controlled by cylinder temperature as was shown by the effects of engine heat transfer.

CONTROL STRATEGIES AS AN EFFECTIVE MEANS OF COMBUSTION CONTROL

• Combinations of the various control strategies can be used effectively to control HCCI combustion phasing throughout the operating range.

• Most control strategies are suitable for HCCI operation, however mixture temperature control is difficult due to the thermal inertia and associated delay in obtaining desired mixture temperatures

• It is possible to correlate heat transfer from a small engine by utilising motored pressure traces at one speed and transferring the correlation to other engine speeds. Modifications of the Woschni Heat Transfer Correlation seem to produce good accuracy even when modelling engine combustion. Wall temperature measurements increase the error due to thermocouple placement and cylinder temperature variations throughout the cycle. The adjusted correlation over predicts heat loss during the expansion stroke; however estimation of engine operation during the compression cycle is critical in modelling of fuel autoignition during engine operation.

• The major discrepancy between the different Heat loss model variations suggests that heat loss experienced in small engines during operation is primarily related to engine size and characteristics and not the mode of combustion.

• Having obtained good heat transfer model accuracy, auto-ignition can be accurately modelled.

ACKNOWLEDGMENTS

This study was funded and supported by Sasol Technology Fuels Technology which is headed by Paul Morgan.

REFERENCES

1. [1] D. of Energy, E. E. R. Energy, and O. of Transportation Technologies, “Homogeneous charge compression ignition: (HCCI) technology a report to the U.S. congress,” Report to Congress, 2001.
2. [2] F. Zhao, Homogeneous Charge Compression Ignition (HCCI) Engines: key research and development issues. SAE, 2003.
3. [3] J. Bengtsson, Closed-Loop Control of HCCI Engine Dynamics. Lund University: Department of Automatic Control, 2004.
4. [4] K. Collair and G. Floweday, “Understanding HCCI characteristics in Mini HCCI Engines,” SAE 2008-01-1662.
5. [5] M. Murphy, J. Taylor, and R. McCormick, Compendium of Experimental Cetane Number Data. Colorado: National Renewable Energy Laboratory, 2004.
6. [6] M. Shukla, T. Bhaskar, A. Jain, S. Singal, and M. Garg, “Bio-ethers as transportation fuel: A review,” Indian Institute of Petroleum Dehradun, 2007.
7. [7] J. Mack, D. Flowers, B. Buchholz, and R. Dibble, “Using biofuel tracers to study alternative combustion regimes,” Nuclear Instruments and Methods in Physics Research, 2007.
8. [8] J. Mack, D. Flowers, B. Buchholz, and R. Dibble, “Investigation of HCCI combustion of diethyl ether and ethanol mixtures using carbon 14 tracing and numerical simulations,” Proceedings of the Combustion Institute, 2005.
9. [9] A. D. Yates and C. L. Viljoen, “An improved empirical model for describing auto-ignition,” SAE 2008-01- 1629.
10. [10] J. Yang, T. Culp, and T. Kenney, “Development of a gasoline engine system using HCCI technology - the concept and the test results,” SAE 2002-01-2832.
11. [11] H. Persson, M. Agrell, J.-O. Olsson, and B. Johansson, “The effect of intake temperature on HCCI operation using negative valve overlap,” SAE 2004-01- 0944.
12. [12] T. Aroonsrisopon, D. Foster, T. Morikawa, and M. Iida, “Comparison of HCCI operating ranges for combinations of intake temperature, engine speed and fuel composition,” SAE 2002-01-1924.
13. [13] M. Sjoberg and J. Dec, “Comparing late-cycle autoignition stability for single- and two-stage ignition fuels in HCCI engines,” Combustion Institute, 2007.
14. [14] M. Sjoberg and J. Dec, “Egr and intake boost for managing HCCI low-temperature heat release over wide ranges of engine speed,” SAE 2007-01-0051.
15. [15] Z. Chen and K. Mitsuru, “How to put the HCCI engine to practical use: Control the ignition timing by compression ratio and increase the power output by supercharge,” SAE 2003-01-1832.
16. [16] A. Maiboom, X. Tauzia, J.-F. Hetet, M. Cormerais, M. Tounsi, T. Jaine, and S. Blanchin, “Various effects of egr on combustion and emissions on an automotive di diesel engine: numerical and experimental study,” SAE 2007-01-1834.
17. [17] X.-C. Lu, W. Chen, and Z. Huang, “A fundamental study on the control of the HCCI combustion and emissions by fuel design concept combined with controllable egr. part 2: Effect of operating conditions and egr on HCCI combustion,” Fuel, 2005.
18. [18] J. Heywood, Internal Combustion Engine Fundamentals. Singapore: McGraw-Hill Book CO, 1988.
19. [19] K. Hansen, C. Nielsen, S. Sorenson, and J. Schramm, “A 50cc two-stroke di compression ignition engine fuelled by dme,” SAE 2008-01-1535.
20. [20] J. Chang, O. Guralp, Z. Filipi, D. Assanis, T.-W. Kuo, P. Najt, and R. Rask, “New heat transfer correlation for an HCCI engine derived from measurements of instantaneous surface heat flux,” SAE 2004-01-2996.

CONTACT

Mr Gareth Floweday
SASOL Advanced Fuels Laboratory
Mechanical Engineering Department
University of Cape Town
Tel: +27 21 650 5306
email: gareth.floweday@sasol.com
www.safl.uct.ac.za

DEFINITIONS, ACRONYMS, ABBREVIATIONS

Φ: Air/Fuel Ratio
After Top Dead Centre (ATDC): crank angle degrees reverse rotation required to bring the piston to its highest position.
Before Top Dead Centre (**BTDC**): crank angle degrees forward rotation required to bring the piston to its highest position.
Burn Duration: Time from Start if Ignition until Heat Release Rate is zero which can be specified either in CAD or a time measurement.
Cooperative Fuels Research (CFR) Engine: Device used in the ASTM test methods for determining the octane ratings of gasoline
Cumulative Heat Release: Total heat released during combustion (J).
Field Programmable Gate Array (FPGA) Card: An electronic integrated circuit chip which allows user programming using logic circuit diagrams or source code to implement logical functions.
Heat Release Rate (HRR): Is defined as the heat release rate per crank angle degree during combustion specified in J/CAD.
Homogeneous Charge: Infers a well mixed mixture of charge, being fuel and air.
Homogeneous Charge Compression Ignition (HCCI) engine: an internal combustion engine which ignites a premixed charge by compression without an ignition device.
Ignition Delay (ID): Time measured in CAD from time of injection to the point of ignition.
Indicated Mean Effective Pressure (IMEP): A theoretical pressure that if applied constantly, will produce the same work per cycle as the engine produces (kPa).
Primary Reference Fuels (PRF's): n-Heptane and iso-Octane are Primary Reference Fuels and are used for octane rating in internal combustion engines.
Start of Combustion (SOC): Is the start of ignition, which is specified as the crank angle corresponding to 50% (CA50) of the magnitude of the peak heat release.
Start of Injection (SOI): Crank angle at which fuel injection begins

APPENDIX A

Figure 24: Side View of Thermocouple Placement for Cylinder Temperature Measurements

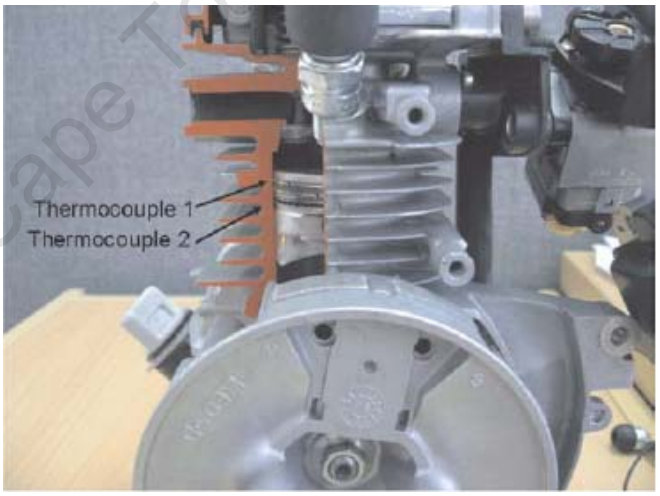

Figure 25: Relative Depth Placements of Thermocouples for Cylinder Temperature Measurements

APPENDIX B

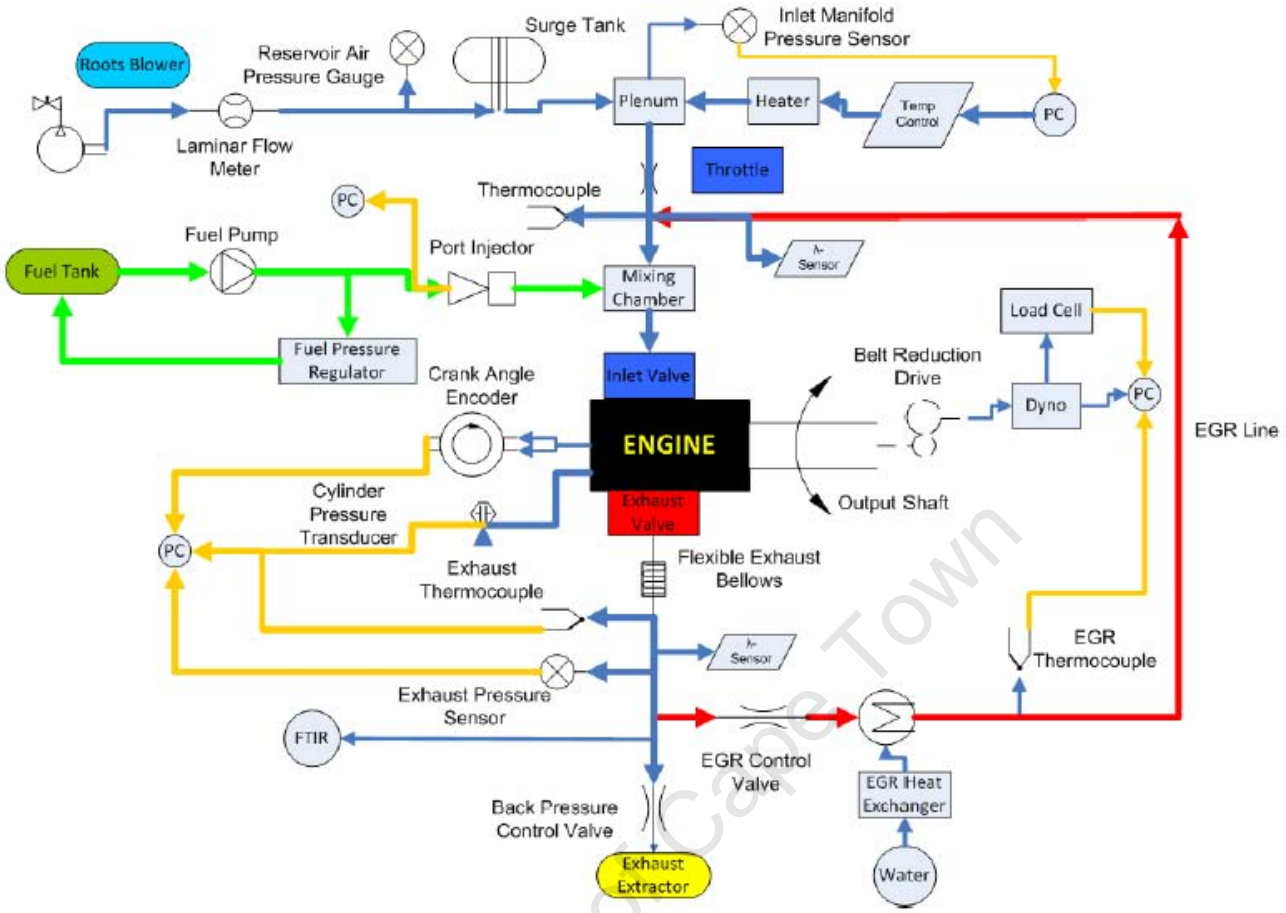

Figure 25: Experimental Setup with DAQ System Layout

APPENDIX C

Engine: Engine specifications given in Table 1
Dynamometer: Leeson TMDC Permanent Magnet Motor, Rated Power 1.1 kW @ 3000rpm
DC Motor Controller: Phantom DC Motor Controller, 3.7 kW @ 30 A and 260 VDC
Load Cell Amplifier: P3500 Strain Gauge Indicator. 40μV/μ analogue output
Cylinder Pressure Transducer: AVL QH33D Water-Cooled Piezoelectric Pressure Transducer. Sensitivity 17.48 pC/bar. Max. Pressure 250 bar. Max Temperature 4000C.
Transducer Amplifier: Kistler Charge Amplifier type 5105
Lambda Sensor type and Display Unit: BOSCH LS17025 Broadband Lambda Sensor connected to ETAS LA4 Display Unit: λ 0.7 to 32.767 and O2 0 to 20.41%.
Pressure Sensors: GEMS Absolute Pressure Sensors, (0 - 2.5 bar) and (0 - 6 bar).
FPGA Card: National Instruments NI 7831-R

Cost Analysis		
Engine Hardware	Engine	R2500
	Dynamometer	R10 000
	Dyno Control	R15 000
Measuring Devices	Load Cell and Amp	R20 000
	Cyl. Pressure Transducer	R30 000
	Transducer Amplifier	R20 000
	Lambda Sensors	R60 000
	Thermocouples	R2000
	Pressure Sensors	R4000
Data Acquisition	FPGA Card	R30 000
Control Hardware	PC	R10 000
	Injector	R1500
	Air Heater	R450
	Water Pump	R400
	Temperature Controller	R2000
Consumables	Materials	R10 000
	Fuel Line	R2000
	TOTAL	± R226 000
		± $22 000*

*Note: Rand to U.S dollar conversion at R10.27

Appendix E: SAE Paper 2008-01-1662

The experimental work contained in this appendix was presented at the 2008 SAE Powertrain, Fuels and Lubricants Conference and published in the conference proceedings

It should be noted that this project was conceived and supervised by Mr Gareth Floweday. The experimental work, however, was conducted by Mr Kyle Collair

SAE 2008-01-1662

Understanding HCCI Characteristics in Mini HCCI Engines

Kyle Collair, Gareth Floweday
Sasol Advanced Fuels Laboratory, University of Cape Town

ABSTRACT

This paper examines the successful use of HCCI combustion in a standard issue model-aero "diesel" engine. This two-stroke engine, unlike the more common glow-plug versions, operates without any form of combustion initiator. The fuel and air are premixed using a simple carburettor and ignited by piston compression only. The engine therefore operates in HCCI mode even though it is referred to as a "model diesel engine". Of particular interest is the fact that the engine is easily started from cold, warm and hot conditions. It runs stably from idle to over 11000rpm and is shown to run at high load points across the speed range with extremely conservative pressure rise rates. Furthermore, this engine is shown not to exhibit any knocking (high pressure oscillations) within its normal range of operation.

The speed-load operational envelope of the engine is mapped out using a range of propellers and a propeller speed-load calibration rig. Air/fuel ratio, inlet air and exhaust gas temperatures are examined within this operational envelope. Areas of unstable operation and extremities in stable operation are also mapped out and discussed. The engine's use of inlet throttling, crankcase pumping and residual exhaust gas metering is modelled and discussed.

The standard model-aero engine fuel (a mixture of paraffin, ether, castor oil and ignition improver) is tested in an Ignition Quality Tester™ and in a larger 4-stroke variable compression ratio HCCI engine. These results are then compared with the HCCI operating characteristics of n-heptane in this larger engine.

INTRODUCTION

HCCI engines are typically limited in their speed-load operational envelopes, with cold starting and extremities of conventional engine speed and load points remaining difficult to attain.

HCCI engines present two major benefits over conventional gasoline and diesel engines; namely the possibility for high efficiency and low emissions [1]. An HCCI engine aspirates and compresses a homogeneous air-fuel mixture (like a gasoline engine). This mixture is auto-ignited purely by compression, with no external control mechanism (such as a spark-plug, glow-plug or fuel injection). The homogeneous bulk combustion of the mixture results in relatively low temperature combustion which in turn lowers NOx formation [2]. The homogeneity of the combustion also decreases particulate formation as there are no locally rich zones to initiate particulate formation [3]. In addition, the autoignition combustion mechanism is not limited to a near-stoichiometric mixture, but allows for leaner, more efficient combustion [1, 4]. Unlike a diesel, which may have a lean bulk air-fuel ratio with locally rich areas, the entire mixture in an HCCI engine has a nominally identical air-fuel ratio and thus burns more uniformly. HCCI engines also have the ability to operate without a throttle (like a diesel) which eliminates pumping losses at part-load, and increase efficiency.

In an HCCI engine the start of combustion, burn duration and combustion phasing are all controlled purely by combustion chemistry. The lack of external control over the ignition point and combustion behaviour has made wide-range HCCI operation a challenge [5, 6]. Transient operation is also a challenge due to the available methods of load and speed control. Varying the speed or load often simultaneously affects any number of critical factors such as air-fuel ratio, inlet pressure or the residence time of reactants. Each of these (and other) factors affect the chemical kinetics of the combustion and autoignition-reactions. As a result, the optimum operating conditions for one point are not easily changed to match the optimum operating conditions at another point [7, 8].

MODEL-AERO ENGINE DESCRIPTION – The model-aero engine is most commonly used to power R/C model aircraft. Despite being referred to as "model diesel engine", the engine used in this study is in fact an HCCI engine, as it combusts a homogenous mixture purely using the heat of compression. Of particular interest is the way this engine operates over a similar load-speed range to conventional glow-plug model aero engines. Transient operation presents no problem for the model-aero engine which has the ability to rapidly change load and speed by varying the throttle position.

The model aero engine utilises a two-step breathing process. Air and fuel are first aspirated into the crank case, where the mixture is then pressurised before entering the cylinder. A regular barrel-type throttle valve on the carburettor controls the mass of air and fuel admitted to the crank-case by varying the inlet pressure of air entering the crank-case. During the compression stroke, the rising piston creates an expanding volume in the crank-case. As a result, a fresh charge is sucked into the crank-case due to the pressure differential. Shortly after TDC, the crank-case inlet port closes and the crank gasses are pressurised by the descending piston (in the sealed crank-case). Pressurised crank-case pumping means the mixture in the crank-case is always above atmospheric when the cylinder inlet valves open. This improves exhaust gas scavenging and significantly increases the performance of two-stroke engines.
The engine, however, is not boosted and since the exhaust ports (open to nominally atmospheric) are the last to close, the pressure at EVC is also always close to atmospheric. Therefore only the mass of fresh charge admitted to the cylinder varies with different throttle positions, with the balance made up of exhaust residuals. Therefore closing the throttle not only decreases engine speed (and load due to decreased fuelling), but also increases exhaust residuals.

Various control strategies have been used in an attempt to extend the operating range and transient operation of HCCI engines. Most of these involve trying to mitigate the changes to the combustion chemistry caused by varying operating conditions. These include, but are not limited to: heated intakes, variable EGR, boosting and variable compression ratios; all with limited success [8]. Often these methods of control are too slow to respond to the rapidly changing operating conditions [8]. The model-aero engine is, by contrast, extremely simple and operates without any of these complex controls. Although it has a variable compression ratio, this is used almost exclusively for setting up the engine before starting from cold and then adjusting it once warmed up (for specific operating conditions). Once correctly set up, the engine is able to run comfortably over a variety of loads and speeds much like any other type of model-aero engine. Once the air-fuel ratio and compression ratio are correctly set up, one needs only adjust the throttle to vary the load/speed of the engine. This method of control is not particularly desirable for an HCCI engine since it results in pumping losses without affecting the inlet pressure (as would normally occur with a throttle valve), due to the layout of the engine's piston porting system. The effect of the throttle in this engine is similar to certain variable-valve-timing control strategies. This type of engine is of particular interest largely because it operates as a self-regulating HCCI engine over a wide range without any undesirable effects.

Table 1 shows the manufacturers' specifications for the model-aero test engine and Figure 1 shows the physical layout of engine, including the mechanism for varying compression ratio.

	Value	Unit
Displacement	6.55	cm^3
Bore	20.32	Mm
Stroke	20.08	Mm
Compression Ratio	variable	
Speed range	4000-11500	rpm
Rated Output	708	Watts
Max Prop	13x8	
Min Prop	10x6	

Table 1: PAW40 engine specifications. All values as quoted by Progress Aero Works except bore, stroke and displacement which were measured.

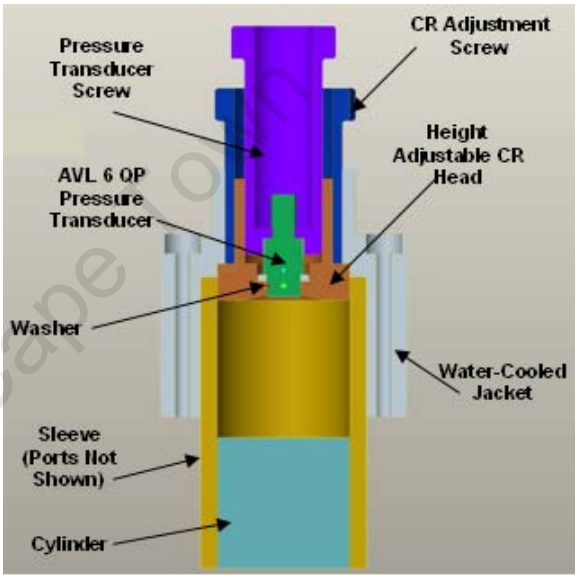

Figure 1: Engine Head and Cylinder Cross Section

Two-Stroke engines combine the expansion and exhaust cycles into one stroke, while the intake and compression cycles also share a single stroke. Therefore the whole combustion cycle is completed in a single crank revolution. This improves the power to displacement ratio of the engine, but compromises the gas-exchange process due to the resultant breathing process. In these engines, a large amount of exhaust residuals are mixed with the incoming fresh charge. HCCI combustion is greatly affected, as exhaust residuals have a significant influence on the combustion chemistry and in-cylinder conditions.

The model-aero engine uses a unique fuel blend of conventional Kerosene, Di-Ethyl-Ether, Iso-Propyl-Nitrate and Castor Oil with the blend ratios shown in Table 2.

D1000 Fuel Composition		
Component	**%**	**Properties**
Kerosene	35	Diesel like paraffinic fuel
Di-Ethyl-Ether	35	High cetane, good vaporisation

Castor Oil	28	2-Stroke lubricant
Iso-Propyl-Nitrate	2	Very high cetane ignition improver

Table 2: D1000 fuel specifications and properties

Model-Aero Engine Operating Cycle from TDC:

1. BDC @ -180^o
2. Crank case port opens @ -133^o
3. Aspiration of fresh charge into crank case
4. Cylinder intake port closes @ -126^o
5. Exhaust port closes @ -116^o
6. Compression of in-cylinder reactants
7. Combustion (SOC close TDC for typical timing)
8. TDC @ 0^o
9. Expand combusted gasses
10. Crank case port closes @ 45^o
11. Crank case gas compression (by descending piston)
12. Exhaust port opens (blowdown) @ 116^o
13. Cylinder intake port opens @ 126^o
14. Fresh charge fills cylinder when $P_{cylinder} < P_{crank\ case}$
15. BDC @ 180^o

A graphic representation of the operating characteristics and pressure traces are shown in Figure 2.

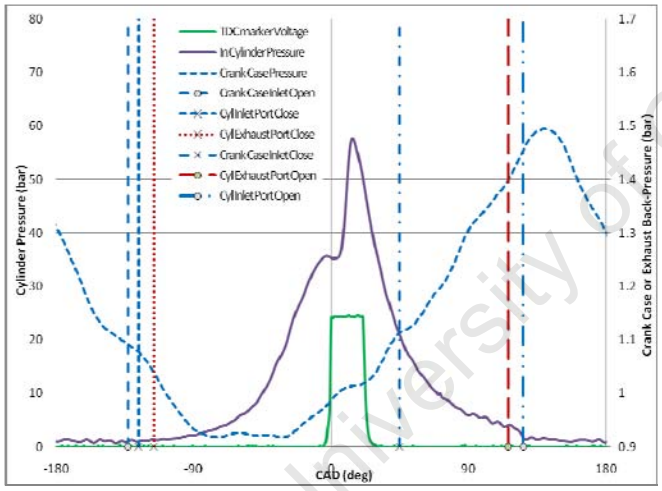

Figure 2: Data Capture from the Oscilloscope while running the engine with the 12x6 propeller at 8596rpm – Note the valve timing. Note also that although there may appear to be cool flame combustion near TDC, analysis of the heat release data showed no such event. This peak just before TDC is due to compression with the location attributed to significant heat loss in the small model aero engine.

This project sought to investigate the operating range of the standard engine. Of particular interest were the limits of stable combustion and beyond, as the intention was to determine the operating boundaries of the engine and then understand which factors limited HCCI combustion in these areas. It was of value to investigate the combustion behaviour outside of the engine's comfortable operating range (i.e. knocking or misfiring).

MODEL AERO PROPELLERS – The propellers used in this study were all fixed-pitch, Master Airscrew K-series types. The naming convention (eg "12x6") refers to the diameter in inches X the pitch in inches (at 75% of the blade radius). The pitch of a propeller refers to the distance travelled by the propeller for a single revolution (analogous to screw threads). For two propellers of the same diameter, the one with the larger pitch will require more torque for a given rpm [9, 10, 11]. Given two propellers with the same pitch, the one with the larger diameter would require a larger torque for a given rpm [9, 10, 11]. It is not possible to decouple the speed-load characteristics of a fixed pitch propeller and as a result, the very regular behaviour of such a propeller was described using the following equation:

$$T = C_t(\rho n^2 \phi^5) \text{ [10, 11]}$$

- T = Torque (Nm)
- C_t = Torque performance coefficient
- ρ = Air Density (kg/m^3)
- n = propeller rotational velocity in (rps)
- Φ = Propeller diameter (m)

A graphic representation of this behaviour is displayed in Figure 3, showing the load increasing as speed increases.

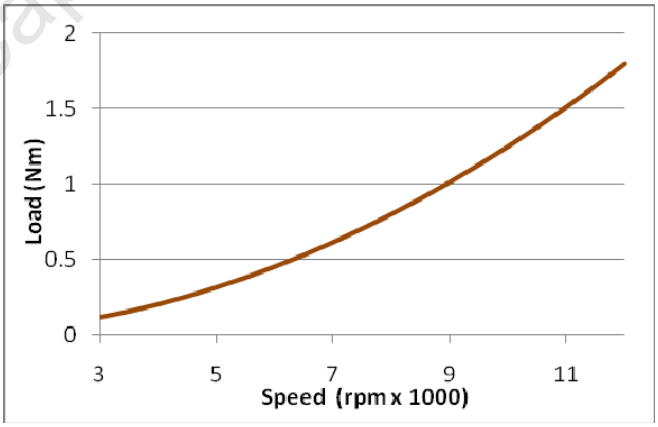

Figure 3: Typical Load vs. Speed behaviour for a fixed pitch propeller, as modelled using the aforementioned equation for a 15x10 propeller.

THIS STUDY – The model-aero engine has three major differences when compared to almost all other HCCI research engines:

- It runs on a unique fuel-blend which consists mainly of two fuels: Di-Ethyl-Ether, which shows single-stage autoignition behaviour (in a similar fashion to Ethanol, MTBE and TAME) [12, 13], and Kerosene, which (as a paraffinic fuel) shows strong two-stage autoignition behaviour [12, 13]. Castor oil is used as a two-stroke lubricant, but initially had an unknown effect on the autoignition properties of the fuel.
- Small physical size

- Unique effect of throttle-controlled residual exhaust gas control and its known effect on autoignition [14, 15]

The aim of this study was therefore to investigate this engine in terms of these fundamental differences, in order to establish the reasons for this engine's successful wide range and transient HCCI operation.

Experimental work included:

- Fuel and fuel-component testing in an Ignition Quality Tester
- Comparative fuel testing between the model-aero fuel and n-heptane in a Ricardo E6 test engine operating in HCCI mode
- Characterising the speed vs. load properties of the propellers used for testing the model-aero engine
- Running the model-aero engine at a variety of speed-load points, thus mapping out its operating range

Modelling work included:

- Modelling the speed vs. load characteristics of a variety of propellers thus, determining the most suitable sizes for testing
- CFD modelling of the engine's breathing characteristics to determine:
  1) The in-cylinder temperature profile.
  2) The effect of residual exhaust-gas fraction on associated reactant composition and temperature.
  3) The effects of breathing through the crank-case, and the cylinder inlet flow conditions.

CHARACTERISING THE PROPELLERS

The rig used to characterise the various propellers was conceptualised as an effective method of dynamometer testing the model-aero engine without a dynamometer. The main reason for choosing to use propellers and an intermediate calibration rig (instead of directly connecting the engine to a dynamometer) was that the maximum speed for a given propeller also represented the point of maximum power for that propeller. This therefore also represented the optimum engine setup for maximum power from that propeller (as any other setup resulted in a lower speed). Maximum power required optimised combustion phasing [16, 17, 18, 19] and tuning the engine in this manner provided a convenient method of altering various engine parameters for optimum combustion phasing.

NUMERICAL MODELLING - Initially it was unclear which propellers were most suitable for testing the extended operating range of the model-aero engine. Modelling a range of propellers was useful in guiding the selection of propellers which were tested (in the calibration rig) and eventually used for testing on the model-aero engine. The full range of Master Airscrew K-series propellers was modelled in MATLAB using a simplified version of Glauert Blade Element Theory [11] to generate the torque vs. speed curves. Evaluation of the model results led to the selection of the following seven propellers which gave the widest possible range for testing: 11x5 (equivalent to the minimum prop suggested by the manufacturers, to ensure a safe maximum operating speed), 11x5, 11x6, 12x6 (recommended propeller size), 13x8, 14x8, 15x8 and 15x10.

EXPERIMENTAL TESTING – The premise behind the propeller experiments was that each propeller had a unique torque coefficient describing its torque vs. speed characteristics. Once known, this performance coefficient was used to calculate the torque required to drive the propeller at any speed (for any operating conditions). The results from the propeller rig showed the operating envelope for a given set of propellers, thus defining the possible test boundaries of the engine using those propellers.

The rig was constructed using a conventional woodworking router motor (with a similar power and speed rating to the model-aero engine) to drive the propellers. This motor was mounted on trunion bearings so that any applied torque caused it to rotate freely. A balance beam was then attached to the motor and weights were hung from the beam in order to counteract the torque supplied by the motor. The layout of the rig is shown in Figure 4. A given combination of weights and lever arm distances resulted in a known torque value for that configuration. The speed of motor was measured using a photo-tachometer, thus generating data points of torque vs. speed from which the propeller torque coefficient could be calculated.

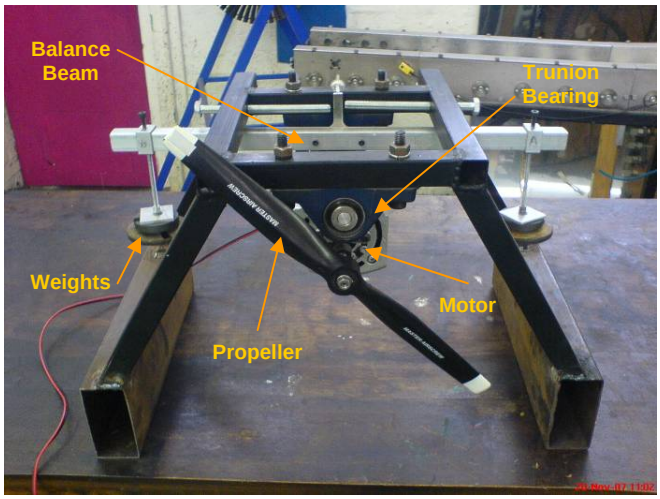

Figure 4: Propeller Testing Rig

Experimental Results - The experimental rig produced excellent results and clearly showed the expected trends for all the tested propellers. It was also possible to use

the averaged torque coefficient to calculate the rpm required for each tested load point. This provided a useful method of evaluating the quality of the data by observing the scatter for each data set.

The data showed very little scatter for all the tested propellers. By using the averaged torque coefficient (calculated from ten readings per propeller) it was possible to calculate the speed vs. load characteristics for each propeller and extrapolate their behaviour beyond the tested range using the torque coefficient and the aforementioned relationship between propeller torque and speed. Figure 6 shows all the data points superimposed onto the characteristic speed vs. load curves of all the tested propellers.

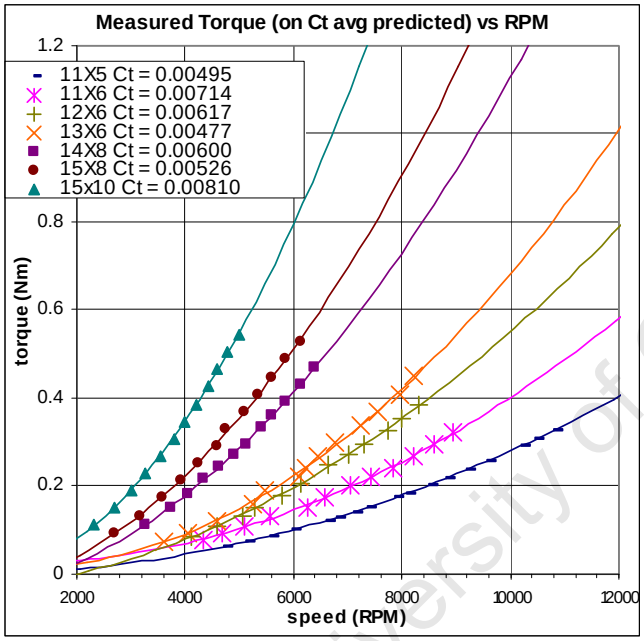

Figure 6: Test points superimposed onto the extrapolated Load vs. Speed behaviour for all the tested propellers

FUEL ANALYSIS & COMBUSTION PROPERTIES

The autoignition characteristics of a fuel are heavily dependent on its reaction to increases in temperature and pressure [20]. Increasing the temperature of an air-fuel mixture generally shortens the autoignition delay of the mixture. However, some fuels exhibit a limited range of "negative temperature coefficient" behaviour where increasing test temperatures results in increased ignition delay times as shown in Figure 7 [20]. This NTC behaviour is associated with a "cool flame" reaction which precedes the main heat release. The cool flame reaction causes a relatively small temperature rise and significantly influences the ignition delay of the main heat release.

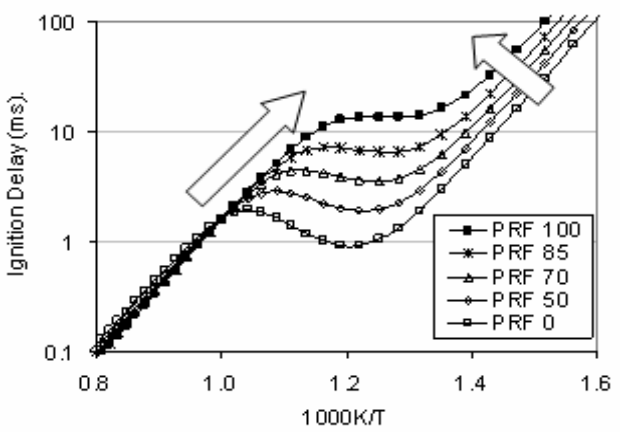

Figure 7: Fuels with pronounced NTC behaviour (resulting in two-stage autoignition with cool flame heat release) [20]

The difficulty with the model-aero fuel blend, D1000, is that the two main combusting fuel components have very different autoignition characteristics. Di-Ethyl-Ether is a single-stage (no cool flame) autoignition fuel whereas Kerosene shows definite two-stage ignition behaviour [12, 13].

The autoignition behaviour of the unique fuel used by the model-aero engine required some form of characterisation. This analysis took two forms; fuel component testing in an Ignition Quality Tester, and comparative blended-fuel testing in a Ricardo E6 test engine.

IQT™ TESTING – The Ignition Quality Tester is a type of combustion bomb commonly used for industrial fuel quality testing. It is used to test the ignition delay and cetane rating of a fuel by comparing the ignition delay of a fuel to the known ignition delay of n-heptane.

Experimental Methodology – The IQT™ is used to evaluate diesel-like fuels (fuels prone to autoignition) in a non-homogeneous, diesel-like, combustion environment. Fuel is sprayed through a high pressure injector into a hot, pressurized environment (in order to aid autoignition). The instrumentation in the IQT™ ultimately measures the ignition delay of the fuel for a fixed set of test conditions. The testing procedure involves first adjusting the test conditions so that the known ignition delay of n-heptane is achieved as a reference. The cetane rating of the fuel is then calculated based on ignition delay of the fuel relative to n-heptane over an average of thirty tests. [21]

Various blends of the fuel components were tested and compared to 100% Kerosene in an attempt to understand the effect of each component. 100% Castor oil could not be tested as it caused injector spray difficulties.

Experimental Results - Testing in the IQT™ clearly showed the cetane effects of each fuel component as shown in Table 3. Using 100% Kerosene as a baseline,

increased concentrations of Castor Oil showed very little effect on cetane number as shown in Figure 9. Once again using 100% Kerosene as baseline, increased concentrations of Iso-Propyl-Nitrate (ignition improver) increased the cetane rating of the fuel significantly as shown in Figure 8. [Pure Di-Ethyl-Ether was found to have a higher cetane than the average for D1000 and thus added to the D1000's high overall cetane in addition to providing good vaporisation.

Percentage Blend by Volume				
Ether	**Kero**	**IsoPropNitro**	**Castor**	**Cetane**
100.0	0.0	0.0	0.0	**198**
0.0	100.0	0.0	0.0	**45**
0.0	99.0	0.0	1.0	**46**
0.0	95.0	0.0	5.0	**46**
0.0	90.0	0.0	10.0	**46**
0.0	85.0	0.0	15.0	**45**
0.0	80.0	0.0	20.0	**43**
0.0	99.0	1.0	0.0	**62**
0.0	98.5	1.5	0.0	**66**
0.0	98.0	2.0	0.0	**71**
0.0	97.5	2.5	0.0	**74**
35.0	35.0	2.0	28.0	**93**

Table3: IQT™ test matrix showing blend compositions and results

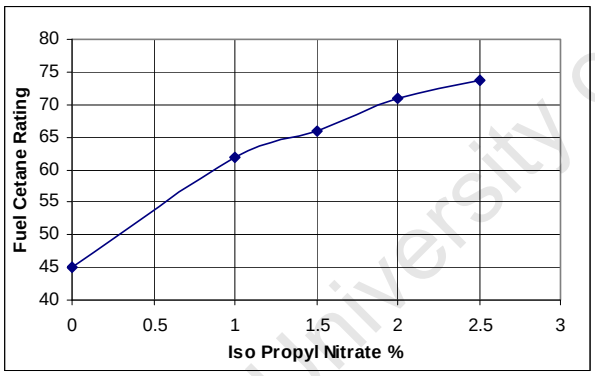

Figure 8: Effect of blending small percentages of Iso-Propyl-Nitrate with Kerosene. Blending even small amounts of Iso-Propyl-Nitrate resulted in a significant cetane improvement.

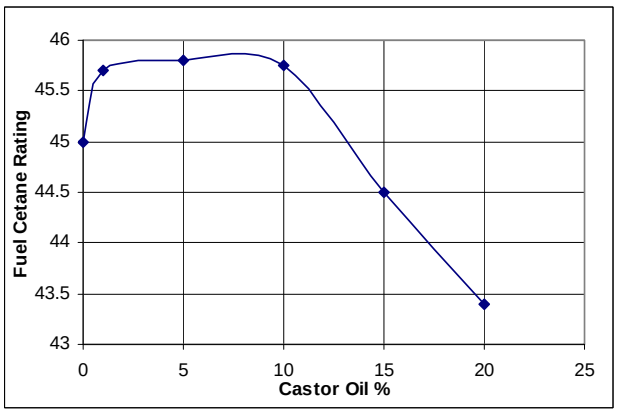

Figure 9: Effect of blending Castor Oil with Kerosene. Noting the scale of the graph, even large amounts of castor oil had very little effect on the cetane rating of the fuel.

Linear extrapolation of the test results for Iso-Propyl-Nitrate and Castor Oil allowed for the cetane value for those fuel components to be calculated as shown in Table 4.

Component	Cetane
Kerosene	45
Di-Ethyl-Ether	198
Castor Oil	~25
Iso-Propyl-Nitrate	~1200
D1000 Measured	93

Table 4: Fuel Component Cetane Properties

RICARDO E6 ENGINE TESTING – D1000 model-aero fuel was evaluated as an HCCI fuel in a Ricardo E6 single cylinder, variable compression ratio research engine. The engine specifications are given in Table 5 below.

	Value	Unit
Displacement	507	cm^3
Bore	76.2	Mm
Stroke	111.1	Mm
Compression Ratio	Variable 4.5:1 to 20:1	
Speed range	1000-3000	Rpm

Table 5: Ricardo E6 engine specifications

The D1000 was compared with a similar formulation, excluding the castor oil component as well as N-heptane and a Low Temperature Fischer Tropsch "Gas to Liquid" Naphtha. IQT-derived Cetane values for the test fuels are shown in Table 6 below.

Test fuel	IQT Cetane #
D1000	93
D1000 minus castor oil	96.5 (estimated)
N-heptane	53
LTFT GTL Naphtha	43.8

Table 6: IQT-derived Cetane values for the test fuels

The aim of this simple testing was to answer the following questions:

1. Does D1000 exhibit unique and unusually favourable HCCI combustion properties compared with other HCCI fuels [22]? For example, does D1000 show a particular insensitivity to T, AFR or exhaust residuals?
2. Does the castor oil blend component reduce combustion heat release rates, or otherwise benefit HCCI combustion?

The tests were run with a fixed heated inlet temperature of 400^{o}C at engine speeds of 600, 1200 and 1800 rpm. Air fuel ratios tested included λ =1.5, 2.0, 2.5, 3.0 and 3.5. Compression ratios were adjusted during testing of each matrix point in order to attain peak pressure phasing at approximately 10 CAD ATDC. Note that many of the test points in this matrix could not be achieved either due to knocking intensity, instability related to misfire or inability to achieve high fuelling (e.g. for D1000 at λ =1.5).

Results - The extremely high ignition quality of the model-aero fuel enabled HCCI combustion at very low compression ratios – stable HCCI combustion was achieved with D1000 minus the castor oil component at a compression ratio of 4.5:1. The slight increase in ignition quality resulting from omission of the castor oil blend component resulted in slightly advanced main heat release timing. In spite of the significantly lower compression ratios afforded by the model-aero fuels (and associated higher trapped exhaust gas residual fractions), the trends in knock and stability limits of speed and air-fuel ratio operating ranges were very similar to the other test fuels.

The answers to the test motivation were therefore as follows:

1. D1000 does not exhibit unique and unusually favourable HCCI combustion properties compared with other HCCI fuels.
2. The Castor oil blend component does not reduce combustion heat release rates, or otherwise benefit HCCI combustion in any significant manner.
3. The D1000 exhibits 2-stage heat release in the Ricardo E6 engine as shown in Figure 10, while exhibiting single stage heat release in the model-aero engine. This indicates that D1000 is in fact a 2-stage ignition fuel, but the NTC area of the fuel is not accessed by the pressure-temperature history in the model-aero engine.

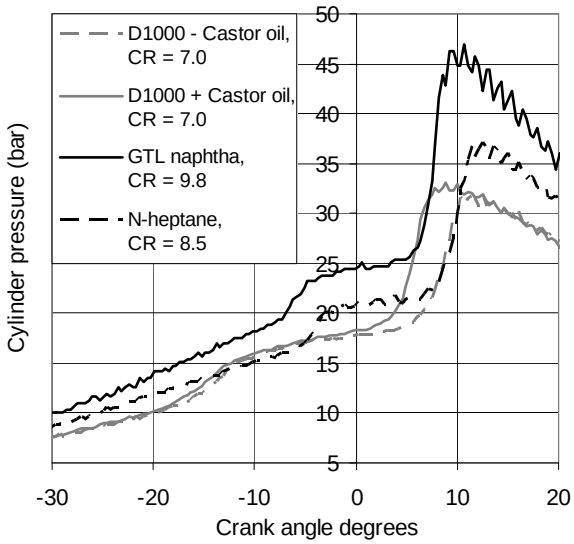

Figure 10: Pressure traces for the 4 test fuels at λ=2.5 (Incipient knocking conditions), indicating compression ratios required for indicated combustion phasing

MODEL-AERO ENGINE CHARACTERISTICS

ENGINE TESTING – Controlled testing of the model-aero engine provided the most insight into the operating characteristics of the engine.

Experimental Philosophy – By using a variety of suitable propellers, it was possible to plot out the operational envelope of the engine and also analyse areas outside that range (i.e. knocking or misfiring).

The rig was fitted with a suitable in-cylinder pressure transducer and a TDC marker (used to measure both engine speed and crank angle degrees). The relative pressure transducer readings were calibrated by pegging the cylinder at 1 bar at BDC. Due to the more extensive nature of this study, further instrumentation and slight modifications were required to measure test factors known to influence HCCI operation as shown in Table 7.

These test factors were limited to:

Factor	Measuring Method
In Cylinder conditions	pressure transducer in cylinder
Inlet Pressure	pressure transducer in crank-case
Inlet Temperature	thermocouple in crank-case
Air-Fuel Ratio	lambda sensor in exhaust
Compression Ratio	measured geometrically

Table 7: Techniques used to measure factors which are known to influence HCCI operating [8]

The engine was adjusted while running to achieve the maximum speed (and therefore power) for a given propeller. Table 8 shows the factors which were adjusted for maximum engine speed:

Adjustment	Effect
Throttle opening	air-fuel mixture inducted
Mixture Needle	Air-Fuel ratio
CR screw	Compression Ratio

Table 8: Engine adjustments and effects

Experimental Methodology – Sufficiently detailed engine testing required further instrumentation of the model-aero engine. Due to the engine's small size, not all instrumentation could be fitted to the engine at the same time.

The engine's air-cooled head had also been replaced by a water-cooled unit as shown in Figure 11, with temperature control to limit engine wear during prolonged testing and control the temperature conditions across different test conditions [23]. The ability to vary the compression ratio was retained.

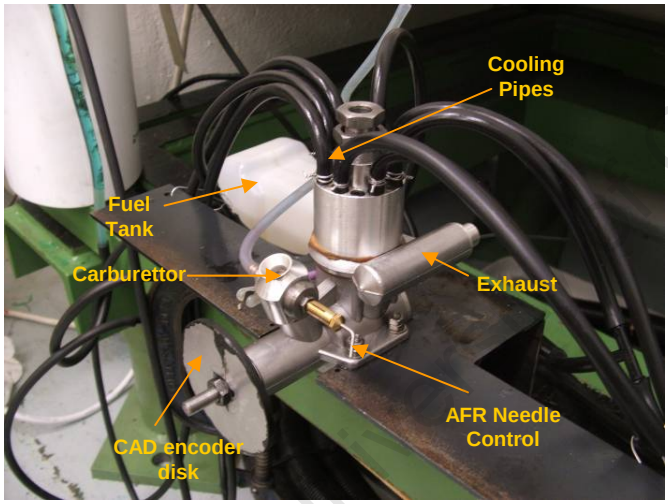

Figure 11: Un-instrumented model-aero engine

The engine was later modified so that a water-cooled pressure transducer or thermocouple could be placed inside the crank case. The pressure trace from the crank-case pressure transducer was used as an inlet port boundary condition in the CFD model.

An oil trap and lambda sensor were built into the exhaust system as shown in Figure 12, although testing with this setup compromised exhaust scavenging performance slightly. A thermocouple was also fitted next to one of exhaust ports of the engine to measure the exhaust gas temperature.

In addition, a thermocouple was placed in the head instead of the pressure transducer as a means of gaining insight into the average head temperature trends.

Fuel was supplied using a conventional gravity feed model-aero fuel tank. The needle-type air-fuel ratio mixture control was retained along with the original throttle valve.

A hand-operated model-aero starter motor was used to start the engine, as well as to spin the engine while recording motored traces.

All maximum speed points were operated with the throttle wide open. Minimum speed points utilised whichever throttle and mixture combinations optimised stability at the compression ratio being tested.

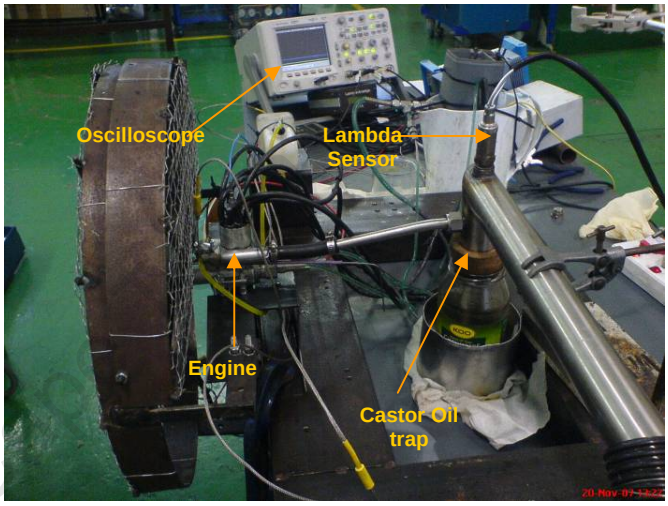

Figure 12: Model-aero engine test rig

Experimental Results – Careful adjustment of the throttle, mixture and compression ratio resulted in a much larger operating range than could be achieved with the recommended propellers with the full operating range shown in Figure 13. Within this area there was no evidence of knocking (at any of the high-load points) or misfiring (at any of the low-load points). It was found that testing on just three propellers provided a suitably large operating range for the engine. The 11x5 propeller was chosen for low-load, high-speed operation. The 12x6 propeller represented the normal load-speed profile for the engine and the 15x10 propeller was chosen for its high-load, low-speed characteristics.

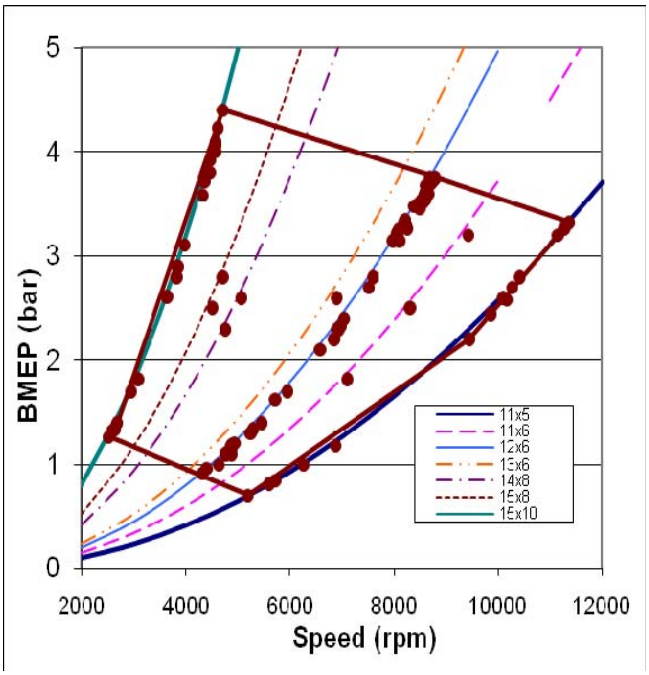

Figure 13: Model-aero operating range showing the test points superimposed on the speed-load curves of the tested propellers. The slight discrepancy between the speed-load curves and the test points is due to the speed-load curves being calculated using a constant air density, whereas the test points were calculated using the actual air density for each test.

Table 9 shows the operating conditions and Table 10 shows the combustion behaviour for the test points at the extremes of the tested operating range.

Prop	RPM	BMEP bar	CR	Lambda	T amb °C
15x10	4706	4.4	9.2	~1.4	17
15x10	2521	1.3	18.8	~0.93	17
12x6	8797	3.8	14.8	1	20
12x6	4316	0.9	13.1	0.98	20
11x5	11363	3.3	17	~0.95	16
11x5	5195	0.7	14.8	1	22.5

Table 9: The maximum and minimum operating speeds for the tested propellers and the associated operating conditions

Combustion Behaviour					
Prop	**Speed**	**CR**	**Lambda**	**SOC** 1%	**Burn** 1-99%
11x5	11363	17	~0.95	-2	8
11x5	5195	14.8	1	5	31
12x6	8797	14.8	1	2.5	10.5
12x6	4316	13.1	0.98	5	28
15x10	4706	9.2	~1.4	1	7
15x10	2521	18.8	~0.93	0	29

Table 10: Combustion behaviour at the operating limits of the model-aero engine.

It was difficult to isolate the factors which most affected the combustion behaviour of the model-aero engine, as a variety of factors were varied simultaneously to try and achieve the optimum engine setup. Figure 14 shows the pressure traces of the maximum speed points for each propeller. Table 11 describes the maximum pressure rise rates and maximum pressures at the upper operating extremes, which were relatively conservative [24] and did not result in knock.

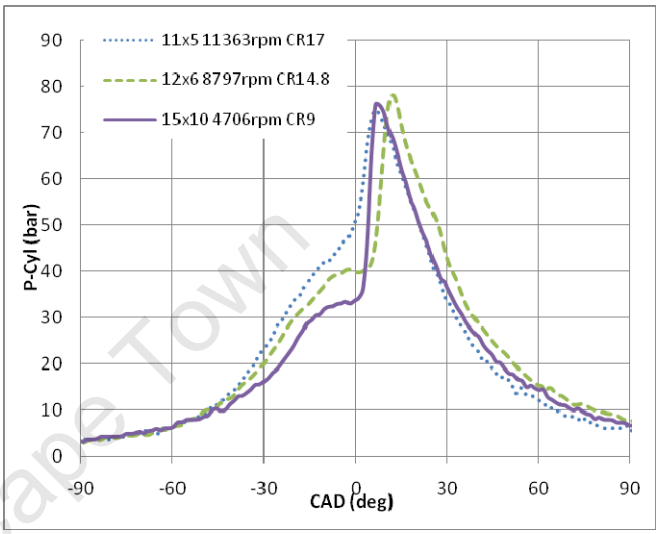

Figure 14: Overlay pressure traces of the maximum speed points for each propeller.

Prop	RPM	Max ΔP bar/deg	@CAD deg	Pmax bar	@CAD Deg
15x10	4706	12	5	76	6.4
12x6	8797	8.1	9.4	78	11.5
11x5	11363	5.1	3.5	74.8	6.2

Table 11: Combustion Characteristics at the maximum-speed operating extremes

Fig 15 to 17 and Tables 12 to 14 show the results of an investigation into the model-aero engine's ability to naturally compensate for conditions which would normally change combustion phasing. It was suspected that two individually conflicting effects cancelled out when combined together:

- Increased Speed Retards timing due to time effects on the autoignition delay
- Increased Load Advances timing due to decreased residuals and increased fuelling

Testing the individual effects in isolation produced the expected results. Combining the effects showed that the model aero engine was able to maintain constant phasing for varying speed/load points along the 12x6 speed/load profile with the increase in speed and load achieved through throttle adjustment only.

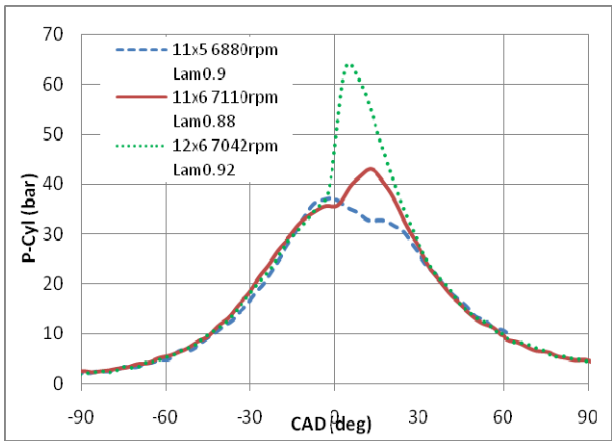

Figure 15: Constant Speed Test results at ~7000rpm

Prop	Speed	BMEP	Lam	1-99% MFB	Pmax	at CAD
ΦXpitch	rpm	Bar		deg	bar	deg
11x5	6881	1.18	0.9	25.6	37	-1.3
11x6	7110	1.82	0.87	21.9	43.1	13
12x6	7042	2.4	0.92	8.7	64.1	4.5

Table 12: Operating Conditions for Constant Speed Tests

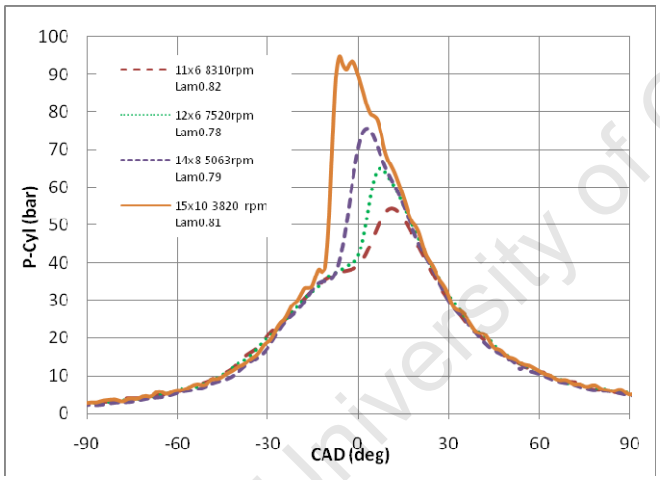

Figure 16: Constant Load Test results at ~2.6bar BMEP

Prop	Speed	BMEP	Lam	Max PRR	at CAD	1-99% MFB	Pmax	at CAD
ΦXpitch	rpm	bar		bar/deg	deg	deg	bar	deg
11x6	8310	2.5	0.82	2	5.2	20	54.4	11.2
12x6	7518	2.7	0.78	4.75	3.5	13.3	65	7.1
14x8	5063	2.6	0.79	5.3	-2.9	10.2	75.4	3.2
15x10	3822	2.8	0.81	18.1	-8.7	7.1	94.6	-6.4

Table 13: Operating Conditions for Constant Load Tests

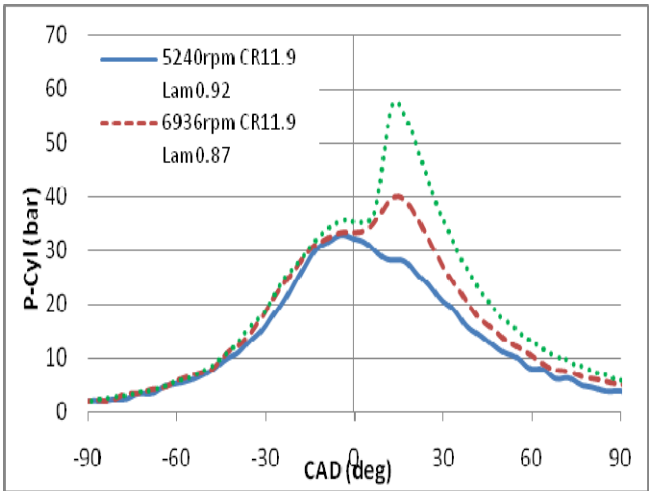

Figure 17: Natural Compensation results on 12x6 prop

Speed	BMEP	Lam	Pmax	at CAD	1-99% MFB
rpm	bar		bar	deg	Deg
5240	1.3	0.92	28.3	14	25
6936	2.3	0.87	40	14.5	24
8596	3.6	0.9	57.6	13.4	15.7

Table 14: Combustion Characteristics of points along standard load-profile. Note that the slowest-speed point achieved such late, low-magnitude heat release (due to highly throttled operation) resulting in peak pressure near TDC and not during combustion. The provided pressure peak due to combustion does, however, occur at a similar CAD when compared to the other test points.

Table 15 and Figure 18 are examples of the effect of varying the compression ratio while keeping the speed, throttle and mixture relatively constant. With increasing CR one would expect the burn duration to decrease, SOC to advance and max ΔP to increase, both of which were observed in testing.

CR	RPM	λ	SOC	Burn	Max PRR	CAD
			1%	1-99%	bar/deg	deg
17.3	8670	~1	-1.5	8	9	2.8
13.3	8620	~1	1	10	5.3	6.2
10.8	8522	~1	2.5	15.5	4.2	11

Table 15: CR Effect on Combustion using 12x6 Prop

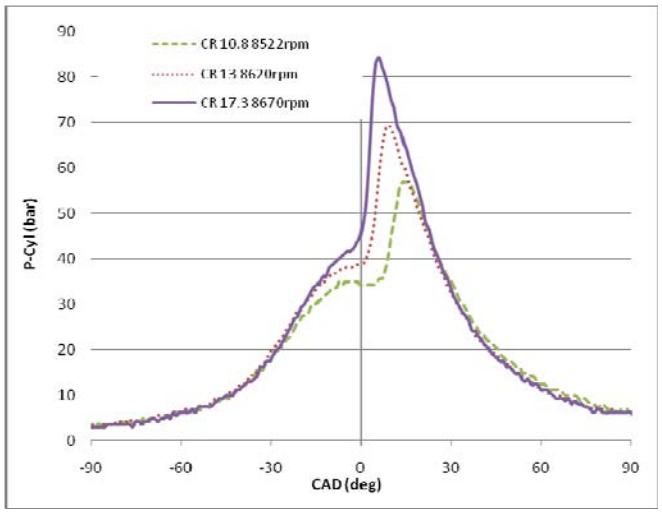

Figure 18: Overlay pressure traces of varying CR effects using the 12x6 propeller

Analysis of the heat release data obtained from the pressure traces was difficult due to significant noise, even after Fourier Transform smoothing. Even with the noisy signal, it appeared as if there was no significant cool flame reaction at the limits of the operating range of the engine, as shown in Figure 19 and Figure 20. The signal noise was attributed to heat flux in the pressure transducer as it was not directly water-cooled. Engine vibration could also have contributed to the noisy signal.

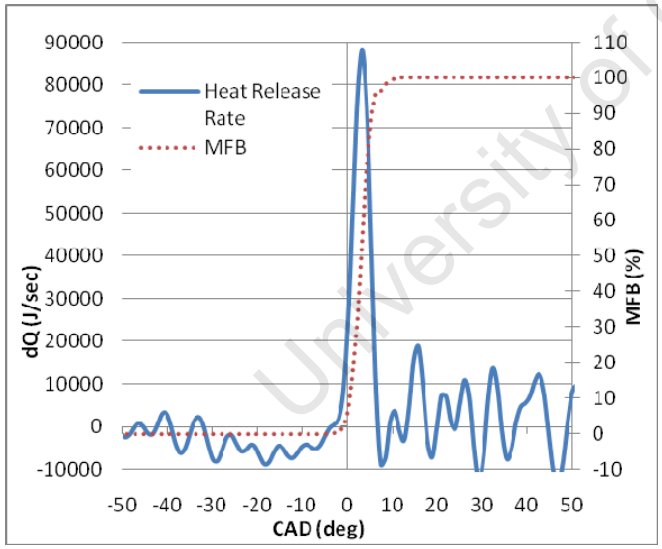

Figure 19: Example of maximum power heat release with no cool flame component (12x6 prop at 8646rpm). Note the large amount of signal noise.

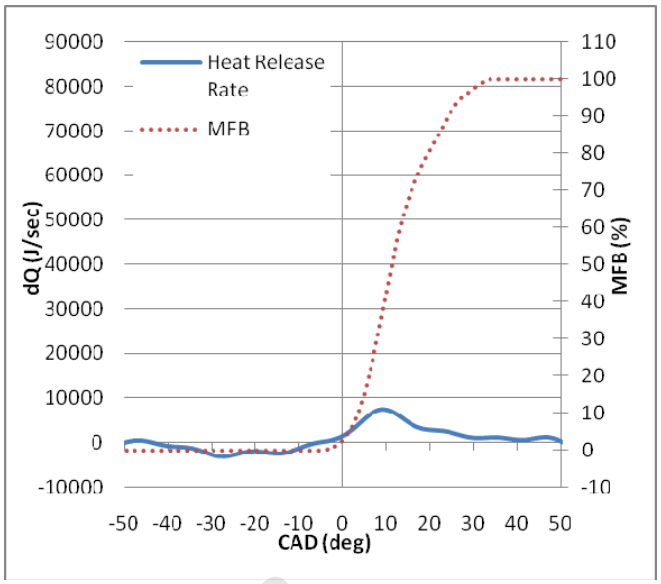

Figure 20: Minimum stable speed heat release example with no cool flame (12x6 prop at 4898rpm). Shown on the same scale as maximum speed point above in fig 19

The upper limits of the operating range were significantly reduced when using a fixed compression ratio (in this case 15:1), as shown in Figure 21. The effect on the lower limits of the operating range was negligible. The 15x10 propeller was limited by undesirable knock at a higher compression than optimum for the same air-fuel ratio and throttle setting (lower CR resulted in better performance). A CR of 15:1 was practically identical to optimum setting for the 12x6 propeller. The 11x5 propeller ran best with a higher compression ratio which better matched the phasing required by higher speeds.

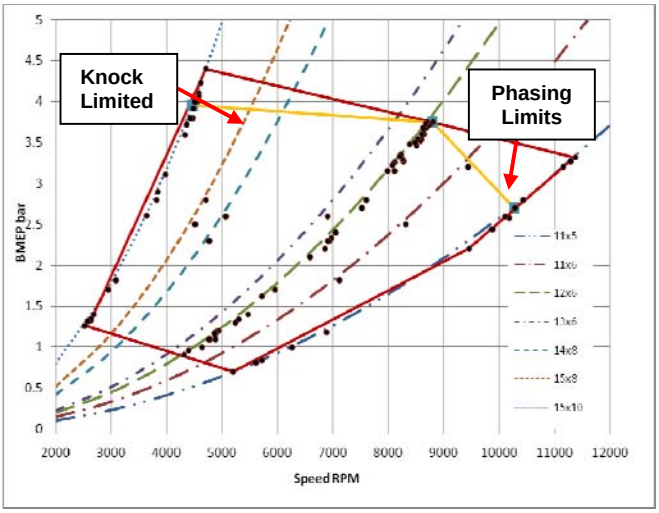

Figure 21: Effect on operating range of using a fixed compression ratio of 15:1. The new upper limits of the operating are shown superimposed onto the full operating range

The engine could be made to knock under certain conditions as shown in Figure 22 and Table 16. Unlike any of the other tested propellers, the 15x10 propeller could not run with the throttle wide open at the same engine settings used for low speed operation. This was why the engine required a much lower compression ratio at maximum power using the 15x10 propeller than if it were using any other propeller. The knock manifested as high pressure oscillations on the pressure trace and as an audible noise (which was not present at other operating conditions). Despite the negative effect on performance, the engine ran without misfire while knocking and with no noticeable engine damage.

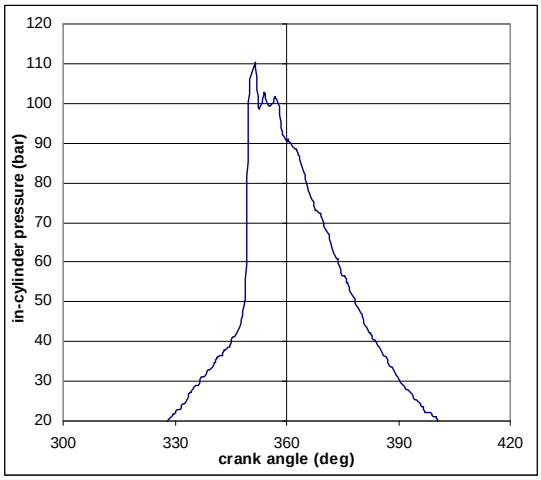

Figure 22: Pressure trace showing knock-related high pressure oscillations using the 15x10 propeller and a compression ratio of 17.3. Note the extremely advanced timing and high pressure rise rate.

Severe Knocking Conditions	
Propeller	15x10
Compression Ratio	17.3
Lambda	~1
Ambient Temperature	17 ^{o}C
Speed	3845 rpm
Maximum ΔP	44 bar/deg
at CAD	-8 deg
Maximum Pressure	110 bar
at CAD	-7
Burn 1-99% MFB	~4 deg
SOC 1% MFB	-10deg

Table 16: Operating Conditions for knocking pressure trace (where TDC = 0^{o} or 360^{o})

Discussion of Experimental Results – The extended operating range and characteristics revealed by the experimental work showed the versatility of the model-aero engine. The extended operating range of the engine exceeds the low-speed limits recommended by the manufacturers. The BMEP values achieved during testing also exceed those found in the literature for similar (model-aero) engines although the rated output of the engine could not be achieved [25, 26].

This is likely due to the engine running on D1000 instead of the "maximum performance" blend, D3000, which has a lower volume fraction of castor oil and more isopropyl nitrate (see Table 18 in appendix for D3000 formulation).

There was a general trend showing that as the engine speed increased, the CR for maximum power also increased. This is likely due to the increased CR compensating the shorter residence time of the combustion gasses at higher speeds. Increasing CR increases the pressure and temperature of the cylinder gasses thus shortening ignition delay and advancing timing. For very low speeds (at maximum power) the CR was knock-limited. This was attributed to the longer residence time, as a result of slower speeds affecting the autoignition chemistry of the reactants.

Adjusting the compression ratio had the largest effect on the upper limits of the operating range of the engine, with a combination of the highest allowable compression ratio and leanest air-fuel ratio yielding the maximum power. In certain cases the engine couldn't run any leaner due to limitation imposed by the carburettor. The available AFR was therefore unable to complement a higher compression ratio. This suggests that the carburettor was not correctly tuned by the manufacturers to correctly compensate for varied speed/load operation. Running leaner with a lower compression ratio caused the engine to run into the lean-auto-ignition-misfire limits of the fuel.

No cool flame was observed during the analysis of the heat-release data from the upper extremes of the operating range. This suggests that the fuel exhibits single-stage autoignition behaviour under those operating conditions.

Running the engine at maximum power using a fixed compression ratio (of ~15:1) showed that the engine was knock-limited at low speeds whereas the compression ratio could not be adjusted high enough at higher speeds to maintain optimum combustion phasing.

NUMERICAL MODELLING - The engine modelling was split into two sections; breathing and combustion. Data from the engine tests was used as input conditions for both models where appropriate.

CFD Breathing Modelling Philosophy – A CFD model was formulated to simulate the in-cylinder conditions from exhaust valve opening (EVO) to TDC. It predicted the in-cylinder temperature distribution and showed the effects of trapped residual gasses. Results from this model were then used as an appropriate guide for aspects (such as heat loss or EGR fraction) of the combustion model.

CFD Breathing Modelling Methodology – Fluent 6.3 was used for modelling the breathing characteristics of the engine. Temperature and pressure data (crank-case, exhaust and in-cylinder) from an engine test at EVO were used in the CFD program as inlet boundary conditions, with the model running from EVO to TDC.

A single representative data point was selected and modelled. This point was chosen as it represented the maximum power for one of the propellers recommended by the manufacturers. That specific propeller was chosen as its point of maximum power was achieved near a compression ratio which gave the widest overall operating range for the engine (representative of the most versatile engine setup). The test conditions are shown below in Table 17 and the pressure trace in Figure 23:

CFD Data Point Test Conditions	
Propeller	11x6
Compression Ratio	15:1
Lambda	0.97
Ambient Temperature	22 °C
Speed	9433 rpm
Coolant Temperature	65 °C
Exhaust Temperature	290 °C
Avg Head Temperature	158 °C
Crank Case Temperature	55 °C

Table 17: CFD data point operating conditions

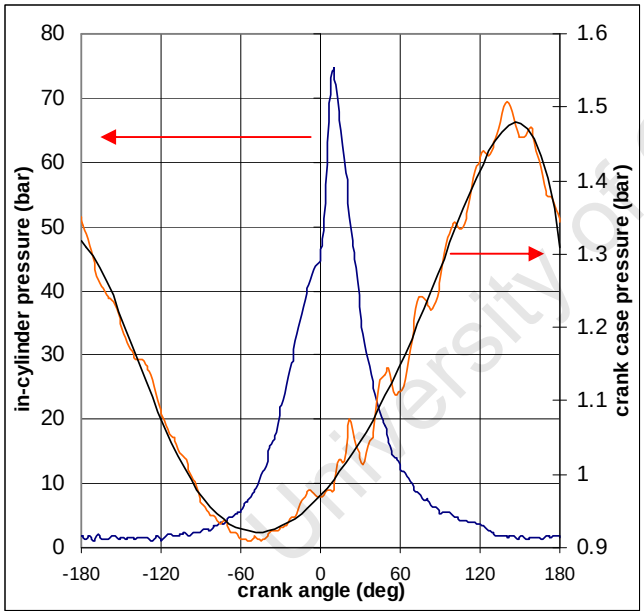

Figure 23: Pressure trace associated with the data point used in CFD simulation and the 6th order polynomial used to approximate the crank-case pressure trace.

Fluent CFD Breathing Modelling Results – The CFD model successfully showed the temperature distribution and residual exhaust gas fraction inside the engine. The CFD model showed a definite thermal boundary layer at the wall for the simulated data point as shown in Figure 24.

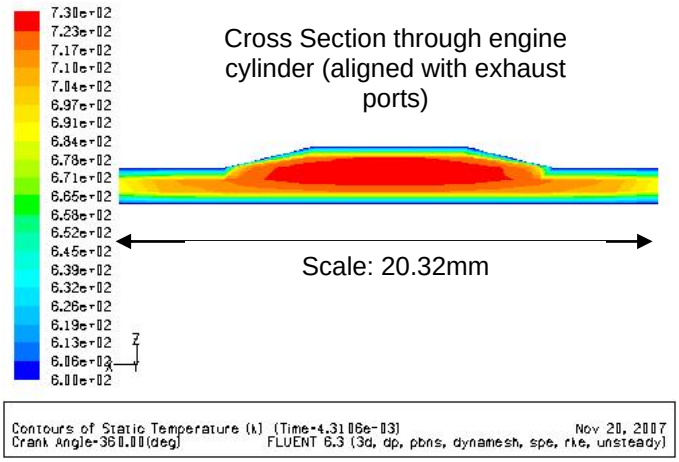

Figure 24: TDC (with clipped temperature scale) – Note the definite thermal boundary layer. The full thermal scale has been clipped to show better definition.

The thermal boundary layer predicted by the CFD was between 0.3mm and 0.4mm, which was approximately half the value found in the literature [25,27]. It was found that the thermal boundary layer occupied approximately 40% of the cylinder volume at TDC. Pronounced thermal stratification (as shown in this engine) is known to greatly affect the peak pressure rise rate and potentially improves the HCCI operating range [28, 29, 30].

Figures 25 to 27 show the distribution of fresh charge in the cylinder as these gasses are compressed up to TDC. All three images clearly show the concentration of fresh charge around the intake ports. The images also show fresh charge near the exhaust ports which indicates short-circuiting of the fresh charge.

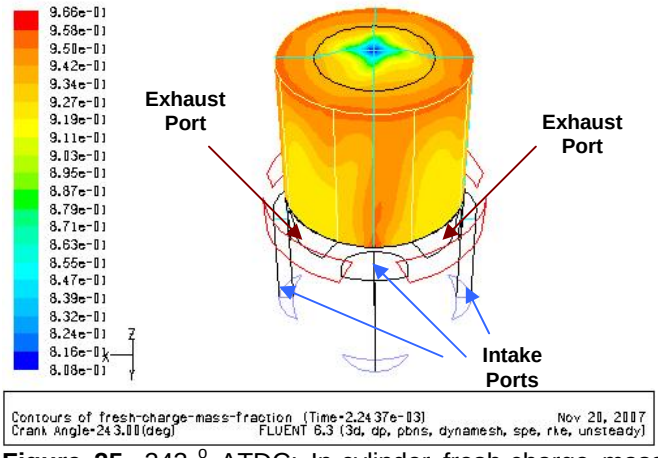

Figure 25: 243 ° ATDC: In-cylinder fresh-charge mass fraction at EVC. Note the symmetrical intake and exhaust port layout

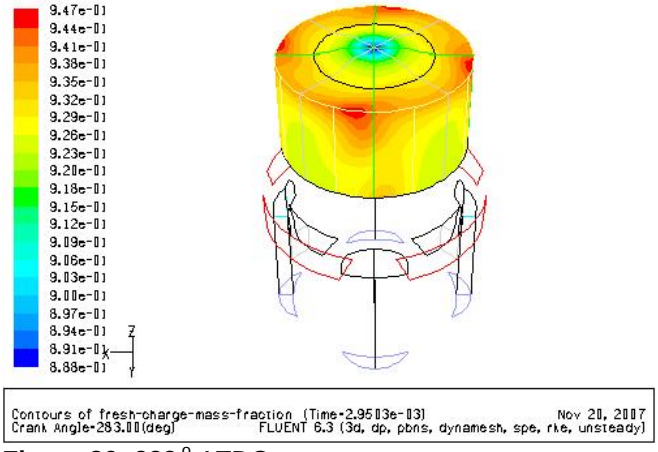

Figure 26: 283 ^{o} ATDC

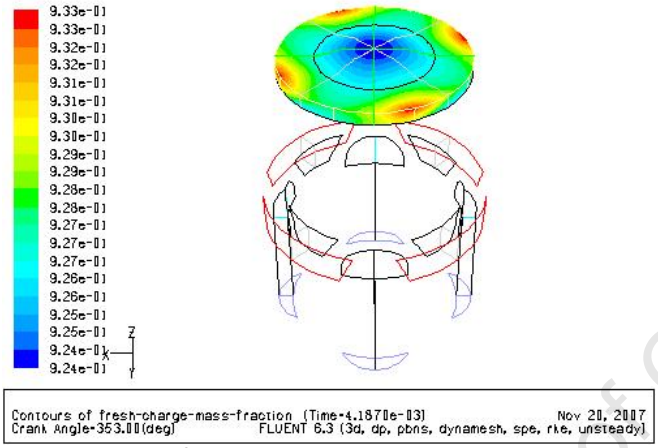

Figure 27: 353 ^{o} ATDC

Figures 28 and 29 show the slightly heterogeneous mixture distribution at TDC. More of the fresh charge is concentrated into four areas aligned with the intake ports with a notable “dead” zone of exhaust gas at the centre of the combustion chamber

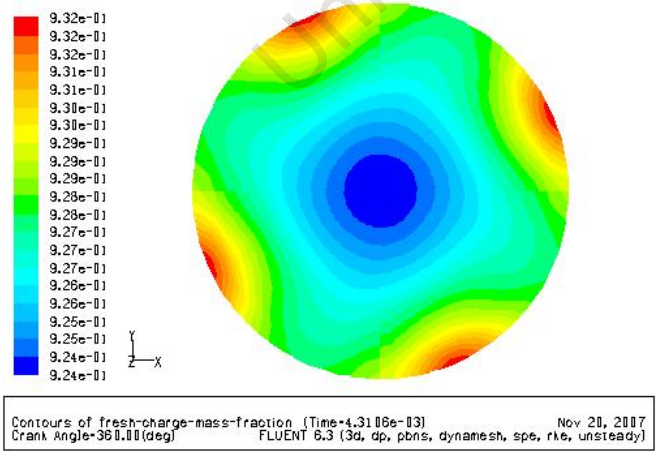

Figure 28: TDC: Clearly shows zones of higher fresh charge concentration aligned with the intake ports

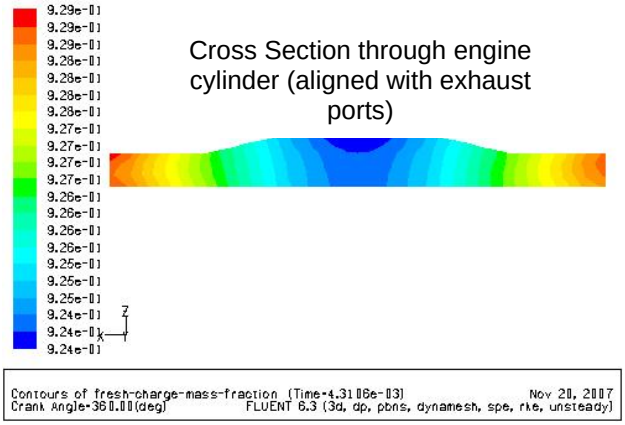

Figure 29: TDC fresh charge mass fraction distribution.

The CFD findings as shown in Figures 25 to 29 matched the non-uniform burn patterns which were found on the cylinder head as shown in Figure 30. This star shaped pattern suggested a non-uniform mixture distribution in the cylinder, most likely as a result of the engine’s intake and exhaust port layout. The formation of these deposits was attributed to undiluted zones and possibly liquid fuel droplets impinging on the cylinder head. This burn pattern showed up in the same location regardless of speed or load and was observed every time the engine was dismantled. Subsequent investigation showed the markings were aligned with the intake ports of the engine.

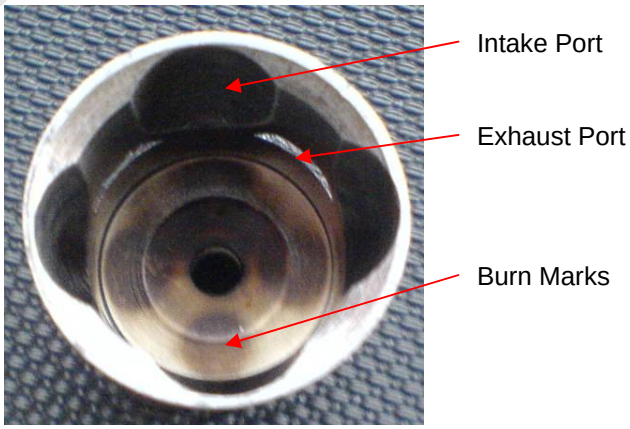

Figure 30: Burn pattern on the head of the model-aero engine aligned with intake ports

It’s likely that this small degree of mixture in-homogeneity results in similarly inhomogeneous burning as shown in figure 30, with combustion being initiated in the four zones of higher fresh charge concentration. It appears as if this engine has four auto-ignition zones with “cascading autoignition”. Depending on the levels of dilution, combustion could be extinguished as it proceeds towards the centre of the combustion chamber which has a lower fresh-charge concentration. The effects of what would normally be a rapidly combusting mixture are cushioned by the “dead zone” of undiluted exhaust gas. The highly concentrated EGR zone combined with the four “cascading autoignition” zones are likely the cause of the

conservative peak pressure rates and knock resistance of this engine.

Engine Modelling - A discreet explicit engine model combined with an Arrhenius form Auto-ignition Integral Method fuel autoignition model was used to investigate the speed and size effects of this engine. The details of the model formulation and results are given in the accompanying paper by Floweday and Yates [SAE 2008-01-1661]. Unfortunately the autoignition model coefficients for D1000 were not known, but trends in engine speed convergence effects were investigated single and two-stage fuels. This investigation revealed that this very small engine would probably exhibit speed convergence at the upper end of its speed range.

CONCLUSIONS

PROPELLER LOAD/SPEED CHARACTERISTICS –

- The numerical model under-predicted the load-speed performance of the propellers, but was still a useful tool in guiding the design of the propeller testing rig.
- The propeller characterisation rig successfully mapped the load-speed curves of a suitable variety of propellers.
- Combining the information from the propeller testing rig with the proposed method of tuning the engine for maximum propeller speed provided a useful method of optimising combustion phasing (and overall engine setup).

FUEL TESTING –

- IQT^{TM} testing of the fuel revealed the cetane blending effects of each component
- The D1000 represents a very useful fuel for HCCI operation in the model-aero engine as it has a very high ignition quality and vaporises easily
- The castor oil was shown to have very little effect on ignition quality and combustion characteristics of the fuel blend with a significant portion passing unburned into the exhaust. Testing in the Ricardo E6 showed that it detracted slightly from the autoignition stability of the fuel.

ENGINE TESTING –

- With proper adjustment, the engine exhibited no signs of undesirable combustion behaviour (knock, noise from excessive heat release rate or misfiring) over its full operating range
- The levels of BMEP achieved were slightly higher than those observed in previous studies using similar engines
- No two-stage combustion phenomena were observed in the model-aero engine, although two-stage ignition was observed for the same fuel in the Ricardo E6 engine. This is attributed to the vastly different compression ratios and heat loss characteristics of the two engines and their effect on pressure-temperature histories in conjunction with the autoignition behaviour of the fuel.
- Fixing the compression ratio of the engine (to ~15:1) limited lower speed maximum power operation due to knocking. This compression ratio was also not high enough to produce maximum power at high speed operation.
- Maximum power for all the tested propellers was achieved using the leanest possible air-fuel ratio while still avoiding the lean-misfire limits.

ENGINE MODELLING –

- The CFD model showed significant thermal stratification
- It also reproduced the observed fresh-charge in-homogeneities inside the cylinder, due the port layout as validated by the burn marks observed on the head.
- The in-homogeneous fresh-charge distribution and temperature profiles have a significant effect on the auto-ignition and ‘cascading combustion” dynamics in the model-aero engine, and likely contribute to the conservative pressure rise rates and knock-resistance of this engine.

ACKNOWLEDGMENTS

This study was funded and supported by the Sasol Technology Fuels Research team which is headed by Dr J.J. Botha.

The authors extend their gratitude the following people for their contributions to this project:

- Dr Martin Hepperle (Institute of Aerodynamics ,Gernamy) for his guidance in setting up the propeller characteristics model
- Owen Metcalfe (Sasol Advanced Fuels Laboratory, University of Cape Town) for his CFD breathing model
- Ian Lemberger (Sasol Advanced Fuels Laboratory, University of Cape Town) for his help in constructing the engine testing rig
- Prof. Andy Yates (Sasol Advanced Fuels Laboratory, University of Cape Town) for his support, guidance and motivation

REFERENCES

1. U.S. Department of Energy - Office of Transportation Technologies, Homogeneous Charge Compression Ignition (HCCI) Technology Page 11, April 2001
2. Heywood JB, Internal Combustion Engine Fundamentals, Page 572, McGraw-Hill Singapore, 1988

3. Heywood JB, Internal Combustion Engine Fundamentals, Page 626, McGraw-Hill Singapore, 1988
4. Heywood JB, Internal Combustion Engine Fundamentals, Page 492, McGraw-Hill Singapore, 1988
5. Onishi S, Hong Jo S, Shoda K, Do Jo P, Kato S, "Active Thermo-Atmosphere Combustion (ATAC)-A New Combustion Process for Internal Combustion Engines", SAE paper 790501
6. Ishibashi Y, "Basic Understanding of Activated Radical Combustion and its Two-Stroke Engine Application and Benefits", SAE paper 2000-01-1836
7. Zhao F, Dennis N. Assanis DN, Najt PM, Dec JE, Eng JA, Asmus TN, (2003), Homogeneous charge compression ignition (HCCI) engines: key research and development issues Page 327, 1st edition, Warrendale, PA, Society of Automotive Engineers
8. Smith JR, Aceves SM, Dibble RW, Flowers DL, Martinez-Frias J, HCCI Engine Control By Thermal Management, SAE International, Paper Submitted to 2000 SAE Conference in Baltimore
9. Swihart JM, Experimental and Calculated Static Characteristics of a two-blade NACA 10-(3)(062) -045 Propeller, National Advisory Committee for Aeronautics, 1954
10. Diehl WS, Report 447 "Static Thrust of Airplane Propellers", National Advisory Committee for Aeronautics, Date not Published
11. Auld DJ and Srivinas K, Aeronautics for Students, AMME University of Sydney, 1996-2006
12. Viljoen CJ, An Investigation of the Ignition Delay Character of Different Fuel Components and an Assessment of Various Autoignition Characteristics, SAE International, 2005-01-2084
13. Owen K and Coley T, Automotive Fuels Handbook Page 229, SAE Inc USA, 1990,
14. Shoji H, Yoshida K, Goto K, Iijima A, Analysis of the Characteristics of HCCI Combustion and ATAC Combustion Using the Same Test Engine, SAE Japan, 2004-32-0097
15. Martinez-Frias J, Aceves SM, Flowers D, Smith JR, Dibble R, HCCI Engine Control By Thermal Management, SAE International, Paper Submitted to 2000 SAE Conference in Baltimore
16. Bunting B, Szybist JP, Cetane Number and Engine Speed Effects on Diesel HCCI Performance and Emissions, 2005-01-3723
17. Heywood JB, Internal Combustion Engine Fundamentals, McGraw-Hill Singapore, 1988, Page 375
18. Bengttson J, Closed Loop Control of HCCI Engine Dynamics, Media Tryck Sweden, 2004
19. Zhao F, Dennis N. Assanis DN, Najt PM, Dec JE, Eng JA, Asmus TN, (2003), Homogeneous charge compression ignition (HCCI) engines: key research and development issues Page 325, 1st edition, Warrendale, PA, Society of Automotive Engineers.
20. Yates ADB et al, An Improved Model for Describing Auto-Ignition, SAE International, Paper submitted for 2008 SAE conference in China
21. ASTM Standard D6890-04, Standard Test Method for Determination of Ignition Delay and Derived Cetane Number of Diesel Fuel Oils by Combustion in a Constant Volume Chamber, ASTM International, 2004
22. Ryan T Matheaus A, Fuel Requirements for HCCI Engine Operation, SAE International, 2003-01-1813
23. Aberg E et al, HCCI 2-stroke – Study of HCCI in a Model Engine (title translated from Swedish), 2001
24. Dec J , Sjoberg M, Hwang W, An Investigation of Thermal Stratification in HCCI Engines Using Chemiluminescence Imaging, SAE International, 2006-01-1518
25. Johansson B, Tunestal P, Manente V, Mini High Speed HCCI Engine Fuel with Ether: Load Range, Emission Characteristics and Optical Analysis, SAE International, 2007-01-3606
26. Johansson B, Tunestal P, Manente V, Influence of Inlet Temperature and Hot Residual Gases on the Performance of a Mini High Speed Glow Plug Engine, SAE International, SAE 2006-32-0057
27. Manente V et al, A Study of a Glow Plug Ignition Engine by Chemiluminescence Images, SAE International, SAE 2007-01-1884
28. Sjöberg and Dec, Effects of Engine Epeed, Fueling Rate and Combustion Phasing on the Thermal Stratification Required to Limit HCCI Knocking Intensity,SAE Internaional, SAE 2005-01-2125
29. Berntsson and Denbratt, HCCI Combustion using Charge Stratification for Combustion Control, SAE International, SAE 2007-01-0210
30. Inagaki K, Ueda M, Akihama K, Kuzuyama H, Machida M, A Study on Natural Gas Fueled Homogeneous Charge Compression Ignition Engine - Expanding the Operating Range and Combustion Mode Switching, SAE International, SAE 2007-01-0176

CONTACT

Kyle Collair
Sasol Advanced Fuels Laboratory
University Of Cape Town
Email: kcollair@gmail.com

Gareth Floweday
SASOL Advanced Fuels Laboratory
Mechanical Engineering Department
University of Cape Town
Tel: +27 21 650 5306
email: gareth.floweday@uct.ac.za
www.safl.uct.ac.za

DEFINITIONS, ACRONYMS, ABBREVIATIONS

AI: Autoignition (see Autoignition)
Angle Of Attack: The angle of deviation from horizontal for a wing section.
Auto-ignite/Auto-ignition: Spontaneous combustion without any form of external initiation (such a spark or glow-plug). Characterised by the simultaneous bulk combustion of the reactants
BDC: Bottom dead centre – the piston is at its lowest position in the cylinder
BMEP: Break Mean Effective Pressure – A concept used to describe the performance of engines with different displacement.
Cetane: Concept used to describe to autoignition performance of (usually diesel-like) fuels. A higher cetane number implies a propensity for autoignition
CFD: Computational Fluid Dynamics
Chord: The characteristic length of a wing cross section
CR: Compression Ratio. Unless otherwise stated refers to the geometric compression ratio
DEE: Di-Ethyl-Ether
EGR: Exhaust Gas Recirculation
EVC: Exhaust Valve Closing
EVO: Exhaust Valve Opening
HCCI: Homogeneous Charge, Compression Ignition
IQT^{TM}: Ignition Quality Tester
IVC: Inlet Valve Closing
IVO: Inlet Valve Opening
Knock/Knocking: High pressure oscillations caused by simultaneous, uncontrolled autoignition of un-reacted combustion gasses. The high pressure oscillations are caused by resulting shock waves reflecting off the inside of the combustion chamber. Often knock may be heard as a "pinging" or "hammering" sound accompanied by rough running. Knock is usually detrimental to engine performance and longevity
MFB: Mass Fraction Burned referring the fraction of fuel burned
n-heptane: Paraffinic hydrocarbon with seven carbon atoms and saturated with hydrogen. Primary reference fuel with zero octane rating often used to calibrate the performance of other fuels. n-heptane has a strong tendency to auto-ignite.
NOx: Undesirable generic Nitrous Oxide gasses formed during combustion.
NTC: Negative Temperature Coefficient
PAW: Progress Aero Works – The manufacturers of the engine used in this study
R/C: Radio Controlled
Scavenging: Combined intake and exhaust procedure utilised in two-stroke engines. As both intake and exhaust valve opening usually have overlap in a two-stroke engine a positive pressure differential between the intake and exhaust is required to drive fresh charge into the cylinder and remove as much of the remaining exhaust gas as possible
Short Circuiting: Undesirable consequence of having the intake and exhaust valve opening overlap in a two-stroke engine is that some fresh charge usually passes straight through the cylinder and out the exhaust port without combusting.
SOC: Start of Combustion
Stalling: The air velocity flowing over a wing section is too low to produce any lift
Stoichiometric: Theoretical chemically correct mixture resulting in the hypothetical complete reaction of all reactants.
TDC: Top Dead Centre – the piston is at its highest position in the cylinder
Windmillling: When a propeller is auto-rotated by the incoming air velocity causing drag without providing and thrust

APPENDICES

Propeller rig motor type and specification: "SKIL 1830" speed range: 0-28000rpm, 4.9A 230V AC, rated power: 1100W

Photo tachometer type and specification: LT type "DT-2236" Range: 5 to 99999rpm, Resolution: 1rpm

IQT^{TM} type and specification: Advanced Engine Technologies' "IQT^{TM}- Laboratory Model" compliant with ASTM D6890 testing standard

In-Cylinder Pressure Transducer type and specification: "AVL GU12P" sensitivity: 0-200bar temperature range: 400^{o}C or "AVL 6 QP 500a" sensitivity: 0-100bar temperature range: 0-240^{o}C connected to Kistler Charge Amplifier type 5105

Oscilloscope type and specification: "Agilent Technologies DSO6014A" 4-channel with sampling rate: 100MHz (2Gsa/s)

CC TP type, specification and charge amp: "Kistler Piezoresistive 4073" sensitivity: 0-10bar (absolute) water-cooled jacket connected to Kistler Charge Amplifier type 4603

Thermocouple type and display: All K-type thermocouples connected to "Fluke 52" thermocouple display

Lambda sensor type and specification: "Bosch LSM11 0 258 104 002" connected to "ETAS LA2" power supply and display unit

Starter motor type: "Thunder Tiger 12V type 2674 Deluxe Hi-Torque"

D3000 Fuel Composition	
Component	**%**
Kerosene	47.5
Di-Ethyl-Ether	30
Castor Oil	20
Iso-Propyl-Nitrate	2.5

Table 18: D3000 fuel specifications and properties

Appendix F: Chemistry derivations used in the global model formulations

This appendix provides the chemistry derivations used in the formation of the new functional global model. These derivations are not novel and can be found in standard chemistry thermodynamic and engine modelling texts [1-3].

For the dissociation equilibrium reaction of carbon dioxide:

1 CO + ½ O_2 <=> 1 CO_2

The calculation of a reverse reaction rate from the forward reaction rate and the thermo-chemical properties:

Consider the balanced equilibrium reaction:

aA + bB <=> cC + dD

at equilibrium: forward reaction rate = reverse reaction rate

$\therefore [A]^a [B]^b K_{fwd} = [C]^c [D]^d K_{rev}$

$\therefore K_c = K_{fwd}/K_{rev} = [C]^c [D]^d /[A]^a [B]^b$

From $PV = n R_u T$

$[\,] = n / V = P / R_u T$

Since $[x_i] = n_f P / R_u T = P_i / R_u T$

from Appendix C:

$$\Delta G^* = -g_A^0 \nu_A - g_B^0 \nu_B + g_C^0 \nu_C + g_D^0 \nu_D$$

$$and\ \Delta G^* = -R_u T \ln\left[\frac{P_C^{\nu_C} P_D^{\nu_D}}{P_A^{\nu_A} P_B^{\nu_B}}\right]$$

$$and \quad K_{p1} = e^{-\Delta G^* / R_u T}$$

$K_p = K_c (R_u T / P)^{c+d-a-b}$

$\therefore K_c = K_p (R_u T / P)^{a+b-c-d}$

$$K_c = \frac{K_{fwd}}{K_{rev}} \quad and \quad K_{rev,(T)} = A_{rev}\, e^{\left(\frac{B_{rev}}{T}\right)}$$

$$\therefore K_{fwd,(T)} = K_{c,(T)}\; A_{rev}\, e^{\left(\frac{B_{rev}}{T}\right)}$$

$$\ln\left(K_{fwd,(T)}\right) = \ln\left(K_{c,(T)}\right) + \ln\left(A_{rev}\right) + \left(\frac{B_{rev}}{T}\right)$$

solve symaltaneously at two arbitrary temperatures :

$$\begin{bmatrix} \ln(A_{rev}) \\ B_{rev} \end{bmatrix} = \begin{bmatrix} 1 & 1/T_1 \\ 1 & 1/T_2 \end{bmatrix}^{-1} \begin{bmatrix} \ln\left(K_{fwd,(T_1)}\right) - \ln\left(K_{c,(T_1)}\right) \\ \ln\left(K_{fwd,(T_2)}\right) - \ln\left(K_{c,(T_2)}\right) \end{bmatrix}$$

Quasi-steady state approximation:

$$F + O_2 \underset{2}{\overset{1}{\rightleftarrows}} J \xrightarrow{3} I$$

$$\mathrm{RR}_1 = [F][O_2]K_1$$
$$\mathrm{RR}_2 = [J]K_2$$
$$\mathrm{RR}_3 = [J]K_3$$

Assuming fast equilibrium of $\mathrm{F} + O_2$ and J :

$$\mathrm{RR}_1 = \mathrm{RR}_2$$
$$\therefore \quad [F][O_2]K_1 = [J]K_2$$
$$\therefore \quad [F] = \frac{[J]}{[O_2]}\frac{K_2}{K_1}$$

consider the lumped species :

$$[\mathrm{X_F}] = [F] + [J]$$
$$[J] = [\mathrm{X_F}] - [F]$$
$$= [\mathrm{X_F}] - \frac{[J]}{[O_2]}\frac{K_2}{K_1}$$
$$\therefore \quad [J] = \frac{[\mathrm{X_F}]}{1 + \frac{K_2}{[O_2]\,K_1}}$$

then:

$$RR_3 = [J]K_3 = \frac{[X_F]K_3}{1 + \frac{K_2}{[O_2]K_1}}$$

$$= \frac{[X_F]}{\frac{1}{K_3} + \frac{K_2}{[O_2]K_1K_3}}$$

considering F as a generic description for X_F:

$$RR_3 = \frac{[F]}{\frac{1}{K_a} + [O_2]^{-1}K_b}$$

References

[1] Y. Cengel and M. Boles, *Thermodynamics: An Engineering Approach*, 2nd ed McGraw-Hill, Inc., 1994.

[2] D. D. Ebbing and M. S. Wrighton, *General Chemistry*, 4th ed Houghton Mifflin Company, 1993.

[3] D. W. Oxtoby, H. P. Gillis, and N. H. Nachtrieb, *Principles of Modern Chemistry*, 4th ed Saunders Collage Publishing, 1999.

Appendix G: Agreement of predictions between the new functional global model and detailed kinetic simulations

The new functional global model developed in this study was fitted to each of the four 2-stage ignition fuels (n-heptane, iso-octane, 1-hexene and the quaternary gasoline surrogate) using 48 carefully selected data points. For the single stage ignition fuels (toluene and methanol) 72 data points were used. This process therefore generated a total of 336 temperature-time profiles. It is therefore impractical to present this data comprehensively and correlation plots are therefore used in the figures of this Appendix in order to demonstrate the agreement between the predictions of the new functional global model and those of the detailed chemical kinetics model.

It should be noted that the fitness function used for the optimisation of the model parameters calculated a normalised difference between the temperature-time profiles. Identification of the exact position and magnitude of the cool flame heat release posed a challenge and the correlation presented in the figures below does not do justice to the satisfying cool flame heat release agreement as demonstrated by the temperature-time profiles presented in the main thesis document.

In the correlation plots below, DKM refers to Detailed Kinetic Model, while FGM refers to Functional Global Model.

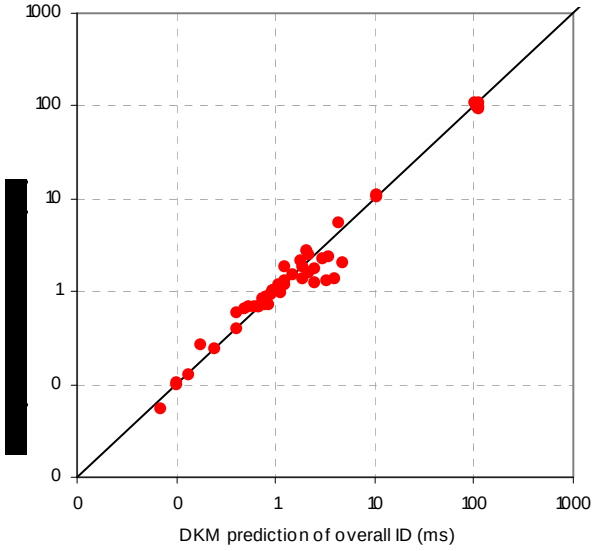

Figure G 1: Correlation of predicted overall ignition delay for n-heptane

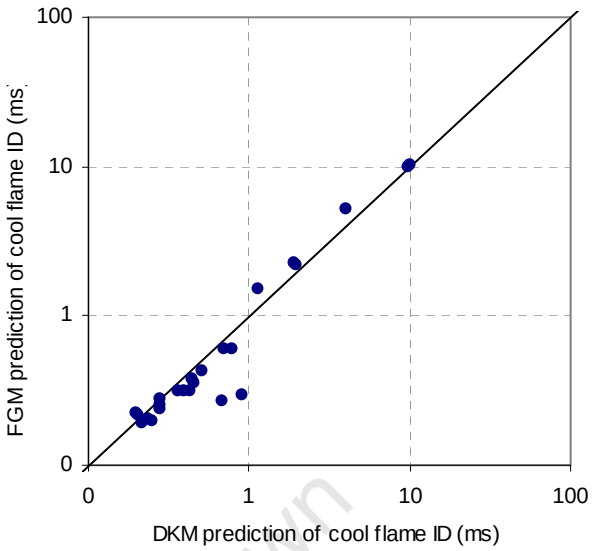

Figure G 2: Correlation of cool flame ignition delay for n-heptane

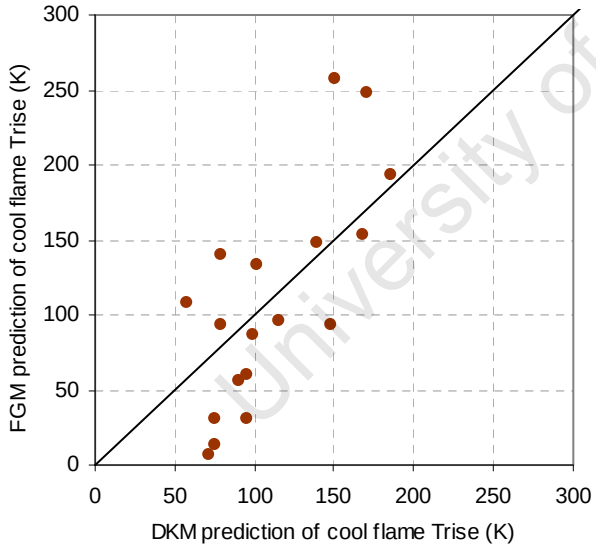

Figure G 3: Correlation of predicted cool flame temperature rise for n-heptane

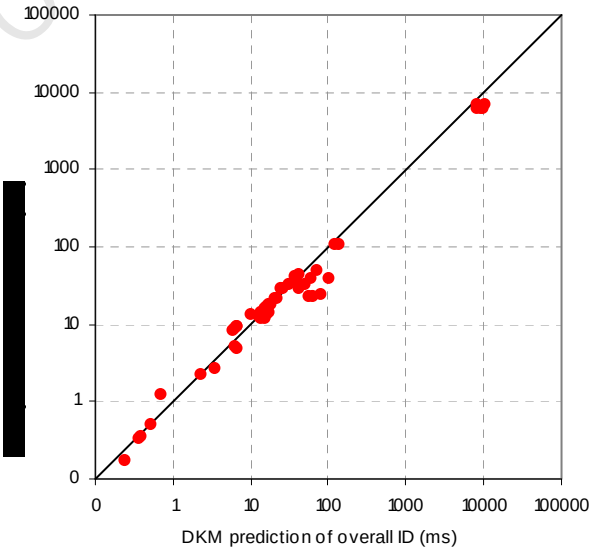

Figure G 4: Correlation of predicted overall ignition delay for iso-octane

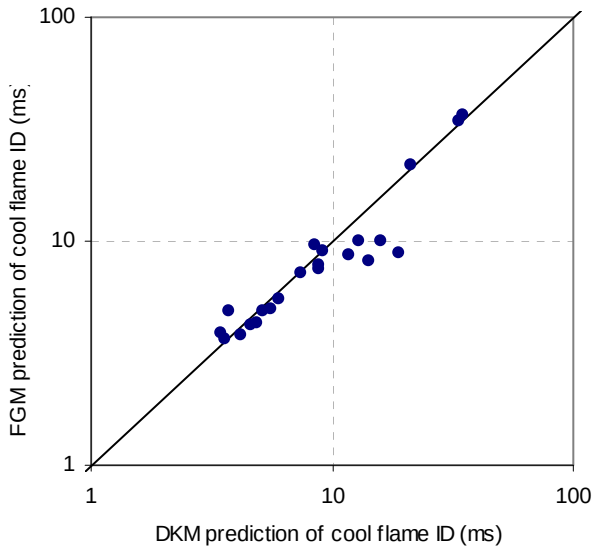

Figure G 5: Correlation of cool flame ignition delay for iso-octane

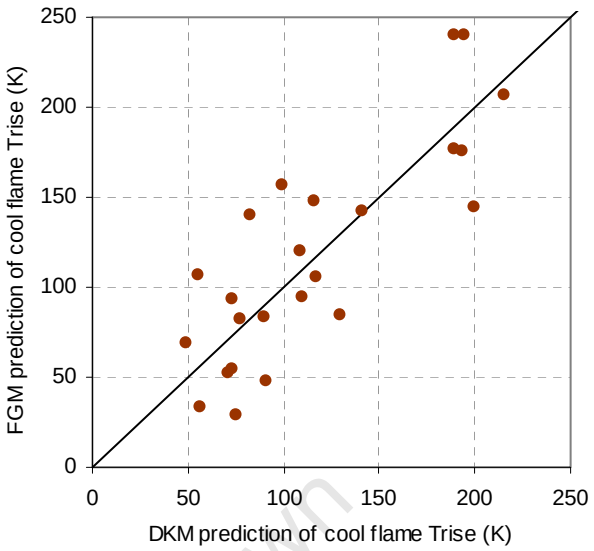

Figure G 6: Correlation of predicted cool flame temperature rise for iso-octane

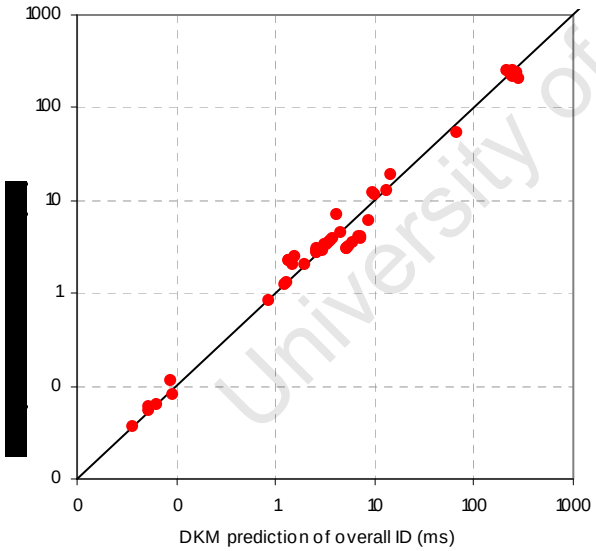

Figure G 7: Correlation of predicted overall ignition delay for 1-hexene

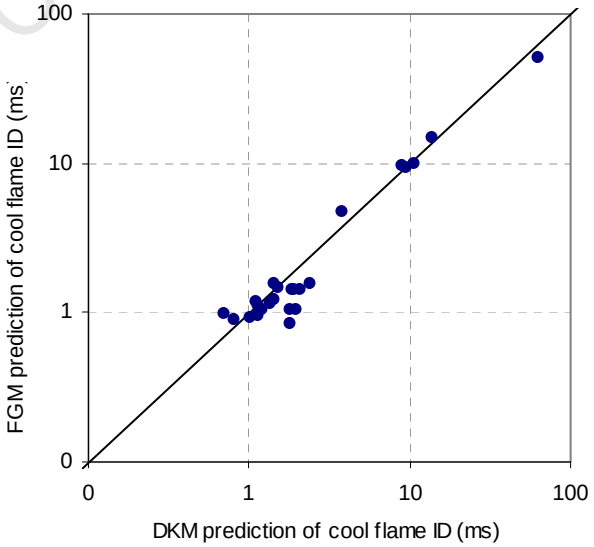

Figure G 8: Correlation of cool flame ignition delay for 1-hexene

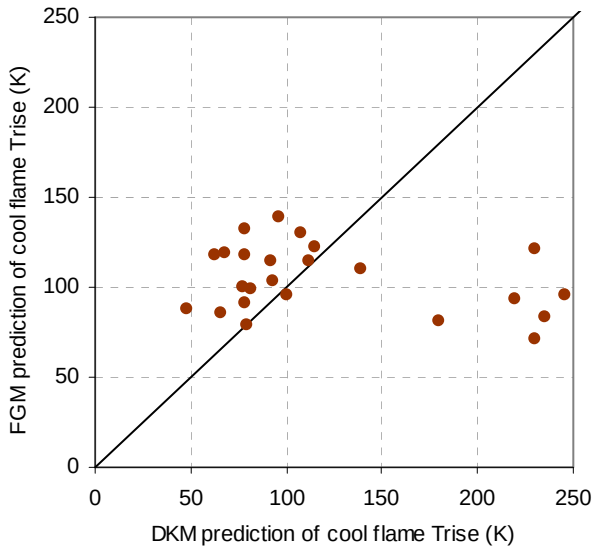

Figure G 9: Correlation of predicted cool flame temperature rise for 1-hexene

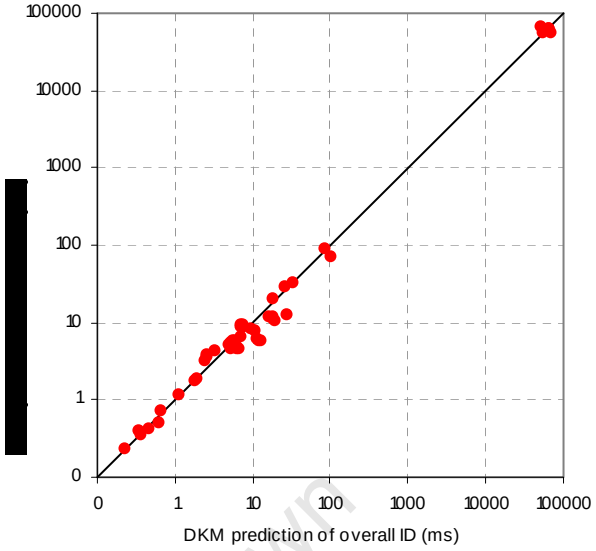

Figure G 10: Correlation of predicted overall ignition delay for the gasoline surrogate

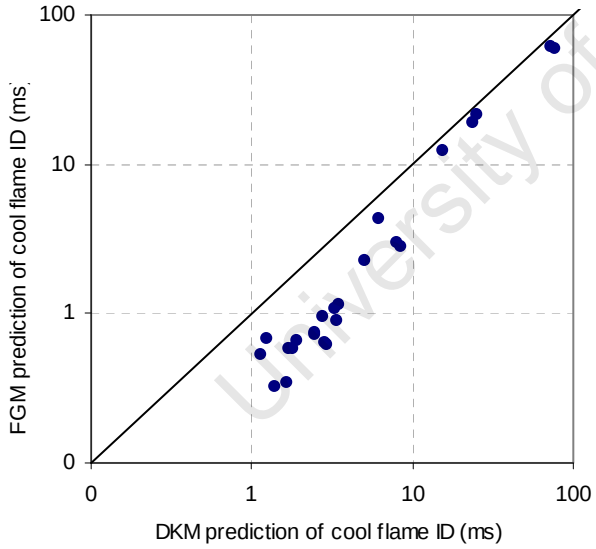

Figure G 11: Correlation of cool flame ignition delay for the gasoline surrogate

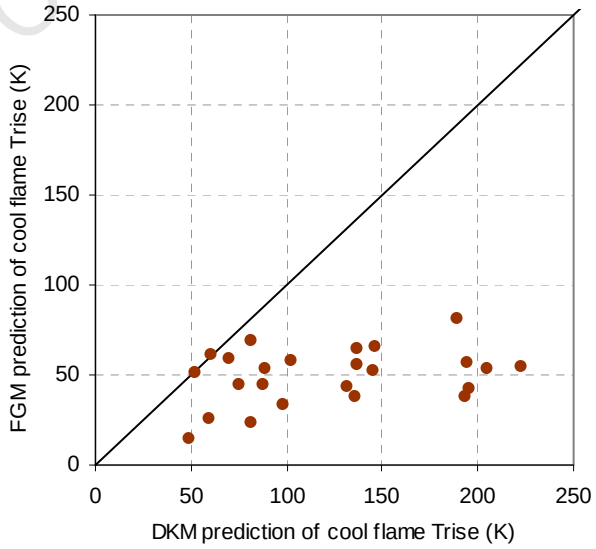

Figure G 12: Correlation of predicted cool flame temperature rise for the gasoline surrogate

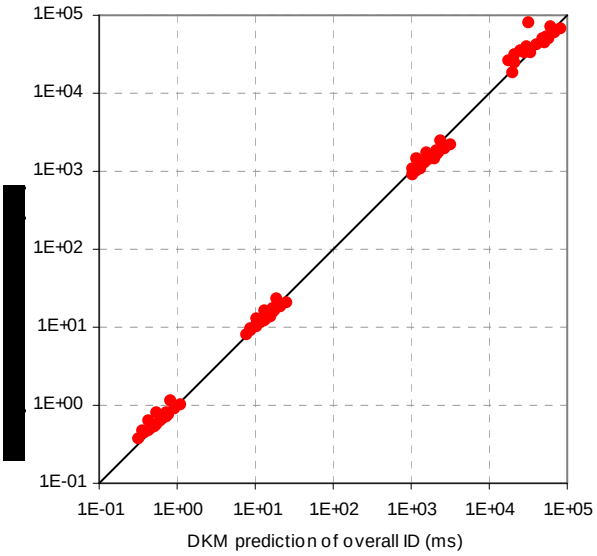

Figure G 13: Correlation of predicted overall ignition delay for toluene

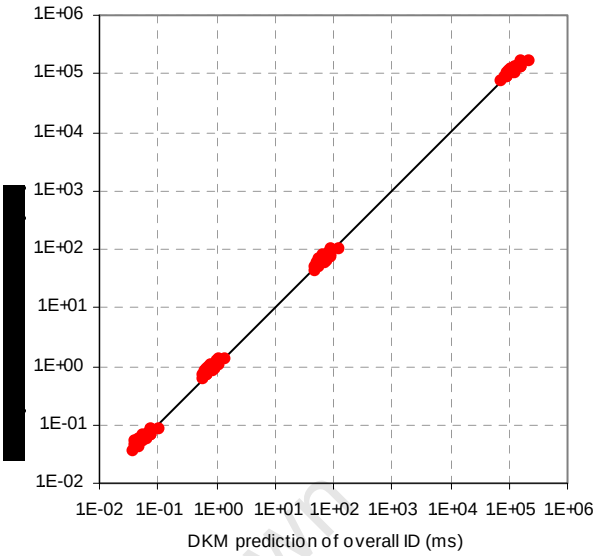

Figure G 14: Correlation of predicted overall ignition delay for methanol

Appendix H: VBA codes used in the MS Excel implementation of the functional global model

The new functional global model made extensive use of VBA programming in its Microsoft Excel 2003 implementation. These codes are given below.

Specific heat calculation worksheet function

```
Function CpMix(T, nCO2, nCO, nH2O, nH2, nO2, nN2, nETOH, nPROP, nHEX, nTOL, nHEPT, nOCT, nMEOH)
' solves the Cp value of a mixture at a given temperature using the Cp polynomial coefficients given
' in the JANEF tables in the "thermodata" worksheet for the various temperature ranges
' The function also interpolates between high T and Low T values of Cp in the 20K transition between HT and LT
Application.Volatile
'
ntot = nCO2 + nCO + nH2O + nH2 + nO2 + nN2 + nETOH + nPROP + nHEX + nTOL + nHEPT + nOCT + nMEOH

'==================
' calculat speces HT Cp values
CO2CpHT = CO2CpaHT + CO2CpbHT * T + CO2CpcHT * T ^ 2 + CO2CpdHT * T ^ 3 + CO2CpeHT * T ^ 4
COCpHT = COCpaHT + COCpbHT * T + COCpcHT * T ^ 2 + COCpdHT * T ^ 3 + COCpeHT * T ^ 4
H2OCpHT = H2OCpaHT + H2OCpbHT * T + H2OCpcHT * T ^ 2 + H2OCpdHT * T ^ 3 + H2OCpeHT * T ^ 4
H2CpHT = H2CpaHT + H2CpbHT * T + H2CpcHT * T ^ 2 + H2CpdHT * T ^ 3 + H2CpeHT * T ^ 4
O2CpHT = O2CpaHT + O2CpbHT * T + O2CpcHT * T ^ 2 + O2CpdHT * T ^ 3 + O2CpeHT * T ^ 4
N2CpHT = N2CpaHT + N2CpbHT * T + N2CpcHT * T ^ 2 + N2CpdHT * T ^ 3 + N2CpeHT * T ^ 4
MEOHCpHT = MEOHCpaHT + MEOHCpbHT * T + MEOHCpcHT * T ^ 2 + MEOHCpdHT * T ^ 3 + MEOHCpeHT * T
^ 4
'=================
' calculat speces LT Cp values
CO2CpLT = CO2CpaLT + CO2CpbLT * T + CO2CpcLT * T ^ 2 + CO2CpdLT * T ^ 3 + CO2CpeLT * T ^ 4
COCpLT = COCpaLT + COCpbLT * T + COCpcLT * T ^ 2 + COCpdLT * T ^ 3 + COCpeLT * T ^ 4
H2OCpLT = H2OCpaLT + H2OCpbLT * T + H2OCpcLT * T ^ 2 + H2OCpdLT * T ^ 3 + H2OCpeLT * T ^ 4
H2CpLT = H2CpaLT + H2CpbLT * T + H2CpcLT * T ^ 2 + H2CpdLT * T ^ 3 + H2CpeLT * T ^ 4
O2CpLT = O2CpaLT + O2CpbLT * T + O2CpcLT * T ^ 2 + O2CpdLT * T ^ 3 + O2CpeLT * T ^ 4
N2CpLT = N2CpaLT + N2CpbLT * T + N2CpcLT * T ^ 2 + N2CpdLT * T ^ 3 + N2CpeLT * T ^ 4
MEOHCpLT = MEOHCpaLT + MEOHCpbLT * T + MEOHCpcLT * T ^ 2 + MEOHCpdLT * T ^ 3 + MEOHCpeLT * T ^
4
'==================
' calculat speces Cp values
ETOHCp = ETOHCpa + ETOHCpb * T + ETOHCpc * T ^ 2 + ETOHCpd * T ^ 3 + ETOHCpe * T ^ 4
PROPCp = PROPCpa + PROPCpb * T + PROPCpc * T ^ 2 + PROPCpd * T ^ 3 + PROPCpe * T ^ 4
HEXCp = HexCpa + HexCpb * T + HexCpc * T ^ 2 + HexCpd * T ^ 3 + HexCpe * T ^ 4
TOLCp = tolCpa + tolCpb * T + tolCpc * T ^ 2 + tolCpd * T ^ 3 + tolCpe * T ^ 4
HEPTCp = HEPTCpa + HEPTCpb * T + HEPTCpc * T ^ 2 + HEPTCpd * T ^ 3 + HEPTCpe * T ^ 4
OCTCp = OctCpa + OctCpb * T + OctCpc * T ^ 2 + OctCpd * T ^ 3 + OctCpe * T ^ 4
' Select correct Cp according to temperature range and interpolate across the transition
If T < 990 Then
   CO2Cp = CO2CpLT
   COCp = COCpLT
   H2OCp = H2OCpLT
   H2Cp = H2CpLT
   O2Cp = O2CpLT
   N2Cp = N2CpLT
   MEOHCp = MEOHCpLT
ElseIf T > 1010 Then
   CO2Cp = CO2CpHT
   COCp = COCpHT
   H2OCp = H2OCpHT
   H2Cp = H2CpHT
```

```
    O2Cp = O2CpHT
    N2Cp = N2CpHT
    MEOHCp = MEOHCpHT
Else
    CO2Cp = ((1010 - T) / 20) * CO2CpLT + ((T - 990) / 20) * CO2CpHT
    COCp = ((1010 - T) / 20) * COCpLT + ((T - 990) / 20) * COCpHT
    H2OCp = ((1010 - T) / 20) * H2OCpLT + ((T - 990) / 20) * H2OCpHT
    H2Cp = ((1010 - T) / 20) * H2CpLT + ((T - 990) / 20) * H2CpHT
    O2Cp = ((1010 - T) / 20) * O2CpLT + ((T - 990) / 20) * O2CpHT
    N2Cp = ((1010 - T) / 20) * N2CpLT + ((T - 990) / 20) * N2CpHT
    MEOHCp = ((1010 - T) / 20) * MEOHCpLT + ((T - 990) / 20) * MEOHCpHT
End If
' calculate mixture Cp according to species CPs and mole fractions

CpMix = CO2Cp * nCO2 / ntot + COCp * nCO / ntot + H2OCp * nH2O / ntot + H2Cp * nH2 / ntot + O2Cp * nO2 / ntot
+ N2Cp * nN2 / ntot + ETOHCp * nETOH / ntot + PROPCp * nPROP / ntot + HEXCp * nHEX / ntot + TOLCp * nTOL /
ntot + HEPTCp * nHEPT / ntot + OCTCp * nOCT / ntot + MEOHCp * nMEOH / ntot

End Function
```

Internal energy calculation worksheet function

```
Function IntE(T, nCO2, nCO, nH2O, nH2, nO2, nN2, nETOH, nPROP, nHEX, nTOL, nHEPT, nOCT, nMEOH)
' solves the Internal energy value of a mixture at a given temperature using the Cp polynomial coefficients given
' in the JANEF tables in the "thermodata" worksheet for the various temperature ranges
' The function distinguishes between high T and Low T range values of the Cp coefficients
'
Application.Volatile
ntot = nCO2 + nCO + nH2O + nH2 + nO2 + nN2 + nETOH + nPROP + nHEX + nTOL + nHEPT + nOCT + nMEOH

' ==================================
If T > 1000 Then
    ' read in HT Cp coeff values
    CO2Cpa = CO2CpaHT
    CO2Cpb = CO2CpbHT
    CO2Cpc = CO2CpcHT
    CO2Cpd = CO2CpdHT
    CO2Cpe = CO2CpeHT

    COCpa = COCpaHT
    COCpb = COCpbHT
    COCpc = COCpcHT
    COCpd = COCpdHT
    COCpe = COCpeHT

    H2OCpa = H2OCpaHT
    H2OCpb = H2OCpbHT
    H2OCpc = H2OCpcHT
    H2OCpd = H2OCpdHT
    H2OCpe = H2OCpeHT

    H2Cpa = H2CpaHT
    H2Cpb = H2CpbHT
    H2Cpc = H2CpcHT
    H2Cpd = H2CpdHT
    H2Cpe = H2CpeHT

    O2Cpa = O2CpaHT
    O2Cpb = O2CpbHT
    O2Cpc = O2CpcHT
    O2Cpd = O2CpdHT
    O2Cpe = O2CpeHT

    N2Cpa = N2CpaHT
    N2Cpb = N2CpbHT
```

```
    N2Cpc = N2CpcHT
    N2Cpd = N2CpdHT
    N2Cpe = N2CpeHT

    MEOHCpa = MEOHCpaHT
    MEOHCpb = MEOHCpbHT
    MEOHCpc = MEOHCpcHT
    MEOHCpd = MEOHCpdHT
    MEOHCpe = MEOHCpeHT

    ' read in HT (dhf298-hsens298) chemkin ref values
    CO2hfhs = CO2hfhsHT
    COhfhs = COhfhsHT
    H2Ohfhs = H2OhfhsHT
    H2hfhs = H2hfhsHT
    O2hfhs = O2hfhsHT
    N2hfhs = N2hfhsHT
    MEOHhfhs = MEOHhfhsHT
Else
    ' read in LT Cp coeff values
    CO2Cpa = CO2CpaLT
    CO2Cpb = CO2CpbLT
    CO2Cpc = CO2CpcLT
    CO2Cpd = CO2CpdLT
    CO2Cpe = CO2CpeLT

    COCpa = COCpaLT
    COCpb = COCpbLT
    COCpc = COCpcLT
    COCpd = COCpdLT
    COCpe = COCpeLT

    H2OCpa = H2OCpaLT
    H2OCpb = H2OCpbLT
    H2OCpc = H2OCpcLT
    H2OCpd = H2OCpdLT
    H2OCpe = H2OCpeLT

    H2Cpa = H2CpaLT
    H2Cpb = H2CpbLT
    H2Cpc = H2CpcLT
    H2Cpd = H2CpdLT
    H2Cpe = H2CpeLT

    O2Cpa = O2CpaLT
    O2Cpb = O2CpbLT
    O2Cpc = O2CpcLT
    O2Cpd = O2CpdLT
    O2Cpe = O2CpeLT

    N2Cpa = N2CpaLT
    N2Cpb = N2CpbLT
    N2Cpc = N2CpcLT
    N2Cpd = N2CpdLT
    N2Cpe = N2CpeLT

    MEOHCpa = MEOHCpaLT
    MEOHCpb = MEOHCpbLT
    MEOHCpc = MEOHCpcLT
    MEOHCpd = MEOHCpdLT
    MEOHCpe = MEOHCpeLT

    ' read in LT (dhf298-hsens298) chemkin ref values
    CO2hfhs = CO2hfhsLT
    COhfhs = COhfhsLT
    H2Ohfhs = H2OhfhsLT
    H2hfhs = H2hfhsLT
```

```
    O2hfhs = O2hfhsLT
    N2hfhs = N2hfhsLT
    MEOHhfhs = MEOHhfhsLT
End If

' calculat species h values
CO2h = CO2hfhs + CO2Cpa * T + (CO2Cpb / 2) * T ^ 2 + (CO2Cpc / 3) * T ^ 3 + (CO2Cpd / 4) * T ^ 4 + (CO2Cpe / 5) * T ^ 5
COh = COhfhs + COCpa * T + (COCpb / 2) * T ^ 2 + (COCpc / 3) * T ^ 3 + (COCpd / 4) * T ^ 4 + (COCpe / 5) * T ^ 5
H2Oh = H2Ohfhs + H2OCpa * T + (H2OCpb / 2) * T ^ 2 + (H2OCpc / 3) * T ^ 3 + (H2OCpd / 4) * T ^ 4 + (H2OCpe / 5) * T ^ 5
H2h = H2hfhs + H2Cpa * T + (H2Cpb / 2) * T ^ 2 + (H2Cpc / 3) * T ^ 3 + (H2Cpd / 4) * T ^ 4 + (H2Cpe / 5) * T ^ 5
O2h = O2hfhs + O2Cpa * T + (O2Cpb / 2) * T ^ 2 + (O2Cpc / 3) * T ^ 3 + (O2Cpd / 4) * T ^ 4 + (O2Cpe / 5) * T ^ 5
N2h = N2hfhs + N2Cpa * T + (N2Cpb / 2) * T ^ 2 + (N2Cpc / 3) * T ^ 3 + (N2Cpd / 4) * T ^ 4 + (N2Cpe / 5) * T ^ 5
MEOHh = MEOHhfhs + MEOHCpa * T + (MEOHCpb / 2) * T ^ 2 + (MEOHCpc / 3) * T ^ 3 + (MEOHCpd / 4) * T ^ 4 + (MEOHCpe / 5) * T ^ 5
ETOHh = ETOHhfhs + ETOHCpa * T + (ETOHCpb / 2) * T ^ 2 + (ETOHCpc / 3) * T ^ 3 + (ETOHCpd / 4) * T ^ 4 + (ETOHCpe / 5) * T ^ 5
PROPh = PROPhfhs + PROPCpa * T + (PROPCpb / 2) * T ^ 2 + (PROPCpc / 3) * T ^ 3 + (PROPCpd / 4) * T ^ 4 + (PROPCpe / 5) * T ^ 5
HEXh = Hexhfhs + HexCpa * T + (HexCpb / 2) * T ^ 2 + (HexCpc / 3) * T ^ 3 + (HexCpd / 4) * T ^ 4 + (HexCpe / 5) * T ^ 5
TOLh = tolhfhs + tolCpa * T + (tolCpb / 2) * T ^ 2 + (tolCpc / 3) * T ^ 3 + (tolCpd / 4) * T ^ 4 + (tolCpe / 5) * T ^ 5
HEPTh = HEPThfhs + HEPTCpa * T + (HEPTCpb / 2) * T ^ 2 + (HEPTCpc / 3) * T ^ 3 + (HEPTCpd / 4) * T ^ 4 + (HEPTCpe / 5) * T ^ 5
OCTh = Octhfhs + OctCpa * T + (OctCpb / 2) * T ^ 2 + (OctCpc / 3) * T ^ 3 + (OctCpd / 4) * T ^ 4 + (OctCpe / 5) * T ^ 5

' calculate mixture enthalpy value per unit mole of mixture (J/mol)
hmixpm = CO2h * nCO2 / ntot + COh * nCO / ntot + H2Oh * nH2O / ntot + H2h * nH2 / ntot + O2h * nO2 / ntot + N2h * nN2 / ntot + ETOHh * nETOH / ntot + PROPh * nPROP / ntot + HEXh * nHEX / ntot + TOLh * nTOL / ntot + HEPTh * nHEPT / ntot + OCTh * nOCT / ntot + MEOHh * nMEOH / ntot
' calculate and return the total internal energy of the mixture in Joules
IntE = ntot * (hmixpm - Ru * T)

End Function
```

Temperature pseudo-explicit solver worksheet function

```
Function TsolveE(Uold, Tprev, Tnext, nCO2, nCO, nH2O, nH2, nO2, nN2, nETOH, nPROP, nHEX, nTOL, nHEPT, nOCT, nMEOH)
Application.Volatile
ncount = 0
ntot = nCO2 + nCO + nH2O + nH2 + nO2 + nN2 + nETOH + nPROP + nHEX + nTOL + nHEPT + nOCT + nMEOH
'================================================
'calculate Uprev and dUprev
T = Tprev
'choose correct Cp coefficient and chemkin ref values
If T > 1000 Then
    CO2Cpa = CO2CpaHT
    CO2Cpb = CO2CpbHT
    CO2Cpc = CO2CpcHT
    CO2Cpd = CO2CpdHT
    CO2Cpe = CO2CpeHT

    COCpa = COCpaHT
    COCpb = COCpbHT
    COCpc = COCpcHT
    COCpd = COCpdHT
    COCpe = COCpeHT

    H2OCpa = H2OCpaHT
    H2OCpb = H2OCpbHT
    H2OCpc = H2OCpcHT
    H2OCpd = H2OCpdHT
```

```
    H2OCpe = H2OCpeHT

    H2Cpa = H2CpaHT
    H2Cpb = H2CpbHT
    H2Cpc = H2CpcHT
    H2Cpd = H2CpdHT
    H2Cpe = H2CpeHT

    O2Cpa = O2CpaHT
    O2Cpb = O2CpbHT
    O2Cpc = O2CpcHT
    O2Cpd = O2CpdHT
    O2Cpe = O2CpeHT

    N2Cpa = N2CpaHT
    N2Cpb = N2CpbHT
    N2Cpc = N2CpcHT
    N2Cpd = N2CpdHT
    N2Cpe = N2CpeHT

    MEOHCpa = MEOHCpaHT
    MEOHCpb = MEOHCpbHT
    MEOHCpc = MEOHCpcHT
    MEOHCpd = MEOHCpdHT
    MEOHCpe = MEOHCpeHT

    CO2hfhs = CO2hfhsHT
    COhfhs = COhfhsHT
    H2Ohfhs = H2OhfhsHT
    H2hfhs = H2hfhsHT
    O2hfhs = O2hfhsHT
    N2hfhs = N2hfhsHT
    MEOHhfhs = MEOHhfhsHT
Else
    CO2Cpa = CO2CpaLT
    CO2Cpb = CO2CpbLT
    CO2Cpc = CO2CpcLT
    CO2Cpd = CO2CpdLT
    CO2Cpe = CO2CpeLT

    COCpa = COCpaLT
    COCpb = COCpbLT
    COCpc = COCpcLT
    COCpd = COCpdLT
    COCpe = COCpeLT

    H2OCpa = H2OCpaLT
    H2OCpb = H2OCpbLT
    H2OCpc = H2OCpcLT
    H2OCpd = H2OCpdLT
    H2OCpe = H2OCpeLT

    H2Cpa = H2CpaLT
    H2Cpb = H2CpbLT
    H2Cpc = H2CpcLT
    H2Cpd = H2CpdLT
    H2Cpe = H2CpeLT

    O2Cpa = O2CpaLT
    O2Cpb = O2CpbLT
    O2Cpc = O2CpcLT
    O2Cpd = O2CpdLT
    O2Cpe = O2CpeLT

    N2Cpa = N2CpaLT
    N2Cpb = N2CpbLT
    N2Cpc = N2CpcLT
```

```
    N2Cpd = N2CpdLT
    N2Cpe = N2CpeLT

    MEOHCpa = MEOHCpaLT
    MEOHCpb = MEOHCpbLT
    MEOHCpc = MEOHCpcLT
    MEOHCpd = MEOHCpdLT
    MEOHCpe = MEOHCpeLT

    CO2hfhs = CO2hfhsLT
    COhfhs = COhfhsLT
    H2Ohfhs = H2OhfhsLT
    H2hfhs = H2hfhsLT
    O2hfhs = O2hfhsLT
    N2hfhs = N2hfhsLT
    MEOHhfhs = MEOHhfhsLT
End If
' calculat species h values
CO2h = CO2hfhs + CO2Cpa * T + (CO2Cpb / 2) * T ^ 2 + (CO2Cpc / 3) * T ^ 3 + (CO2Cpd / 4) * T ^ 4 + (CO2Cpe /
5) * T ^ 5
COh = COhfhs + COCpa * T + (COCpb / 2) * T ^ 2 + (COCpc / 3) * T ^ 3 + (COCpd / 4) * T ^ 4 + (COCpe / 5) * T ^ 5
H2Oh = H2Ohfhs + H2OCpa * T + (H2OCpb / 2) * T ^ 2 + (H2OCpc / 3) * T ^ 3 + (H2OCpd / 4) * T ^ 4 + (H2OCpe /
5) * T ^ 5
H2h = H2hfhs + H2Cpa * T + (H2Cpb / 2) * T ^ 2 + (H2Cpc / 3) * T ^ 3 + (H2Cpd / 4) * T ^ 4 + (H2Cpe / 5) * T ^ 5
O2h = O2hfhs + O2Cpa * T + (O2Cpb / 2) * T ^ 2 + (O2Cpc / 3) * T ^ 3 + (O2Cpd / 4) * T ^ 4 + (O2Cpe / 5) * T ^ 5
N2h = N2hfhs + N2Cpa * T + (N2Cpb / 2) * T ^ 2 + (N2Cpc / 3) * T ^ 3 + (N2Cpd / 4) * T ^ 4 + (N2Cpe / 5) * T ^ 5
MEOHh = MEOHhfhs + MEOHCpa * T + (MEOHCpb / 2) * T ^ 2 + (MEOHCpc / 3) * T ^ 3 + (MEOHCpd / 4) * T ^ 4 +
(MEOHCpe / 5) * T ^ 5
ETOHh = ETOHhfhs + ETOHCpa * T + (ETOHCpb / 2) * T ^ 2 + (ETOHCpc / 3) * T ^ 3 + (ETOHCpd / 4) * T ^ 4 +
(ETOHCpe / 5) * T ^ 5
PROPh = PROPhfhs + PROPCpa * T + (PROPCpb / 2) * T ^ 2 + (PROPCpc / 3) * T ^ 3 + (PROPCpd / 4) * T ^ 4 +
(PROPCpe / 5) * T ^ 5
HEXh = Hexhfhs + HexCpa * T + (HexCpb / 2) * T ^ 2 + (HexCpc / 3) * T ^ 3 + (HexCpd / 4) * T ^ 4 + (HexCpe / 5) * T
^ 5
TOLh = tolhfhs + tolCpa * T + (tolCpb / 2) * T ^ 2 + (tolCpc / 3) * T ^ 3 + (tolCpd / 4) * T ^ 4 + (tolCpe / 5) * T ^ 5
HEPTh = HEPThfhs + HEPTCpa * T + (HEPTCpb / 2) * T ^ 2 + (HEPTCpc / 3) * T ^ 3 + (HEPTCpd / 4) * T ^ 4 +
(HEPTCpe / 5) * T ^ 5
OCTh = Octhfhs + OctCpa * T + (OctCpb / 2) * T ^ 2 + (OctCpc / 3) * T ^ 3 + (OctCpd / 4) * T ^ 4 + (OctCpe / 5) * T ^
5

' calculate mixture enthalpy value per unit mole of mixture (J/mol)
hmixpm = CO2h * nCO2 / ntot + COh * nCO / ntot + H2Oh * nH2O / ntot + H2h * nH2 / ntot + O2h * nO2 / ntot + N2h
* nN2 / ntot + ETOHh * nETOH / ntot + PROPh * nPROP / ntot + HEXh * nHEX / ntot + TOLh * nTOL / ntot + HEPTh
* nHEPT / ntot + OCTh * nOCT / ntot + MEOHh * nMEOH / ntot
' calculate and return the total Ucalcrnal energy of the mixture in Joules
Ucalc = ntot * (hmixpm - Ru * T)
Uprev = Ucalc
dUprev = Uprev - Uold
' ================================================================
'calculate Unext and dUnext
T = Tnext
'choose correct Cp coefficient and chemkin ref values
If T > 1000 Then
    CO2Cpa = CO2CpaHT
    CO2Cpb = CO2CpbHT
    CO2Cpc = CO2CpcHT
    CO2Cpd = CO2CpdHT
    CO2Cpe = CO2CpeHT

    COCpa = COCpaHT
    COCpb = COCpbHT
    COCpc = COCpcHT
    COCpd = COCpdHT
    COCpe = COCpeHT

    H2OCpa = H2OCpaHT
    H2OCpb = H2OCpbHT
```

```
    H2OCpc = H2OCpcHT
    H2OCpd = H2OCpdHT
    H2OCpe = H2OCpeHT

    H2Cpa = H2CpaHT
    H2Cpb = H2CpbHT
    H2Cpc = H2CpcHT
    H2Cpd = H2CpdHT
    H2Cpe = H2CpeHT

    O2Cpa = O2CpaHT
    O2Cpb = O2CpbHT
    O2Cpc = O2CpcHT
    O2Cpd = O2CpdHT
    O2Cpe = O2CpeHT

    N2Cpa = N2CpaHT
    N2Cpb = N2CpbHT
    N2Cpc = N2CpcHT
    N2Cpd = N2CpdHT
    N2Cpe = N2CpeHT

    MEOHCpa = MEOHCpaHT
    MEOHCpb = MEOHCpbHT
    MEOHCpc = MEOHCpcHT
    MEOHCpd = MEOHCpdHT
    MEOHCpe = MEOHCpeHT

    CO2hfhs = CO2hfhsHT
    COhfhs = COhfhsHT
    H2Ohfhs = H2OhfhsHT
    H2hfhs = H2hfhsHT
    O2hfhs = O2hfhsHT
    N2hfhs = N2hfhsHT
    MEOHhfhs = MEOHhfhsHT
Else
    CO2Cpa = CO2CpaLT
    CO2Cpb = CO2CpbLT
    CO2Cpc = CO2CpcLT
    CO2Cpd = CO2CpdLT
    CO2Cpe = CO2CpeLT

    COCpa = COCpaLT
    COCpb = COCpbLT
    COCpc = COCpcLT
    COCpd = COCpdLT
    COCpe = COCpeLT

    H2OCpa = H2OCpaLT
    H2OCpb = H2OCpbLT
    H2OCpc = H2OCpcLT
    H2OCpd = H2OCpdLT
    H2OCpe = H2OCpeLT

    H2Cpa = H2CpaLT
    H2Cpb = H2CpbLT
    H2Cpc = H2CpcLT
    H2Cpd = H2CpdLT
    H2Cpe = H2CpeLT

    O2Cpa = O2CpaLT
    O2Cpb = O2CpbLT
    O2Cpc = O2CpcLT
    O2Cpd = O2CpdLT
    O2Cpe = O2CpeLT

    N2Cpa = N2CpaLT
```

```
    N2Cpb = N2CpbLT
    N2Cpc = N2CpcLT
    N2Cpd = N2CpdLT
    N2Cpe = N2CpeLT

    MEOHCpa = MEOHCpaLT
    MEOHCpb = MEOHCpbLT
    MEOHCpc = MEOHCpcLT
    MEOHCpd = MEOHCpdLT
    MEOHCpe = MEOHCpeLT

    CO2hfhs = CO2hfhsLT
    COhfhs = COhfhsLT
    H2Ohfhs = H2OhfhsLT
    H2hfhs = H2hfhsLT
    O2hfhs = O2hfhsLT
    N2hfhs = N2hfhsLT
    MEOHhfhs = MEOHhfhsLT
End If
' calculat species h values
CO2h = CO2hfhs + CO2Cpa * T + (CO2Cpb / 2) * T ^ 2 + (CO2Cpc / 3) * T ^ 3 + (CO2Cpd / 4) * T ^ 4 + (CO2Cpe /
5) * T ^ 5
COh = COhfhs + COCpa * T + (COCpb / 2) * T ^ 2 + (COCpc / 3) * T ^ 3 + (COCpd / 4) * T ^ 4 + (COCpe / 5) * T ^ 5
H2Oh = H2Ohfhs + H2OCpa * T + (H2OCpb / 2) * T ^ 2 + (H2OCpc / 3) * T ^ 3 + (H2OCpd / 4) * T ^ 4 + (H2OCpe /
5) * T ^ 5
H2h = H2hfhs + H2Cpa * T + (H2Cpb / 2) * T ^ 2 + (H2Cpc / 3) * T ^ 3 + (H2Cpd / 4) * T ^ 4 + (H2Cpe / 5) * T ^ 5
O2h = O2hfhs + O2Cpa * T + (O2Cpb / 2) * T ^ 2 + (O2Cpc / 3) * T ^ 3 + (O2Cpd / 4) * T ^ 4 + (O2Cpe / 5) * T ^ 5
N2h = N2hfhs + N2Cpa * T + (N2Cpb / 2) * T ^ 2 + (N2Cpc / 3) * T ^ 3 + (N2Cpd / 4) * T ^ 4 + (N2Cpe / 5) * T ^ 5
MEOHh = MEOHhfhs + MEOHCpa * T + (MEOHCpb / 2) * T ^ 2 + (MEOHCpc / 3) * T ^ 3 + (MEOHCpd / 4) * T ^ 4 +
(MEOHCpe / 5) * T ^ 5
ETOHh = ETOHhfhs + ETOHCpa * T + (ETOHCpb / 2) * T ^ 2 + (ETOHCpc / 3) * T ^ 3 + (ETOHCpd / 4) * T ^ 4 +
(ETOHCpe / 5) * T ^ 5
PROPh = PROPhfhs + PROPCpa * T + (PROPCpb / 2) * T ^ 2 + (PROPCpc / 3) * T ^ 3 + (PROPCpd / 4) * T ^ 4 +
(PROPCpe / 5) * T ^ 5
HEXh = Hexhfhs + HexCpa * T + (HexCpb / 2) * T ^ 2 + (HexCpc / 3) * T ^ 3 + (HexCpd / 4) * T ^ 4 + (HexCpe / 5) * T
^ 5
TOLh = tolhfhs + tolCpa * T + (tolCpb / 2) * T ^ 2 + (tolCpc / 3) * T ^ 3 + (tolCpd / 4) * T ^ 4 + (tolCpe / 5) * T ^ 5
HEPTh = HEPThfhs + HEPTCpa * T + (HEPTCpb / 2) * T ^ 2 + (HEPTCpc / 3) * T ^ 3 + (HEPTCpd / 4) * T ^ 4 +
(HEPTCpe / 5) * T ^ 5
OCTh = Octhfhs + OctCpa * T + (OctCpb / 2) * T ^ 2 + (OctCpc / 3) * T ^ 3 + (OctCpd / 4) * T ^ 4 + (OctCpe / 5) * T ^
5

' calculate mixture enthalpy value per unit mole of mixture (J/mol)
hmixpm = CO2h * nCO2 / ntot + COh * nCO / ntot + H2Oh * nH2O / ntot + H2h * nH2 / ntot + O2h * nO2 / ntot + N2h
* nN2 / ntot + ETOHh * nETOH / ntot + PROPh * nPROP / ntot + HEXh * nHEX / ntot + TOLh * nTOL / ntot + HEPTh
* nHEPT / ntot + OCTh * nOCT / ntot + MEOHh * nMEOH / ntot
' calculate and return the total Ucalcrnal energy of the mixture in Joules
Ucalc = ntot * (hmixpm - Ru * T)
Unext = Ucalc
dUnext = Unext - Uold
' ========================================================================
' start Newton's method iteration loop
Do While dUnext ^ 2 > 0.000001
'counter update and non convergence exit
ncount = ncount + 1
If ncount > 5 Then Exit Do
'
Slope = (dUnext - dUprev) / (Tnext - Tprev)
Intrcpt = dUnext - Slope * Tnext
Tnewnext = -Intrcpt / Slope
' ========================================================================
'calculate Unewnext and dUnewnext
T = Tnewnext
'choose correct Cp coefficient and chemkin ref values
If T > 1000 Then
    CO2Cpa = CO2CpaHT
    CO2Cpb = CO2CpbHT
```

```
    CO2Cpc = CO2CpcHT
    CO2Cpd = CO2CpdHT
    CO2Cpe = CO2CpeHT

    COCpa = COCpaHT
    COCpb = COCpbHT
    COCpc = COCpcHT
    COCpd = COCpdHT
    COCpe = COCpeHT

    H2OCpa = H2OCpaHT
    H2OCpb = H2OCpbHT
    H2OCpc = H2OCpcHT
    H2OCpd = H2OCpdHT
    H2OCpe = H2OCpeHT

    H2Cpa = H2CpaHT
    H2Cpb = H2CpbHT
    H2Cpc = H2CpcHT
    H2Cpd = H2CpdHT
    H2Cpe = H2CpeHT

    O2Cpa = O2CpaHT
    O2Cpb = O2CpbHT
    O2Cpc = O2CpcHT
    O2Cpd = O2CpdHT
    O2Cpe = O2CpeHT

    N2Cpa = N2CpaHT
    N2Cpb = N2CpbHT
    N2Cpc = N2CpcHT
    N2Cpd = N2CpdHT
    N2Cpe = N2CpeHT

    MEOHCpa = MEOHCpaHT
    MEOHCpb = MEOHCpbHT
    MEOHCpc = MEOHCpcHT
    MEOHCpd = MEOHCpdHT
    MEOHCpe = MEOHCpeHT

    CO2hfhs = CO2hfhsHT
    COhfhs = COhfhsHT
    H2Ohfhs = H2OhfhsHT
    H2hfhs = H2hfhsHT
    O2hfhs = O2hfhsHT
    N2hfhs = N2hfhsHT
    MEOHhfhs = MEOHhfhsHT
Else
    CO2Cpa = CO2CpaLT
    CO2Cpb = CO2CpbLT
    CO2Cpc = CO2CpcLT
    CO2Cpd = CO2CpdLT
    CO2Cpe = CO2CpeLT

    COCpa = COCpaLT
    COCpb = COCpbLT
    COCpc = COCpcLT
    COCpd = COCpdLT
    COCpe = COCpeLT

    H2OCpa = H2OCpaLT
    H2OCpb = H2OCpbLT
    H2OCpc = H2OCpcLT
    H2OCpd = H2OCpdLT
    H2OCpe = H2OCpeLT

    H2Cpa = H2CpaLT
```

```
    H2Cpb = H2CpbLT
    H2Cpc = H2CpcLT
    H2Cpd = H2CpdLT
    H2Cpe = H2CpeLT

    O2Cpa = O2CpaLT
    O2Cpb = O2CpbLT
    O2Cpc = O2CpcLT
    O2Cpd = O2CpdLT
    O2Cpe = O2CpeLT

    N2Cpa = N2CpaLT
    N2Cpb = N2CpbLT
    N2Cpc = N2CpcLT
    N2Cpd = N2CpdLT
    N2Cpe = N2CpeLT

    MEOHCpa = MEOHCpaLT
    MEOHCpb = MEOHCpbLT
    MEOHCpc = MEOHCpcLT
    MEOHCpd = MEOHCpdLT
    MEOHCpe = MEOHCpeLT

    CO2hfhs = CO2hfhsLT
    COhfhs = COhfhsLT
    H2Ohfhs = H2OhfhsLT
    H2hfhs = H2hfhsLT
    O2hfhs = O2hfhsLT
    N2hfhs = N2hfhsLT
    MEOHhfhs = MEOHhfhsLT
End If
' calculat species h values
CO2h = CO2hfhs + CO2Cpa * T + (CO2Cpb / 2) * T ^ 2 + (CO2Cpc / 3) * T ^ 3 + (CO2Cpd / 4) * T ^ 4 + (CO2Cpe /
5) * T ^ 5
COh = COhfhs + COCpa * T + (COCpb / 2) * T ^ 2 + (COCpc / 3) * T ^ 3 + (COCpd / 4) * T ^ 4 + (COCpe / 5) * T ^ 5
H2Oh = H2Ohfhs + H2OCpa * T + (H2OCpb / 2) * T ^ 2 + (H2OCpc / 3) * T ^ 3 + (H2OCpd / 4) * T ^ 4 + (H2OCpe /
5) * T ^ 5
H2h = H2hfhs + H2Cpa * T + (H2Cpb / 2) * T ^ 2 + (H2Cpc / 3) * T ^ 3 + (H2Cpd / 4) * T ^ 4 + (H2Cpe / 5) * T ^ 5
O2h = O2hfhs + O2Cpa * T + (O2Cpb / 2) * T ^ 2 + (O2Cpc / 3) * T ^ 3 + (O2Cpd / 4) * T ^ 4 + (O2Cpe / 5) * T ^ 5
N2h = N2hfhs + N2Cpa * T + (N2Cpb / 2) * T ^ 2 + (N2Cpc / 3) * T ^ 3 + (N2Cpd / 4) * T ^ 4 + (N2Cpe / 5) * T ^ 5
MEOHh = MEOHhfhs + MEOHCpa * T + (MEOHCpb / 2) * T ^ 2 + (MEOHCpc / 3) * T ^ 3 + (MEOHCpd / 4) * T ^ 4 +
(MEOHCpe / 5) * T ^ 5
ETOHh = ETOHhfhs + ETOHCpa * T + (ETOHCpb / 2) * T ^ 2 + (ETOHCpc / 3) * T ^ 3 + (ETOHCpd / 4) * T ^ 4 +
(ETOHCpe / 5) * T ^ 5
PROPh = PROPhfhs + PROPCpa * T + (PROPCpb / 2) * T ^ 2 + (PROPCpc / 3) * T ^ 3 + (PROPCpd / 4) * T ^ 4 +
(PROPCpe / 5) * T ^ 5
HEXh = Hexhfhs + HexCpa * T + (HexCpb / 2) * T ^ 2 + (HexCpc / 3) * T ^ 3 + (HexCpd / 4) * T ^ 4 + (HexCpe / 5) * T
^ 5
TOLh = tolhfhs + tolCpa * T + (tolCpb / 2) * T ^ 2 + (tolCpc / 3) * T ^ 3 + (tolCpd / 4) * T ^ 4 + (tolCpe / 5) * T ^ 5
HEPTh = HEPThfhs + HEPTCpa * T + (HEPTCpb / 2) * T ^ 2 + (HEPTCpc / 3) * T ^ 3 + (HEPTCpd / 4) * T ^ 4 +
(HEPTCpe / 5) * T ^ 5
OCTh = Octhfhs + OctCpa * T + (OctCpb / 2) * T ^ 2 + (OctCpc / 3) * T ^ 3 + (OctCpd / 4) * T ^ 4 + (OctCpe / 5) * T ^
5

' calculate mixture enthalpy value per unit mole of mixture (J/mol)
hmixpm = CO2h * nCO2 / ntot + COh * nCO / ntot + H2Oh * nH2O / ntot + H2h * nH2 / ntot + O2h * nO2 / ntot + N2h
* nN2 / ntot + ETOHh * nETOH / ntot + PROPh * nPROP / ntot + HEXh * nHEX / ntot + TOLh * nTOL / ntot + HEPTh
* nHEPT / ntot + OCTh * nOCT / ntot + MEOHh * nMEOH / ntot
' calculate and return the total Ucalcrnal energy of the mixture in Joules
Ucalc = ntot * (hmixpm - Ru * T)
Unewnext = Ucalc
dUnewnext = Unewnext - Uold
' ================================================================
' shift values for next Newton's method iteration
Tprev = Tnext
Tnext = Tnewnext
dUprev = dUnext
```

```
dUnext = dUnewnext
Loop
' return the T value which satisfies the energy equation
TsolveE = Tnext

End Function
```

Iterative stable time step calculation worksheet function

```
Function dtstep(ChemkID, IDdev, Tres, Cp, dHFCO, dHCOCO2, volume, dTdtprev, Lopp, nCO2, nCO, nH2O, nO2,
nF, nI, nQ, nY, dndtCO2, dndtCO, dndtH2O, dndtO2, dndtF, dndtI, dndtQ, dndtY, T)
'function calculates the optimised time step in miliseconds according to 4 criteria
Application.Volatile
'=========================================================================
' 1) set default large time step
dtdefault = ChemkID / IDdev
'=========================================================================
' 2) calculate the max alowable time step to avoid negative concentrations
' (only species that can reduce [] are considerred)
'
' first check the direction of each rate and calculate the time step for each species
If dndtCO2 >= 0 Then
   dtRCO2 = dtdefault
Else
   dtRCO2 = -1000 * nCO2 / dndtCO2
End If
'
If dndtCO >= 0 Then
   dtRCO = dtdefault
Else
   dtRCO = -1000 * nCO / dndtCO
End If
'
If dndtO2 >= 0 Then
   dtRO2 = dtdefault
Else
   dtRO2 = -1000 * nO2 / dndtO2
End If
'
If dndtF >= 0 Then
   dtRF = dtdefault
Else
   dtRF = -1000 * nF / dndtF
End If
'
If dndtI >= 0 Then
   dtRI = dtdefault
Else
   dtRI = -1000 * nI / dndtI
End If
'
If dndtQ >= 0 Then
   dtRQ = dtdefault
Else
   dtRQ = -1000 * nQ / dndtQ
End If
'
If dndtY >= 0 Then
   dtRY = dtdefault
Else
   dtRY = -1000 * nY / dndtY
End If
'
dtR = 1 * Application.WorksheetFunction.Min(dtRCO2, dtRCO, dtRO2, dtRF, dtRI, dtRQ, dtRY)
'=========================================================================
```

```
' 3) calculate the time step size for the specified temperature resolution value based on reaction rates
'calculate the net rate of fuel to CO energy release (J/s)
dHFCOdt = (-dndtF - dndtI - dndtQ - dndtY) * dHFCO * volume
'calculate the net rate of CO to CO2 energy release (J/s)
dHCOCO2dt = dndtCO2 * dHCOCO2 * volume
'calculate the net rate of energy release (J/s)
dHdt = dHFCOdt + dHCOCO2dt
'calculate time step size for the specified temperature resolution value
'use a factor of 41.667 to compensate for the lack of proper dH calculation?
If dHdt < -1E-20 Then
   dtTres = -1000 * Cp * (41.667) * Tres / dHdt
Else
   dtTres = dtdefault
End If

If T > 1200 Then
   dtTres = dtdefault
End If
'=========================================================================
' 4) calculate the time step size based on temperature curvature
' this scales the dTdt space into dydx space using ID/2500K
'it then determines the previous and current slopes and the angle formed
If dTdtprev < 1E-100 Then
   dtCurv = dtdefault
Else
   alpha = Atn(dTdtprev * (ChemkID / 2500))
   dTdt = -dHdt / (1000 * Cp * (41.667))
   phi = Atn(dTdt * (ChemkID / 2500))
   theta = Abs(phi - alpha)
   'it then uses the given length of the opp side to determine the hypotonuse
   hypot = Lopp / (2 * Sin(theta / 2))
   'it then determines the dx from the slope and hypotenuse and scales dx back to dt
   dx = hypot * Cos(phi)
   dtCurv = dx * ChemkID
End If
'=========================================================================
'calculate the minimum time step from each of the 4 criteria
If dtTres <= 0 Then
   dtstep = Application.WorksheetFunction.Min(dtdefault, dtR, dtCurv)
Else
   dtstep = Application.WorksheetFunction.Min(dtdefault, dtR, dtTres, dtCurv)
End If

End Function
```

Shape error calculation function

```
Function ShapeError(Ckntimes, CknTemps, FRAIMtimes, FRAIMTemps, Tcutoff)
'worksheet function to calculate Temperature trace shape error value
'
'check that each function reaches the cutoff Temperature
If CknTemps(100) >= Tcutoff Then

If FRAIMTemps(100) >= Tcutoff Then

' get time for each function at the Tcutoff
CknTcutID = Application.WorksheetFunction.Lookup(Tcutoff, CknTemps, Ckntimes)
FRAIMTcutID = Application.WorksheetFunction.Lookup(Tcutoff, FRAIMTemps, FRAIMtimes)
'set the time ingrement to give 100 time values (99 steps) to the larger ID
IntegrIDtime = Application.WorksheetFunction.Max(CknTcutID, FRAIMTcutID)
IntegrIDtstep = IntegrIDtime / 99
RiemannArea = 0
For step = 1 To 99
   Integrtime = IntegrIDtstep * step
```

```
    'get Chemkin Temperature at the specified time or use the Tcutoff
    If Integrtime >= CknTcutID Then
        CknfnTemp = Tcutoff
    Else
        'get lower and upper values for Chemkin times and temperatures
        Cknarrayindex! = Application.WorksheetFunction.Match(Integrtime, Ckntimes)
        CknLowerTime = Ckntimes(Cknarrayindex)
        CknUpperTime = Ckntimes(Cknarrayindex + 1)
        CknLowerTemp = CknTemps(Cknarrayindex)
        CknUpperTemp = CknTemps(Cknarrayindex + 1)
        'interpolate to get the function Temperature at the given time
        CknfnTemp = CknLowerTemp + (Integrtime - CknLowerTime) * (CknUpperTemp - CknLowerTemp) /
(CknUpperTime - CknLowerTime)
    End If

    'get FRAIM Temperature at the specified time or use the Tcutoff
    If Integrtime >= FRAIMTcutID Then
        FRAIMfnTemp = Tcutoff
    Else
        'get lower and upper values for Chemkin times and temperatures
        FRAIMarrayindex! = Application.WorksheetFunction.Match(Integrtime, FRAIMtimes)
        FRAIMLowerTime = FRAIMtimes(FRAIMarrayindex)
        FRAIMUpperTime = FRAIMtimes(FRAIMarrayindex + 1)
        FRAIMLowerTemp = FRAIMTemps(FRAIMarrayindex)
        FRAIMUpperTemp = FRAIMTemps(FRAIMarrayindex + 1)
        'interpolate to get the function Temperature at the given time
        FRAIMfnTemp = FRAIMLowerTemp + (Integrtime - FRAIMLowerTime) * (FRAIMUpperTemp -
FRAIMLowerTemp) / (FRAIMUpperTime - FRAIMLowerTime)
    End If
    'calculate Riemann integral
    fnerror = Abs(CknfnTemp - FRAIMfnTemp)
    RiemanndA = fnerror * IntegrIDtstep
    RiemannArea = RiemannArea + RiemanndA
Next
'normalise the Riemann area integral

 ShapeError = 1000 * RiemannArea / (Tcutoff * CknTcutID)

Else
'    ShapeError = 1 / 0
End If

Else
    'ShapeError = 1 / 0
End If

End Function
```

FGM parameter set solver

```
Private Sub CommandButton11_Click()
' solves the shape error function using sets of FRAIM variables
""
' set counters to zero
Range("B43").Value = "set"
VarUnchCnt = 0
IterCnt = 0
SolverReset
SolverOptions Derivatives:=1, Convergence:=0.1, MaxTime:=1800
"
Do While IterCnt < 50
    Do While VarUnchCnt < 8
        IterCnt = IterCnt + 1
        Range("C43").Value = IterCnt
        VarUnchCnt = 0
```

```
' ----------------------------------------------------------
' 1) solve C ID set
Range("D43").Value = 1
Ecur = Range("B45").Value
SolverOk SetCell:="$B$45", MaxMinVal:=2, ValueOf:="0", ByChange:=Range("D4:D6")
SolverSolve UserFinish:=True
Enew = Range("B45").Value
If 100 * (Abs(Ecur - Enew)) / Ecur <= 0.01 Then
   VarUnchCnt = VarUnchCnt + 1
End If

' 2) solve CFh ID set
Range("D43").Value = 2
Ecur = Range("B45").Value
SolverOk SetCell:="$B$45", MaxMinVal:=2, ValueOf:="0", ByChange:=Range("D2:D3", "D7:D9")
SolverSolve UserFinish:=True
Enew = Range("B45").Value
If 100 * (Abs(Ecur - Enew)) / Ecur <= 0.01 Then
   VarUnchCnt = VarUnchCnt + 1
End If

' 3) solve CF kill set
Range("D43").Value = 3
Ecur = Range("B45").Value
SolverOk SetCell:="$B$45", MaxMinVal:=2, ValueOf:="0", ByChange:=Range("D10:D14")
SolverSolve UserFinish:=True
Enew = Range("B45").Value
If 100 * (Abs(Ecur - Enew)) / Ecur <= 0.01 Then
   VarUnchCnt = VarUnchCnt + 1
End If

' 4) solve post CF ID set
Range("D43").Value = 4
Ecur = Range("B45").Value
SolverOk SetCell:="$B$45", MaxMinVal:=2, ValueOf:="0", ByChange:=Range("D15:D19")
SolverSolve UserFinish:=True
Enew = Range("B45").Value
If 100 * (Abs(Ecur - Enew)) / Ecur <= 0.01 Then
   VarUnchCnt = VarUnchCnt + 1
End If

' 5) solve HT ID set
Range("D43").Value = 5
Ecur = Range("B45").Value
SolverOk SetCell:="$B$45", MaxMinVal:=2, ValueOf:="0", ByChange:=Range("D20:D24")
SolverSolve UserFinish:=True
Enew = Range("B45").Value
If 100 * (Abs(Ecur - Enew)) / Ecur <= 0.01 Then
   VarUnchCnt = VarUnchCnt + 1
End If

' 6) solve LT Qrel set
Range("D43").Value = 6
Ecur = Range("B45").Value
SolverOk SetCell:="$B$45", MaxMinVal:=2, ValueOf:="0", ByChange:=Range("D25:D29")
SolverSolve UserFinish:=True
Enew = Range("B45").Value
If 100 * (Abs(Ecur - Enew)) / Ecur <= 0.01 Then
   VarUnchCnt = VarUnchCnt + 1
End If

' 7) solve HT Qrel set
Range("D43").Value = 7
Ecur = Range("B45").Value
SolverOk SetCell:="$B$45", MaxMinVal:=2, ValueOf:="0", ByChange:=Range("D30:D34")
SolverSolve UserFinish:=True
Enew = Range("B45").Value
```

```
        If 100 * (Abs(Ecur - Enew)) / Ecur <= 0.01 Then
            VarUnchCnt = VarUnchCnt + 1
        End If

        ' 8) solve CO2 dissoc set
        Range("D43").Value = 8
        Ecur = Range("B45").Value
        SolverOk SetCell:="$B$45", MaxMinVal:=2, ValueOf:="0", ByChange:=Range("D34:D38")
        SolverSolve UserFinish:=True
        Enew = Range("B45").Value
        If 100 * (Abs(Ecur - Enew)) / Ecur <= 0.01 Then
            VarUnchCnt = VarUnchCnt + 1
        End If
        ' ---------------------------------------------------------
        If IterCnt >= 50 Then
            VarUnchCnt = 100
        End If
        If VarUnchCnt >= 8 Then
            IterCnt = 1000
        End If
    Loop
Loop
End Sub
```

Step-through FGM parameter solver

```
Private Sub CommandButton8_Click()
' step through solver method solver which performs solver iterations on each
' variable before stepping to the next variable.
' declare and load variables
Dim varoffset(37) As Integer
Dim varnum As Integer
"""
varoffset(0) = 0
varoffset(1) = 1
varoffset(2) = 2
varoffset(3) = 3
varoffset(4) = 4
varoffset(5) = 5
varoffset(6) = 6
varoffset(7) = 7
varoffset(8) = 8
varoffset(9) = 9
varoffset(10) = 10
varoffset(11) = 11
varoffset(12) = 12
varoffset(13) = 13
varoffset(14) = 14
varoffset(15) = 15
varoffset(16) = 16
varoffset(17) = 17
varoffset(18) = 18
varoffset(19) = 19
varoffset(20) = 20
varoffset(21) = 21
varoffset(22) = 22
varoffset(23) = 23
varoffset(24) = 24
varoffset(25) = 25
varoffset(26) = 26
varoffset(27) = 27
varoffset(28) = 28
varoffset(29) = 29
varoffset(30) = 30
varoffset(31) = 31
```

```
varoffset(32) = 32
varoffset(33) = 33
varoffset(34) = 34
varoffset(35) = 35
varoffset(36) = 36

'
'varoffset(?) =?
''
' set counters to zero
Range("D43").Value = "individ"
VarUnchCnt = 0
IterCnt = 0
'reset and set solver function to central difference method
SolverReset
SolverOptions Derivatives:=1, Convergence:=0.1, MaxTime:=1800
'
Do While IterCnt < 100
   Do While VarUnchCnt < 37
      IterCnt = IterCnt + 1
      Range("C43").Value = IterCnt
      VarUnchCnt = 0
      For varnum = 0 To 36
         Range("B43").Value = Range("A2").Offset(varoffset(varnum), 0).Value
         Vcur = Range("D2").Offset(varoffset(varnum), 0).Value
         SolverOk SetCell:="$B$45", MaxMinVal:=2, ValueOf:="0", ByChange:=Range("D2").Offset(varoffset(varnum),
0)
         SolverSolve UserFinish:=True
         Vnew = Range("D2").Offset(varoffset(varnum), 0).Value
         If 100 * (Abs(Vcur - Vnew)) / Vcur <= 0.01 Then
            VarUnchCnt = VarUnchCnt + 1
         End If
      Next
      If IterCnt >= 100 Then
         VarUnchCnt = 1000
      End If
      If VarUnchCnt >= 37 Then
         IterCnt = 10000
      End If
   Loop
Loop
End Sub
```